Ⅳ．研究成果の刊行物・別刷

快をささえる
難病ケア スターティングガイド

［編集］ 河原仁志・中山優季

［執筆］
和田美紀
河原仁志
山田隆司
高木憲司
大山良子
小倉加恵子
佐藤仙務
小川一枝
川村佐和子
中島隆信
中山優季
多田羅勝義
近藤真生
難波玲子
深谷圭孝
西牧謙吾
鈴木信行
服部絵美
福永秀敏
秋山正子
塩田琴美
松木満里子
佐藤伸彦
伊藤佳世子
星野尾美幸
輪竹一義
たむらあやこ
田中勇次郎
香取久之
梶山　滋
中島　孝

難病療養は長期戦である。家族の支援も欠かせない。家族の快も一面で保障されるべきである

食の快を保障することは、人生を支えること

原病の進行による食欲の低下と決めつける前に，好きな食事なのか，彩りはよいのかなど，食欲が湧くように工夫されているか

難病患者であっても、自分の希望を叶えるためにでき得る限りの自助努力が求められるのは、健常者と同じである

訪問1回目から利用者さんとうまくいくことはあまりないので，何回もくりかえしやっていくなかで，本人の表情などで反応を見ながら進めていくことが在宅難病ケアの基本

本人が願う非日常が，こんなにも大きな力を引き出す

在宅難病ケアの悩ましい点として，「ケア要求が高い方」への対応があります。それは一概にわがままと言えるものではなく，疾患特性として「もう治らない障害」という大きなストレスと，今後の見通しの不透明さからくる当然の反応

石畳の凸凹は自然のタッピングとなり、橋の中央付近で吸引をすることになり介護士が傘で目隠しをし、OTが荷物を持って看護師が吸引をするという具合である。珍道中であるが、Aさんが本当に楽しそうなことが私たちに力を与えてくれる

「誰かを好きになること」は人間普遍の権利

在宅療養と入院療養は決して対立する概念ではなく、お互いに補完しあい、響きあい、高めあう関係

医学書院

ISBN978-4-260-02758-8
C3047 ¥3200E

9784260027588

定価：本体 3,200 円 +税

1923047032003

社会や医療を変えていくのは患者自身の力だ

寝たきりの生活でありながら、やる気さえあれは可能性は無限大に広がっていきます。近い将来、私も死を迎えます。死を前にしていかに生きるか、その答えは過去にこだわらず、常に前向きに一生懸命に生きていくことではないでしょうか。今日が終わらなければ明日はこない。今日を楽しむことが全てです

私たち患者の日頃の生活態度・成人患者としての自覚にも問題があったのではないか。患者も自分で考え行動できる大人でありたい

自分らしく生きていくには在宅以外考えられません

「病院は安全で良い」と言われ，「在宅療養は安定しない」と言われます。私が住んでいた病院は安全だと思わなかったし，在宅で関わる人との信頼関係，それが一番の安全と安心になるのだということを実感しています

寝たきりだと下を向けない，後ろも振り向けないから

自分で自分の生活をコントロールすることができないと，よりよく生きることなど困難です。それがひいては自らの余命にまで影響し，結果として支援システムが育たない。僕は支援システムを育てるのは，実は我々被支援者自身なのではないかと最近考えるようになりました

患者は弱い。でも，それで終わってはいけない

快をささえる難病ケアスターティングガイド,
医学書院, 編集：河原仁志／中山優季
,222-223,2016.7.15

My Column

患者の主観評価に基づく難病ケア

患者・ご家族の「笑顔」を目標としないケアは本来ありえない。しかし，現代医療では医学の名のもとで必ずしもケアはこのように行なわれていない。大変残念である。何故だろうか。多くの人は，真の幸せにたどりつくために，苦痛に満ちた努力がなければならないと思っているからなのだろうか。人は病気が治らなくても笑顔になれることを内心は知っているにもかかわらず，それでは科学的なケアにはならないと思いこんでいる。

科学的なケアを行なおうとする際に，人（保健医療福祉従事者など）は客観的な健康概念を参照して，少しでも健康の方向に近づけるようと努力する。無限の努力のもとでも，すこしも健康になれないにしても，また，医療がたとえ苦痛に満ちていてもである。この健康概念は身体的，精神的および社会的に完全に良好であること（complete well-being）であり，単に病気や病弱ではないことではない」（1948年世界保健機関憲章前文）に由来している。このwell-beingは単に良い状態という言葉でしかないにもかかわらず，意味を探求し混乱し，このwell-beingの官報訳が福祉である一方で，現代用語での「福祉」が「非医療系サービス」と言う意味に使われていることからさらに混乱におちいっている。

健康関連QOL評価で，well-beingを操作的に測定評価する際には，再度ジレンマが生ずる，健康な人々のデータをもとにして，計量心理学的に自己のwell-beingを主観尺度化する研究なのか，健康でない人も含めて尺度化すべきなのかという問題である。ここでは，健康か非健康かをあらかじめ定義する矛盾が起きている。

オランダの医学者であるHuber博士は「健康とは社会的，身体的，感情的問題に直面したときに適応し自ら管理する（何とかやりくりする）能力（…The authors propose changing the emphasis towards the ability to adapt and self manage in the face of social, physical, and emotional challenges）」と定義しようとしており，この適応能力が損なわれた状態が病気であり，その際支援するのが医療であるとする。この定義を使うと，客観的な絶対値としての健康を最初に定義する必要はなく，患者が変化する力がないのが病気であるとすればよいだけになる。

この新たな健康概念の導入は通常の医療技術と何ら矛盾を起こさないばかりか，治らない難病，根治し得ない悪性腫瘍，超高齢障害者のケアを著しく促進する。例えば，急性期医療において，細菌性肺炎になった場合に，自らの免疫機序により治癒することができないから，病気とし医療を行なうのであり，胃がんの手術であっても同様といえる。治らない悪性腫瘍や難病では，完全に治らなくても，その人が，その病気の状態に適応できるような症状コントロールや疾患コントロールを行なえればよいのだ。これは1967年に英国シデナムでシシリー・ソンダースが実践を始めたホスピス・緩和ケアにおける適切なケア・緩和概念と同義である。

患者さんの主観評価を科学していくためにはいくつかのポイントがある。人は現在を過去と比較し，また，現在から未来を予想しようとする。そのとき，人は時系列のエピソード記憶を保持するが，過去の意味づけを常に変えようとする。その様式は徐々に解明されてきており，reprioritization（再優先付け），reframe（再枠組化）といった意味の再構成（meaning reconstruction）と同時に，評価・判断におけるrecalibration（目盛り再調整）などであることがわかってきた。これは新たな状況に対して人が再度適応するために自動的に行なわれる神経心理現象であり，それが心理的にうまくいかないときに必要になるのが心理カウンセリングである。この現象をより科学的に評価するためにはSEIQoLやDRS（Decision Regret Scale）が有用であると思われる。

このような患者・家族の主観評価をどのように科学的に評価すればよいのかという研究はもちろん必要であるが，今日から，医学の意味を再構成し患者・家族の主観評価を高める目的にパラダイ

ムを切り替えることができれば，既存の難病ケアは再び力を取り戻せ，患者・家族を笑顔にすることができるだろう。このように保健医療福祉従事者が切り替えることができれば，病気が治癒にいたらなくても，患者・家族はすぐさま，適応的，自律的な力を取り戻していける。

中島　孝

資料
- 松田純：神経難病における健康概念と現代医療倫理学，総合診療，25 (3)：258-260, 2015.
- 大生定義，中島孝：個人の生活の質QOLとPRO評価とは何か，総合診療，25 (3)：222-226, 2015.
- 丹野清美，高木安雄：日本語版 Decision Regret Scaleと健康関連QOL，患者要因の関係―鼠径ヘルニア，胆石症，胆嚢炎，胆嚢ポリープ患者における横断研究，日本医療・病院管理学会誌，52 (4)：189-199, 2015.

世界保健機関（WHO）は1948年に，健康を「単に疾患がないとか虚弱でない状態ではなく，身体的・心理的・社会的に完全に良い状態（a state of complete physical, mental and social well-being and not merely the absence of disease or infirmity）」と定義した。この定義は当時，広範で野心的なものと評価されたが，その後，たえず批判にさらされてきた。そもそも，「完全なる健康状態」は存在するのか，健康／病気という明確な二分法が成り立つのか等々，さまざまな疑問が提起されてきた。WHOもこれを改正しようと試みたが，実現しないまま今日に至っている。結果として，65年以上にもわたって，この定義は一度も改定されていない。

これが策定されたのは，西洋近代医学が感染症に対して圧倒的な勝利をおさめつつあった時代である。ところが今日では，新しいタイプの感染症の脅威はあるものの，医学の主要な対象が，治癒が困難な難病や慢性疾患や加齢に伴う機能低下などになってきた。Machteld Huberらの国際的な研究グループは，「高齢化や疾患傾向が変化している現代において，WHOの定義は望ましくない結果を生む可能性すらある」として，新たな健康概念の開拓に取り組んできた。その成果として，「社会的・身体的・感情的問題に直面したときに適応し自らを管理する能力（the ability to adapt and self manage in the face of social, physical, and emotional challenges）」という新しい健康概念を提起した。WHOの「身体的・心理的・社会的に完全に良い状態」という定義が静態的な目標であるのに対して，問題に対処する（cope）能力という動的な捉え方になっている点に特徴がある。これは健康観の転換のみならず，医療全般，とりわけ難病医療の捉え方を大きく変える可能性すらはらんでいる。

〔松田純：神経難病における健康概念と現代医療倫理学，総合診療，25 (3)：258-259，2015.〕

Column

難病治療に新たな時代の幕開け

中島　孝

筋萎縮性側索硬化症（ALS）などの難治性の神経・筋疾患患者に対し，装着型ロボット（HAL）を用いた治療の有効性が正式に厚生労働省から認められました。しかしながら，HAL については「ずっと身体に装着しておくもの」などという誤解が多いのが現実です．

HAL とは

HAL は腰モデルのように作業を助けるモデルもありますし，将来は長時間装着するモデルも市販される可能性もあるでしょう．しかし，医療機器としての HAL は，補装具でも義足でもありません．医療機器の法的定義は「人若しくは動物の疾病の診断，治療若しくは予防に使用されること，又は人若しくは動物の身体の構造若しくは機能に影響を及ぼすことが目的とされている機械器具等であって，政令で定めるもの」ですので，HAL を一定時間装着使用し，外した後に体によい変化がおきることが使用目的となります．使っているときだけ効能がある電動車椅子や筋電義足は，医療機器とは言いません．

医療機器としての HAL 医療用（下肢タイプ）は，歩行障害を治療する機器です．つまり，HAL を使って歩いた後に，脳，脊髄，運動神経，筋が再調整され，HAL を脱いだ後に，歩行が改善することを目指しています．病気自体を根治させる治療法ではありません．現在，体幹の筋力がない方，補助具を使っても立位ができない方は HAL を使うことは不可能です．何とかぎりぎり介助や，つかまって歩こうとしている方が対象となります．

ALS と HAL

私は HAL を研究するにあたり，ALS を含む神経・筋疾患を最初のテーマとしました。もっとも困難で困られている対象患者さんが使え，臨床効果があれば，他の疾患にも容易に使えると考えたからです．狙いどおり，完成した HAL 医療用（下肢モデル）は，性能的には脳梗塞，脊髄損傷から，パーキンソン病，筋ジストロフィー，ALS までカバーしうるものとなりました．すでに，レンタルされている HAL 福祉用との性能上の差を出す必要があったことも重要でした。HAL 福祉用で動かない疾患・患者で有効性を示す必要があったからでもあります．

技術革新は難病を対象とすることで進歩するというのは山海嘉之先生（筑波大）と私に共通する考えであり，ALS 患者さんや患者団体の応援があったこと，日本には難病対策が施策として確立し，研究費をいただけたことも大きな理由です．ある人は，戦争によって科学技術は進歩・発展すると総括しますが，科学技術の進歩の最前線は難病医学研究と探検（月や火星，地中や深海探検）だと私は思っています．いずれも，人の世界認識や世界観を広げるものですから，応用技術と同時に学問も進歩するのです．

皮膚表面から装着者の運動意図を分析

ここで HAL 福祉用と医療用の違いについて考えてみましょう．HAL 福祉用は，残念ながら ALS，筋ジストロフィー患者さんでは使うことがほとんどできません．いろいろな施設で使おうとして挫折したモデルです．その無念さをバネに，HAL 医療用では ALS や脊髄性筋萎縮症，筋ジストロフィー患者さんの皮膚表面から，脊髄運動ニューロンが支配する骨格筋由来の電気信号を捉え，リアルタイムに装着者の運動意図を分析できるように技術開発してもらいました．

その患者さんたちの生体電位は微弱でまばらだったにもかかわらず，あらたな技術開発により，動かない四肢からも運動意図に対応した電位が出ることがわかったのは驚きでした。リアルタイムの分析結果をモータトルクに出力し歩行パターンを再学習可能とするのが HAL ですが，もう一つの研究として，意思伝達装置，環境制御装置や PC にスイッチ出力するサイバニックスイッチの領域があります。JALSA の岡部さんや橋本さんの協力で実際にできることがわかり，2015 年からその実用化研究を開始し，商品化も実現するという目を見張る展開となりました．

山海先生との出会い

10 数年以上になりますが，山海先生は人工臓器の研究をしていました。私も神経内科医ですから脳梗塞も臨床研究していましたが，血栓を検出したり溶解したりするディバイスを作ろうとか，夢のスパコンを医療のために作ろうと考えていました。それが山海先生との出会いのきっかけです。私はまだ医長，山海先生は准教授だったと思います．山海先生は 1991 年から HAL の開発を始めていましたが，私は 2004 年ころから国の研究費の支援も得て，難病患者用の HAL の開発研究を山海先生と一緒に始めました．

HAL の基盤技術である機器と人間をつなぐサイバニクス技術は，人工臓器研究と同じです．ALS 医療では，人工呼吸器は医療機器ですが，身体接続があるためある意味でサイボーグ型ロボットといえ，山海先生と気持ちが一緒にできた理由だと思います。

今後の展望

読者の皆さんは，今後の展望について気になることかと思います。まず，治験（法的に定められた検証のための臨床試験）が終了した 8 疾患（脊髄性筋萎縮症，球脊髄性筋萎縮症，ALS，シャルコー・マリー・トゥース病，遠位型ミオパチー，先天性ミオパチー，筋ジストロフィー，封入体筋炎）では短期効果が検証され，医療機器承認が得られ，2016 年春に，健康保険が適用されました．

その病名と診断された患者さんで，治験の基準と同じ程度の症状の患者さんは，HAL が適正に使用できる施設（HAL 適正使用ガイド参照，日本神経学会，日本神経治療学会，日本リハビリテーション医学会で監修）で効能を体験してみることをお勧めします．1 回 30 分くらい，ホイストなどの転倒予防装置をつけ，HAL 装着歩行練習を行い，少なくとも 9 回くらい行うことで歩行改善効果がでてくると思います．

治験では，具体的には「歩行不安定なため，杖，歩行器などを使わず，つかまらず，10 m を安全に自立歩行できない患者で，軽介助があるか，つかまるか，歩行器又は移動型ホイストを使うことで，10 m 以上歩行が可能な患者。下肢補装具は必要時使用可」で有効性が検証されました．長期効果はまだ検証試験をしていませんが，ぜひ今後，製造販売後調査のデータ収集にも協力していただき，HAL の長期効果を試してもらいたいと思っています。難病患者さんの場合は一時的な改善効果があっても，全体的には，病気の進行による歩行機能の悪化が緩やかになることが使用目的となります．また，上記の基準より，やや軽症，やや重症の人にも，周囲の状況などが満たし，使用できる方から効果があるか検証してもらいたいと思っています．

さいごに

ALS など神経・筋疾患は HAL を使ったとしても依然として進行性の難病ですので，今後，新規薬剤と HAL との複合療法が最終的な治療法になると思われます．今回は薬以外にも有効な治療法がみつかったことが驚きだと思いますが，画期的な薬物療法等が開発されても，神経と筋の機能を再度つなぐ必要がありますので，HAL による脳・神経・筋の可塑性を促進する治療メカニズムは，その時，さらに重要になると確信しています．

Magn Reson Med Sci

MAJOR PAPER

E-pub ahead of print by J-STAGE
doi:10.2463/mrms.mp.2015-0015

Quantitative Assessment of Head Motion toward Functional Magnetic Resonance Imaging during Stepping

Kousaku Saotome[1,2]*, Akira Matsushita[1,3], Kei Nakai[3], Hideki Kadone[1], Hideo Tsurushima[3], Yoshiyuki Sankai[1,4], and Akira Matsumura[3]

[1]*Center for Cybernics Research, University of Tsukuba, 1-1-1 Tennoudai, Tsukuba, Ibaraki 305-8577, Japan*
[2]*Graduate School of Comprehensive Human Science Majors of Medical Sciences, University of Tsukuba*
[3]*Department of Neurosurgery, University of Tsukuba*
[4]*Graduate School of Systems and Information Engineering, University of Tsukuba*
(Received February 4, 2015; Accepted September 15, 2015; published online November 6, 2015)

Purpose: Stepping motions have been often used as gait-like patterns in functional magnetic resonance imaging (fMRI) to understand gait control. However, it is still very difficult to stabilize the task-related head motion. Our main purpose is to provide characteristics of the task-related head motion during stepping to develop robust restraints toward fMRI.

Methods: Multidirectional head and knee position during stepping were acquired using a motion capture system outside MRI room in 13 healthy participants. Six phases in a stepping motion were defined by reference to the left knee angles and the mean of superior-inferior head velocity (V_{mean}) in each phase was investigated. Furthermore, the correlation between the standard deviation of the knee angle (θ_{sd}) and the maximum of the head velocity (V_{max}) was evaluated.

Results: The standard deviation of each superior-inferior head position and pitch were significantly larger than the other measurements. V_{mean} showed a characteristic repeating pattern associated with the knee angle. Additionally, there were significant correlations between θ_{sd} and V_{max}.

Conclusions: This is the first report to reveal the characteristics of the task-related head motion during stepping. Our findings are an essential step in the development of robust restraint toward fMRI during stepping task.

Keywords: ***head movements, motion, kinesis, magnetic resonance imaging, quantitative assessment***

Introduction

Stepping motion has often been used as the multi-joint leg task in functional magnetic resonance imaging (fMRI).[1–3] This consists of coordinated movements where both legs extend and flex alternately and comprise multi-joint interlocking movements of the hip, knee, and ankle joints. Complex motion activates wide regions of the primary motor cortex, premotor cortex, supplementary motor cortex, and sensorimotor cortex.[4–9] These studies are important as they challenge our understanding of gait control in healthy participants and patients with gait disorders.

fMRI using blood oxygenation level dependence is a common approach to the imaging of regions involved in cognition and motor control, and is now widely used throughout neuroscience.[10–13] It has advantages over positron emission tomography, single photon emission computed tomography, and near-infrared spectroscopy in that it does not require the administration of a contrast medium, and acquires high-resolution images. In fMRI, the translational and rotational head motion during image acquisition is a major source of motion artifact and makes it very difficult to assess brain activity.[14–17] Past studies have attempted to suppress head motion using restraints, however, these are still challenging.[1,2,18–20] Moreover, a number of strategies using fast acquisition have been developed in recent years.[14,15,21–25] However, these techniques cannot often acquire satisfactory images because of excessive head motion.

To develop the robust restraint for stepping motion toward fMRI, the investigation of the characteristics of

* Corresponding author, Phone: +81-29-853-5858, Fax: +81-29-853-5852, E-mail: saotome84@gmail.com

head motion during stepping is required. Seto et al. quantitatively showed the amount of head motion during hand and ankle tasks in fMRI in detail.[26] Though head motion tends to increase during multi-joint movement tasks such as stepping than single joint tasks,[1,2,26–29] the quantitative assessment of head motion during stepping has not been investigated. The development of the task-suitable restraint for stepping could be an essential step towards the research of brain function for gait control using fMRI.

Our study measured the head and leg motion (three orthogonal translation directions and three rotations) of healthy participants during stepping, and investigated the relationship between the head position and the knee angle, velocity, using a motion capture system. Measurements were performed in a motion capture laboratory outside the MRI roomand used 12 cameras to acquire multidirectional head position and the knee angle data. Our data provide accurate and detailed three-dimensional information for the head positions and knee angles, and reveal the characteristics of head motion.

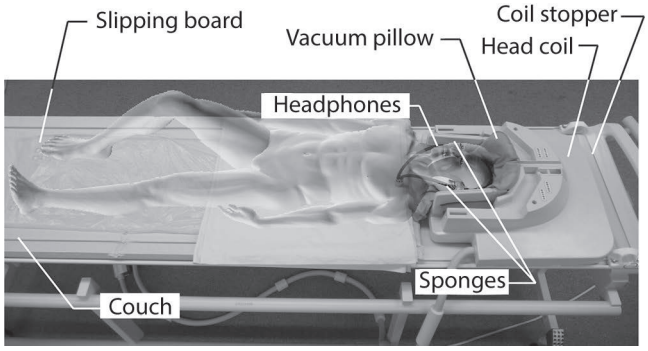

Fig. 1. Couch setup. The 32-channel SENSE head coil was set on the couch. The anterior part of the head coil was displaced to measure the head position by motion capture. A homemade coil stopper was placed above the head coil to prevent it from sliding. A slippery board made of acrylic and wrapped in a polyethylene bag was aligned on the bed so that it would touch the soles during stepping to achieve fluid motion of the legs. The participant was positioned on the scanner bed in a supine position and their head was placed in the head coil. The head was restrained using sponges, a beaded vacuum pillow, and magnetic resonance-compatible headphones, which are generally used in most magnetic resonance imaging examinations.

Materials and Methods

Subjects

Thirteen young healthy male volunteers participated in this study. The mean ± standard deviation of the participants' age was 23.2 ± 2.5 years. Each subject gave written informed consent before entering this study. The protocol was approved by the University of Tsukuba Ethics Committee (No. 745). Prior to participating, volunteers were also screened using checklists. Participants were excluded if they had a history of neurological impairments or physical conditions contraindicative to exercise.

Experimental setup

The couch: The couch, which was the same shape as the one in the MRI scanner (Philips Medical Systems, Eindhoven, Netherlands), was set up in a motion capture laboratory outside the MRI room (Fig. 1). A 32-channel SENSE head coil was set on the couch, but the anterior part of the head coil was displaced to allow measurement of head position by motion capture. A homemade coil stopper was placed at the top of the head coil to prevent the head coil from sliding. Participants wore socks. A slippery board made of acrylic and wrapped in a polyethylene bag was aligned on the bed so that it would touch the soles during stepping to allow fluid motion of the legs. Participants were positioned on the scanner bed in a supine position and their head was placed in the head coil. The head was restrained using sponges and a beaded vacuum pillow (Tatsuno Cork Industries Co. Ltd., Tatsuno, Hyogo) formed to the shape of each participant's head, and magnetic resonance compatible headphones, which are generally used in most MRI examinations.

The motion capture system: The motion of the head and the lower limbs was measured using an MAC3D motion capture system (Motion Analysis, Santa Rosa, California, USA) in a laboratory outside the MRI room. The system consisted of 12 Raptor-4 (2352 × 1728 pixels) cameras arranged around the couch, and a desktop computer with operating software (Fig. 2). Optical markers were placed on the face of the participant on the middle of the forehead, the right and left cheek bones, and the chin, to compute each three-rotation (roll, pitch, yaw) and three-translation [S-I; superior-inferior, R-L; right-left, and A-P; anterior-posterior of the head (Fig. 3A)]. Markers were also placed bilaterally on the greater trochanter, the lateral epicondyle of the femur, and the lateral malleolus of the fibula to obtain the flexion/extension angle of the knee joint (Fig. 3B). Additionally, a marker was placed on the middle of the clavicles, and six additional markers were also placed on the iliac crest, thigh, medial epicondyle of the femur, shank, medial malleolus, and instep of both legs (Fig. 3B). These were used for supportive purposes in three-dimensional reconstruction of the other markers. The system was calibrated following a standard procedure guided by the software provided by the supplier. After calibration of the camera position and orientation, the residual error in the reconstruction of the three markers on the wand, which was used to collect data for calibration, was

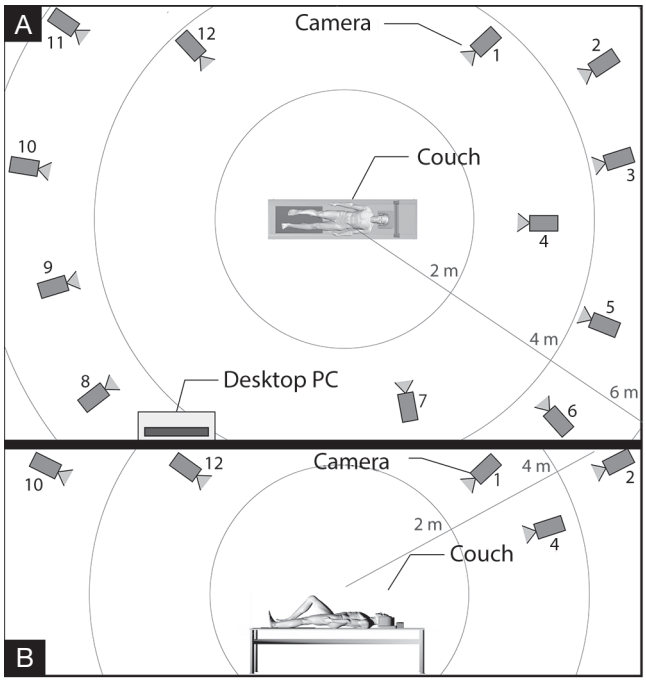

Fig. 2. (**A**) Top view and (**B**) side view of the motion capture laboratory. The 12 cameras were set around the couch. The desktop computer with operating software was set unobtrusively on the edge of the examination room.

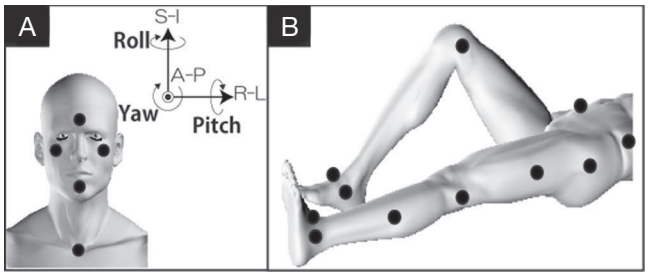

Fig. 3. Optical marker positions on (**A**) the face and (**B**) the legs. On the face, markers were placed on the middle of the forehead, the right and left cheekbones, and the chin. On the legs, markers were placed bilaterally on the greater trochanter and lateral epicondyle of the femur and the lateral malleolus of the fibula. Additionally, a marker that was used for supportive purposes in the three-dimensional reconstruction of the other makers was placed on the middle of the clavicles, and five additional markers were also placed on the iliac crest, thigh, medial epicondyle of the femur, shank, medial malleolus, and instep of both legs. Each three-rotation (roll, pitch, yaw) and three-translation (S-I; superior-inferior, R-L; right-left, and A-P; anterior-posterior) was defined as shown.

0.539 mm on average with 0.224 mm standard deviation throughout the whole capture area. The system recorded the marker positions at 120 Hz (approximately 8 ms/fr), and the data was calculated in each 56 ms. This is because 56 ms is realistic situation of one slice acquisition for time resolution in typical fMRI sequence.

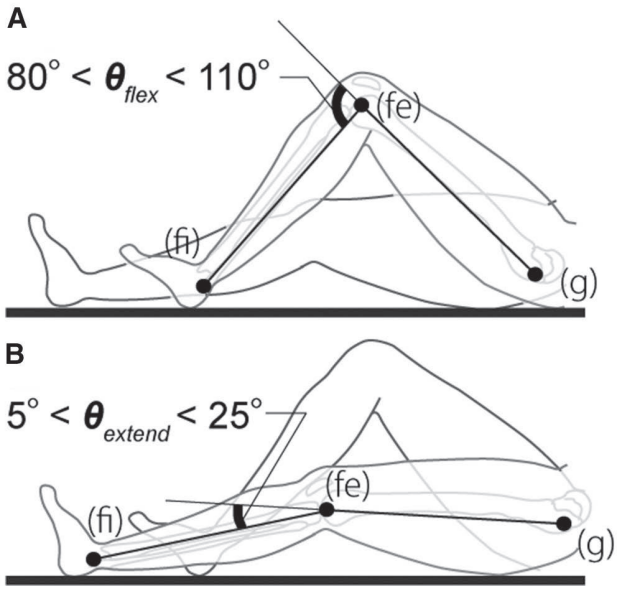

Fig. 4. (**A**) Flexion target angle (θ_{flex}) and (**B**) extension target angle (θ_{extend}) of the knee joints. θ is defined as the angle between the line connecting the greater trochanter of the femur with the lateral epicondyle of the femur and the line connecting the lateral epicondyle of the femur with the lateral epicondyle of the fibula. (g), the greater trochanter of the femur; (fe), the lateral epicondyle of the femur; (fi), the lateral epicondyle of the fibula.

Stepping task

All participants performed stepping in supine position. Participants were instructed as follows: (1) the start position was to entirely extend both legs; (2) the left leg was first flexed; (3) when the knee joint angle (θ) was defined as the angle between the line connecting the greater trochanter of the femur with the lateral epicondyle of the femur and the line connecting the lateral epicondyle of the femur with the lateral epicondyle of the fibula, the flexion target angle of the knee joints (θ_{flex}) was $80° < \theta_{flex} < 110°$ (Fig. 4A); (4) when one side of the leg started to extend, the other side started to flex; (5) the extension target angle of the knee joints (θ_{extend}) was $5° < \theta_{extend} < 25°$ (Fig. 4B); (6) this exercise was continued for 30 s after the cue; (7) stepping was performed at approximately 1.67 Hz (100 beats per second), which was given using a metronome; and (8) participants kept their eyes open to concentrate their gaze on a single point on the ceiling during measurement. Before each measurement, participants practiced the above exercise for 30 s. Moreover, participants were instructed to keep their heads as still as possible during the exercise.

Data analyses

First, the position of the center of the four markers on the face (middle forehead, right and left cheekbones, and chin), was calculated and used to define the head

position. Using these markers' position, the roll, pitch, and yaw rotation angles of the head was computed, around the S-I, A-P, and P-L axes, respectively (Fig. 3A).

Second, the angles of the knee joints were calculated using the position of the three markers on the legs (greater trochanter of the femur, lateral knee joints, and ankles).

The below five metrics were used to calculate the head motion during stepping: (1) the standard deviation of the head position (M_{sd}); (2) the mean of the head velocity (V_{mean}); (3) the maximum of the head velocity (V_{max}); and (4) the standard deviation of the angle of the knee joints (θ_{sd}). M_{sd} is described by the formula

$$\mathbf{M}_{sd} = \sqrt{\frac{\sum_{i=1}^{N}\left(X_i - \bar{X}\right)^2}{N-1}}$$

where X_i is the head position measurement at a particular time i, X is the mean of the head position measurements in each of the three orthogonal translation directions or rotations, and N is the number of data points. V_{mean} was calculated as

$$v = \frac{dX}{dt}$$

$$\boldsymbol{V_{mean}} = \frac{\sum_{i=1}^{N-1} \boldsymbol{v_i}}{N-1}$$

where v is the velocity of the head and t is each measurement time. V_{max} was calculated as

$$\boldsymbol{V_{max}} = |\boldsymbol{v}|_{\boldsymbol{max}}$$

where v_{max} is the maximum head velocity in each of the three orthogonal translation directions (S-I; superior-inferior, R-L; right-left, and A-P; anterior-posterior). θ_{sd} was calculated as

$$\boldsymbol{\theta_{sd}} = \sqrt{\frac{\sum_{i=1}^{N}\left(\boldsymbol{Y_i} - \bar{\boldsymbol{Y}}\right)^2}{\boldsymbol{N}-1}}$$

where Y_i is the angle of the knee joint at a particular time i, and $\bar{Y}$ is the mean of all the knee joint angles. M_{sd} and V_{mean} were applied to each of the three orthogonal translation directions (S-I, R-L, A-P) and each of the three rotations (roll, pitch, yaw). Additionally, six phases in stepping were defined by reference to the left knee joint angles to interpret the relation between the head velocity and the angle of the knee joint (Fig. 5); (I) $0° < \theta < 30°$, which indicates the beginning of flexion; (II) $31° < \theta < 60°$; (III) $61° < \theta < 110°$, which indicates the end of flexion; (IV) $110° < \theta < 61°$, which indicates the beginning of extension; (V) $60° < \theta < 31°$; (VI) $30° < \theta < 0°$, which indicates the end of extension. Then, the V_{mean} in each of the six phases was calculated.

Statistical analyses were performed using SPSS (IBM Statistical Package for the Social Sciences, version 21.0, Chicago, Illinois, USA). A Mann–Whitney test of three orthogonal translation directions (S-I, R-L, A-P) and three rotations (roll, pitch, yaw) were performed for M_{sd}. A Mann–Whitney test of the six phases of the knee joint angle was also performed for V_{mean}. Furthermore, we used the Spearman's correlation coefficient (r) to evaluate the correlations between θ_{sd} and V_{max}. The level of statistical significance for all measures was set at $P < 0.05$.

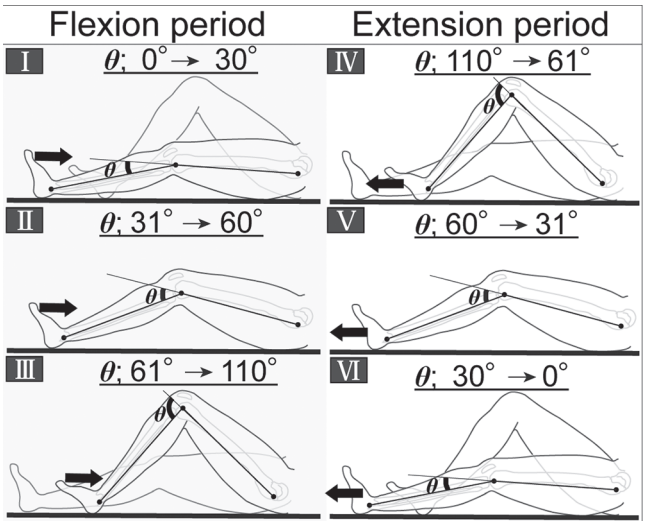

Fig. 5. Six phases by reference to the angle of the left knee joint. θ shows the angle of the left knee joint. The flexion period consists of phases I, II, and III. The extension period consists of phases IV, V, and VI; (I) $0° < \theta < 30°$, indicates the beginning of flexion; (II) $31° < \theta < 60°$; (III) $61° < \theta < 110°$, indicates the end of flexion; (IV) $110° < \theta < 61°$, indicates the beginning of extension; and (V) $60° < \theta < 31°$; (VI) $30° < \theta < 0°$, indicates the end of extension.

Results

The standard deviation of the head position (M_{sd})

Figure 6A, B are box-and-whisker plots showing the median and interquartile ranges of the standard deviation of the head position (M_{sd}) with three rotations (roll, pitch, yaw) and three orthogonal translation directions (S-I, R-L, A-P). Among the three rotations, there was a strong statistically significant difference between roll and pitch ($P < 0.001$), but no significant difference between yaw and the others. Furthermore, among the three orthogonal translation directions, there were also strong statistically significant differences between S-I and the others ($P < 0.001$), respectively, but no significant difference between R-L and A-P.

The relationship between the mean of the head velocity (V_{mean}) and the phases of knee angle (I–VI)

Figure 7 is box-and-whisker plots showing the median and interquartile ranges of the mean of the

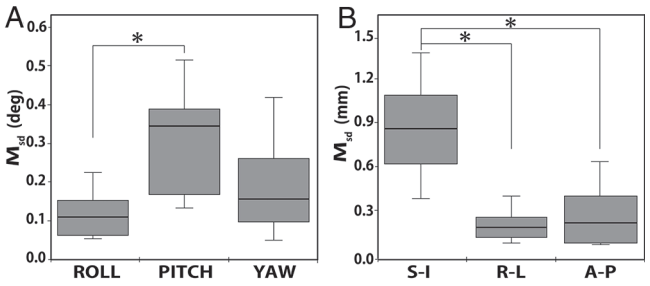

Fig. 6. Box-and-whisker plot of the standard deviation of the head position (M_{sd}) with (**A**) three rotations (roll, pitch, yaw) and (**B**) three orthogonal translation directions (S-I; superior-inferior, R-L; right-left, and A-P; anterior-posterior). Box-and-whisker plots show the median and interquartile ranges of the M_{sd}. (**A**) There was strong statistically significant difference between roll and pitch. (**B**) There were also strong statistically significant differences between S-I and the others, respectively. Note the difference in vertical scales. *$P < 0.001$, Mann–Whitney tests.

head velocity (V_{mean}) with S-I in each phase (I–VI) of knee angle. There were statistically significant ($P < 0.01$) differences between phase I and phases III, V, and VI. There were also statistically significant ($P < 0.01$) differences between phase II and phase VI. There were also statistically significant ($P < 0.01$) differences between phase IV and phases III, V, and VI. V_{mean} of phase I and phase IV showed a larger positive velocity. However, V_{mean} of phase III and phase VI showed a larger negative velocity. Thus, the larger positive velocity occurred at the beginning of flexion and the beginning of extension. In contrast, these also showed that a larger negative velocity occurred at the end of flexion and the end of extension.

The correlation between the standard deviation of knee angle (θ_{sd}) and the maximum of the head velocity (V_{max})

Figure 8 shows the correlations between the standard deviation of knee joint angle (θ_{sd}) and the maximum of the head velocity V_{max}. There were significant correlations between θ_{sd} and V_{max} for both caudo-cranial and cranio-caudal directions (r = 0.657, $P < 0.01$ and r = 0.696, $P < 0.01$). The mean ± standard deviations of V_{max} in the caudo-cranial and cranio-caudal directions were 34.1 ± 14.0 mm/s and 35.4 ± 19.1 mm/s, respectively.

Discussion

The measurements were performed in a motion capture laboratory outside the MRI room. Prior to an in-depth discussion of our results, we need to describe the differences between the motion capture laboratory and the actual environment within an MRI scanner. The only notable difference was that there were no loud

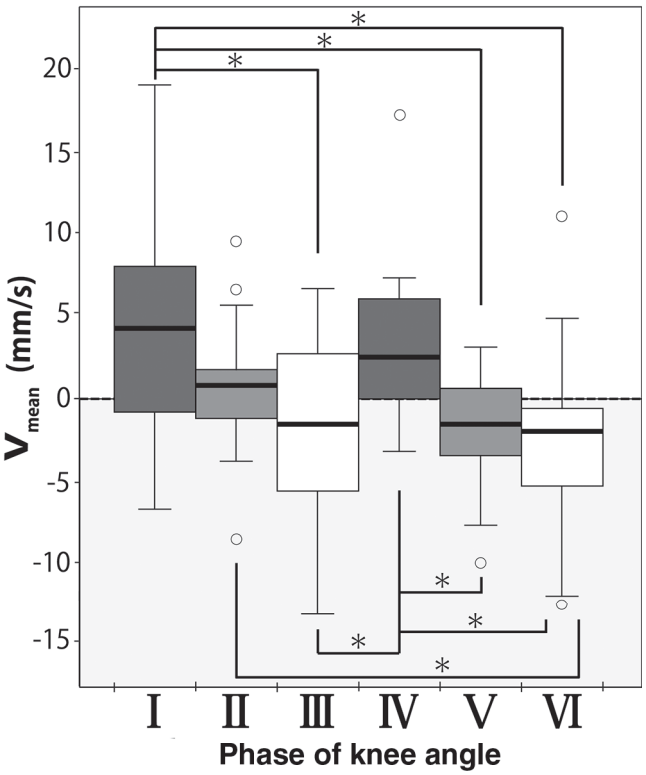

Fig. 7. Box-and-whisker plot of the mean of the superior-inferior head velocity (V_{mean}). Box-and-whisker plots show the median and interquartile ranges of the V_{mean} in each phase (I–VI) of the left knee angle. There were statistically significant differences between phase I and phases III, V, and VI. There were also statistically significant differences between phase II and phase VI. There were also statistically significant differences between phase IV and phases III, V, and VI. *$P < 0.01$, Mann–Whitney tests.

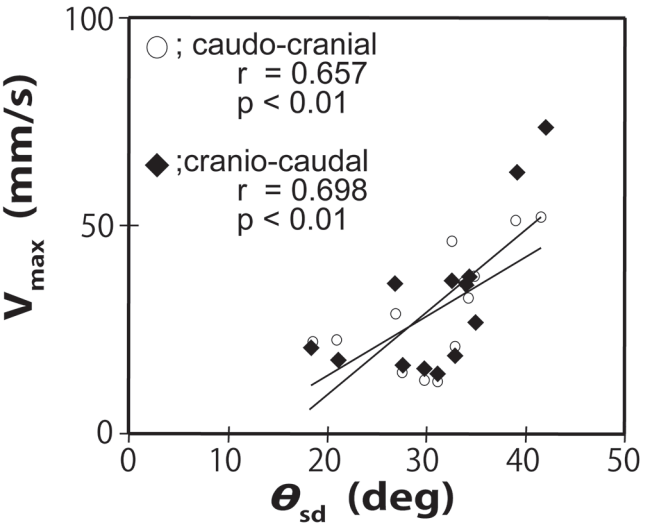

Fig. 8. Correlation scatter plot of the standard deviation of left knee angle (θ_{sd}) in the maximum of the head velocity (V_{max}). Circles show θ_{sd} in the caudo-cranial and diamond shapes show θ_{sd} in the cranio-caudal directions. There were significant correlations between θ_{sd} and V_{max} for both caudo-cranial and cranio-caudal directions (r = 0.697, $P < 0.01$ and r = 0.723, $P < 0.01$).

sounds emanating from an MRI scanner in the motion capture laboratory. However, the head motion induced by loud sounds is significantly less than the head motion associated with multi-joint leg movements.[30] Regarding other differences, there was little influence on the measurements for the following reasons. In the motion capture laboratory, a couch of the same shape and material as that of an MRI scanner was used. In addition, the same head coil, coil stopper, and restraints as those of an MRI scanner were used. Therefore, similar head motion and stepping motion might be possible within the confines of an MRI scanner.

Head motion is dependent on the task and the subject group in fMRI.[1,26] Seto et al., who investigated the amount of head motion during hand and foot task in stroke subjects and age-matched controls in fMRI, revealed that the head motion in stroke subject with foot task was largest, especially S-I translation. Our result in S-I translation exhibited approximately twice the head motion compared to that of stroke subjects with foot task. Furthermore, all rotation and R-L and A-P translation exhibited the head motion at the same level as that of stroke subjects. Our findings mean that we should pay special attention to suppress the head motion in S-I translation.

Fig. 8 shows V_{max} during stepping in each 60 ms. If the head velocity is 40.0 mm/s, the head moves 2.4 mm during acquiring an echo in a plane, which is a very short period (approximately 60 ms following generally fMRI echo planar imaging sequences; repetition time (TR)/echo time/image matrix/number of slice/slice thickness = 3000 ms/35 ms/128/40 slices/4 mm). This displacement corresponds to 60% of slice thickness. This means that approximately 60% of the plane excited by the slice selection gradient has deviated from its original position at the echo acquisition time on the sequence. Previous studies, which approached fMRI during multi-joint movements of the legs by using trunk restraints in addition to head restraints, stated that the offset value of motion correction algorithm of the SPM software (Wellcome Department of Cognitive Neurology, Queen Square, London) implemented in the Matlab (MathWorks, Natick, Massachusetts, USA) has to be limited to a range of 2 mm over a period of a TR to justify the effect of their restraints.[1,2,20,27] It is reasonable to refer to this value on the SPM software in the single joint movement, however, it would be enough to refer to only this value in multi-joint movement of the legs. This is because that the problems in huge head motion are not only the misregistration of image voxel locations with brain anatomy but also signal loss in a slice plane leading either to false-positive activation or to false-negative activation.[14,15,31] The motion correction algorithm in the SPM can correct the volume-by-volume displacement acquired in each TR up to a few millimeters. However, this algorithm cannot correct signal loss occurring during acquiring the echoes in a plane. There are many other motion correction algorithms for slice-by-slice and volume-by-volume, however, none of them can correct signal loss in a plane.[21,22,32–35] Therefore, we should focus on the robust restraint toward fMRI during stepping, which can reduce the head velocity in S-I translation.

The robust restraint against multi-joint movements of the legs is still challenging and should be suiting the characteristics of the task. At the same time, it should be noted that applying excessive pressure on the head could cause severe head pain to the subjects. Some past studies suffered from the head motion associated with the tasks even though they paid close attention to head motion by restraining the head and the trunk.[1,2] Considering this as well as the problem of causing head pain, some methods to exempt or isolate the force reached into the trunk and the head from the legs might be expected and is the topic of our further study.

Furthermore, our results showed that the head moves repeatedly up and down with regularity in association with the knee angle. This finding is supported by Fig. 7. Mostly positive velocities (caudo-cranial) occurred at the beginning of right extension (phase I) and at the beginning of left extension (IV), and mostly negative velocities (cranio-caudal) occurred at the end of left extension (III) and at the end of right extension (VI), and phases with smaller velocities (II and V) occurred between the phases associated with the positive velocities and negative velocities. These mean that the head moved up and down twice in a stepping cycle, which includes an extension and a flexion for each leg. Here we make an observation that the initial extension of the knee and hip of motion of one leg pushed the head upward, and then the head stopped a while, and then the stretching motion of one leg at the end of extension pulled the head down to its original position. In concurrence with one leg started to flex, the other leg just started to extend and then the head moved up and down once again. Noteworthy, it is interesting that there are two phases including smaller head motion in a stepping. By acquiring image data only in these phases using moderated fast acquisition techniques, the data set with minimum motion might be accomplished. In addition, our findings showed that the larger the knee joint motion range, the larger the head velocity in both caudo-cranial and cranio-caudal. It is therefore important that we need to select an adequate task that has the motion range of knee joint as small as the study's objective permits.

Understanding the characteristic of head motion during stepping is essential to build the task-suitable restraints in fMRI. To the best of the authors' knowledge, this is the first report that has quantitatively assessed head motion during stepping in depth. Our future works are the building of the robust restraint and task setting toward fMRI. Then, it could be an essential step toward the investigation of brain function for gait control using fMRI. The limitations of this study are that the measurements were performed outside of an MRI examination room. However, as already described, we assume that similar head motion and stepping motion are possible within the confines of an MRI scanner. Furthermore, only a stepping motion with a single repetition rate as a multi-joint leg movement was performed in this study. Other multi-joint movements and a slower or faster repetition rate might show different results. These cases require further study.

Conclusion

In this study, the head position and the knee angle during stepping toward fMRI were measured using a motion capture system. All measurements were performed in a motion capture laboratory outside the MRI room to acquire multidirectional head position and knee angle data using a number of cameras. Our results showed the relationship between the head displacement, velocity, and knee angle. During stepping, the superior-inferior translation and pitch rotation were the largest. The mean of the superior-inferior head velocity showed a characteristic repeating pattern associated with the knee angle. There were positive significant correlations between the standard deviation of the knee joint angle and the superior-inferior maximum head velocity. This is the first report that quantitatively assessed the head motion during stepping for fMRI. Our findings might help the building of the robust restraint and the adequate environment against stepping motion to assess brain activity in fMRI.

Acknowledgments

This work was supported by Japan Society for the Promotion of Science Kakenhi Grant No. 25870090. In addition, this work was supported by the "Center for Cybernics Research (CCR)—World Leading Human-Assistive Technology Supporting a Long-Lived and Healthy Society" granted through the "Funding Program for World-Leading Innovative R&D on Science and Technology (FIRST Program)" initiated by the Council for Science and Technology Policy (CSTP). Finally, the authors would like to thank the anonymous reviewers for their useful comments.

Informed Consent and Ethical Approval

The study was performed in accordance with the ethical standards laid down in the 1964 Declaration of Helsinki and its later amendments. Each subject gave written informed consent before entering this study. Details that could disclose the identity of the subjects under study were omitted. The protocol was approved by the University of Tsukuba Ethics Committee (No. 745).

References

1. Mehta JP, Verber MD, Wieser JA, Schmit BD, Schindler-Ivens SM. A novel technique for examining human brain activity associated with pedaling using fMRI. J Neurosci Methods 2009; 179:230–239.
2. Hollnagel C, Brügger M, Vallery H, et al. Brain activity during stepping: a novel MRI-compatible device. J Neurosci Methods 2011; 201:124–130.
3. Sahyoun C, Floyer-Lea A, Johansen-Berg H, Matthews PM. Towards an understanding of gait control: brain activation during the anticipation, preparation and execution of foot movements. Neuroimage 2004; 21:568–575.
4. Christensen LO, Johannsen P, Sinkjaer T, Petersen N, Pyndt HS, Nielsen JB. Cerebral activation during bicycle movements in man. Exp Brain Res 2000; 135:66–72.
5. la Fougère C, Zwergal A, Rominger A, et al. Real versus imagined locomotion: a [18F]-FDG PET-fMRI comparison. Neuroimage 2010; 50:1589–1598.
6. Hanakawa T, Katsumi Y, Fukuyama H, et al. Mechanisms underlying gait disturbance in Parkinson's disease: a single photon emission computed tomography study. Brain 1999; 122 (Pt 7):1271–1282.
7. Fukuyama H, Ouchi Y, Matsuzaki S, et al. Brain functional activity during gait in normal subjects: a SPECT study. Neurosci Lett 1997; 228:183–186.
8. Miyai I, Tanabe HC, Sase I, et al. Cortical mapping of gait in humans: a near-infrared spectroscopic topography study. Neuroimage 2001; 14:1186–1192.
9. Miyai I, Suzuki M, Hatakenaka M, Kubota K. Effect of body weight support on cortical activation during gait in patients with stroke. Exp Brain Res 2006; 169:85–91.
10. Le Bihan D, Karni A. Applications of magnetic resonance imaging to the study of human brain function. Curr Opin Neurobiol 1995; 5:231–237.
11. Soros P, Sokoloff LG, Bose A, McIntosh AR, Graham SJ, Stuss DT. Clustered functional MRI of overt speech production. Neuroimage 2006; 32:376–387.
12. Schulz M, Chau W, Graham SJ, et al. An integrative MEG-fMRI study of the primary somatosensory cortex using cross-modal correspondence analysis. Neuroimage 2004; 22:120–133.
13. Ogawa S, Lee TM, Nayak AS, Glynn P. Oxygenation-sensitive contrast in magnetic resonance image of rodent brain at high magnetic fields. Magn Reson Med 1990; 14:68–78.
14. Field AS, Yen YF, Burdette JH, Elster AD. False cerebral activation on BOLD functional MR images: study

of low-amplitude motion weakly correlated to stimulus. AJNR Am J Neuroradiol 2000; 21:1388–1396.
15. Friston KJ, Williams S, Howard R, Frackowiak RS, Turner R. Movement-related effects in fMRI time-series. Magn Reson Med 1996; 35:346–355.
16. Bhavsar S, Zvyagintsev M, Mathiak K. BOLD sensitivity and SNR characteristics of parallel imaging-accelerated single-shot multi-echo EPI for fMRI. Neuroimage 2014; 84:65–75.
17. Turner R, Howseman A, Rees GE, Josephs O, Friston K. Functional magnetic resonance imaging of the human brain: data acquisition and analysis. Exp Brain Res 1998; 123:5–12.
18. Green MV, Seidel J, Stein SD, et al. Head movement in normal subjects during simulated PET brain imaging with and without head restraint. J Nucl Med 1994; 35:1538–1546.
19. Ruttimann UE, Andreason PJ, Rio D. Head motion during positron emission tomography: is it significant? Psychiatry Res 1995; 61:43–51.
20. Hollnagel C, Vallery H, Schädler R, et al. Non-linear adaptive controllers for an over-actuated pneumatic MR-compatible stepper. Med Biol Eng Comput 2013; 51:799–809.
21. Rotenberg D, Chiew M, Ranieri S, Tam F, Chopra R, Graham SJ. Real-time correction by optical tracking with integrated geometric distortion correction for reducing motion artifacts in functional MRI. Magn Reson Med 2013; 69:734–748.
22. Speck O, Hennig J, Zaitsev M. Prospective real-time slice-by-slice motion correction for fMRI in freely moving subjects. MAGMA 2006; 19:55–61.
23. Fellner C, Doenitz C, Finkenzeller T, Jung EM, Rennert J, Schlaier J. Improving the spatial accuracy in functional magnetic resonance imaging (fMRI) based on the blood oxygenation level dependent (BOLD) effect: benefits from parallel imaging and a 32-channel head array coil at 1.5 Tesla. Clin Hemorheol Microcirc 2009; 43:71–82.
24. Nishimura DG, Irarrazabal P, Meyer CH. A velocity k-space analysis of flow effects in echo-planar and spiral imaging. Magn Reson Med 1995; 33:549–556.
25. Yun SD, Reske M, Vahedipour K, Warbrick T, Shah NJ. Parallel imaging acceleration of EPIK for reduced image distortions in fMRI. Neuroimage 2013; 73: 135–143.
26. Seto E, Sela G, McIlroy WE, et al. Quantifying head motion associated with motor tasks used in fMRI. Neuroimage 2001; 14:284–297.
27. Thijs Y, Vingerhoets G, Pattyn E, Rombaut L, Witvrouw E. Does bracing influence brain activity during knee movement: an fMRI study. Knee Surg Sports Traumatol Arthrosc 2010; 18:1145–1149.
28. Hajnal JV, Myers R, Oatridge A, Schwieso JE, Young IR, Bydder GM. Artifacts due to stimulus correlated motion in functional imaging of the brain. Magn Reson Med 1994; 31:283–291.
29. Gopinath K, Crosson B, McGregor K, et al. Selective detrending method for reducing task-correlated motion artifact during speech in event-related FMRI. Hum Brain Mapp 2009; 30:1105–1119.
30. Rosenberg DR, Sweeney JA, Gillen JS, et al. Magnetic resonance imaging of children without sedation: preparation with simulation. J Am Acad Child Adolesc Psychiatry 1997; 36:853–859.
31. Zeffiro T. Clinical functional image analysis: artifact detection and reduction. Neuroimage 1996; 4(3 Pt 3): S95–100.
32. Biswal BB, Hyde JS. Contour-based registration technique to differentiate between task-activated and head motion-induced signal variations in fMRI. Magn Reson Med 1997; 38:470–476.
33. Muraskin J, Ooi MB, Goldman RI, et al. Prospective active marker motion correction improves statistical power in BOLD fMRI. Neuroimage 2013; 68:154–161.
34. Schulz J, Siegert T, Bazin PL, et al. Prospective slice-by-slice motion correction reduces false positive activations in fMRI with task-correlated motion. Neuroimage 2014; 84:124–132.
35. Wu DH, Lewin JS, Duerk JL. Inadequacy of motion correction algorithms in functional MRI: role of susceptibility-induced artifacts. J Magn Reson Imaging 1997; 7:365–370.

Taylor & Francis
Taylor & Francis Group

The Journal of Spinal Cord Medicine

ISSN: 1079-0268 (Print) 2045-7723 (Online) Journal homepage: http://www.tandfonline.com/loi/yscm20

Decrease of spasticity after hybrid assistive limb® training for a patient with C4 quadriplegia due to chronic SCI

Akira Ikumi, Shigeki Kubota, Yukiyo Shimizu, Hideki Kadone, Aiki Marushima, Tomoyuki Ueno, Hiroaki Kawamoto, Yasushi Hada, Akira Matsumura, Yoshiyuki Sankai & Masashi Yamazaki

To cite this article: Akira Ikumi, Shigeki Kubota, Yukiyo Shimizu, Hideki Kadone, Aiki Marushima, Tomoyuki Ueno, Hiroaki Kawamoto, Yasushi Hada, Akira Matsumura, Yoshiyuki Sankai & Masashi Yamazaki (2016): Decrease of spasticity after hybrid assistive limb® training for a patient with C4 quadriplegia due to chronic SCI, The Journal of Spinal Cord Medicine, DOI: 10.1080/10790268.2016.1225913

To link to this article: http://dx.doi.org/10.1080/10790268.2016.1225913

Published online: 20 Oct 2016.

Research Article

Decrease of spasticity after hybrid assistive limb® training for a patient with C4 quadriplegia due to chronic SCI

Akira Ikumi[1], Shigeki Kubota[1,2], Yukiyo Shimizu[3], Hideki Kadone[4], Aiki Marushima[5], Tomoyuki Ueno[3], Hiroaki Kawamoto[6]Yasushi Hada[3], Akira Matsumura[5], Yoshiyuki Sankai[6], Masashi Yamazaki[1,4]

[1]Department of Orthopaedic Surgery, Faculty of Medicine, University of Tsukuba, Ibaraki, Japan, [2]Division of Regenerative Medicine for Musculoskeletal System, Faculty of Medicine, University of Tsukuba, Ibaraki, Japan, [3]Department of Rehabilitation Medicine, University of Tsukuba Hospital, Ibaraki, Japan, [4]Center for Innovating Medicine and Engineering (CIME), University of Tsukuba Hospital, Ibaraki, Japan, [5]Department of Neurosurgery, Faculty of Medicine, University of Tsukuba, Ibaraki, Japan, [6]Faculty of Systems and Information Engineering, University of Tsukuba, Ibaraki, Japan

Context: Recently, locomotor training with robotic assistance has been found effective in treating spinal cord injury (SCI). Our case report examined locomotor training using the robotic suit hybrid assistive limb (HAL) in a patient with complete C4 quadriplegia due to chronic SCI. This is the first report examining HAL in complete C4 quadriplegia.

Findings: The patient was a 19-year-old man who dislocated C3/4 during judo 4 years previously. Following the injury, he underwent C3/4 posterior spinal fusion but remained paralyzed despite rehabilitation. There was muscle atrophy under C5 level and no sensation around the anus, but partial sensation of pressure remained in the limbs. The American Spinal Injury Association impairment scale was Grade A (complete motor C4 lesion).

HAL training was administered in 10 sessions (twice per week). The training sessions consisted of treadmill walking with HAL. For safety, 2 physicians and 1 therapist supported the subject for balance and weight-bearing. The device's cybernic autonomous control mode provides autonomic physical support based on predefined walking patterns.

We evaluated the adverse events, walking time and distance, and the difference in muscle spasticity before and after HAL-training using a modified Ashworth scale (mAs).

No adverse events were observed that required discontinuation of rehabilitation. Walking distance and time increased from 25.2 meters/7.6 minutes to 148.3 meter/15 minutes. The mAs score decreased after HAL training.

Conclusion: Our case report indicates that HAL training is feasible and effective for complete C4 quadriplegia in chronic SCI.

Keywords: Hybrid assistive limb (HAL), Spinal cord injury, Locomotor training, Robotics, Spasticity

Introduction

Rehabilitation robotics emerged in the 1980s with the aim of using robotic technology to assist people with movement dysfunction.[1] Robotic devices have recently been developed for use in clinical settings.

Tefertiller *et al.*[2] reviewed 30 articles (14 randomized controlled trials, 16 nonrandomized controlled trials) that examined the effects of locomotor training with robotic assistance in patients after stroke, spinal cord injury (SCI), multiple sclerosis, traumatic brain injury, and Parkinson's disease. The review supports the conclusion that locomotor training with robotic assistance is beneficial for improving walking function in individuals after stroke and SCI.[2]

The development of main gait training machines followed. These machines either involve an exoskeleton robotic device (e.g. Lokomat®, LOPES exoskeleton

Correspondence to: Akira Ikumi, Department of Orthopaedic Surgery, Faculty of Medicine, University of Tsukuba, 1-1-1, Tennodai, Tsukuba, Ibaraki, 305-8575, Japan. Email: ikumi@tsukuba-seikei.jp

DOI 10.1080/10790268.2016.1225913

robot)[3,4] or a robotic device with foot-driven plates (e.g. Gait Trainer GT I®, Haptic Walker).[5,6] The exoskeleton robotic device is equipped with programmable drives or passive elements that flex the knees and hips during the swing phase, whereas with the other type of robotic device, the feet are placed on footplates whose trajectories simulate the stance and swing phases.

Other than robotic gait training and conventional therapy, another treatment approach involves treadmill training with partial body weight support.[7] However, this approach requires considerable involvement of a physical therapist, and generally, 3 therapists are required to induce movement of the paretic leg during the swing phase and to shift the patient's weight onto the stance limb.

The potentially positive common benefits of robotic gait training are that it involves repeatedly undergoing sufficient and accurate training for a prolonged period. Lokomat is the first robotic-driven gait orthosis with electromechanical drives to assist the walking movements of gait-impaired patients on a treadmill by supporting the body weight.[8,9] Husemann *et al.*[10] compared a Lokomat group that received 30 minutes of robotic training with a control group that received 30 minutes of conventional physiotherapy. After 4 weeks of therapy, although there was no significant difference in walking ability between the groups, the walking ability in both groups as expressed by functional ambulation classification was significantly improved. The researchers reported that the Lokomat group demonstrated an advantage for robotic training over conventional physiotherapy in the improvement of gait abnormality and body tissue composition.[10]

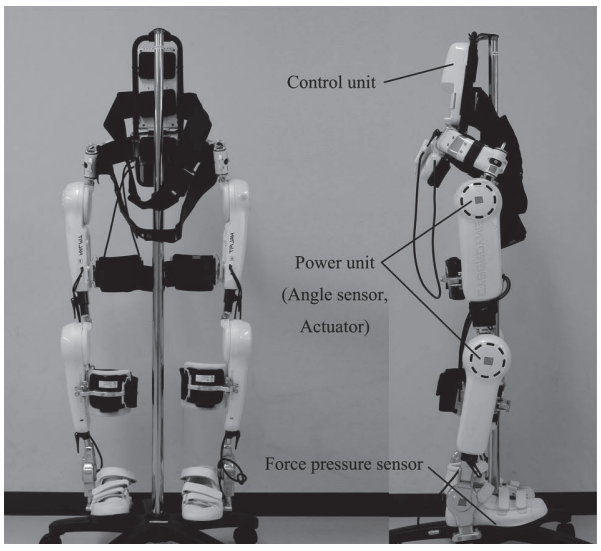

Figure 1. The robotic suit HAL. (Colour online)

However, in a recent randomized controlled study[11] that compared robot-assisted locomotor training with therapist-assisted locomotor training in chronic stroke patients, the results indicated that greater improvements in speed and single limb stance time on the impaired leg were observed in subjects who received therapist-assisted locomotor training. Thus, the usefulness of robot-assisted rehabilitation is controversial.

The hybrid assistive limb® (HAL®; Cyberdyne Inc, Ibaraki, Japan)[12–15] is a wearable robotic suit that assists in voluntary control of knee- and hip-joint motion (Fig. 1). Signals from force-pressure sensors in the shoes and muscle action potentials detected through electrodes on the surface of the skin are processed through a computer, and assisted motions are provided to the patient. Power units on the hip and knee joints on both sides consist of angular sensors and actuators, and the control system consists of a cybernic voluntary control (CVC) and a cybernic autonomous control (CAC) subsystem.[12]

HAL has been reported to be useful in the functional recovery of various mobility disorders.[12,16–18] To the best of our knowledge, however, there is no published report to clarify the feasibility of rehabilitation with HAL for a patient with complete quadriplegia. Therefore, the efficacy and safety of HAL for complete quadriplegia remains unclear.

In the current case report, HAL training was performed for a patient with complete quadriplegia after SCI, and efficiency and safety were evaluated. This study was conducted with the approval of the Ethics Committee of the Tsukuba University Faculty of Medicine.

Case presentation

Patient

A 19-year-old man who was injured while participating in judo 4 years previously was diagnosed with a cervical vertebral fracture-dislocation (C3/4). Emergency surgery (posterior spinal fusion) was performed. After surgery, the patient required respiratory care with a ventilator, but at one month postoperatively, he no longer required the ventilator. Complete paralysis and serious sensory dysfunction inferior to the C5 level were present from the time of injury. He continued the rehabilitation during the hospital stay and ambulatory rehabilitation after discharge. In spite of the aggressive rehabilitation, his paralysis had scarcely improved, and he required assistance with all activities of daily living. He was hospitalized in our facility to undergo rehabilitation using the robotic suit HAL.

Physical examination findings on admission indicated that the patient required comprehensive care, including feeding, changing clothes, bathing and egestion. He used the chin-controlled electric wheelchair to move outside. The neurologic examination revealed muscle weakness with a manual muscle testing (MMT) score of 5/5 in the trapezius muscle and an MMT score of 0/0 below the deltoid muscle (C5 level). The patient had severe sensory disturbances below the C5 level. A slight sense of pressure remained in his right upper extremity and both lower extremities, but there was none in other areas. No articular contracture was observed. No urinary bladder or bowel function remained. The results of the blood and urine tests were normal.

The computed tomography (CT) and the magnetic resonance imaging (MRI) immediately after injury showed a C3/4 vertebral fracture-dislocation and interlocking of the right facets. The spinal cord was compressed tightly (Fig. 2). The radiographic findings after surgery showed posterior spinal fusion between C3 and C4. The vertebral dislocation was reduced well (Fig. 3). The CT and MRI findings on admission showed no loosening of the implant and decompression at the injury site of the spinal cord. A signal change (low signal at T1WI and high signal at T2WI) of the spinal cord was observed (Fig. 4).

Clinical evaluation before HAL training showed the following: the American Spinal Injury Association (ASIA) impairment scale (AIS) was grade A (complete motor C4 lesion); the ASIA motor score (lower limb total) was 0 points; the ASIA sensory score for light touch was 62 points (right: 31 points; left: 31 points); the Frankel classification was grade B2; the Spasm Frequency Score was 3 (spasm occurred 1 to 10 times per hour); the Barthel Index was 5/100 points; the Total Functional Independence Measure Score was 53/126 points (motor 18/91 points, cognitive 35/35 points); and the Functional Balance Scale was 0/56 points.

HAL training

The patient received additional HAL training 2 times per week for 5 weeks (10 sessions) in addition to standard physical and occupational therapy. HAL training lasted 60 minutes, including rests and time for attaching/detaching the device. At the initiation of HAL training, the robot was fitted, and the sitting/standing motion was confirmed. The training sessions consisted of treadmill walking with HAL. A body weight support system (945-480 Unweighing System, BIODEX®, Shirley, NY, USA) with a harness was used for safety.

The cybernic autonomous control (CAC) mode provides autonomic physical support based on predefined walking patterns from able-bodied persons. For safety reasons, 2 physicians and 1 therapist supported the subject in balance and weight bearing (Fig. 5).

We evaluated the walking time and distance, the modified Ashworth scale score (mAs)[19] before and after HAL training, and adverse events associated with HAL training.

The time from attaching the device to setting the unweighing system was an average of 10 minutes. Walking distance and time increased from 25.2 meters/7.6 minutes (first session) to 148.3 meters/7.6 minutes (last session) (Figs. 6 and 7). The total mAs score (Score: 0–144; the number of joints: 36) was evaluated before and after HAL training. The score before HAL training was 15.13 ± 2.80 points; after HAL training, it was 5.75 ± 2.38 points. No joint change for the worse after training was observed (Fig. 8). The average number of joints decreased, and the spasticity was 7. The efficiency continued for approximately 30 minutes after HAL training. There were no adverse events requiring discontinuation of the HAL training. A transient blood pressure change (systolic blood pressure <90 or >180) was observed 6 times/10 sessions (0.6 times/session), but the blood pressure returned to baseline after a few minutes of resting.

Discussion

Aach *et al.*[18] demonstrated the clinical potential of HAL training based on voluntary drive in patients suffering from chronic SCI. Fujii *et al.*[20] reported that the training using an advanced robotic device may affect the patient's motivation for rehabilitation based on the analysis of questionnaires from patients undergoing HAL training.

On the other hand, Maeshima *et al.*[16] reported that the HAL suit should not be used in a patient with paralysis severe enough to cause muscle contraction or whose bioelectric signals cannot be sensed. Thus, the use of HAL for patients with severe chronic SCI is still controversial.

In this case, we investigated the feasibility of rehabilitation using a robotic suit HAL for C4 quadriplegia, and confirmed that HAL training could be implemented safely. No serious HAL training-related adverse events occurred. Furthermore, the walking time and distance had increased as the rehabilitation continued, suggesting the learning effect of the HAL training for the patient with complete C4 quadriplegia.

In our case, a certain effect on decreasing the spasticity was also confirmed after HAL training. Spasticity

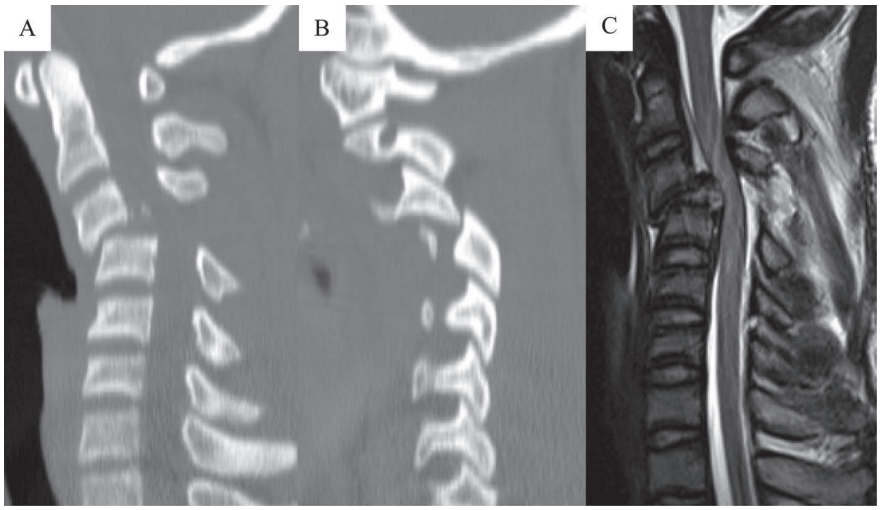

Figure 2. Mid-sagittal (A) and right-lateral (B) reconstruction images of CT and a mid-sagittal view of T2-weighted MR image immediately after injury. The CT images show the cervical vertebral fracture-dislocation at C3/4 (A, B). The MR image shows the compressed spinal cord at C3/4 (C).

was defined as "a motor disorder characterized by velocity-dependent increase in tonic stretch reflexes (muscle tone) with exaggerated tendon jerks, resulting from hyper-excitability of stretch reflexes, as a main component of upper motoneuron syndrome.[21] The spasticity after SCI is a serious hindrance factor at the start of active rehabilitation.[22] The decrease of spasticity is directly linked to the functional improvement of the SCI patient. Powell *et al*. [23] reported the usefulness of combined therapy in transvertebral direct current stimulation (tvDCS) and locomotor training on a robot-assisted gait orthosis (LT-RGO) for spasticity, and Duffel *et al*.[24] reported that robotic locomotor training with anti-spastic medication improves the walking ability by decreasing spasticity. On the other hand, a systematic review found that the effects of robot-assisted therapy on muscle spasticity were inconsistent.[25] Several studies have reported that prolonged passive muscle stretching reduces spasticity.[26–28] Sustained ambulation activity due to HAL training have possibility to effect similar decreasing of spasticity as

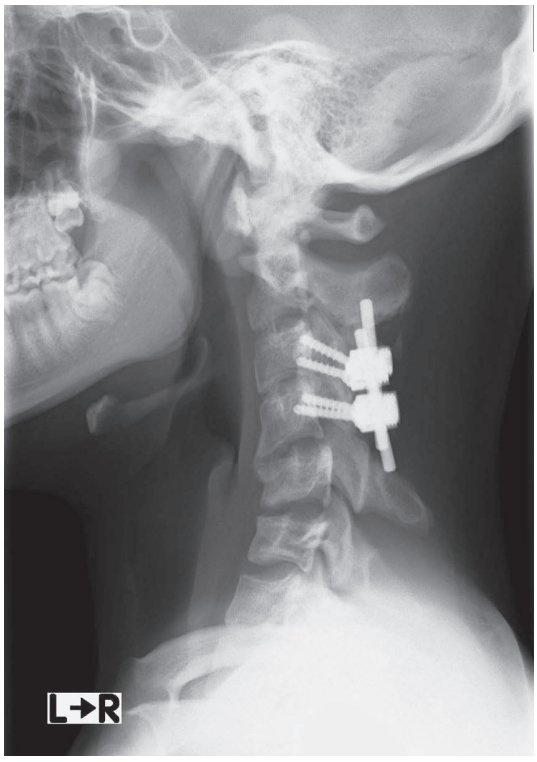

Figure 3. A cervical lateral radiograph 4 years after surgery, showing the completion of C3/4 posterior spinal fusion.

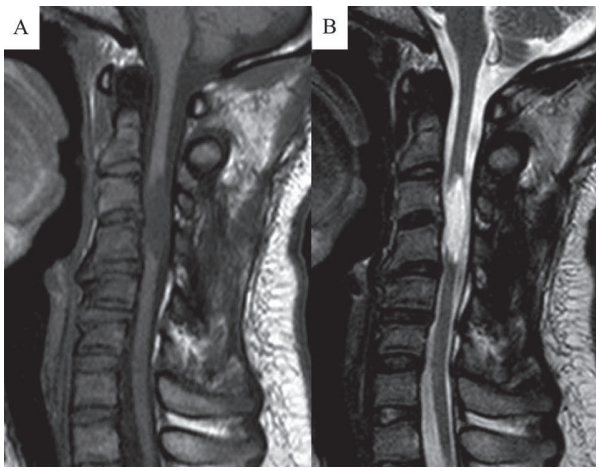

Figure 4. Mid-sagittal T1-weighted (A) and T2-weighted (B) MR images 4 years after surgery. The MR images show the signal changes in the spinal cord at the C3/4 level.

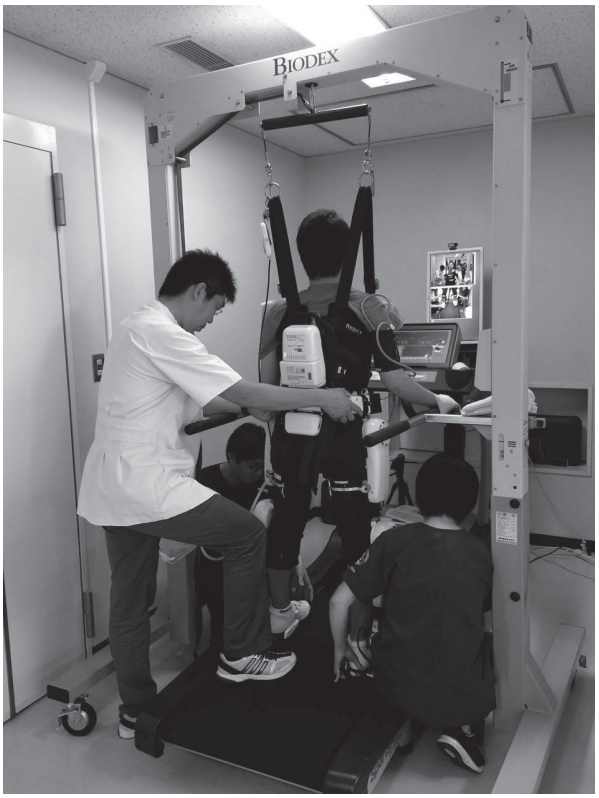

Figure 5. Gait training using the robotic suit HAL with a body weight support system (BIODEX). (Colour online)
2 physicians and 1 therapist support the subject in balance and weight-bearing.

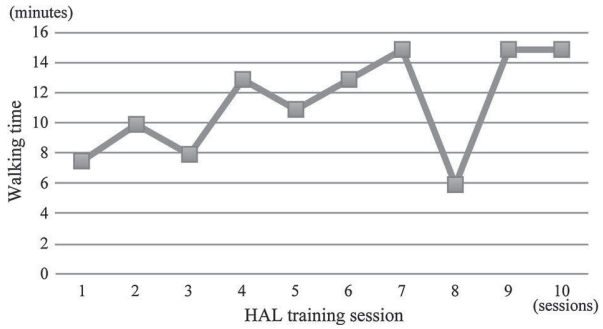

Figure 6. Walking time in each HAL session.

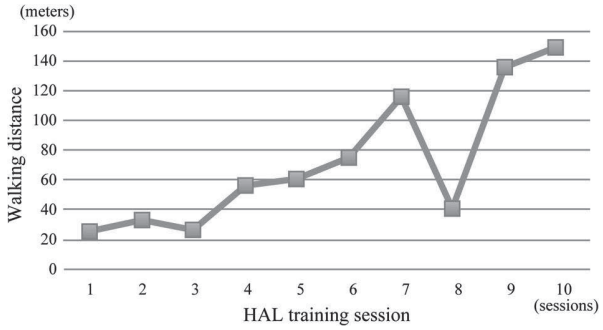

Figure 7. Walking distance in each HAL session.

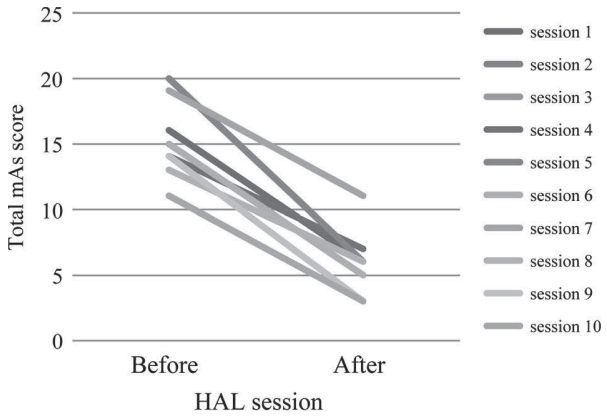

Figure 8. Change in the total modified Ashworth scale score before and after training in each HAL session. (Colour online)

passive muscle stretching. More studies are required in order to verify the availability of HAL training. To the best of our knowledge, however, there has been no report that a single robotic locomotor training decreased the spasticity of patients with SCI. In this meaning, this is the first report that the HAL training has a possibility to decrease the spasticity of patients with SCI, in spite of the fact that the decrease of spasticity in our patient was temporary (lasting approximately 30 minutes after HAL training).

In summary, the HAL training for a patient with complete C4 quadriplegia and chronic SCI decreased the spasticity, indicating the feasibility and efficiency of rehabilitation using a robotic suit HAL for quadriplegia patients.

Acknowledgements

We thank Mayuko Sakamaki and Yumiko Ito, Center for Innovative Medicine and Engineering (CIME), University of Tsukuba Hospital, for their excellent technical assistance. This study was supported by the Industrial Disease Clinical Research Grants of the Ministry of Health Labour and Welfare, Japan (14060101-01).

Disclaimer statements

Contributors None.

Funding None.

Conflicts of interest None.

Ethics approval None.

ORCiD

Akira Ikumi http://orcid.org/0000-0001-6034-1593

References

1 van Vliet P, Wing AM. A new challenge: robotics in the rehabilitation of the neurologically motor impaired. Phys Ther 1991;71(1): 39–47.
2 Tefertiller C, Pharo B, Evans N, Winchester P. Efficacy of rehabilitation robotics for walking training in neurological disorders: a review. J Rehabil Res Dev 2011;48(4):387–416.
3 Colombo G, Joerg M, Schreier R, Dietz V. Treadmill training of paraplegic patients using a robotic orthosis. J Rehabil Res Dev 2000;37(6):693–700.
4 Veneman JF, Kruidhof R, Hekman EE, Ekkelenkamp R, Van Asseldonk EH, van der Kooij H. Design and evaluation of the LOPES exoskeleton robot for interactive gait rehabilitation. IEEE Trans Neural Syst Rehabil Eng 2007;15(3):379–86.
5 Hesse S, Uhlenbrock D, Werner C, Bardeleben A. A mechanized gait trainer for restoring gait in nonambulatory subjects. Arch Phys Med Rehabil 2000;81(9):1158–61.
6 Schmidt H, Werner C, Bernhardt R, Hesse S, Kruger J. Gait rehabilitation machines based on programmable footplates. J Neuroeng Rehabil 2007;4:2.
7 Visintin M, Barbeau H, Korner-Bitensky N, Mayo NE. A new approach to retrain gait in stroke patients through body weight support and treadmill stimulation. Stroke 1998;29(6):1122–8.
8 Lunenburger L, Colombo G, Riener R, Dietz V. Biofeedback in gait training with the robotic orthosis Lokomat. Conf Proc IEEE Eng Med Biol Soc 2004;7:4888–91.
9 Neckel N, Wisman W, Hidler J. Limb alignment and kinematics inside a Lokomat robotic orthosis. Conf Proc IEEE Eng Med Biol Soc 2006;1:2698–701.
10 Husemann B, Muller F, Krewer C, Heller S, Koenig E. Effects of locomotion training with assistance of a robot-driven gait orthosis in hemiparetic patients after stroke: a randomized controlled pilot study. Stroke 2007;38(2):349–54.
11 Hornby TG, Campbell DD, Kahn JH, Demott T, Moore JL, Roth HR. Enhanced gait-related improvements after therapist- versus robotic- assisted locomotor training in subjects with chronic stroke: a randomized controlled study. Stroke 2008;39(6):1786–92.
12 Kawamoto H, Sankai Y. Power assist method based on phase sequence and muscle force condition for HAL. Adv Robot 2005; 19:717–34.
13 Lee S, Sankai Y. Virtual impedance adjustment in unconstrained motion for an exoskeletal robot assisting the lower limb. Adv Robot 2005;19:773–95.
14 Suzuki K, Gouji M, Kawamoto H, Hasegawa Y, Sankai Y. Intention- based walking support for paraplegia patients with robot suit HAL. Adv Robot 2007;21:1441–69.
15 Tsukahara A, Kawanishi R, Hasegawa Y, Sankai Y. Sit-to-stand and stand-to-sit transfer support for complete paraplegic patients with robot suit HAL. Adv Robot 2010;24:1615–38.
16 Maeshima S, Osawa A, Nishio D, Hirano Y, Takeda K, Kigawa H, *et al*. Efficacy of a hybrid assistive limb in post-stroke hemiplegic patients: a preliminary report. BMC Neurol. 2011;11:116.
17 Kubota S, Nakata Y, Eguchi K, Kawamoto H, Kamibayashi K, Sakane M, *et al*. Feasibility of rehabilitation training with a newly developed wearable robot for patients with limited mobility. Arch Phys Med Rehabil 2013;94(6):1080–7.
18 Aach M, Cruciger O, Sczesny-Kaiser M, Hoeffken O, Meindl R, Tegenthoff M, *et al*. Voluntary driven exoskeleton as a new tool for rehabilitation in chronic spinal cord injury: a pilot study. Spine J. 2014;14(12):2847–53.
19 Bohannon RW, Smith MB. Inter-rater reliability of a modified Ashworth scale of muscle spasticity. Phys Ther 1987;67:206–7.
20 Fujii K, Abe T, Kubota S, Marushima A, Kawamoto H, Ueno T, *et al.* The voluntary driven exoskeleton Hybrid Assistive Limb (HAL) for postoperative training of thoracic ossification of the posterior longitudinal ligament: a case report. J Spinal Cord Med 2016;Feb 9. [Epub ahead of print]
21 Lance JW. What is spasticity? Lancet 1990;335(8689):606.
22 van Cooten IP, Snoek GJ, Nene AV, de Groot S, Post MW. Functional hindrance due to spasticity in individuals with spinal cord injury during inpatient rehabilitation and 1 year thereafter. Spinal Cord 2015;53(9):663–7.
23 Powell ES, Carrico C, Raithatha R, Salyers E, Ward A, Sawaki L. Transvertebral direct current stimulation paired with locomotor training in chronic spinal cord injury: a case study. NeuroRehabilitation 2016;38(1):27–35.
24 Duffell LD, Brown GL, Mirbagheri MM. Facilitatory effects of anti-spastic medication on robotic locomotor training in people with chronic incomplete spinal cord injury. J Neuroeng Rehabil 2015;12:29.
25 Peter O, Fazekas G, Zsiga K, Denes Z. Robot-mediated upper limb physiotherapy: review and recommendations for future clinical trials. Int J Rehabil Res 2011;34(3):196–202.
26 Pin T, Dyke P, Chan M. The effectiveness of passive stretching in children with cerebral palsy. Dev Med Child Neurol 2006;48(10): 855–62.
27 Stevenson VL. Rehabilitation in practice: spasticity management. Clin Rehabil 2010;24(4):293–304.
28 Tremblay F, Malouin F, Richards CL, Dumas F. Effects of prolonged muscle stretch on reflex and voluntary muscle activations in children with spastic cerebral palsy. Scand J Rehabil Med 1990;22(4):171–80.

Hindawi Publishing Corporation
Case Reports in Orthopedics
Volume 2016, Article ID 9610745, 6 pages
http://dx.doi.org/10.1155/2016/9610745

Case Report

Knee-Extension Training with a Single-Joint Hybrid Assistive Limb during the Early Postoperative Period after Total Knee Arthroplasty in a Patient with Osteoarthritis

Tomokazu Yoshioka,[1,2] Hisashi Sugaya,[1,2] Shigeki Kubota,[1,2] Mio Onishi,[2] Akihiro Kanamori,[2] Yoshiyuki Sankai,[3] and Masashi Yamazaki[2]

[1]*Division of Regenerative Medicine for Musculoskeletal System, Faculty of Medicine, University of Tsukuba, 1-1-1 Tennodai, Tsukuba, Ibaraki 305-8575, Japan*
[2]*Department of Orthopedic Surgery, Faculty of Medicine, University of Tsukuba, 1-1-1 Tennodai, Tsukuba, Ibaraki 305-8575, Japan*
[3]*Faculty of Systems and Information Engineering, University of Tsukuba, 1-1-1 Tennodai, Tsukuba, Ibaraki 305-8577, Japan*

Correspondence should be addressed to Tomokazu Yoshioka; yoshioka@md.tsukuba.ac.jp

Received 5 June 2016; Revised 22 August 2016; Accepted 18 September 2016

Academic Editor: Werner Kolb

The knee range of motion is an important outcome of total knee arthroplasty (TKA). According to previous studies, the knee range of motion temporarily decreases for approximately 1 month after TKA due to postoperative pain and quadriceps dysfunction following surgical invasion into the knee extensor mechanism. We describe our experience with a knee-extension training program based on a single-joint hybrid assistive limb (HAL-SJ, Cyberdyne Inc., Tsukuba, Japan) during the acute recovery phase after TKA. HAL-SJ is a wearable robot suit that facilitates the voluntary control of knee joint motion. A 76-year-old man underwent HAL-SJ-based knee-extension training, which enabled him to perform knee function training during the acute phase after TKA without causing increased pain. Thus, he regained the ability to fully extend his knee postoperatively. HAL-SJ-based knee-extension training can be used as a novel post-TKA rehabilitation modality.

1. Introduction

The knee range of motion is an important outcome of total knee arthroplasty (TKA), a procedure commonly used to treat osteoarthritis of the knee [1]. According to previous studies, the knee range of motion decreases temporarily for approximately 1 month after TKA due to postoperative pain and quadriceps dysfunction following surgical invasion of the knee extensor mechanism. These previous studies have also indicated that this decrease in the knee range of motion correlates significantly with decreases in joint function and the patient's degree of satisfaction [2, 3]. Currently, no joint function exercises intended to maintain the range of passive knee extension obtained through surgery can be performed without pain, even when using active extension. Therefore, a new treatment strategy is needed to prevent the prolongation of extension lag after TKA.

The single-joint hybrid assistive limb (HAL) (HAL-SJ, Cyberdyne Inc., Tsukuba, Japan) is a wearable robot suit that facilitates the voluntary control of knee joint motion (Figure 1). With this suit, signals from muscle action potentials are detected through electrodes on the surface of the skin and processed through a computer, after which the patient is provided with assisted joint motions. The power unit on the knee joint comprises angular sensors and actuators, and the control system comprises a cybernetic voluntary control (CVC) and cybernetic autonomous control (CAC) system [4]. The HAL has been reported to be effective in the functional recovery of various mobility disorders [5–8]. Although studies have reported successful outcomes for acute

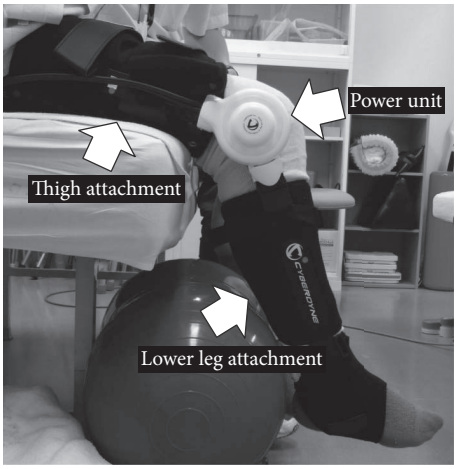

Figure 1: Lateral image of the single-joint hybrid assistive limb on the patient's right knee joint. Thigh and lower leg attachments are adjusted to the patient's body and connected by a power unit.

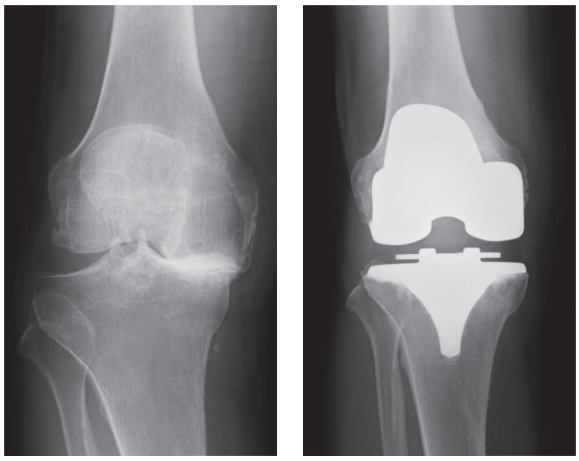

(a) (b)

Figure 2: Preoperative (a) and postoperative (b) frontal radiographs of the knee.

or chronic mobility disorders, there have been no reports on the use of HAL-SJ for degenerative joint diseases or related postoperative recovery to date. Accordingly, we describe our experience with a HAL-SJ-based knee-extension training program during the acute recovery phase after TKA.

2. Case Presentation

A 76-year-old man underwent right TKA (Vanguard, Zimmer Biomet Inc., Warsaw, IN, USA) for grade 4 (Kellgren-Lawrence scale) osteoarthritis of the knee (Figures 2 and 3). The HAL treatment program was divided into the following five phases.

2.1. Preoperative Observation Phase (Day of Hospital Admission to the Day of Surgery). The patient's thigh circumference and lower leg length were measured preoperatively, thus allowing us to adjust the HAL-SJ to the patient's size to ensure accurate training (Figure 1). We palpated the patient's quadriceps muscles (vastus medialis, rectus femoris, and vastus lateralis) and attached electrodes to each muscle to detect the bioelectric potentials of the long axes along the belly of each muscle. Then, we instructed the patient to perform knee-extension exercises and contract his quadriceps. We asked the patient to simulate the knee-extension training exercises, which were to be performed postoperatively, by performing 10 knee extensions with HAL-SJ assistance; the muscle that exhibited the highest bioelectric potential amplitude was used. The patient sat with his lower leg hanging down naturally, and we adjusted the height of the chair so his feet were not in contact with the floor (Figure 1).

2.2. Surgery Phase (Day of Surgery). TKA was performed through a longitudinal incision with a medial parapatellar approach. We cemented the femoral and tibial components using the modified gap technique and a posterior stabilized-type device.

2.3. Postoperative Observation Phase (Postoperative Days 1–7). On the first day after surgery, the patient was able to place full body weight on his leg; subsequently, he began rehabilitation (sitting, standing, and walking training; joint range of motion training; muscle strength maintenance; and muscle strengthening training) under the guidance of a physical therapist. Until discharge, he engaged in rehabilitation exercises for 20–40 min 5 days per week. Continuous passive motion (CPM) training began on the second postoperative day after the intra-articular drain was removed, and it was performed for 1 hour per day until discharge. On the seventh postoperative day, we attached electrodes to the quadriceps muscle again to detect the bioelectric potential along the long axis of the rectus femoris muscle belly (Figure 4(a)). Then, the patient was instructed to perform active knee-extension exercises to contract his quadriceps and thus simulate training with the HAL-SJ (Figure 4(b)).

2.4. HAL-SJ Therapy Phase (Postoperative Day 8 to Discharge). After 1 week of postoperative observation, we confirmed that his general condition had stabilized, and we decided to initiate HAL-SJ therapy. The CVC mode of the HAL-SJ, which was used in this study, can support a patient's voluntary motion according to the voluntary muscle activity and assistive torque provided to the knee joint [7]. This mode also allows the operator to adjust the degree of physical support to achieve patient comfort while gradually reducing support as training progresses. In addition to conventional rehabilitation (Figure 5(a)), the patient also performed HAL-SJ-assisted knee-extension exercises in a seated position at a frequency of 10 exercises/set for 5 sets twice weekly (HAL-SJ range of motion: 0–120°; Figure 5(b)). Training was performed 3 times (postoperative days 8, 10, and 17). The mean duration of a HAL-SJ training session was 26 min, which included the total time for which the HAL-SJ was worn and the duration of training (39, 22, and 17 min on postoperative days 8, 10, and 17, resp.).

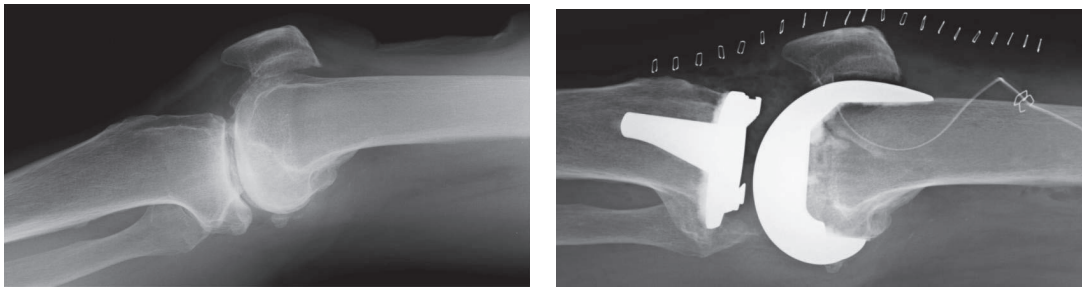

(a) (b)

Figure 3: Lateral radiographs of the knee. (a) Preoperative passive knee extension without anesthesia. (b) Passive extension under postoperative anesthesia immediately postoperatively. Full knee extension was restricted preoperatively but it was possible immediately postoperatively.

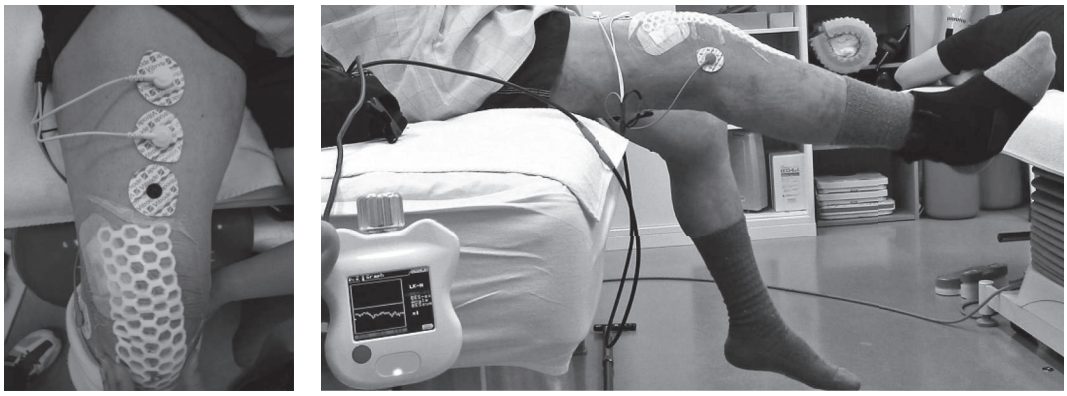

(a) (b)

Figure 4: Bioelectric potential detection and simulation before single-joint hybrid assistive limb training. Electrodes were attached to the muscle belly of the quadriceps (a), and rectus femoris simulation (b) was performed. Electrodes were placed to avoid surgical wound.

2.5. Post-HAL-SJ Therapy Observation Phase (Discharge to 3 Months after the End of HAL-SJ Therapy). There were no adverse effects related to HAL-SJ training. The patient was able to walk using a T cane, and he was discharged on postoperative day 21. Posttherapy assessments were conducted on an outpatient basis at 1 and 3 months after the end of the third HAL-SJ therapy session.

The following assessments were conducted: extension lag (maximum knee joint extension angle during passive exercise and that during active exercise), knee pain (visual analog scale, VAS), and isometric knee-extension muscle strength (IKEMS) before surgery, before and after HAL-SJ training, and at 1 and 3 months after training ended. The knee range of motion was measured using goniometry at accuracy of up to 1.0°, as goniometric measurements of range of motion have been reported to be more reliable than visual observation [9]. The measurement landmarks were the greater trochanter of the femur, proximal head of the fibula, and lateral malleolus. The maximal IKEMS of the operated leg was assessed while the patient was seated with 90° flexion in the hips and knees. Two measurements were taken using a μTas F-1 handheld dynamometer (Anima Corp., Tokyo, Japan) that was fixed to the chair. Each trial lasted for 3–5 s, with a 30-second rest period between trials. The higher of the two valid measurements was recorded. All measurements were performed by a single trained physical therapist to eliminate interobserver variability.

The extension lag, VAS, and IKEMS results are shown in Table 1. The extension lag was 15° preoperatively; this value decreased gradually over time to 1° at 3 months after therapy, indicating improvement. Comparisons before and after HAL-SJ therapy indicated that the 3 intervention sessions yielded respective improvements of 5°, 9°, and 5°. The VAS decreased from 55 mm before surgery to 17 mm at 3 months after the end of HAL-SJ therapy. Notably, training was not stopped because of increased knee pain from the HAL-SJ intervention. The maximum IKEMS value of 35.2 kgf was recorded before surgery. This value decreased markedly postoperatively and was measured as 18.3 kgf at 3 months after the end of the third HAL-SJ therapy session. Although this final value did not indicate recovery to the preoperative level, our comparison of IKEMS before and after HAL-SJ therapy indicated a slight improvement over the 3 intervention sessions (0.4, 0.0, and 1.8 kgf, resp.).

Clinical outcomes were assessed using the Japanese Orthopedic Association score [10]. The preoperative score of 55 points (pain, walking ability: 15 points; pain, ability to ascend/descend stairs: 5 points; flexion angle: 25 points;

Table 1: Chronological changes in EL, VAS, and IKEMS.

	Preoperative	First HAL-SJ (***POD 8)		Second HAL-SJ (POD 10)		Third HAL-SJ (POD 17)		At discharge (POD 21)	Following the end of the third HAL-SJ	
		*IPO	**IFO	IPO	IFO	IPO	IFO		1 month	3 months
EL (degrees)	15	10	5	12	3	10	5	4	4	1
VAS (mm)	55	28	4	20	20	32	46	40	18	17
IKEMS (kg)	35.2	8.7	9.1	5.6	5.6	10.7	12.5	16.9	16.9	18.3

EL: extension lag; VAS: visual analog scale; IKEMS: isometric knee-extension muscle strength; HAL-SJ: single-joint hybrid assistive limb.
*IPO: immediately before the intervention.
**IFO: immediately following the intervention.
***POD: postoperative day.

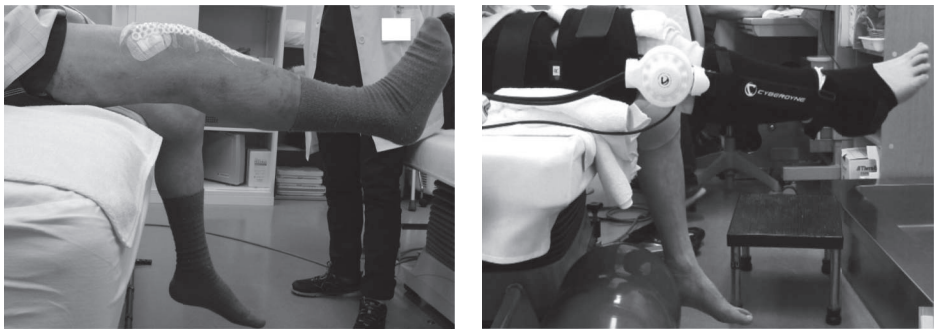

(a) (b)

Figure 5: Knee-extension training on postoperative day 8. Active knee extension (a) did not result in full extension, whereas extension with single-joint hybrid assistive limb assistance resulted in full knee extension (b).

swelling: 10 points) improved to 90 points (pain, walking ability: 30 points; pain, ability to ascend/descend stairs: 20 points; flexion angle: 30 points; swelling: 10 points) at 3 months after the end of HAL-SJ therapy.

3. Discussion

The patient's clinical course described herein has yielded two important clinical findings. First, knee-extension training with HAL-SJ, performed as part of the acute phase of post-TKA rehabilitation, resulted in immediate improvements in extension lag. Second, knee-extension training with HAL-SJ could be performed without increased pain.

We will first address the immediate improvement in extension lag. According to a recent review, CPM with a knee-range-of-motion training device commonly used for acute post-TKA rehabilitation resulted in early improvements in the knee flexion range of motion, compared to not using CPM; however, neither the range of active nor that of passive knee extension improved with CPM [11]. Restricted post-TKA knee extension (decreased or poor extension range) has been significantly correlated with decreases in the Oxford Knee Score and clinical outcomes related to standing, as indicated by the Short Form-36 physical component score [2]. Therefore, maintenance of the improved knee-extension range obtained through surgery is extremely important to improving knee function. In the present study, HAL-SJ-based knee-extension training led to an immediate improvement in extension lag even though the quadriceps did not exhibit significant strengthening. This result suggests that this improvement resulted from the facilitation of the muscular and neural functions of the quadriceps by HAL-SJ, which allowed the knee to extend fully because of the presence of a bioelectric potential in the quadriceps and the degree of feedback strength.

As mentioned before, HAL-SJ-based knee-extension training, even during the acute postoperative stage, did not cause an increase in knee pain. Although isometric quadriceps training is performed during the acute post-TKA phase to address decreased or dysfunctional knee extension related to surgical invasion of the knee-extension mechanism, it is difficult for patients to sufficiently perform knee-extension training because of pain and swelling caused by the operation [2, 11, 12]. HAL-SJ-based knee-extension training, however, can be performed during the acute post-TKA phase without increased pain. We believe that this is due to the knee-assistive function of HAL-SJ.

Two case reports on postoperative interventional training using HAL have been published in the field of orthopedic surgery. Both reports described improvements in walking ability when HAL was used in patients with thoracic vertebra ossification of the posterior longitudinal ligament [8, 13]. In contrast, the present study is the first to report on the use of HAL-SJ knee-extension training during the acute phase following TKA for osteoarthritis of the knee.

In conclusion, HAL-SJ-based knee-extension training allows the performance of knee function training during the acute post-TKA phase without causing increased pain, thus maintaining the patient's surgically recovered ability to fully extend the knee. Although inability to fully extend the knee is a cause of reduced knee function and decreased satisfaction in patients after TKA, there is currently no effective modality for the recovery of knee-extension function. Therefore, HAL-SJ-based knee-extension training can be used as a novel post-TKA rehabilitation modality. Reduced medical costs can also be anticipated, as early recovery of knee function would reduce hospital stays and the nursing care burden consequent to improved patient independence. However, the mechanism underlying the immediate improvement in extension lag remains unknown; therefore, further study from a neurophysiological perspective is required.

Ethical Approval

The study was carried out in accordance with the Declaration of Helsinki and within the appropriate ethical framework.

Consent

Written informed consent was obtained from the patient for publication of this case report and any accompanying images.

Competing Interests

A commercial party having a direct financial interest in the results of the research supporting this article has conferred or will confer a financial benefit on one of the authors. Yoshiyuki Sankai is CEO of Cyberdyne Inc., Ibaraki, Japan. Cyberdyne is the manufacturer of the robot suit (hybrid assistive limb). Cyberdyne was not directly involved in the study design; collection, analysis, or interpretation of data; writing the report; or the decision to submit the paper for publication. No commercial party having a direct financial interest in the results of the research supporting this article has or will confer a benefit on the authors or on any organization with which the authors are associated (Tomokazu Yoshioka, Hisashi Sugaya, Shigeki Kubota, Mio Onishi, Akihiro Kanamori, and Masashi Yamazaki).

References

[1] K. Y. Chiu, T. P. Ng, W. M. Tang, and W. P. Yau, "Review article: knee flexion after total knee arthroplasty," *Journal of Orthopaedic Surgery*, vol. 10, no. 2, pp. 194–202, 2002.

[2] Z. Zhou, K. S. A. Yew, E. Arul et al., "Recovery in knee range of motion reaches a plateau by 12 months after total knee arthroplasty," *Knee Surgery, Sports Traumatology, Arthroscopy*, vol. 23, no. 6, pp. 1729–1733, 2015.

[3] R. L. Mizner, S. C. Petterson, and L. Snyder-Mackler, "Quadriceps strength and the time course of functional recovery after total knee arthroplasty," *The Journal of Orthopaedic and Sports Physical Therapy*, vol. 35, no. 7, pp. 424–436, 2005.

[4] H. Kawamoto and Y. Sankai, "Power assist method based on phase sequence and muscle force condition for HAL," *Advanced Robotics*, vol. 19, no. 7, pp. 717–734, 2005.

[5] H. Kawamoto, K. Kamibayashi, Y. Nakata et al., "Pilot study of locomotion improvement using hybrid assistive limb in chronic stroke patients," *BMC Neurology*, vol. 13, article 141, 2013.

[6] S. Kubota, Y. Nakata, K. Eguchi et al., "Feasibility of rehabilitation training with a newly developed wearable robot for patients with limited mobility," *Archives of Physical Medicine and Rehabilitation*, vol. 94, no. 6, pp. 1080–1087, 2013.

[7] M. Aach, O. Cruciger, M. Sczesny-Kaiser et al., "Voluntary driven exoskeleton as a new tool for rehabilitation in chronic spinal cord injury: A pilot study," *Spine Journal*, vol. 14, no. 12, pp. 2847–2853, 2014.

[8] K. Fujii, T. Abe, S. Kubota et al., "The voluntary driven exoskeleton Hybrid Assistive Limb (HAL) for postoperative training of thoracic ossification of the posterior longitudinal ligament: a case report," *The Journal of Spinal Cord Medicine*, 2016.

[9] A. F. Lenssen, E. M. van Dam, Y. H. F. Crijns et al., "Reproducibility of goniometric measurement of the knee in the in-hospital phase following total knee arthroplasty," *BMC Musculoskeletal Disorders*, vol. 8, article 83, 2007.

[10] M. Okuda, S. Omokawa, K. Okahashi, M. Akahane, and Y. Tanaka, "Validity and reliability of the Japanese Orthopaedic Association score for osteoarthritic knees," *Journal of Orthopaedic Science*, vol. 17, no. 6, pp. 750–756, 2012.

[11] J. B. Mistry, E. D. Elmallah, A. Bhave et al., "Rehabilitative guidelines after total knee arthroplasty: a review," *Journal of Knee Surgery*, vol. 29, no. 3, pp. 201–217, 2016.

[12] Y.-H. Pua, "The time course of knee swelling post total knee arthroplasty and its associations with quadriceps strength and gait speed," *Journal of Arthroplasty*, vol. 30, no. 7, pp. 1215–1219, 2015.

[13] H. Sakakima, K. Ijiri, F. Matsuda et al., "A newly developed robot suit hybrid assistive limb facilitated walking rehabilitation after spinal surgery for thoracic ossification of the posterior longitudinal ligament: a case report," *Case Reports in Orthopedics*, vol. 2013, Article ID 621405, 4 pages, 2013.

Physiotherapy Practice and Research 37 (2016) 91–100
DOI 10.3233/PPR-160074
IOS Press

Hybrid Assistive Limb enhances the gait functions in sub-acute stroke stage: A multi single-case study

Kenichi Yoshikawa[a,*], Masafumi Mizukami[b], Hiroaki Kawamoto[c], Ayumu Sano[a], Kazunori Koseki[a], Yuko Hashizume[a], Yasutsugu Asakawa[b], Koji Iwamoto[b], Yutaka Kohno[d], Hiroshi Nagata[e], Kei Nakai[d,f] and Hideo Tsurushima[f]

[a]*Department of Physical Therapy, Ibaraki Prefectural University of Health Sciences Hospital, Ami Ibaraki, Japan*
[b]*Department of Physical Therapy, Ibaraki Prefectural University of Health Sciences, Ami Ibaraki, Japan*
[c]*Faculty of Systems and Information Engineering, University of Tsukuba, Tsukuba Ibaraki, Japan*
[d]*Department of Neurology, Ibaraki Prefectural University of Health Sciences Hospital, Ami Ibaraki, Japan*
[e]*Center for Medical Sciences, Ibaraki Prefectural University of Health Sciences, Ami Ibaraki, Japan*
[f]*Faculty of Medicine, University of Tsukuba, Tsukuba Ibaraki, Japan*

Abstract.
BACKGROUND: Hybrid Assistive Limb (HAL) is a new robotics walking training device consisting of a wearable robot that interactively provides motion according to the wearer's voluntary drive. The ability of HAL to enhance walking speed has not been clarified in sub-acute people with stroke, and few studies have focused on changes in walking pattern.
OBJECTIVES: To assess clinical availability of HAL in sub-acute stroke stage, we conduct a multi single-case study.
METHOD: An A-B-A single case study design was used in 4 patients. The intervention was conventional training in period A1 for 5 weeks and period A2 for 4 or 5 weeks and training with HAL and conventional training in period B for 5 weeks. The primary outcomes were maximum walking speed (MWS), cadence, and mean step length assessed each week. The secondary outcomes were Functional Ambulation Category, Berg Balance Scale, Fugl-Meyer Motor Assessment, and asymmetry rate in single-limb support time, as assessed before and after period B.
RESULTS: The significant increases in MWS was found in three patients through period B. The cadence, mean step length, FAC and AR were also increased in one, three, two and two patients, respectively.
CONCLUSIONS: It was found that HAL training of people with sub-acute stroke is an effective walking training to enhance the walking speed with the change of walking pattern in our clinical setting. Further studies are needed including control trials to analyze satirical difference.

Keywords: Hybrid Assistive Limb, robotics walking training, stroke

1. Introduction

Stroke is a major cause of walking disability worldwide [1]. More than 60% of people with stroke have walking disability and approximately 50% find it impossible to walk at disease onset [2]. Improving the walking ability of stroke is therefore an important goal, and various interventions have been tested in the past.

In 2003, Hesse et al. [3] pointed out that automated motor rehabilitation offers a fascinating new perspective on treatment, diagnosis, and interdisciplinary cooperation to the benefit of all participants, although a robot can never replace multi-level interaction between patients and therapist. Since then, research into the

*Corresponding author: Kenichi Yoshikawa, 4733 Ami, Ami-Machi, Inashiki-County, Ibaraki 300-0394, Japan. Tel.: +81 29 888 9216; Fax: +81 29 888 9279; E-mail: yoshikawak@ami.ipu.ac.jp.

effects of robotic rehabilitation of the upper and lower limbs on central nervous disabilities has increased. A systematic review of electromechanical-assisted training for walking after stroke [4, 5] revealed that using electromechanical-assisted gait training devices in combination with physiotherapy increases the chance of regaining independent walking ability in people after stroke.

The Hybrid Assistive Limb (HAL) was developed by Cyberdyne Corporation (Tsukuba, Japan). HAL is a wearable robot that interactively provides motion according to the wearer's voluntary drive [6]. HAL detects the bioelectrical signals generated by the patient's muscle activity or the floor-reaction-force signals caused by the patient's intended weight shifts, or both. HAL enables locomotor training with voluntary drive, and it has the advantages of both voluntary drive and ambulatory performance. Other exoskeletons use autonomously generated predefined motion. In contrast, HAL generates motion in response to the wearer's voluntary drive. The wearer operates HAL by adjusting his or her muscle activity. Thus HAL is able to conduct locomotor training by providing motion support in response to the user's voluntary drive. This assistance mechanism differs completely from those of other exoskeletons. In addition, other exoskeletons are designed for walking on a treadmill; therefore, they provide a simulated gait that differs from that of walking on a flat floor. In contrast, as a wearable system, HAL delivers locomotor training in an actual ambulatory environment. Kubota et al. [7] reported that the gait speed of patients with limited mobility, including people with chronic stroke, increases after gait training with HAL.

A recent randomized controlled trial comparing HAL gait training with conventional gait training showed that participants in the former group were significantly more able to walk independently after training [8]. Watanabe et al. remarked that the optimum duration of rehabilitation, the duration of each training session, the intervention frequency, and the long-term effects of HAL needed to be examined. In a previous unpublished study, we examined the effect of HAL training in people with sub-acute stroke. Motor recovery and walking function were greatly improved in all participants in the early recovery stage. However, improvement rates differed greatly among individuals. Large numbers of participants are therefore needed to detect any statistically significant effects of HAL training in a randomized controlled trial.

We therefore designed an intervention to occur at a time when improvement of walking speed was stable, in the late recovery stage of stroke, to clarify the effects of HAL walking training. We then tentatively evaluated the validity of this design in this pilot study. The first purpose of the study was to use a single case study design to explore the walking speed–enhancing effect of HAL gait training in people with sub-acute stroke whose walking speed had stabilized in the late recovery stage of their disease.

In addition, little has been reported on the effects of HAL gait training on cadence, step length (SL), and walking asymmetry in people with stroke. The second purpose of this study was therefore to examine changes in walking pattern and asymmetry after gait training with HAL.

2. Methods

2.1. Participants

Participants were recruited from an inpatient rehabilitation unit in Ibaraki Prefectural University of Health Sciences Hospital, Japan. All participants were admitted to our hospital between October 2013 and December 2013 through acute care hospitals to receive acute medical care and acute rehabilitation.

Inclusion criteria were diagnosis of first cerebral infarction or cerebral hemorrhage with hemiparesis and, for suitability for HAL, height from 150 to 185 cm and weight from 40 to 80 kg.

Exclusion criteria were high-risk heart disease, uncontrollable or severe high blood pressure, severe chronic respiratory disease, severe diabetes mellitus, severe aphasia, severe cognitive deficit lesion of the cerebellum or brain stem, subarachnoid hemorrhage, a need for severe risk control in physical therapy, severe sensory aphasia, ability to walk independently without cane or orthosis and live in the community, severe contracture and deformities of the lower limb, and use of an active implantable medical device.

The ethics committee of Ibaraki Prefectural University of Health Sciences approved the study, and written informed consent to participate was given by all participants or their legal representatives. This study was part of a research project, the protocol of which was registered with the University Hospital Medical Information Network Clinical Trials Registry (UMIN 000012760).

2.2. Case description

Four patients participated in the study. Table 1 gives the participant profiles in terms of age, sex, weight, side of paresis, time from stroke to admission, and time from stroke to intervention. The first participant (Case 1) was post-left corona radiata infarction. Case 2 was post-right frontal lobe and parietal lobe hemorrhage. Case 3 was post-right putamen hemorrhage, and case 4 was post-right parietal lobe and capsula interna hemorrhage.

2.3. Design

An A-B-A design was used. Maximum walking speed was recorded during the baseline in period A (A1 = before B; A2 = after B). In period A, patients were treated by conventional physical therapy, which included gait training, muscle strength training, range of motion training, up- and downstairs training, and other types of individual training for 60 min 5 days a week for 5 weeks. In period B, patients were given HAL gait training for 20 min and conventional physical therapy for 40 min a day, 4 or 5 days a week (excluding Saturdays, Sundays, and national holidays) for 5 weeks. In all periods, patients were given occupational therapy and speech therapy as needed.

Because of the great degree of functional improvement in the subacute stage after stroke, it is difficult to discriminate between the results of one type of training and those of others. We therefore intervened at a time when the improvement in walking speed was stable. To determine when to start the intervention, we evaluated the patients' walking speed by means of a 10-m walk test every week. The simple moving average (SMA) of walking speed in the preceding 3 weeks was then calculated. To assess the improvement rate, we calculated the change in the rate by dividing the difference between the present SMA and the previous week's SMA by the previous SMA. We intervened at a time when the improvement in walking speed was stable. We defined this as occurring when the change in the rate was less than 10% in the first, second and third week and 5% in the fourth and fifth weeks consecutively. We then monitored whether or not the change in rate was stable for 5 consecutive weeks.

2.4. Intervention

The single-leg version of HAL was placed on the participant's paretic side. To prevent falling, the HAL

Table 1
Participant characteristics, case description and secondly outcomes

	Age	Sex	Type of stroke	Side of paresis	Weight (kg)	Time from stroke to ad (days)	Time from stroke to intervention (days)	Number of training session	FAC			BBS			FMA-LE			AR	
									ad	Start	End	ad	Start	End	ad	Start	End	Start	End
Case 1	73	M	I	R	73.8	35	108	23	1	3	4	37	48	56	22	25	27	2.17 ± 0.59	1.17 ± 0.30*
Case 2	48	M	H	R	72.5	39	115	24	2	4	4	41	50	53	19	20	20	2.03 ± 0.29	1.10 ± 0.02*
Case 3	58	M	H	L	73.4	30	129	24	1	3	4	9	48	52	19	30	32	1.75 ± 0.68	1.25 ± 0.35
Case 4	26	F	H	L	51.4	48	160	22	3	5	5	32	55	56	23	23	24	1.57 ± 0.40	1.37 ± 0.68

Abbreviation: M male, F female, H hemorrhage, I infarct, L left, R right, ad admission to our hospital, FAC Functional Ambulation Category, BBS Bergs Balance Scale, FMA-LE the Lower Extremity part of the Fugl-Meyer Motor Assessment, AR asymmetry ratio, Start Start of period B, End End of period B. * $p < 0.05$.

Fig. 1. Walking training with HAL and a mobile suspension system.

attached to the patient was connected to a mobile suspension system (All-In-One Walking Trainer, Ropox A/S, Næstved, Denmark) without the patient bearing weight (Fig. 1). During the intervention, gait training was implemented at a speed judged by the therapists to be as fast as possible while still maintaining a good gait posture on level ground. Gait training with HAL was done 4 or 5 times a week. One gait training session with HAL took a total of 20 min a day, excluding the device-fitting time and rest time.

During each training session, walking was continuously assisted by HAL, which is a computer-controlled exoskeletal device. The design and control system for HAL have been described in detail elsewhere [9–11, 30]. The exoskeletal frame was fixed to the pelvis and the lower limbs by thigh and lower leg cuffs. Active actuators were installed at the hip joints and knee joints and generated assistive extension or flexion torque of these joints. HAL has two control systems, namely Cybernic Voluntary Control (CVC) mode and Cybernic Autonomous Control (CAC) mode [9]. CVC mode drives the amount and timing of the assistive torque provided to each joint for walking on the basis of bioelectrical signals from the flexor and extensor muscles at the hip and knee [12]. The gain in assistive torque at each joint in response to these bioelectrical signals was controlled by a therapist. The optimal gain and balance of the torque to maintain an appropriate walking pattern were determined by observing the joint trajectories and listening to the patient's comments. If it is difficult for patients to achieve the motion derived from the CVC, the CAC can autonomously generate torque according to the walking pattern by referring to information from the floor reaction force [13]; CAC mode was thus used until the patient became familiar with the CVC.

2.5. Outcome measures

The primary outcomes were maximum walking speed (MWS) [14], cadence, and mean SL, using a 10-m walk test each week. If the participant's Functional Ambulation Category (FAC) [15] was 2, then assistance in the 10-m walk test was needed only to prevent the participant from falling. In every test the physical therapist giving the assistance was different from the one who gave the conventional physical therapy. The evaluator, who was a third person, did not change from admission to discharge. If the FAC was 0 or 1, we waited until the FAC was 2 before we did the 10-m walk test. The time elapsed and number of steps were measured in the intermediate 6 m to allow for acceleration and deceleration. Cadence and mean SL [16] were calculated from the time elapsed and the number of steps in the 10-m section. The best MWS data from three trials were used for the analysis.

The secondary outcomes were the level of independence according to the FAC, the balance function according to the Berg Balance Scale (BBS) [17], motor recovery according to the Lower Extremity part of the Fugl-Meyer Motor Assessment (FMA-LE) [18] and the asymmetry ratio (AR) [19–21] in swing time (equal to single-limb support time). Secondary outcomes were assessed on admission, at the start of period B, and at the end of period B. The evaluator was a different person from the therapist that gave the patient normal physical therapy. AR was evaluated at a self-selected walking speed by motion analysis. Gait motion was captured in the sagittal plane by a video camera (Sony HDR-CX 390, Tokyo, Japan; sampling rate 60 Hz). Motion times were applied to the gait after more than 5 steps from the starting line. The video times were loaded into a computer and used to calculate the single support time (length of time for which one leg was on the ground) in 5 walking cycles by using video editing software (EDIUS Neo 3.5, Grass Valley K.K., Japan).

2.6. Statistical analysis

We defined period A1 as the period of 5 weeks in which the change in improvement rate, as calculated by using the SMA, was less than 10% in the first week and 5% in the subsequent 4 weeks.

MWS, cadence, and SL were plotted on a graph weekly to enable visual analysis [22]. To detect changes in trends between periods A1, B, and A2, changes in plot level during a period, as well as the variability, direction, or slope on the graph, were needed [22]. Least-square lines were also drawn for visual analysis [23].

In addition, non-parametric statistical analyses were done to support the results observed in the graphs. Differences between each period (A1, B, A2) were inferred with the Kruskal-Wallis test.

Serial dependency was also assessed by using an autocorrelation coefficient [24]. Clinical ordinal consecutive data such as those in this report are not independent. Most of the data were autocorrelated ($r > 0.20$). Because autocorrelation increases the probability of type I errors when there is a positive correlation [24], we chose a conservative P value of 0.01 [24, 25].

The differences in AR between the start and end of period B were analyzed by using a Wilcoxon signed-rank test. A P value less than 0.05 was considered statistically significant.

We used SPSS version 21.0 for all statistical analyses.

3. Results

All sessions were held for 20 min and completed safely. The number of sessions per participant ranged from 22 to 24 (Table 1).

Upon visual analysis, the graphs of weekly MWS showed improvement between periods A1 and B in Case

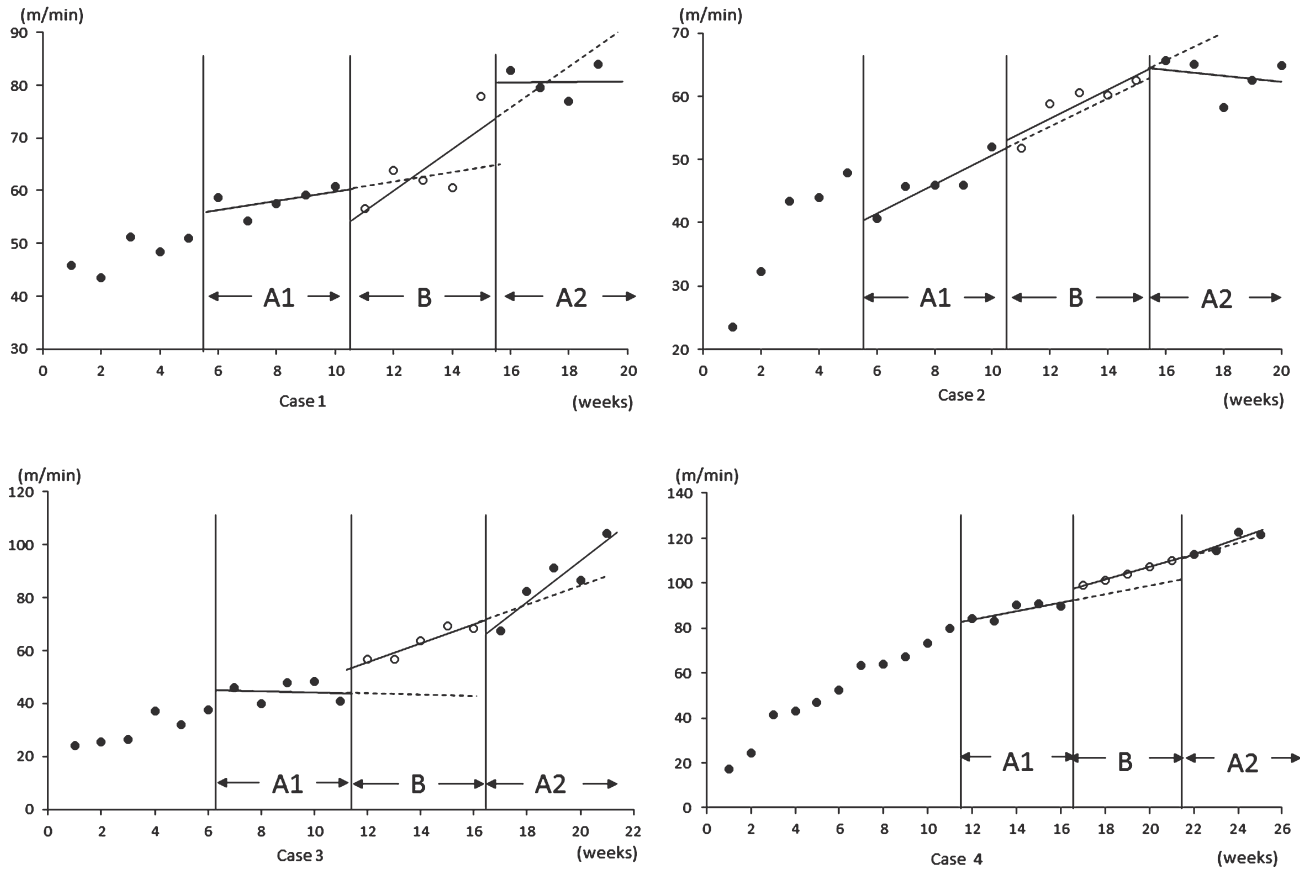

Fig. 2. Walking speeds of 4 participants. Baseline period (A1 and A2): Conventional physical therapy. Intervention period (B): Walking training with HAL and conventional training.

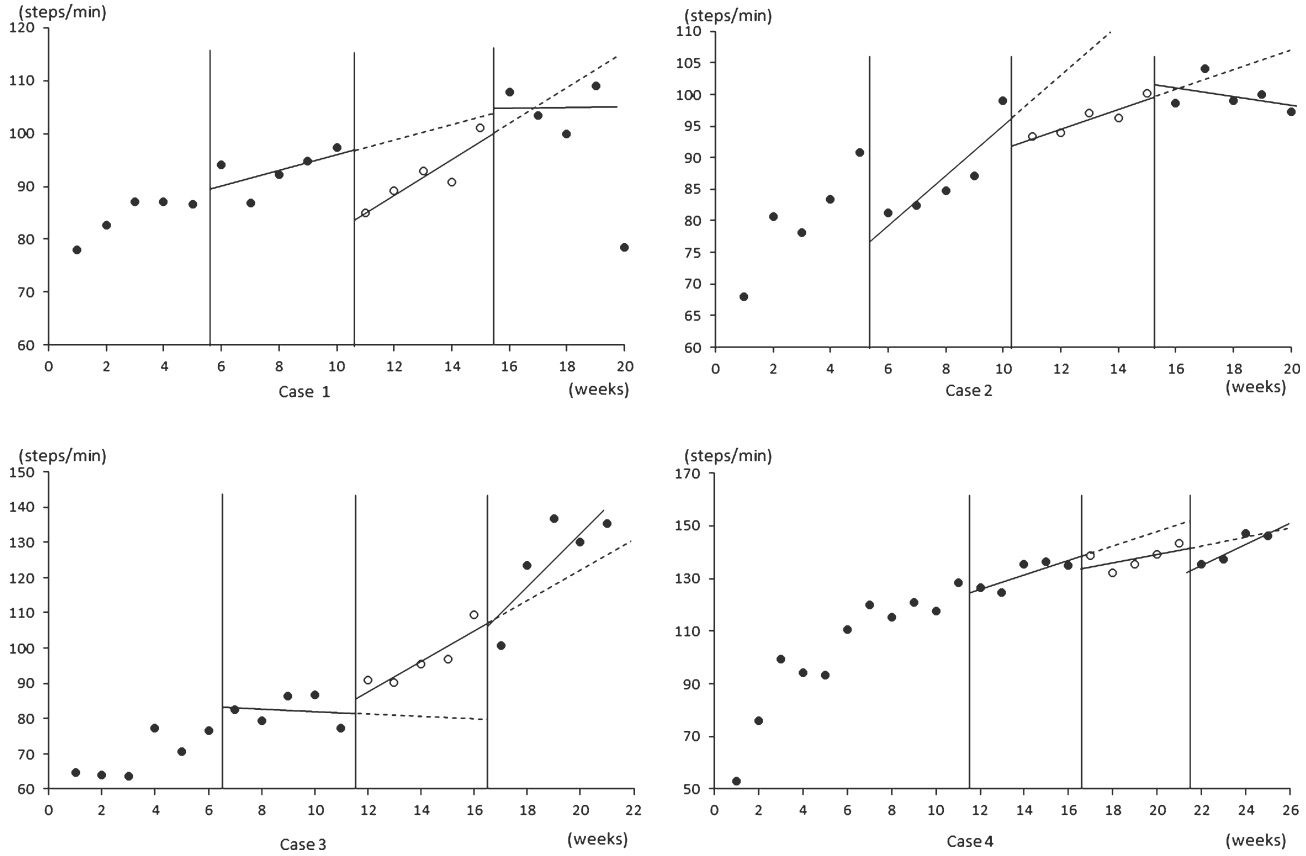

Fig. 3. Cadence in 4 participants. Baseline period (A1 and A2): Conventional training. Intervention period (B): Walking training with HAL and conventional training.

2, 3, and 4 (Fig. 2). The improvement was less clear in case 1. In period A2 the improvement decreased in case 1 and 2 and was constant in case 3 and 4.

The results for the graphs of cadence varied among individuals. There was evident improvement between periods A1 and B in case 3, whereas there was a clear decrease in case 1. There was a continued increase with a slightly smaller slope in period B compared with period A1 in case 2, and virtually no change in case 4 (Fig. 3). In case 1 and 3 the cadence in period A2 was greater than that in period B, whereas in case 4 the cadence was almost unchanged throughout.

The graphs of SL revealed obvious improvement between periods A1 and B in case 1, 2, and 4 (Fig. 4). The graph of SL for case 3 showed a decrease in improvement rate by visual analysis. In period A2 the improvement rate decreased in case 1 and 2 and increased in case 3 and 4.

The results of the non-parametric statistical analyses of MSW supported those of the visual analysis and were as follows: Case 1 to 4, respectively, Kruskal-Wallis $\chi2 = 8.68$, P-value = 0.013; $\chi2 = 9.92$, P-value = 0.0070; $\chi2 = 11.58$, P-value = 0.0031; $\chi2 = 11.57$, P-value = 0.0031. The non-parametric statistical analyses for cadence also supported the visual analysis results and were as follows: $\chi2 = 7.43$, P-value = 0.024; $\chi2 = 7.22$, P-value = 0.027; $\chi2 = 12.02$, P-value = 0.0025; $\chi2 = 4.71$, P-value = 0.095. The non-parametric statistical analyses for SL supported the visual analysis results and were as follows: $\chi2 = 11.79$, P-value = 0.0028; $\chi2 = 10.14$, P-value = 0.0063; $\chi2 = 10.44$, P-value = 0.0054; $\chi2 = 12.69$, P-value = 0.0018.

Table 1 shows the differences in secondary outcomes between the start and the end of period B. FAC improved in case 1 and 2 during period B. FAC in case 4 was 5 at the start of period B. BBS and FMA-LE improved in all participants during period B. AR decreased in all participants and changed significantly in case 1 and 2 ($P < 0.05$).

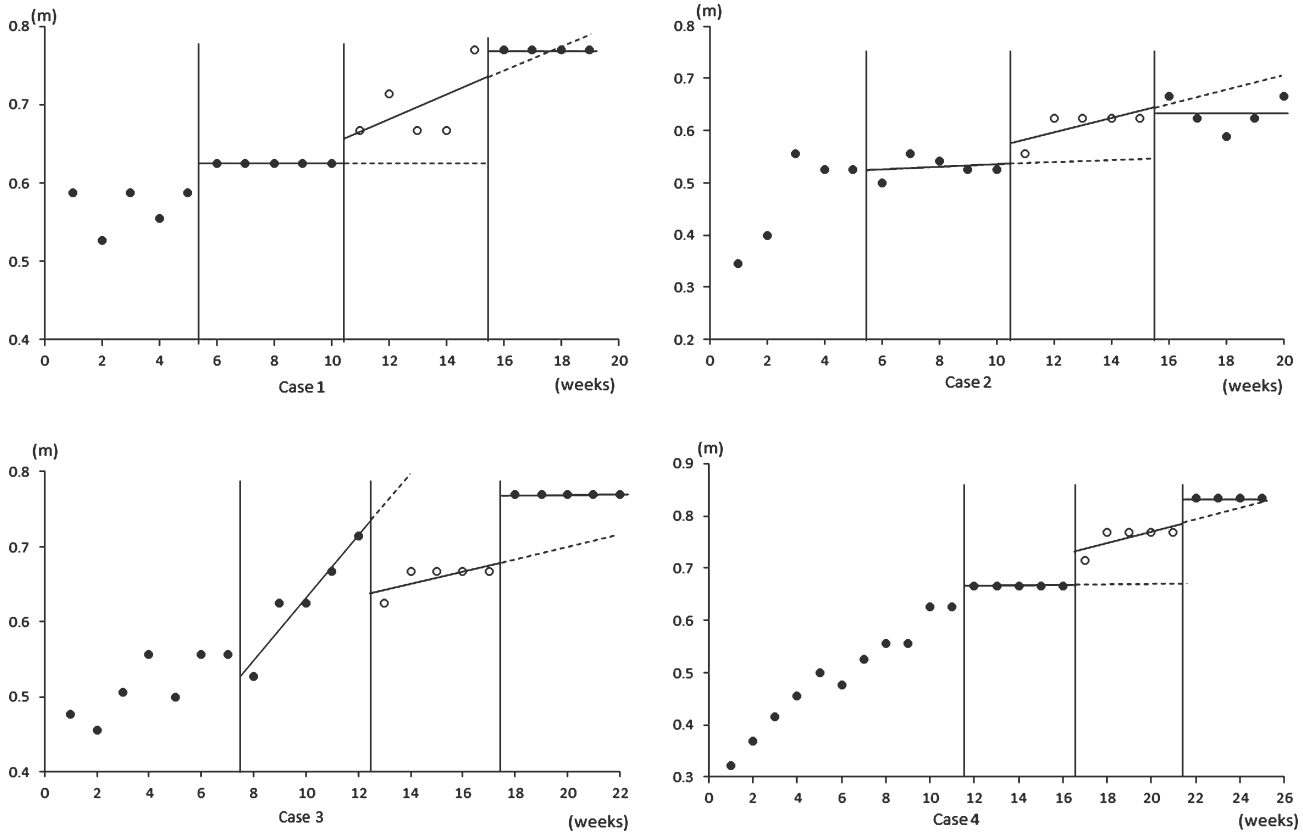

Fig. 4. Step length in 4 participants. Baseline period (A1 and A2): Conventional training. Intervention period (B): Walking training with HAL and conventional training.

4. Discussion

In Japan, it is usual for people with sub-acute stroke that are considered to require more rehabilitation to be transferred to a recovery rehabilitation hospital or unit. In our unpublished pilot study we intervened in the early recovery stage. However, it was difficult to extract the effect of only the HAL training from our results.

Therefore, in this current pilot study we explored the effect of HAL gait training in enhancing walking speed in people with stroke in the late recovery stage. The MWS results clearly showed improvement in period B in case 2, 3, and 4 and a slight improvement in case 1, whereas the participants' MWS values were almost stable in period A1. All participants accordingly started receiving their interventions at more than 100 days. Therefore, we consider that our design, whereby we intervened with HAL when the improvement in walking speed was stable, was reasonable.

Improvements in MWS were caused by an increase in SL in case 1, 2, and 4 and by an increase in cadence in case 3. A recent randomized controlled trial by Watanabe et al. [8] showed a significant difference between a HAL training group and a group receiving conventional training, but only in FAC. We found here that MWS was better in period B than in period A1 in the majority of patients. This difference between the studies may have been caused by the fact that we intervened for longer and more often than in the trial by Watanabe et al., who used HAL for 4 weeks at 3 times a week. However, our number of participants was only small.

In addition, the improvements in MWS in period B were the result of not only an increase in cadence or SL, but also a decrease in the other parameter. For example, in case 1, cadence decreased and SL increased in period B, conversely in case 3 cadence increased and SL decreased in period B. The difference in SL between the HAL group and the conventional group

was not significant in the trials performed by Watanabe et al. However, we found here that the increase or decrease in SL or cadence depended on the individual. In healthy adults, the walk ratio (calculated by dividing SL by cadence) [26] is generally constant; however, because walking speed can be changed, it is affected by SL and cadence speed to the same extent [27, 28]. Furthermore, Suzuki et al. [29] indicated that people with hemiparetic stroke in the recovery stage improved in MWS, with an invariant relationship between stride length and walking rate. Our results suggest that HAL training changed the participants' gait patterns. In fact, our finding that AR decreased in all participants and significantly increased in case 1 and 2 showed that gait symmetry improved. The ability to maintain single-limb support is an important determinant of gait stability [30, 31]. Asymmetry during single-limb support seems to be related to decreased ability to bear weight on the paretic limb [32], and single-support training helps to achieve symmetric gait in people with stroke [33, 34]. Goldie et al. [35] also pointed that increase in single support time on the paretic side is a good indicator of increase in weight bearing on the paretic side, whereas increase in single support time on the non-paretic side is a good indicator of better paretic leg advancement. In addition, training that incorporates active participation whereby the patient voluntarily produces movement, inducing changes in motor performance, cortical activity, and excitability, is considered essential for motor learning of new tasks [36, 37]. Therefore, training with HAL, which interactively provides motion according to the wearer's voluntary drive, may have enhanced walking performance in association with an improvement in walking pattern.

FAC was improved in case 1 and 3. Case 4 already had a perfect FAC score of 5 at the start of period B. BBS in all participants and FMA-LE in 3 participants (excluding case 2) increased; these changes were similar to those in the trial by Watanabe et al. [8].

A limitation of our study was the small number of participants. However, as a feasibility study its aim was to explore the effects of HAL training on walking speed at a time when the improvement in walking speed had stabilized in the late recovery stage, as well as to explore changes in walking pattern and asymmetry. Further studies are needed to explain how HAL training improves walking speed and walking pattern. We intend to use more participants and create a control group that will be treated only with conventional physical therapy and not with HAL training.

The results of this exploratory study suggested that HAL training in people with sub-acute stroke may enhance walking speed in association with an improvement in walking pattern at a time when the rate of improvement in walking speed is stable in the late recovery stage. Further studies with a control group are needed to clarify the effects on walking function.

Acknowledgments

We thank colleagues in Dept. of Physical Therapy, Ibaraki Prefectural University of Health Sciences Hospital and physical therapists in for their help with this study. The authors would particularly like to thank the study participants for their time.

Conflict of interest

Kenichi Yoshikawa, Masafumi Mizukami, Ayumu Sano, Kazunori Koseki, Yuko Hashizume, Yasutsugu Asakawa, Yutaka Kohno, Hiroshi Nagata, Kei Nakai, and Hideo Tsurushima have no competing interests to declare. Hiroaki Kawamoto is a founder, shareholder, and external director of CYBERDYNE Inc., which produces HAL.

Contributors

KY participated in the design of the study, carried out the data collection, analysis and interpretation, drafted and revised the manuscript.

MM participated in the design of the study, collected patient's informed consent and drafted the manuscript.

AS and KK carried out the HAL training.

YH and KI carried out the assessments.

YA participated in the statistical analysis.

HK participated in the design of the study and provided the HAL suits and technical support.

YK, HN, KN and HT participated in the coordination and design of the study, in finalizing the manuscript.

Funding

This work was supported by Grant-in-Aid for Project Research (1247) from Ibaraki Prefectural University of Health Sciences.

References

[1] Feigin VL, Lawes CM, Bennett DA, Barker-Collo SL, Parag V. Worldwide stroke incidence and early case fatality reported in 56 population-based studies: A systematic review. The Lancet Neurology 2009;8(4):355-69.

[2] Jørgensen HS, Nakayama H, Raaschou HO, Vive-Larsen J, Støier M, Olsen TS. Outcome and time course of recovery in stroke. Part II: Time course of recovery. The Copenhagen Stroke Study. Archives of Physical medicine and Rehabilitation 1995;76(5):406-12.

[3] Hesse S, Schmidt H, Werner C, Bardeleben A. Upper and lower extremity robotic devices for rehabilitation and for studying motor control. Current Opinion in Neurology 2003;16(6): 705-10.

[4] Mehrholz J, Elsner B, Werner C, Kugler J, Pohl M. Electromechanical-assisted training for walking after stroke. The Cochrane Database of Systematic Reviews 2013;7: Cd006185.

[5] Mehrholz J, Elsner B, Werner C, Kugler J, Pohl M. Electromechanical-Assisted Training for Walking After Stroke Updated Evidence. Stroke 2013;44(10):e127-e8.

[6] Kawamoto H, Kamibayashi K, Nakata Y, Yamawaki K, Ariyasu R, Sankai Y, et al. Pilot study of locomotion improvement using hybrid assistive limb in chronic stroke patients. BMC Neurology 2013;13:141.

[7] Kubota S, Nakata Y, Eguchi K, Kawamoto H, Kamibayashi K, Sakane M, et al. Feasibility of rehabilitation training with a newly developed wearable robot for patients with limited mobility. Archives of Physical Medicine and Rehabilitation 2013;94(6):1080-7.

[8] Watanabe H, Tanaka N, Inuta T, Saitou H, Yanagi H. Locomotion Improvement Using a Hybrid Assistive Limb in Recovery Phase Stroke Patients: A Randomized Controlled Pilot Study. Archives of Physical Medicine and Rehabilitation 2014.

[9] Suzuki K, Mito G, Kawamoto H, Hasegawa Y, Sankai Y. Intention-based walking support for paraplegia patients with Robot Suit HAL. Advanced Robotics 2007;21(12):1441-69.

[10] Kawamoto H, Taal S, Niniss H, Hayashi T, Kamibayashi K, Eguchi K, et al. editors. Voluntary motion support control of Robot Suit HAL triggered by bioelectrical signal for hemiplegia. Engineering in Medicine and Biology Society (EMBC), 2010 Annual International Conference of the IEEE; 2010: IEEE.

[11] Kawamoto H, Sankai Y. Power assist system HAL-3 for gait disorder person. Computers helping people with special needs 2002;19-29.

[12] Kawamoto H, Sankai Y. Power assist system HAL-3 for gait disorder person. Computers helping people with special needs: Springer; 2002;196-203.

[13] Kawamoto H, Sankai Y. Power assist method based on phase sequence and muscle force condition for HAL. Advanced Robotics 2005;19(7):717-34.

[14] Suzuki K, Imada G, Iwaya T, Handa T, Kurogo H. Determinants and predictors of the maximum walking speed during computer-assisted gait training in hemiparetic stroke patients. Archives of Physical Medicine and Rehabilitation 1999;80(2):179-82.

[15] Raphael C, Briscoe C, Davies J, Ian Whinnett Z, Manisty C, Sutton R, et al. Limitations of the New York Heart Association functional classification system and self-reported walking distances in chronic heart failure. Heart (British Cardiac Society) 2007;93(4):476-82.

[16] Aaslund MK, Helbostad JL, Moe-Nilssen R. Walking during body-weight-supported treadmill training and acute responses to varying walking speed and body-weight support in ambulatory patients post-stroke. Physiotherapy Theory and Practice 2013;29(4):278-89.

[17] Berg K, Wood-Dauphinee S, Williams JI. The Balance Scale: Reliability assessment with elderly residents and patients with an acute stroke. Scandinavian Journal of Rehabilitation Medicine 1995;27(1):27-36.

[18] Fugl-Meyer AR, Jaasko L, Leyman I, Olsson S, Steglind S. The post-stroke hemiplegic patient. 1. a method for evaluation of physical performance. Scandinavian Journal of Rehabilitation Medicine 1975;7(1):13-31.

[19] Patterson KK, Gage WH, Brooks D, Black SE, McIlroy WE. Evaluation of gait symmetry after stroke: A comparison of current methods and recommendations for standardization. Gait & Posture 2010;31(2):241-6.

[20] Patterson KK, Gage WH, Brooks D, Black SE, McIlroy WE. Changes in gait symmetry and velocity after stroke: A cross-sectional study from weeks to years after stroke. Neurorehabilitation and Neural Repair 2010;24(9):783-90.

[21] Lewek MD, Bradley CE, Wutzke CJ, Zinder SM. The relationship between spatiotemporal gait asymmetry and balance in individuals with chronic stroke. Journal of Applied Biomechanics 2014;30(1):31-6.

[22] Kratochwill TR, Hitchcock J, Horner R, Levin JR, Odom S, Rindskopf D, et al. Single-case designs technical documentation. What Works Clearinghouse 2010.

[23] Johnson M, Ottenbacher K. Trend line influence on visual analysis of single-subject data in rehabilitation research. Disability & Rehabilitation 1991;13(2):55-9.

[24] Franklin RD, Allison DB, Gorman BS. Design and analysis of single-case research: Psychology Press; 2014.

[25] Sideridis GD, Greenwood CR. Is human behavior autocorrelated? An empirical analysis. Journal of Behavioral Education 1997;7(3):273-93.

[26] Sekiya N, Nagasaki H. Reproducibility of the walking patterns of normal young adults: Test-retest reliability of the walk ratio (step-length/step-rate). Gait & Posture 1998;7(3):225-7.

[27] Sekiya N, Nagasaki H, Ito H, Furuna T. The invariant relationship between step length and step rate during free walking. Journal of Human Movement Studies 1996;30(6):241-57.

[28] Zijlstra W, Rutgers A, Hof A, Van Weerden T. Voluntary and involuntary adaptation of walking to temporal and spatial constraints. Gait & Posture 1995;3(1):13-8.

[29] Suzuki K, Yamada Y, Handa T, Imada G, Iwaya T, Nakamura R. Relationship Between Stride Length and Walking Rate in Gait Training for Hemiparetic Stroke Patients1. American Journal of Physical Medicine & Rehabilitation 1999;78(2):147-52.

[30] Perry J, Davids JR. Gait analysis: Normal and pathological function. Journal of Pediatric Orthopaedics 1992;12(6):815.

[31] Hendrickson J, Patterson KK, Inness EL, McIlroy WE, Mansfield A. Relationship between asymmetry of quiet standing balance control and walking post-stroke. Gait & Posture 2014;39(1):177-81.

[32] Hsu AL, Tang PF, Jan MH. Analysis of impairments influencing gait velocity and asymmetry of hemiplegic patients after

mild to moderate stroke. Archives of Physical Medicine and Rehabilitation 2003;84(8):1185-93.

[33] Olney SJ, Richards C. Hemiparetic gait following stroke. Part I: Characteristics. Gait & Posture 1996;4(2):136-48.

[34] Aruin AS, Rao N, Sharma A, Chaudhuri G. Compelled body weight shift approach in rehabilitation of individuals with chronic stroke. Topics in Stroke Rehabilitation 2012;19(6): 556-63.

[35] Goldie PA, Matyas TA, Evans OM. Gait after stroke: Initial deficit and changes in temporal patterns for each gait phase. Archives of Physical Medicine and Rehabilitation 2001;82(8): 1057-65.

[36] Lotze M, Braun C, Birbaumer N, Anders S, Cohen LG. Motor learning elicited by voluntary drive. Brain 2003;126(4): 866-72.

[37] Pennycott A, Wyss D, Vallery H, Klamroth-Marganska V, Riener R. Towards more effective robotic gait training for stroke rehabilitation: A review. Journal of Neuroengineering and Rehabilitation 2012;9:65.

Magnetic Resonance Imaging 36 (2016) 32–39

Contents lists available at ScienceDirect

Magnetic Resonance Imaging

journal homepage: www.mrijournal.com

A brain phantom for motion-corrected PROPELLER showing image contrast and construction similar to those of in vivo MRI☆

Kousaku Saotome [a,b,*], Akira Matsushita [a,c,1,2], Koji Matsumoto [d,3], Yoshiaki Kato [e,4], Kei Nakai [c,2], Koichi Murata [f,5], Tetsuya Yamamoto [c,2], Yoshiyuki Sankai [a,g,1,5], Akira Matsumura [c,2]

[a] Center for Cybernics Research, University of Tsukuba, 1-1-1 Tennoudai, Tsukuba, Ibaraki 305-8577, Japan
[b] Graduate School of Comprehensive Human Science Majors of Medical Sciences, University of Tsukuba, 1-1-1 Tennoudai, Tsukuba, Ibaraki 305-8577, Japan
[c] Department of Neurosurgery, Faculty of Medicine, University of Tsukuba, 1-1-1 Tennoudai, Tsukuba, Ibaraki 305-8575, Japan
[d] Department of Radiology, Chiba University Hospital, Chiba, Chiba 260-8677, Japan
[e] Diagnostic Imaging Room, Medical Technology Department, Kameda General Hospital, Kamogawa, Chiba 296-8602, Japan
[f] School of Integrative and Global Majors (SIGMA), University of Tsukuba, 1-1-1 Tennoudai, Tsukuba, Ibaraki 305-8573, Japan
[g] Faculty of Engineering, Information, and Systems, University of Tsukuba, 1-1-1 Tennoudai, Tsukuba, Ibaraki 305-8573, Japan

ARTICLE INFO

Article history:
Received 3 July 2016
Revised 6 September 2016
Accepted 5 October 2016
Available online xxxx

Keywords:
Propeller
Phantom
Brain
Motion correction
3-D prototyping technology

ABSTRACT

Purpose: A fast spin-echo sequence based on the Periodically Rotated Overlapping Parallel Lines with Enhanced Reconstruction (PROPELLER) technique is a magnetic resonance (MR) imaging data acquisition and reconstruction method for correcting motion during scans. Previous studies attempted to verify the in vivo capabilities of motion-corrected PROPELLER in real clinical situations. However, such experiments are limited by repeated, stray head motion by research participants during the prescribed and precise head motion protocol of a PROPELLER acquisition. Therefore, our purpose was to develop a brain phantom set for motion-corrected PROPELLER.

Materials and methods: The profile curves of the signal intensities on the in vivo T_2-weighted image (T_2WI) and 3-D rapid prototyping technology were used to produce the phantom. In addition, we used a homemade driver system to achieve in-plane motion at the intended timing. We calculated the Pearson's correlation coefficient (R^2) between the signal intensities of the in vivo T_2WI and the phantom T_2WI and clarified the rotation precision of the driver system. In addition, we used the phantom set to perform initial experiments to show the rotational angle and frequency dependences of PROPELLER.

Results: The in vivo and phantom T_2WIs were visually congruent, with a significant correlation (R^2) of 0.955 ($p < .001$). The rotational precision of the driver system was within 1 degree of tolerance. The experiment on the rotational angle dependency showed image discrepancies between the rotational angles. The experiment on the rotational frequency dependency showed that the reconstructed images became increasingly blurred by the corruption of the blades as the number of motions increased.

Conclusions: In this study, we developed a phantom that showed image contrasts and construction similar to the in vivo T_2WI. In addition, our homemade driver system achieved precise in-plane motion at the intended timing. Our proposed phantom set could perform systematic experiments with a real clinical MR image, which to date has not been possible in in vivo studies. Further investigation should focus on the improvement of the motion-correction algorithm in PROPELLER using our phantom set for what would traditionally be considered problematic patients (children, emergency patients, elderly, those with dementia, and so on).

☆ Grant support: This study was supported by an Industrial Disease Clinical Research Grant from the Ministry of Health, Labor, and Welfare of Japan (no. 14060101-01). The study was also supported by the Japan Authorize Organization for Magnetic Resonance Technological Specialist (JMRTS).

* Corresponding author at: Center for Cybernics Research (CCR), University of Tsukuba, 1-1-1 Tennoudai, Tsukuba, Ibaraki 305-8577, Japan. Tel.: +81 29 853 5858; fax: +81 29 853 5852.
E-mail address: saotome84@gmail.com (K. Saotome).
[1] Tel.: +81 29 853 5858.
[2] Tel.: +81 29 853 3220.
[3] Tel.: +81 43 222 7171.
[4] Tel.:+81 4 7092 2211.
[5] Tel.:+81 29 853 6246.

http://dx.doi.org/10.1016/j.mri.2016.10.003
0730-725X/

1. Introduction

A fast spin-echo sequence based on the Periodically Rotated Overlapping Parallel Lines with Enhanced Reconstruction (PROPELLER) technique is a magnetic resonance imaging (MRI) data acquisition and reconstruction method for correcting motion during scans [1–3]. Recent advances in motion-correction techniques using PROPELLER have made it possible to reduce artifacts induced by in-plane rotation and translation motion [4–6]. Therefore, PROPELLER has been extensively used in many regions of the body [7–10]. Particularly in the brain, PROPELLER plays an important role in correcting unconscious movements in unsedated pediatric patients, acute stroke patients, and others [11–13].

In previous studies, experiments on the performance of motion-corrected PROPELLER have been attempted using a geometric phantom, which features a simple construction that includes high image contrast [4,5,14]. Although any region of the human body shows complicated image contrast and construction, studies using a phantom that includes image contrasts and construction similar to the target region have not been reported at the time of this study. To verify the capability of motion-corrected PROPELLER in real clinical situations, in vivo experiments have also been attempted. However, such experiments are limited by repeated, stray head motion by research participants during the prescribed and precise head motion protocol of a PROPELLER acquisition [4,6]. Such unsolicited motion has complicated the understanding of the accuracy of the data acquisition method and the motion correction algorithm for PROPELLER. To solve this problem, we need to produce a complex phantom that looks like a brain on a Magnetic Resonance (MR) image and takes this unsolicited motion into account.

Recent advances in 3-dimensional (3-D) rapid prototyping technology have allowed the printing of highly complex structures derived from precise computer data [15–22]. Although this technology has the potential to allow us to develop high-definition MRI phantoms, the field has not been fully developed. We used a 3-D printer to attempt to produce a phantom that shows image contrast and construction similar to the T_2-weighted image (T_2WI) of the brain. In addition, we developed a driver system to move the phantom precisely.

In this paper, we describe the process whereby we created the phantom and calculated the correlation coefficient between the phantom and in vivo MR images. Moreover, we verified the precision of our homemade driver system. We also performed initial experiments on the rotational angle and frequency dependencies of motion-corrected PROPELLER using our phantom and driver system (phantom set).

2. Materials and methods

2.1. Process of creating the phantom

2.1.1. MRI acquisition for the in vivo image

This study was approved by the institutional review board and ethics committee (no. 870) of the University of Tsukuba, and written informed consent to participate in the study was obtained from the research participant. The axial brain T_2WI of a healthy volunteer (36-year-old woman) without any history of severe head trauma or neuropsychiatric disorders was acquired as the in vivo image (Fig. 1). All imaging in this study was performed using an Achieva dStream 3.0 T-TX MRI system (release 5.1.7.0; Philips Medical Systems, Eindhoven, The Netherlands) combined with a 32-channel SENSE head coil. Axial T_2WIs positioned parallel to the intercommissural (AC–PC) line were acquired covering the whole brain using a fast spin-echo sequence (repetition time [TR] = 4500 ms, echo time [TE] = 90 ms, slice thickness = 6 mm, field of view =230 mm, pixel resolution =0.51 × 0.51 mm).

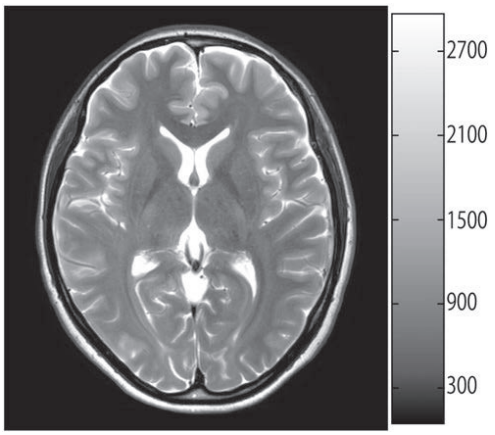

Fig. 1. In vivo T_2-weighted image (T_2WI). The axial brain T_2WI fitting of the intercommissural (AC–PC) line of a healthy volunteer (36-year-old woman) using a fast spin-echo sequence.

2.1.2. Digital imaging and communications in medicine (DICOM) data conversion and printing

Matlab R2015b (MathWorks, Natick, MA, USA) was used to process the DICOM data of the in vivo T_2WI. Fig. 2a shows the profile of the signal intensity of all pixels in the in vivo T_2WI on an x-y plane. Fig. 2b shows the profile curve of the line defined through both posterior limbs of the internal capsules as a typical case. The signal intensity (I) was converted into thickness of the printed layer stack (T) as

$$T = (I_{max} - I)\left\{\left(T_{slice}/T_{layer}\right)/I_{max}\right\}T_{layer} + T_{bottom}$$

where I_{max} is the maximum signal intensity of the in vivo T_2WI, T_{slice} is the slice thickness of the T_2WI, T_{layer} is the thickness of a printed layer, and T_{bottom} is the thickness of the bottom of the phantom. In this study, each value was defined as follows: I_{max} = 2725, T_{slice} = 6 mm, T_{layer} = 0.016 mm, and T_{bottom} = 5 mm. Fig. 2c shows the cross section of the printed layer stack after conversion. Next, the surface configuration of the printed material (indicated by a heavy line in Fig. 2c) was produced to correspond to the configuration of the flipped vertical profile curve shown in Fig. 2b. The converted data were sent to the 3-D printer (Objet Eden350V; Stratasys, Eden Prairie, MN, USA), and printed on plastic (FullCure810 Vero Clear), which has no MR signal. Then, agarose gel was poured; its concentration, T_2-relaxation time, and T_1-relaxation time were 0.4%, 168 ms and 1667 ms, respectively. After enough agarose gel had been poured in to fill the convexo-concave surface of the printed phantom, it was left in the MRI room for 24 h at room temperature to polymerize.

2.1.3. MRI acquisition of the phantom image

The phantom was set in a horizontal position on the head coil. The same image parameters as those for the in vivo image, except for the slice orientation, were used to acquire the T_2WI of the phantom; the in vivo image was acquired on the axial plane. The slice plane was carefully set on the slice position as shown in Fig. 2c. We then calculated the Pearson's correlation coefficient (R^2) between the signal intensities of the in vivo T_2WI and the phantom T_2WI after registration, including rotation and translation, using Matlab R2015b.

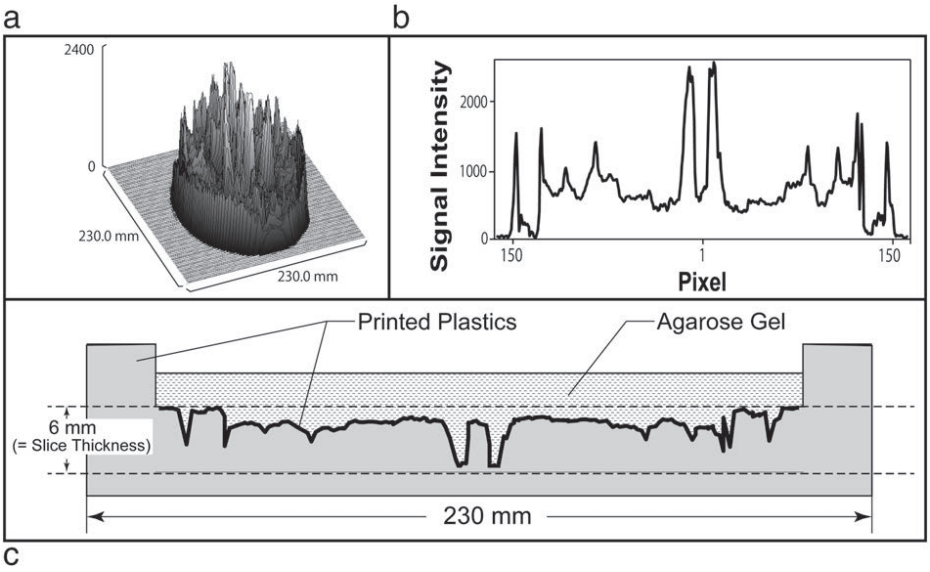

Fig. 2. Phantom design. (a) The profile of the signal intensity of all pixels on an x-y plane in the in vivo T_2-weighted image (T_2WI). (b) Profile curve of the line defined through both posterior limbs of the internal capsule as a typical case. (c) Cross section of the phantom on the line in (b). The signal intensities of the in vivo T_2WI were converted to a depth of 0 to 6 mm by the conversion equation in the text. The heavy line shows the surface configuration of the printed material, which corresponds to the configuration of the flipped vertical profile curve in (b). The gray painted region shows the printed plastics, and the dotted pattern shows the poured agarose gel. The frame was built around the phantom to allow agarose gel to be poured in. The distance between the broken lines was 6 mm, which corresponds to the slice thickness for the T_2WI of the phantom acquisition. The slice position was fitted to this area. The diameter of the phantom is 230 mm.

2.2. Driver system

2.2.1. Structure

We developed a driver system that precisely moves the phantom from outside the MRI gantry. The driver system consists of a supporting table, turntable, and 24 ball bearings ($\varphi = 12$ mm), all made of nonmagnetic materials (Fig. 3a). The diameter of the driver system is 23 cm and can rotate in the head coil. Fig. 3b shows the arrangement of the phantom and driver system in the MRI gantry. The phantom was set securely on the driver system with the vacuumed pillow on the head coil. We marked the side of the turntable every 5° and attached 2 strings to the turntable to rotate it from outside the MRI gantry.

2.2.2. MRI examination for precision

To verify the rotation precision of the driver system, we acquired a T_2WI of the phantom in the pre- and post-rotation positions. At the beginning, the turntable with the phantom was set to zero degree using the turntable marks, and a T_2WI of the phantom was acquired. Next, it was reset to 60° as indicated by the turntable marks, and a T_2WI of the phantom was acquired again. The 60° reset was chosen because in the pre-examination, the maximum limitation angle of the volunteer's head rotation from the face forward to another side was approximately 60° (58°) in the head coil of the MRI system. Therefore, we thought that if we could accurately rotate the phantom to 60° within approximately 1 s, we could also rapidly rotate it to any angle lower than 60° in an equally short time. This examination was repeated 10 times, and the rotation angles of the medial line of the brain in the pre- and post-rotation positions were measured on the T_2WIs to calculate the mean and standard deviation.

2.3. Initial experiment for motion-corrected PROPELLER

Using our phantom set, we performed initial experiments on the rotational angle and frequency dependencies of motion-corrected PROPELLER. All images were acquired using single-slice, coronal, fast spin-echo T_2WI-based PROPELLER with motion correction (eg, MultiVane). The sequence had a TR/TE of 4000/111 ms, field of view of 250 mm^2, slice thickness of 6 mm, resolution of 0.78×0.78 mm^2, 30 turbo spin echo factors, MultiVane percentages of 160%, and total acquisition time of 72 s. Eighteen blades were collected for a single slice (ie, number of TR = 18). The original motion-correction algorithm for the MultiVane sequence (from Philips) was used in the experiments. This sequence included the data acquisition and dead times. The data acquisition time was defined as the time interval for onset of RF pulse, gradient reading, and echo sampling; which was roughly 500 ms. The dead time was defined as the time interval between data acquisition times; this was about 3500 ms, as shown in Fig. 4. The phantom was rotated from zero to any degree once during a dead time in a PROPELLER acquisition without any corrupted blades; the acquired blade data show 2 image groups (zero degree and any degree). Next, the images of a single angle were corrected to another angle by the motion-correction algorithm, with the expectation that the performances of image correspondence by motion correction would differ depending on the rotation angle [2]. On the other hand, when the phantom was rotated once from zero to any degree during the acquisition time, one of the acquired blades suffered from severe corruption. Then, the corrupt data degraded the image quality after correction and it was expected that the adverse implications of corruption would differ depending on the rotation frequency [4,21]. To investigate these 2 dependences described above, reproducibility and precise rotation at the intended timing are essential. We performed the following 2 initial experiments on the rotational angle and frequency dependences of motion-corrected PROPELLER using our phantom set.

2.3.1. Rotational angle dependence

Twelve trials were performed to show the rotational angle dependence. At the beginning of a PROPELLER acquisition, the phantom was set at the zero-degree position, and this position was maintained for the first half of the acquisition (ie, 9 of 18 TRs). When the data acquisition in the ninth TR was finished, the phantom was

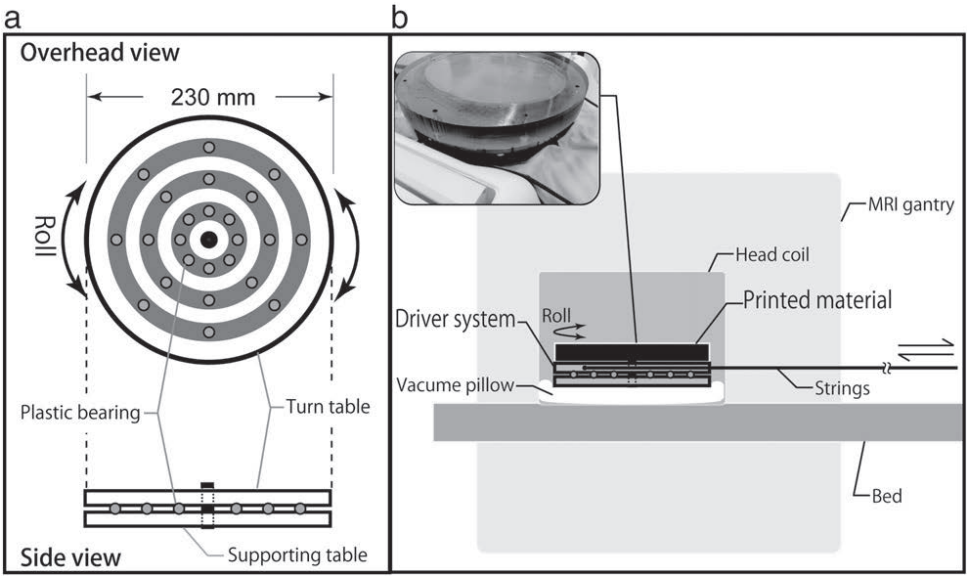

Fig. 3. The homemade driver system. (a) The overhead and side views of the driver system. The diameter of the driver system is 230 mm. It consists of a supporting table, turntable, and 24 ball bearings ($\varphi = 12$ mm) with glycerin, which are made of nonmagnetic materials and able to rotate smoothly. (b) The arrangement of the phantom and the driver system in the MRI gantry. The printed phantom was set firmly on the driver system, which was set on the vacuumed pillow on the head coil. Marks were made every 5° on the side of the turntable, and the 2 strings were attached to the turntable to rotate it from outside the MRI gantry.

then rotated counterclockwise from zero by α degrees (α: 5, 10, 15, 20, 25, 30, 35, 40, 45, 50, 55, 60) during the dead time of the ninth TR (Fig. 4). The phantom was rotated to each degree by the experimenter when the MRI sound stopped at the beginning of the dead time. Then, the other experimenter confirmed that the phantom had stopped before the next MRI sound. After the rotation, the phantom was maintained at the same position until the end of the acquisition. Then, both images with and without motion correction were reconstructed.

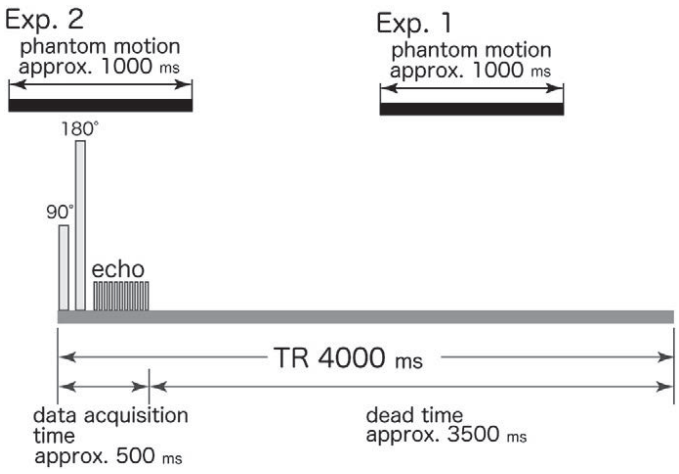

Fig. 4. Timing to rotate the phantom in the initial experiments (experiments 1 and 2) for motion-corrected PROPELLER. This figure shows the simple pulse sequence chart of a single slice fast spin-echo T_2WI-based PROPELLER (TR = 4000 ms). This sequence included the data acquisition and dead times. The data acquisition time is defined as the time interval for onset of RF pulse applying, gradient reading, and echo sampling; it takes about 500 ms. The dead time is defined as the time interval between the data acquisition times; it takes about 3500 ms. In experiment 1, the phantom was rotated clockwise from zero during the dead time for about 1000 ms. On the other hand, in experiment 2, the phantom was rotated during the data acquisition time for about 1000 ms.

2.3.2. Rotational frequency dependence

Nineteen trials were performed to show the rotational frequency dependence. At the beginning of a PROPELLER acquisition, the phantom was set at the zero-degree position. In the first trial, the phantom was kept at the same position throughout the PROPELLER acquisition as a no-motion image. In the second trial, the phantom was rotated once during the first blade acquisition—from zero degree to 30°—and it was maintained at the same position through to the end of the PROPELLER acquisition. In the third trial, the phantom was rotated twice during the first and second blade acquisitions—from zero degree to 30°—and re-rotated from 30° to zero degree, and it was maintained at the same degree position through to the end of the PROPELLER acquisition (Fig. 4). Thus, the number of bipolar motions during the blade acquisitions increased gradually at each trial, and consequently, the phantom was rotated 18 times during all the blade acquisitions in the 19th trial. The experimenter attempted to rotate the phantom about 250 ms before the next MRI sound in the acquisition time, which was guided by sound signals using a metronome. To show if the degree by which the blade data corruption was altered by motion, the correlation coefficient between the T_2WI without motion and each T_2WI with motion was calculated using the same method as that described in Section 2.1.3.

3. Results

Fig. 5a and b shows a photograph of the printed material, and Fig. 5c shows a photograph of the printed material with agarose gel. Fig. 6 shows the T_2WI of the phantom. We can see that the in vivo T_2WI in Fig. 1 and the T_2WI of the phantom were in very good agreement. Fig. 7 is the scatterplot showing the correlation between the signal intensities of the in vivo T_2WI and the phantom T_2WI. There was a significant correlation between these images ($R^2 = 0.955$, $p < .001$). In the experiment on the rotation precision of the driver system, the mean ± standard deviation of the rotation angle of the medial line of the brain was 59.7 ± 0.28°, thus showing high precision as well as accuracy. Furthermore, Fig. 8a-l and a'-l' shows the reconstructed image without and with motion correction,

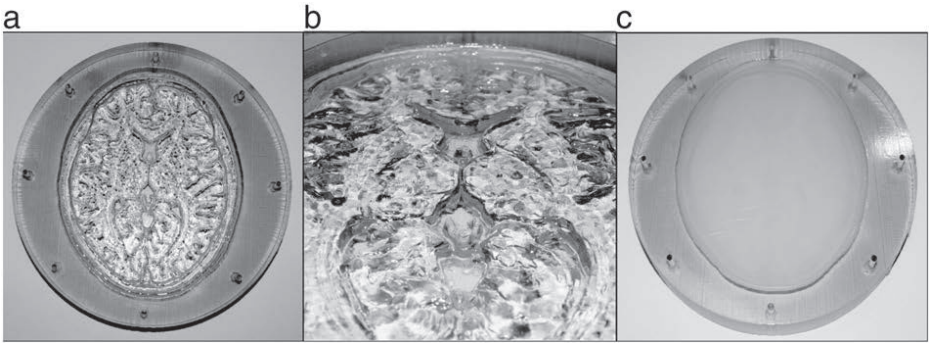

Fig. 5. Photographs of the printed phantom. (a) Without agarose gel; (b) low-angled close-up of center area; (c) with agarose gel.

respectively, in the experiment on rotational angle dependence. Fig. 8a", g" and l" shows the zoomed-in areas from the upper left corners of a', g' and l', respectively. The reconstructed images without motion correction in Fig. 8a-l show the bipolarization at zero and α degrees, respectively. In contrast, the reconstructed images with motion correction in Fig. 8a'-l' show that all the bipolar images were corrected at the zero-degree position in general, but the image discrepancies became increasingly noticeable as the rotational angle became larger. Fig. 9a–r shows each reconstructed image with motion correction, and Fig. 10 shows the correlation coefficient between the T_2WI without motion and each T_2WI with motion with respect to rotational frequency dependence. These results show that the reconstructed images became increasingly blurred by the corruption of the blades as the number of motions increased.

4. Discussion

In this study, we used the profile curves of the signal intensities on the in vivo T_2WI and 3-D rapid prototyping technology to produce a novel phantom for motion-corrected PROPELLER showing image contrasts and construction similar to the in vivo T_2WI. In addition, we used a homemade driver system to achieve the in-plane motion of the phantom at the intended timing, which is considered difficult in in vivo studies. We calculated the correlation coefficient between the in vivo T_2WI shown in Fig. 1 and the phantom T_2WI shown in Fig. 6 and clarified the rotational accuracy of the driver system. The in vivo and phantom T_2WIs showed close congruency, as evidenced by the resulting $R^2 = 0.955$ ($p < .001$). In addition, the driver system worked with objective rotation angles. Moreover, we performed initial experiments showing the rotational angle and frequency dependencies of motion-corrected PROPELLER using our phantom set. The initial experiment on the rotational angle dependence showed image discrepancies among the rotation angles. Furthermore, the rotational frequency dependence showed a graded increase from the adverse effects of the corruption data. Therefore, our phantom set has the potential to investigate the capability of motion-corrected PROPELLER in real clinical situations.

Our process to create the phantom is for a single slice. The motion-correction algorithm works for in-plane motion; therefore, we consider that this single-slice acquisition will play an adequate role in understanding the capability of motion-corrected PROPELLER in-plane [4,6].

Our homemade driver system can perform rotation at the objective angles by virtue of the manual pulling of the two strings attached to the turntable. This means that simple in-plane rotation movement can be implemented to simulate a patient's head rotation. However, for future cases in which complex rotations such as random motion are needed, the driver system needs to be improved to allow automatic operation using an actuator (such as an ultrasonic motor) by receiving the onset signal of each TR from an MR unit. In the present study, the accuracy of the angular velocities was not guaranteed. Particularly in the experiment on the rotational frequency-dependence, the inaccuracy of the angular velocities might have affected the quality of the images after each blade

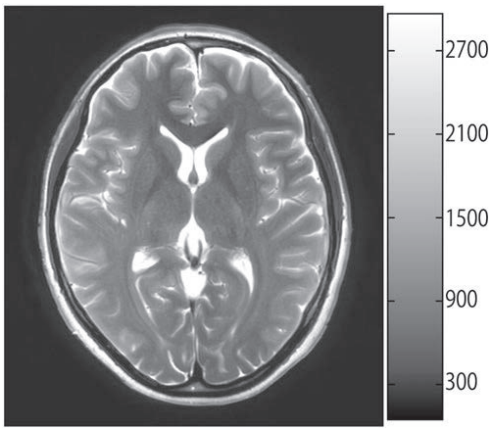

Fig. 6. T_2-weighted image (T_2WI) of the phantom. The image was acquired by using the same image parameters as those of the in vivo T_2WI. This image was in excellent agreement with the in vivo T_2WI (shown in Fig. 1).

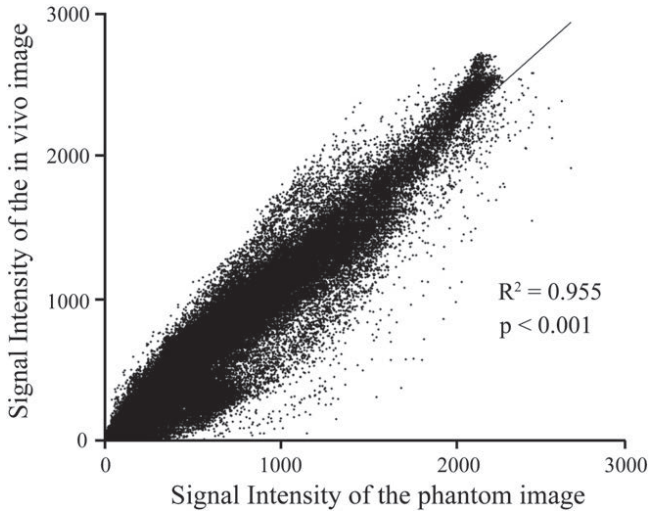

Fig. 7. Correlation between the signal intensities of the in vivo T_2WI and the phantom T_2WI. There was a significant correlation between these images ($R^2 = 0.955$, $p < .001$).

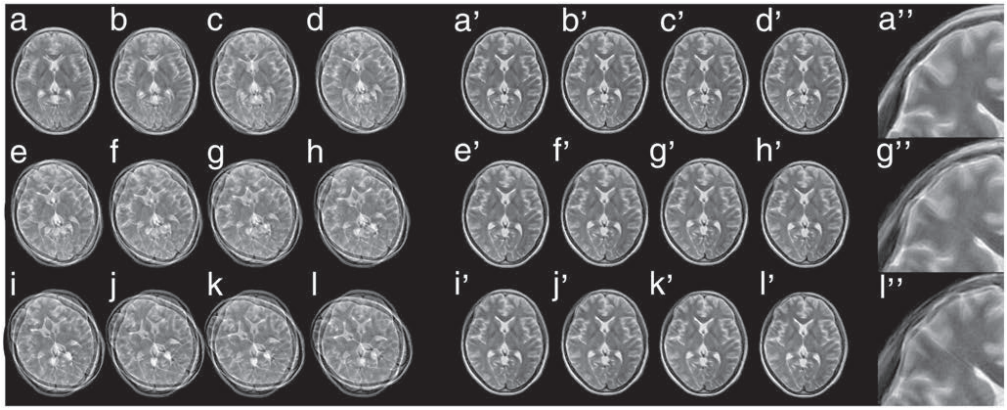

Fig. 8. Results of the rotational angle dependence. (a)–(l) Reconstructed images without motion correction in each 5° rotation: (a) 5, (b) 10, (c) 15, (d) 20, (e) 25, (f) 30, (g) 35, (h) 40, (i) 45, (j) 50, (k) 55, (l) 60°. (a')–(l') Reconstructed images with motion correction in each 5° rotation. (a"), (g"), (l"): zoomed-in areas from the upper left corners of (a'), (g'), and (l'), respectively.

correction. This limitation might be also solved by using the above automatic operation system.

Some methods for developing anatomic structures derived from CT or MRI data of a human subject using 3-D rapid prototyping technology have been suggested by other researchers. Ogden et al. recently examined the factors affecting the dimensional accuracy of 3-D printed material derived from helical CT scan data [21]. Burfeindt et al. recently produced a 3-D-printed breast phantom derived from 3-D T_1-weighted fast field echo MRI data for use in pre-clinical experimental microwave imaging studies [16]. These studies were focused on duplicating the target anatomic structures. In contrast, our method is focused on duplicating the construction and image contrast on an MR image. Therefore, we proposed the following process to create a phantom derived from an in vivo T_2WI: (1) converting the profile curves of the MR signal intensities to the surface configuration of the phantom, (2) printing the plastic phantom, (3) pouring agarose into the phantom. The MRI intensity in a particular voxel depends on the entire content of the corresponding anatomic volume and the sequence that is used. If only a single tissue type is present in the voxel, the signal intensity will be characterized as that tissue type. However, if more than one tissue type is present, the signal will be a combination of the contributions of the different tissues. This is known as the partial volume effect [23]. Therefore, the T_1, T_2, and T_2* relaxation times of the phantom are different from the in vivo ones although the signal intensities of the phantom T_2WI were almost the same as those of the in vivo T_2WI as shown Fig. 7. As shown in Fig. 6, the partial volume effect between the printed plastic and agarose gives various and consecutive signal intensities. Thus, our novel method allows not only the acquisition of similar image contrasts, but also the presentation of a similar structure to the in vivo T_2WI.

In previous studies, the capabilities of motion-correction algorithms with PROPELLER were investigated using geometric phantoms, which have a simple construction including high image contrast [4,5,14]. These phantoms helped to understand PROPELLER'S capabilities in simulation. In vivo studies have been previously performed in addition to phantom studies to understand PROPELLER'S capabilities in real clinical situations [4,5,14]. However, in vivo studies have the essentially unsolvable problem of the difficulty of ensuring that the volunteer achieves the precise in-plane motion of

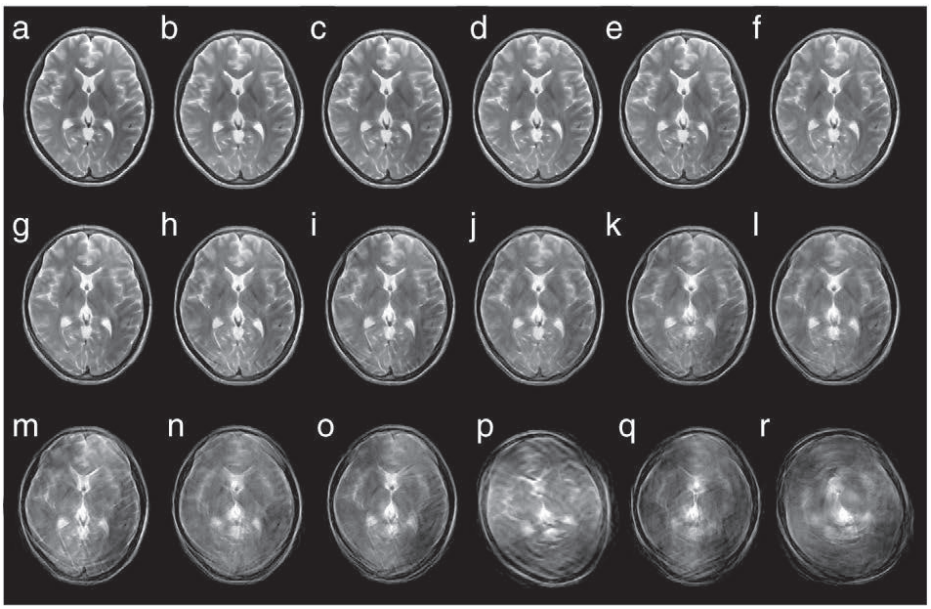

Fig. 9. Results for the rotational frequency dependence. (a)–(r) Reconstructed images with motion correction for each of the 18 rotations.

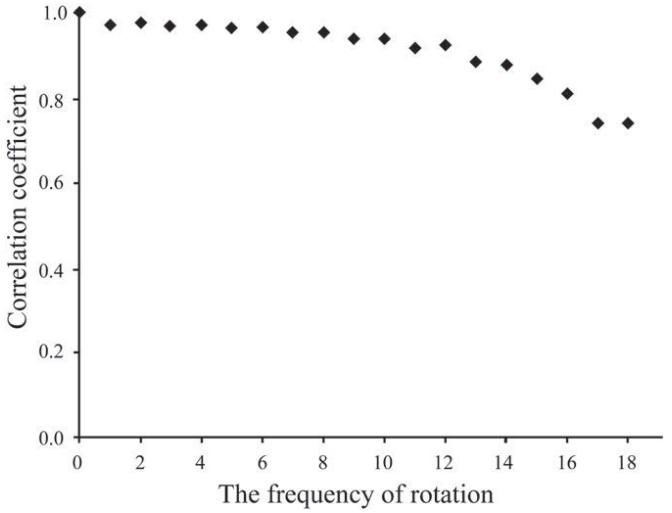

Fig. 10. Correlation coefficients between the T_2WI without motion and each T_2WI with motion in the experiment on rotational frequency dependence.

the head. In past in vivo studies, although the human volunteer was instructed to move his or her head in the scanner to avoid the through-plane motion, there was no way of ensuring an exact movement of the head. If a motion-correction algorithm for PROPELLER was developed based on motion-corrected images with unsolicited motion (such as a through-plane motion), it might be misleading. Liu et al., who recently developed robust reference generation methods to improve PROPELLER reconstruction in both phantom and in vivo experiments, could not obtain desirable results in the in vivo experiments when compared with the phantom experiments [4]. They stated that the volunteer's motion might be insufficient to fully examine their method's performance. They also stated that further systematic clinical studies are warranted to test the method's ability in future studies. The results of our initial experiments using our phantom set showed the motion-corrected images and the correlation coefficients avoiding through-plane motion at the intended timing with the image contrast and construction similar to those of in vivo T_2WI. Namely, our phantom set could perform systematic experiments with a real clinical MR image, which has thus far not been possible in in vivo studies. Thus, our phantom set has the potential to be a powerful tool for future investigations. Further investigations using our phantom set might allow for revision of previous algorithms and development of more robust motion-corrected PROPELLER.

Our process of making a phantom can duplicate not only the brain of a healthy volunteer but also brains with a clinical lesion. Our method requires no change other than selecting a brain T_2WI involving a lesion for the in vivo image. Our method also has the potential to allow comparison of small lesion detectability in some algorithms or among different MRI units. Additionally, although our process showed only the case of T_2WI, theoretically some modifications might be adaptable to a T_1-weighted image and a Fluid Attenuation Inversion Recovery image. For example, as for the phantom of the T_1WI, we select a T_1WI as the in vivo image instead of a T_2WI and, instead of agarose gel, fill the printed material with baby oil or gadolinium diluted with saline, which shows high intensity on T_1WI. Therefore, our novel process of making a phantom might allow for creation of a brain phantom that simulates specific lesions on the image contrasts, which could not be achieved in previous studies. Further investigation should be focused on the improvement of the motion-correction algorithm in PROPELLER using our phantom set for uncooperative patients in emergency situations, unsedated children, or elderly persons, including those with dementia [24–30]. Moreover, the motion-corrected PROPELLER has been used not only generally for the brain but also clinically for the neck, shoulder, abdomen, and others [8–10,31]. In shoulder MRI, which often poses difficulties because of the rise and fall of the patient's breathing, developing an adapted motion-correction algorithm might contribute to detecting the presence of a high signal on the rotator cuff [32]. Our process of making a phantom is adaptable to any region or section of the human body. Therefore, it might be useful to develop a suitable algorithm for multiple target regions in future studies.

5. Conclusions

We developed a phantom set consisting of a printed plastic phantom with agarose and a driver system for motion-corrected PROPELLER. The phantom was produced according to a novel method using a partial volume effect that showed image contrasts and construction similar to the in vivo T_2WI in an MRI. In addition, our homemade driver system achieved precise in-plane motion at the intended timing. Our proposed phantom set could perform systematic experiments with a real clinical MR image, which to date has not been possible in in vivo studies. Therefore, our phantom set might enable further investigation of motion-correction algorithms for PROPELLER. Further investigation should be focused on improvement of the motion-correction algorithm in PROPELLER using our phantom set for what would traditionally be considered problematic patients (children, emergency patients, elderly, those with dementia, and so on).

Acknowledgments

We are grateful to Yoshihiro Ozaki, Tomoyuki Hasegawa, and Hiroki Tsuchiya for assistance with the experiments. Thanks also to Philips Electronics Japan, special application staff, Akira Suwa, Chihiro Naito, and Yukiko Fukuma, for providing information about the PROPELLER technique. We also thank Flaminia Miyamasu and Bryan Mathis (Editor in the Life Sciences [ELS], Medical English Communications Center, University of Tsukuba) for grammatical revision. Finally, we wish to express our appreciation to the Reviewer's insightful comments, which have helped us improve the paper significantly.

References

[1] Forbes KP, Pipe JG, Bird CR, Heiserman JE. PROPELLER MRI: clinical testing of a novel technique for quantification and compensation of head motion. J Magn Reson Imaging 2001;14:215–22.
[2] Pipe JG. Improved in-plane motion correction for PROPELLER MRI. Proceedings of the 9th annual meeting of ISMRM, Glasgow, Scotland; 2001 [Abstract 743].
[3] Pipe JG. Motion correction with PROPELLER MRI: application to head motion and free-breathing cardiac imaging. Magn Reson Med 1999;42:963–9.
[4] Liu Z, Zhang Z, Ying K, Yuan C, Guo H. Improved motion correction in PROPELLER by using grouped blades as reference. J Magn Reson Imaging 2014;39:700–7.
[5] Pipe JG, Gibbs WN, Li Z, Karis JP, Schar M, Zwart NR. Revised motion estimation algorithm for PROPELLER MRI. Magn Reson Med 2014;72:430–7.
[6] Tamhane AA, Arfanakis K. Motion correction in periodically-rotated overlapping parallel lines with enhanced reconstruction (PROPELLER) and turboprop MRI. Magn Reson Med 2009;62:174–82.
[7] Deng J, Miller FH, Salem R, Omary RA, Larson AC. Multishot diffusion-weighted PROPELLER magnetic resonance imaging of the abdomen. Investig Radiol 2006; 41:769–75.
[8] Hirokawa Y, Isoda H, Maetani YS, Arizono S, Shimada K, Okada T, et al. Hepatic lesions: improved image quality and detection with the periodically rotated overlapping parallel lines with enhanced reconstruction technique–evaluation of SPIO-enhanced T2-weighted MR images. Radiology 2009;251:388–97.
[9] Hirokawa Y, Isoda H, Maetani YS, Arizono S, Shimada K, Togashi K. Evaluation of motion correction effect and image quality with the periodically rotated overlapping parallel lines with enhanced reconstruction (PROPELLER) (BLADE) and parallel imaging acquisition technique in the upper abdomen. J Magn Reson Imaging 2008;28:957–62.
[10] Ohgiya Y, Suyama J, Seino N, Takaya S, Kawahara M, Saiki M, et al. MRI of the neck at 3 tesla using the periodically rotated overlapping parallel lines with enhanced reconstruction (PROPELLER) (BLADE) sequence compared with T2-weighted fast spin-echo sequence. J Magn Reson Imaging 2010;32:1061–7.

[11] Chou MC, Huang TY, Chung HW, Hsieh TJ, Chang HC, Chen CY. Q-ball imaging with PROPELLER EPI acquisition. NMR Biomed 2013;26:1723–32.
[12] Forbes KP, Pipe JG, Karis JP, Farthing V, Heiserman JE. Brain imaging in the unsedated pediatric patient: comparison of periodically rotated overlapping parallel lines with enhanced reconstruction and single-shot fast spin-echo sequences. AJNR Am J Neuroradiol 2003;24:794–8.
[13] Forbes KP, Pipe JG, Karis JP, Heiserman JE. Improved image quality and detection of acute cerebral infarction with PROPELLER diffusion-weighted MR imaging. Radiology 2002;225:551–5.
[14] Holmes JH, Beatty PJ, Rowley HA, Li Z, Gaddipati A, Zhao X, et al. Improved motion correction capabilities for fast spin echo T1 FLAIR propeller using non-cartesian external calibration data driven parallel imaging. Magn Reson Med 2012;68:1856–65.
[15] Cao Y, Vacanti JP, Paige KT, Upton J, Vacanti CA. Transplantation of chondrocytes utilizing a polymer-cell construct to produce tissue-engineered cartilage in the shape of a human ear. Plast Reconstr Surg 1997:297–302.
[16] Burfeindt MJ, Colgan TJ, Mays RO, Shea JD, Behdad N, Van Veen BD, et al. MRI-derived 3-D-printed breast phantom for microwave breast imaging validation. IEEE Antennas Wirel Propag Lett 2012;11:1610–3.
[17] Giannatsis J, Dedoussis V. Additive fabrication technologies applied to medicine and health care: a review. Int J Adv Manuf Technol 2007;40:116–27.
[18] Gibson I, editor. Advanced manufacturing technology for medical applications: reverse engineering, software conversion and rapid prototyping. John Wiley & Sons; 2006.
[19] Hopkinson N, Hague R, Dickens P, editors. Rapid manufacturing: an industrial revolution for the digital age. John Wiley & Sons; 2006.
[20] Khalyfa A, Vogt S, Weisser J, Grimm G, Rechtenbach A, Meyer W, et al. Development of a new calcium phosphate powder-binder system for the 3D printing of patient specific implants. J Mater Sci Mater Med 2007;18:909–16.
[21] Ogden KM, Aslan C, Ordway N, Diallo D, Tillapaugh-Fay G, Soman P. Factors affecting dimensional accuracy of 3-D printed anatomical structures derived from CT data. J Digit Imaging 2015;28:654–63.
[22] Weng Y, Cao Y, Arevalo C, Vacanti MP, Vacanti CA. Tissue-engineered composites of bone and cartilage for mandible condylar reconstruction. J Oral Maxillofac Surg 2001;59:185–90.
[23] Gonzalez Ballester MA, Zisserman AP, Brady M. Estimation of the partial volume effect in MRI. Med Image Anal 2002;6:389–405.
[24] Barzo P, Marmarou A, Fatouros P, Hayasaki K, Corwin F. Contribution of vasogenic and cellular edema to traumatic brain swelling measured by diffusion-weighted imaging. J Neurosurg 1997;87:900–7.
[25] Yoshii F, Kozuma R, Takahashi W, Haida M, Takagi S, Shinohara Y. Magnetic resonance imaging and 11C-N-methylspiperone/positron emission tomography studies in a patient with the interval form of carbon monoxide poisoning. J Neurol Sci 1998;160:87–91.
[26] Yagishita A, Nakano I, Ushioda T, Otsuki N, Hasegawa A. Acute encephalopathy with bilateral thalamotegmental involvement in infants and children: imaging and pathology findings. AJNR Am J Neuroradiol 1995;16:439–47.
[27] Arca G, Pacheco E, Alfonso I, Duchowny MS, Melnick SJ. Characteristic brain magnetic resonance imaging (MRI) findings in neonates with tuberous sclerosis complex. J Child Neurol 2006;21:280–5.
[28] Onuma A, Miyabayashi S, Iinuma K, Tada K, Yamada K, Matsuzawa T. Comparative appraisal of CT scan and MRI in the diagnosis of Leigh encephalomyelopathy in two siblings. J Child Neurol 1987;2:324–6.
[29] Otsubo H, Hwang PA, Jay V, Becker LE, Hoffman HJ, Gilday D, et al. Focal cortical dysplasia in children with localization-related epilepsy: EEG, MRI, and SPECT findings. Pediatr Neurol 1993;9:101–7.
[30] Shiomi M. Influenzal encephalopathy. Nihon Rinsho 2003(61 Suppl 2):100–6.
[31] Ciet P, Serra G, Bertolo S, Spronk S, Ros M, Fraioli F, et al. Assessment of CF lung disease using motion corrected PROPELLER MRI: a comparison with CT. Eur Radiol 2016;26:780–7.
[32] Deutsch A, Altchek DW, Veltri DM, Potter HG, Warren RF. Traumatic tears of the subscapularis tendon. Clinical diagnosis, magnetic resonance imaging findings, and operative treatment. Am J Sports Med 1997;25:13–22.

NeuroRehabilitation xx (20xx) x–xx
DOI:10.3233/NRE-161424
IOS Press

Effects of gait training using the hybrid assistive limb® in recovery-phase stroke patients: A 2-month follow-up, randomized, controlled study

Hiroki Watanabe[a], Ryohei Goto[b], Naoki Tanaka[c], Akira Matsumura[d] and Hisako Yanagi[a,*]
[a]*Department of Medical Science and Welfare, Graduate School of Comprehensive Human Sciences, University of Tsukuba, Tsukuba, Japan*
[b]*Department of Primary Care and Medical Education, Graduate School of Comprehensive Human Sciences, University of Tsukuba, Tsukuba, Japan*
[c]*Department of Rehabilitation, Tsukuba Memorial Hospital, Tsukuba, Japan*
[d]*Department of Neurosurgery, Faculty of Medicine, University of Tsukuba, Tsukuba, Japan*

Abstract.
BACKGROUND: Gait training using the Hybrid Assistive Limb® (HAL®) may have beneficial effects on post-stroke gait function and independent walking. However, the long-term and medium-term efficacies of gait training using HAL® in stroke patients remain unclear.
OBJECTIVE: To compare the medium-term efficacy of gait training using a single-leg version of the Hybrid Assistive Limb® (HAL®) on the paretic side with conventional gait training (CGT) in recovery-phase stroke patients.
METHODS: Twenty-four post-stroke participants (HAL® group: $n = 12$, CGT group: $n = 12$) completed the trial. Over 4 weeks, all participants received twelve 20-min sessions of either HAL® (using the single-leg version of HAL® on the paretic side) or conventional (performed by skilled and experienced physical therapists) gait training. Outcome measures were evaluated prior to training, after 12 sessions, and at 8 and 12 weeks after intervention initiation. Functional Ambulation Category (FAC) was the primary outcome measure.
RESULTS: The HAL® group showed significant improvement in FAC after 12 sessions, and at 8 and 12 weeks compared to the conventional group ($P = 0.02$).
CONCLUSIONS: The results suggested that a gait training program based on HAL® may improve independent walking more efficiently than CGT at 1 and 2 months after intervention.

Keywords: Exoskeleton device, rehabilitation, robotics, stroke, walking

1. Introduction

The restoration of independent walking is one of the major goals of post-stroke rehabilitation (Dobkin, 2005). Several studies have investigated the effects of automated electromechanical and robotic-assisted gait training devices for post-stroke improvement

*Address for correspondence: Hisako Yanagi, MD, PhD, Department of Medical Science and Welfare, Faculty of Medicine, University of Tsukuba, 1-1-1 Tennodai, Tsukuba, Ibaraki 305-8577, Japan. Tel.: +81 29 853 3496; Fax: +81 29 853 3039; E-mail: hyanagi@md.tsukuba.ac.jp.

in walking (Geroin et al., 2013; Mehrholz, Elsner, Werner, Kugler, & Pohl, 2013). An exoskeleton, the Robot Suit Hybrid Assistive Limb® (HAL®) has been developed to assist voluntary control of knee and hip joint motion by detecting very weak bioelectric signals on the surface of the skin (Lee & Sankai, 2005). The single-leg version of the HAL® is a new wearable robot for patients with hemiplegia that has the cybernic voluntary control mode and the cybernic autonomous control mode (Kawamoto, & Sankai, 2002; Kawamoto, Hayashi, Sakurai, Eguchi, & Sankai, 2009). The cybernic voluntary control mode provides physical support and actuation according to the operator's voluntary intentions (Suzuki, Mito, Kawamoto, Hasegawa, & Sankai, 2007). The cybernic autonomous control mode can autonomously provide effective physical support based on fundamental motion patterns (Kawamoto, Hayashi, Sakurai, Eguchi, & Sankai, 2009). (Wall, Borg, & Palmcrantz, 2015) reported that gait training using HAL® may have beneficial effects on post-stroke gait function and independent walking. However, well-designed and controlled studies are needed. Because many previous studies did not include control subjects, the benefits of gait training using HAL® in stroke patients require clarification. Therefore, randomized controlled trials are needed to compare the efficacy of HAL®-assisted gait training with conventional gait training (CGT) in terms of the improvement of walking ability in stroke patients.

Our previous study was the first randomized, controlled pilot trial to show the efficacy of gait training using HAL® compared to CGT (Watanabe, Tanaka, Inuta, Saitou, & Yanagi, 2014). However, the long-term and medium-term efficacies of gait training using HAL® in stroke patients remain unclear. Therefore, in this study, we added 2-month follow-up data to compare the medium-term efficacy of gait training using a single-leg version of the HAL® on the paretic side with CGT in recovery-phase stroke patients.

2. Methods

2.1. Participants

Post-stroke patients who were admitted to a recovery-phase rehabilitation ward in Tsukuba Memorial Hospital between February 2013 and December 2013 participated in this study. All patients who participated in the previous study (Watanabe, Tanaka, Inuta, Saitou, & Yanagi, 2014) were included with the addition of two new patients. The final follow-up was conducted in January 2014. The inclusion criteria, exclusion criteria, recruitment and randomization were the same as in our previous study (Watanabe, Tanaka, Inuta, Saitou, & Yanagi, 2014).

In this study the experimental HAL® group was 8 male and 4 female patients (12 total) with a median age of 66.9 ± 16.0 years. 7 of this group had ischemic stroke and 7 had right side paresis. The average time since stroke was 57.0 ± 44.3 days in this group. The control group was 8 male and 4 female patients (12 total) with a median age of 76.8 ± 13.8 years. The average time since stroke in the control group was 48.1 ± 33.3 days. No differences were observed between the groups in either characteristics or baseline clinical data. Patient flow is shown in Fig. 1.

The ethics committees of the University of Tsukuba and of Tsukuba Memorial Hospital approved this study and written informed consent was provided by all of the subjects or their legal representatives. This study is registered in the University Hospital Medical Information Network (UMIN) clinical trials registry in Japan with the registration number UMIN000022335.

2.2. Intervention

HAL® patients performed gait training using HAL® 3 times a week with a total of 12 HAL® training sessions (4 weeks). CGT patients performed CGT 3 times a week with a total of 12 CGT training sessions (4 weeks). The intervention goal and structure in both groups have been described in detail in our previous study (Watanabe, Tanaka, Inuta, Saitou, & Yanagi, 2014).

2.3. Assessment

All measurements were done by physical therapists who were trained to perform standardized assessment procedures. The primary outcome measure was Functional Ambulation Category (FAC). Secondary outcomes measures were maximum walking speed, stride, cadence, 6-min walking distance, timed Up-and-Go test, and Fugl-Meyer Assessment of the lower extremity.

All outcomes were assessed prior to training, after 12 sessions (4 weeks), and at 8 and 12 weeks after intervention initiation. These outcomes were assessed without wearing the HAL® because we wanted to show the effectiveness of the HAL® as

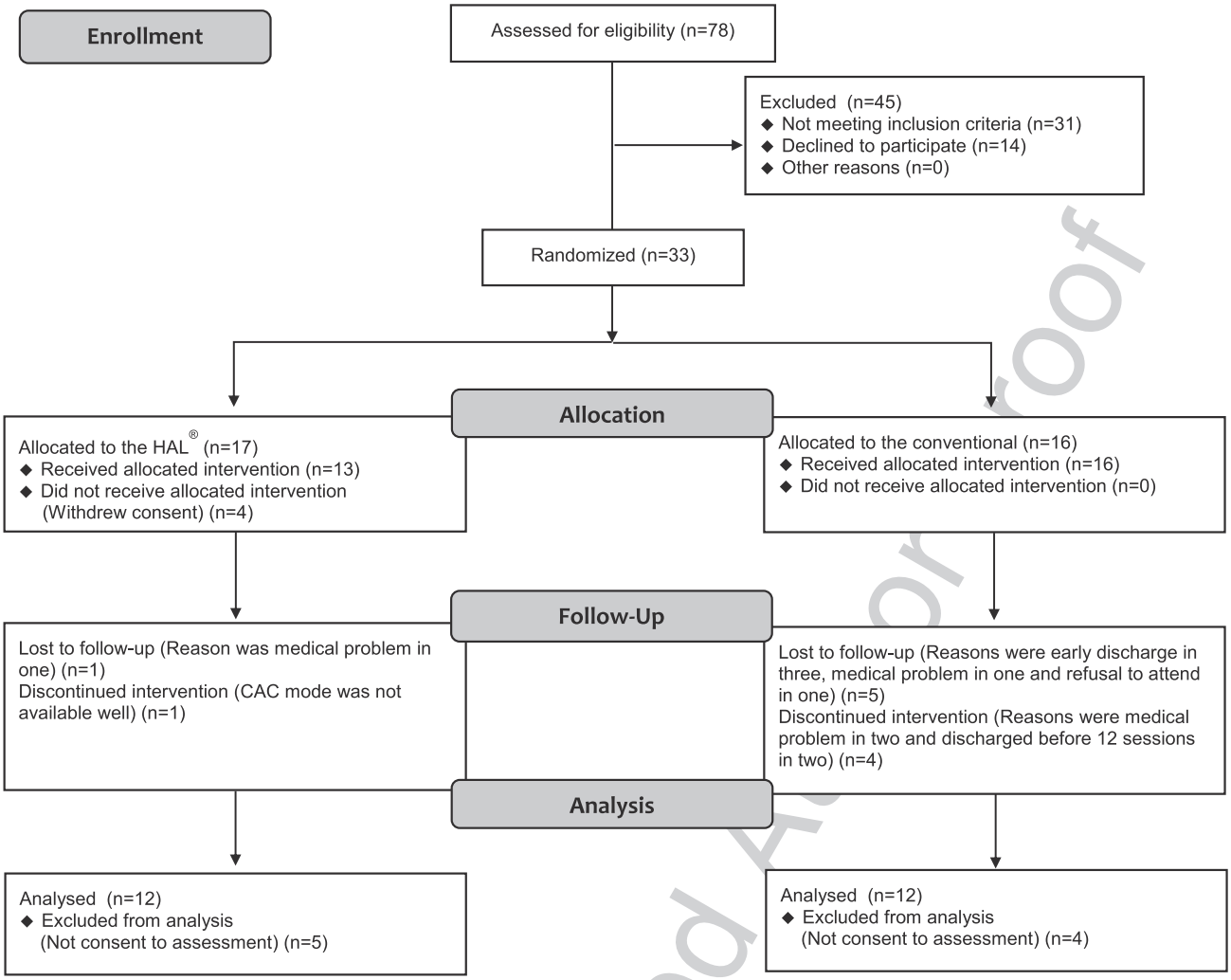

Fig. 1. Flowchart of the study. CAC, cybernic autonomous control.

a rehabilitation device, not as an orthosis for patients with stroke. Participants, therapists, and evaluators were not blinded to the treatment allocation.

2.4. Statistical analysis

The outcome measures in each group were compared prior to training, after 12 sessions (4 weeks), and at 8 and 12 weeks after intervention initiation. Interaction effects of groups (time × effect) were calculated using the mixed-effects model. SPSS version 23.0 was used for all statistical analyses. Statistical significance was set at $P < 0.05$.

3. Results

The HAL® group showed significant improvement in FAC after 12 sessions, and at 8 and 12 weeks post-intervention compared to the conventional group ($P = 0.02$). The interaction effects (time × effect) were significant for FAC. However, the secondary outcome measures did not differ between the two groups (Table 1). Values are expressed as number or mean ± SD.

4. Discussion

The present study is the first randomized controlled trial to compare the medium-term efficacy of gait training using a single-leg version of the HAL® on the paretic side with CGT in recovery-phase stroke patients. The HAL® group showed significant improvement in FAC after 12 sessions, and at 8 and 12 weeks post-intervention compared to the conventional group. The interaction effects (time × effect) were significant for FAC. However, the secondary

Table 1
Differences within groups and differences between groups with a 2-month follow-up

Measures	HAL® Group ($n=12$)				Conventional Group ($n=12$)				P Value #
	Pre	4 weeks	8 weeks	12 weeks	Pre	4 weeks	8 weeks	12 weeks	
FAC	2.0 ± 1.0 ($n=12$)	3.0 ± 1.3 ($n=12$)	3.5 ± 1.5 ($n=11$)	3.6 ± 1.7 ($n=11$)	2.0 ± 0.9 ($n=12$)	2.5 ± 1.3 ($n=12$)	2.4 ± 1.5 ($n=7$)	2.7 ± 1.6 ($n=7$)	0.026
Maximal walking speed (m/s)	0.56 ± 0.43 ($n=9$)	0.85 ± 0.43 ($n=8$)	0.83 ± 0.50 ($n=8$)	0.84 ± 0.51 ($n=8$)	0.45 ± 0.53 ($n=11$)	0.61 ± 0.47 ($n=11$)	0.54 ± 0.35 ($n=6$)	0.57 ± 0.41 ($n=6$)	0.975
Stride (m)	0.37 ± 0.16 ($n=9$)	0.44 ± 0.12 ($n=8$)	0.44 ± 0.14 ($n=8$)	0.46 ± 0.15 ($n=8$)	0.29 ± 0.18 ($n=11$)	0.34 ± 0.18 ($n=11$)	0.37 ± 0.18 ($n=6$)	0.36 ± 0.16 ($n=6$)	0.581
Cadence (steps/min)	81.5 ± 36.3 ($n=9$)	108.4 ± 33.2 ($n=8$)	103.6 ± 46.8 ($n=8$)	99.3 ± 40.3 ($n=8$)	75.1 ± 37.1 ($n=11$)	98.7 ± 26.3 ($n=11$)	83.4 ± 16.2 ($n=6$)	88.9 ± 30.2 ($n=6$)	0.844
6-minute walking distance (m)	92.4 ± 104.2 ($n=12$)	156.7 ± 137.8 ($n=11$)	154.3 ± 139.2 ($n=11$)	166.7 ± 143.9 ($n=11$)	106.9 ± 132.6 ($n=12$)	140.8 ± 127.8 ($n=12$)	142.7 ± 102.1 ($n=7$)	131.0 ± 117.6 ($n=7$)	0.810
TUG (s)	33.9 ± 22.4 ($n=9$)	16.7 ± 6.9 ($n=8$)	29.1 ± 39.7 ($n=8$)	23.1 ± 23.9 ($n=8$)	46.6 ± 24.4 ($n=11$)	28.6 ± 17.9 ($n=11$)	31.3 ± 22.3 ($n=6$)	27.3 ± 18.9 ($n=6$)	0.413
LE Fugl-Meyer Assessment	19.5 ± 6.3 ($n=12$)	20.6 ± 6.3 ($n=11$)	18.7 ± 7.0 ($n=11$)	18.7 ± 7.1 ($n=11$)	21.1 ± 5.4 ($n=12$)	22.5 ± 5.7 ($n=12$)	22.7 ± 6.4 ($n=7$)	23.1 ± 6.5 ($n=7$)	0.131

Values are mean ± standard deVation or as otherwise indicated. FAC, Functional Ambulation Category; TUG, timed Up-and-Go test, LE, lower limb. # P value for Interaction, mixed-effects model.

outcome measures did not differ between the two groups. The data indicate that gait training using HAL® is beneficial for hemiparetic, non-ambulatory, recovery-phase stroke patients.

A recent Cochrane review (Mehrholz, Elsner, Werner, Kugler, & Pohl, 2013) reported that electromechanical-assisted gait training in combination with physical therapy increased the odds of independent walking in participants (odds ratio: 2.39, 95% confidence interval: 1.67–3.43; $P<0.01$). Our data showed similar findings. The HAL® system enables such a repetitive gait training by providing motion assistance in response to the patient's voluntary drive using an exclusive the cybernic voluntary control and the cybernic autonomous control technology (Lee & Sankai, 2005; Suzuki, Mito, Kawamoto, Hasegawa, & Sankai, 2007; Kawamoto, Hayashi, Sakurai, Eguchi, & Sankai, 2009). This new type of HAL®-assisted gait training might improve independent walking in patients with subacute stroke. (Kawamoto et al., 2013) reported that user control over the amount of assistance provided by HAL® is effected by voluntarily adjusting myoelectric activities. Thus, this mechanism forms a proprioceptive feedback loop that adjusts to each user.

Several studies have investigated the effects of locomotion training using HAL® for stroke patients (Kawamoto et al., 2013; Nilsson, Vreede, Häglund, Kawamoto, Sankai, & Borg, 2014; Watanabe, Tanaka, Inuta, Saitou, & Yanagi, 2014; Mizukami et al., 2016). (Kawamoto et al., 2013) reported that the dependent ambulatory levels (FAC 2-3 with chronic stroke) showed significant differences in comfortable walking speed between before and after a total of 16 HAL® training sessions. The cybernic voluntary control mode was used during HAL® locomotor training in most patients. During locomotor training, the patients walked on a floor and were harnessed in a mobile suspension system. (Mizukami et al., 2016) discussed that the harness walker system enabled patients to walk continuously without risk of falling. Therefore, the use of mobile suspension system played an important role in enhancing the HAL® training effect. In this present study, all subacute stroke patients were classified into the dependent ambulatory levels (FAC 0–3) prior to HAL® training but the cybernic voluntary control mode was available for only ten patients. Thus, two patients use had to the cybernic autonomous control mode to complete locomotion training. Of these, 1 subject exhibited reduced dependence on walking assistance and 1 did

not change. It is still unclear whether gait training using HAL® benefits post-stroke patients who could not use the the cybernic autonomous control mode. Further study is needed to discuss the indications and the efficiency of each mode of HAL® for post-stroke gait training.

Other reports in the literature also detail the usage of a gait trainer in improvement of patient condition after stroke. (Chua, Culpan, & Menon, 2016) evaluated long-term efficacy and suggested that the use of an electromechanical gait trainer in combination with conventional physical therapy was as effective as conventional physical therapy alone for improving ambulation in subacute stroke. (Morone et al., 2012) evaluated the long-term efficacy of robotic gait training in stroke patients at approximately 2 years after hospital discharge. To the best of our knowledge, this is the longest follow-up study reported at this time. In our study, the HAL® group showed greater efficiency in the improvement of independent walking compared with that observed with CGT at 1 and 2 months after intervention. Although this is a short-term result, gait training using HAL® was shown to be superior to CGT in subacute stroke patients. Further study is needed to evaluate longer follow-up periods (months to years) of gait training using HAL®. Such data will allow for comparisons with previously published long-term studies.

There are few limitations in our study. The statistical power was low because of the small number of subjects. In addition, we could not exclude observer bias because the same therapists implemented training and assessment; there was no blinding in the treatment allocation. Furthermore, regarding the sufficient duration and the long-term efficacy of gait training using HAL®, we will attempt to answer these questions in our future investigations.

5. Conclusions

In conclusion, the present study is the first randomized controlled trial with a 2-month follow-up period to compare the medium-term efficacy of gait training using a single-leg version of HAL® on the paretic side with CGT in recovery-phase stroke patients. The results suggested that a gait training program based on HAL® may improve independent walking more efficiently than CGT at 1 and 2 months after intervention. Further study is needed to evaluate the long-term efficacy of gait training using HAL®.

Conflict of interest

None to report.

References

Chua, J., Culpan, J., & Menon, E. (2016). Efficacy of an Electromechanical Gait Trainer Poststroke in Singapore: A Randomized Controlled Trial. *Arch Phys Med Rehabil*, *97*, 683-690.

Dobkin, B. H., (2005). Clinical practice. Rehabilitation after stroke. *N Engl J Med*, *352*, 1677-1684.

Geroin, C., Mazzoleni, S., Smania, N., Gandolfi, M., Bonaiuti, D., Gasperini, G., et al. (2013). Systematic review of outcome measures of walking training using electromechanical and robotic devices in patients with stroke. *J Rehabil Med*, *45*, 987-996.

Kawamoto, H., & Sankai, Y. (2002). Power assist system HAL-3 for gait disorder person. *Proceedings of the 8th International Conference on Computers Helping People with Special Needs (ICCHP 2002)*, 196-203.

Kawamoto, H., Hayashi, T., Sakurai, T., Eguchi, K., & Sankai, Y. (2009). Development of single leg version of HAL for hemiplegia. *Annual International Conference of the IEEE Engineering in Medicine and Biology Society Conf Proc IEEE Eng Med Biol Soc*), 5038-5043.

Kawamoto, H., Kamibayashi, K., Nakata, Y., Yamawaki, K., Ariyasu, R., Sankai, Y., et al. (2013). Pilot study of locomotion improvement using hybrid assistive limb in chronic stroke patients. *BMC Neurology*, *13*, 141.

Lee, S., & Sankai, Y. (2005). Virtual impedance adjustment in unconstrained motion for exoskeletal robot assisting lower limb. *Adv Robot*, *19*, 773-795.

Mehrholz, J., Elsner, B., Werner, C., Kugler, J., & Pohl, M. (2013). Electromechanical-assisted training for walking after stroke. *Cochrane Database Syst Rev*, *7*, CD006185.

Mizukami, M., Yoshikawa, K., Kawamoto, H., Sano, A., Koseki, K., Asakawa, Y., et al. (2016). Gait training of subacute stroke patients using a hybrid assistive limb: A pilot study. *Disabil Rehabil Assist Technol*, *26*, 1-8.

Morone, G., Iosa, M., Bragoni, M., Angelis, D. D., Venturiero, V., Coiro, P., et al. (2012). Who may have durable benefit from robotic gait training?: A 2-year follow-up randomized controlled trial in patients with subacute stroke. *Stroke*, *43*, 1140-1142.

Nilsson, A., Vreede, K. S., Häglund, V., Kawamoto, H., Sankai, Y., & Borg, J. (2014). Gait training early after stroke with a new exoskeleton –the hybrid assistive limb: A study of safety and feasibility. *J Neuroeng Rehabil*, *11*, 92.

Suzuki, K., Mito, G., Kawamoto, H., Hasegawa, Y., & Sankai, Y. (2007). Intention-based walking support for paraplegia patients with Robot Suit HAL. *Adv Robot*, *21*, 1441-1469.

Wall, A., Borg, J., & Palmcrantz, S. (2015). Clinical application of the Hybrid Assistive Limb (HAL) for gait training – a systematic review. *Front Syst Neurosci*, *9*, 48.

Watanabe, H., Tanaka, N., Inuta, T., Saitou, H., & Yanagi, H. (2014). Locomotion improvement using a hybrid assistive limb in recovery phase stroke patients: A randomized controlled pilot study. *Arch Phys Med Rehabil*, *95*, 2006-2012.

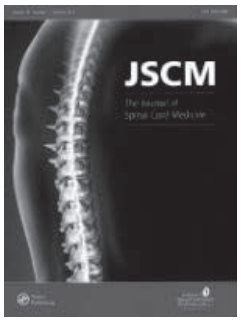

The Journal of Spinal Cord Medicine

ISSN: 1079-0268 (Print) 2045-7723 (Online) Journal homepage: http://www.tandfonline.com/loi/yscm20

Walking ability following Hybrid Assistive Limb treatment for a patient with chronic myelopathy after surgery for cervical ossification of the posterior longitudinal ligament

Shigeki Kubota, Tetsuya Abe, Hideki Kadone, Kengo Fujii, Yukiyo Shimizu, Aiki Marushima, Tomoyuki Ueno, Hiroaki Kawamoto, Yasushi Hada, Akira Matsumura, Yoshiyuki Sankai & Masashi Yamazaki

To cite this article: Shigeki Kubota, Tetsuya Abe, Hideki Kadone, Kengo Fujii, Yukiyo Shimizu, Aiki Marushima, Tomoyuki Ueno, Hiroaki Kawamoto, Yasushi Hada, Akira Matsumura, Yoshiyuki Sankai & Masashi Yamazaki (2017): Walking ability following Hybrid Assistive Limb treatment for a patient with chronic myelopathy after surgery for cervical ossification of the posterior longitudinal ligament, The Journal of Spinal Cord Medicine, DOI: 10.1080/10790268.2017.1313932

To link to this article: http://dx.doi.org/10.1080/10790268.2017.1313932

Published online: 20 Apr 2017.

Case Report

Walking ability following Hybrid Assistive Limb treatment for a patient with chronic myelopathy after surgery for cervical ossification of the posterior longitudinal ligament

Shigeki Kubota[1,2], Tetsuya Abe[2], Hideki Kadone[3], Kengo Fujii[2], Yukiyo Shimizu[4], Aiki Marushima[5], Tomoyuki Ueno[4], Hiroaki Kawamoto[6], Yasushi Hada[4], Akira Matsumura[5], Yoshiyuki Sankai[6], Masashi Yamazaki[2]

[1]Division of Regenerative Medicine for Musculoskeletal System, Faculty of Medicine, University of Tsukuba, Ibaraki, Japan, [2]Department of Orthopaedic Surgery, Faculty of Medicine, University of Tsukuba, Ibaraki, Japan, [3]Center for Innovating Medicine and Engineering (CIME), University of Tsukuba Hospital, Ibaraki, Japan, [4]Department of Rehabilitation Medicine, University of Tsukuba Hospital, Ibaraki, Japan, [5]Department of Neurosurgery, Faculty of Medicine, University of Tsukuba, Ibaraki, Japan, [6]Faculty of Systems and Information Engineering, University of Tsukuba, Ibaraki, Japan

Context: The hybrid assistive limb (HAL) (the wearable robot) can assist kinesis during voluntary control of hip and knee joint motion by detecting the wearer's bioelectric signals on the surface of their skin. The purpose of this study was to report on walking ability following the wearable robot treatment in a patient with chronic myelopathy after surgery for cervical ossification of the posterior longitudinal ligament (OPLL).

Findings: The patient was a 66-year-old woman with cervical OPLL who was able to ambulate independently with the aid of bilateral crutches. The wearable robot treatment was received once every 2 weeks for ten sessions beginning approximately 14 years after surgery. Improvements were observed in gait speed (BL 22.5; post 46.7 m/min), step length (BL 0.36; post 0.57 m), and cadence (BL 61.9; post 81.6 m/min) based on a 10-m walk test and a 2-minute walk test (BL 63.4; post 103.7 m) assessing total walking distance. The improvements in walking ability were maintained after the wearable robot treatment for 6 months.

Conclusion: We report the functional recovery in the walking ability of a patient with chronic cervical myelopathy following the wearable robot treatment, suggesting that as a rehabilitation tool, the wearable robot has the potential to effectively improve functional ambulation in chronic cervical myelopathy patients whose walking ability has plateaued, even many years after surgery.

Keywords: Hybrid assistive limb (HAL), Ossification of the posterior longitudinal ligament (OPLL), Chronic myelopathy, Wearable robot, Rehabilitation

Introduction

The hybrid assistive limb (HAL) (the wearable robot) can assist kinesis during voluntary control of hip and knee joint motion (Fig. 1). Motion is assisted via the detection of bioelectric signals, through an electrode on the anterior and posterior surface of the wearer's thigh and force-pressure sensors in the shoes, which are processed through a computer.[1] The wearable robot has a hybrid control system comprised of cybernic voluntary control (CVC) and cybernic autonomous control (CAC) systems. The CVC mode of the wearable robot can support the patient's voluntary motion using voluntary muscle activity and the assistive torque provided to the hip and knee joint. The CAC mode can provide physical support autonomously, based on output from force-pressure sensors in the shoes. The feasibility and efficacy of the wearable robot has been shown in the functional recovery of multiple disorders in chronic[2–4] and subacute phases.[5–7]

In the current case report, a patient who had a walking disorder in the chronic phase of myelopathy

Correspondence to: Shigeki Kubota, PhD, Division of Regenerative Medicine for Musculoskeletal System, Faculty of Medicine, University of Tsukuba, 1-1-1, Tennodai, Tsukuba, Ibaraki, 305-8575, Japan. Email: s-kubota@md.tsukuba.ac.jp

DOI 10.1080/10790268.2017.1313932

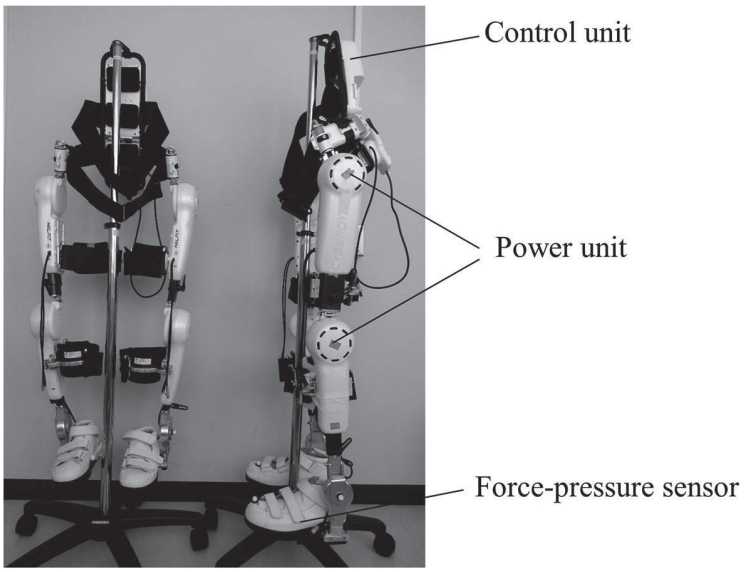

Figure 1 The robot suit HAL®. The wearable robot has a power unit in the hip and knee joints on both lateral sides and force-pressure sensors in the shoes.

after surgery for cervical ossification of the posterior longitudinal ligament (OPLL) received wearable robot treatment. Three similar cases have been reported, but HAL treatment for those patients was provided in the early postoperative period.[8–10] Sakakima *et al.* reported that the walking ability of a thoracic OPLL patient, for whom the outcome of multiple surgeries did not facilitate ambulation, improved with HAL treatment.[8] We have reported that HAL treatment for a postoperative thoracic OPLL patient, in whom reaggravation of paralysis occurred in the sitting position during the postoperative period, improved their walking ability.[9] Furthermore, we reported that HAL treatment, in surgically-treated thoracic OPLL patients with the inability to walk in the early postoperative phase, has the potential to effectively improve functional ambulation.[10] In the present case study, we report on improvements in walking ability following wearable robot treatment of a patient in the chronic phase of myelopathy after surgery for cervical OPLL.

Case report

Patient

A 66-year-old woman, diagnosed with cervical myelopathy due to OPLL 14 years earlier underwent anterior decompression and spinal fusion surgery. Before surgery, her spinal cord was compressed anteriorly by cervical OPLL, and the most stenotic intervertebral level was C5/6 (Figs. 2A and 2B). The preoperative Japanese Orthopaedic Association (JOA) score for cervical myelopathy was 8 out of a total score of 17 (8/17). Immediately after surgery, her myelopathy was slightly recovered and the JOA score increased to 9/17. Two years after surgery, the patient's myelopathy gradually worsened without any apparent cause and decreased to 8/17. Fourteen years after surgery, findings from magnetic resonance imaging (MRI) and computed tomography (CT) scans confirmed the compression of the spinal cord had resolved, but that spinal cord atrophy was present at the C5/6 level (Figs. 2B and 2C). Fourteen years after surgery, the patient wanted to undergo HAL treatment to attempt to improve her ability to walk.

Before wearable robot treatment, the patient scored 3 out of 6 on the bilateral manual muscle tests (MMTs),[11] indicating fair or full motion against gravity, of the iliopsoas, quadriceps femori, hamstring muscles, tibialis anterior, gastrocnemii, and wrist flexors, and scored 4 on the MMTs, good or full motion against gravity and some resistance, of the deltoids, biceps brachii, triceps brachii, and wrist extensors. Numbness in the right lower limb and in the left ulnar nerve was reported by the patient; however, her proprioception in both upper and lower extremities was found to be normal. Using the American Spinal Injury Association (ASIA) impairment scale (AIS),[12] a clinical evaluation showed the patient's grade was D on a scale ranging from grade E (least impaired) to grade A (most impaired). The patient's ASIA motor score (lower extremity) was 30 points (right, 15 points; left, 15 points) out of a total of 50 points and her ASIA sensory score for light touch was 101 points (right, 47 points; left, 54 points)

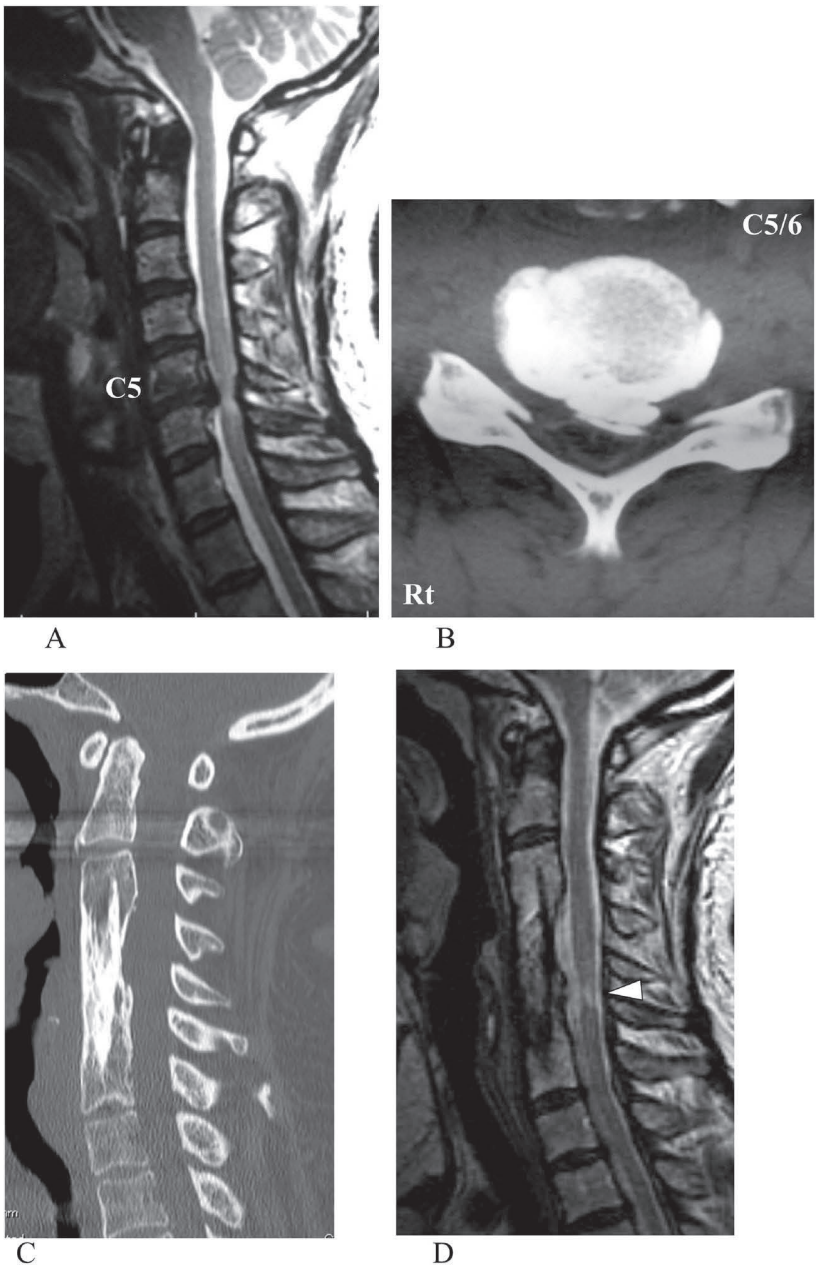

Figure 2 Imaging findings of the cervical spine before and after surgery. (A) Mid-sagittal section of a T2-weighted magnetic resonance image (MRI); (B) an axial section of a computed tomography (CT) myelogram at the C5/6 level before surgery, showing the OPLL that compressed the spinal cord anteriorly. (C) Mid-sagittal CT reconstruction and (D) mid-sagittal section of a T2-weighted MRI 14 years after surgery, showing that the spinal cord compression was resolved but atrophic changes of the spinal cord were present at the C5/6 level (arrowhead).

out of a total 112 points. Based on the Frankel grading classification for spinal injuries on a scale ranging from grade A (complete neurological injury) to grade E (normal motor function), the patient was grade D. Using the Walking Index for Spinal Cord Injury (WISCI) II[13] scale ranging from 0 (inability to walk) to 20 (no walking devices, no braces, no assistance) the patient scored 16 (ambulates with two crutches, no braces and no physical assistance, 10 meters), and using the Functional Independent Measure (FIM)[14,15] motor score based on ADL (activities of daily living), she scored 91 out of 91.

The patient was able to ambulate independently for approximately 300 m outdoors with the aid of bilateral crutches, and was able to walk indoors using props such as a wall or table for support. Although she did

not need supervision during walking with crutches, her gait was unstable and her steps were short. Without the aid of crutches, the patient was not able to ambulate independently due to the high risk of falling.

Functional evaluation

A 10-m walk test and 2-minute walk test were conducted before the period of the wearable robot sessions had begun (baseline) and after it had finished (after training). Initial testing (base line) was performed on the day of the first wearable robot session before starting wearable robot treatment. The final test (after training) was performed on the day of post-evaluation, which was later than the day of the final wearable robot session. The primary outcome was the walking speed (m/minute) of the 10-m walking tests at the initial (baseline) and final (after training) evaluation. The 10 m walking speed and the walking time were measured using a handheld stopwatch. In addition, the number of steps taken between the start and finish line were counted to calculate step length (m). Cadence was calculated based on the number of steps taken over the walking time and converted to steps/minute. During the 10-m walk test; the patient was instructed to walk without the wearing robot on a flat surface at a self-selected comfortable pace. During the 2-minute walk test, the patient was asked to walk for 2 minutes at her chosen maximal pace and the total distance walked was recorded. The 10-m walk test was also performed at each of the wearable robot sessions just before wearing the robot for an additional evaluation.

At every four sessions starting from the first wearable robot session; i.e. at sessions 1, 5 and 9, gait characteristics were measured using a VICON motion capture system (Vicon MX System with 16 T20s cameras; Oxford Metrics Ltd, Oxford, United Kingdom) three times during each of the three session: unassisted gait just prior to treatment with the robot (pre-robot); gait while ambulating with the wearable robot during treatment (robot); and unassisted gait after removal of wearable robot after treatment (post-robot). During these tests, the patient was instructed to walk on a flat surface at a self-selected comfortable pace. While walking with the wearable robot, the patient walked at a self-selected comfortable pace. Auto reflexive markers were attached on the feet following VICON plug-in gait marker placement on the foot; the head of the second metatarsal bone for the toe, lateral malleolus for the ankle and posterior peak of the calcaneus for the heel. Steps were extracted according to heel strikes detected as the lower peaks of the height of the heel markers. Toe lift was computed according to the relative height displacement measured by maximum height minus minimum height of a toe marker for each step and then averaged among the extracted steps. Step length was computed for each step according to the horizontal distance between the position of a heel marker at the moment of a heel strike and the successive heel strike, and then averaged among the extracted steps. Toe lift and step length were computed first separately for the right and left sides and then averaged to obtain a representative value, because our focus was not lateral symmetry. Gait speed and cadence were also computed from the step data for pre-robot and post-robot in the same wearable robot treatment sessions (in the 1st, 5th, 9th sessions). Without the wearable robot the participant walked wearing her own comfortable shoes, and with the wearable robot she walked wearing the shoes of the robot. Since the evaluation of step detection, toe lift and step length depended on relative movement of a marker in each track, the slight differences in the heights of sole and toe cover between these shoes did not affect these evaluation.

Wearable robot treatment

The device used for the research is equivalent to the marketed device that has been given the CE marking certificate (CE0197) for a medical device. In Japan, the device is approved as a medical treatment device used to delay the advancement of slowly progressive rare neuromuscular diseases.

Wearable robot treatment was started approximately 14 years after the patient underwent surgery for anterior decompression and spinal fusion. Upon initiation of the wearable robot treatment, the wearable robot was fitted and sitting and standing mobility was confirmed. The patient received wearable robot treatment once every 2 weeks for ten sessions (Fig. 3). To minimize the risk of falling for the patient, a walking device (AllinOne Walking Trainer; Healthcare Lifting Specialist, Denmark) with a harness was used. The CVC mode for the wearable robot was primarily used with the walking device and harness. Each wearable robot treatment session lasted 60 minutes and included the time taken for attaching/detaching the device, rest, single-leg motion, standing and sitting exercises, and walking on a 25-meter-long circuit several times with the assistance of two therapists and a doctor. One therapist operated the walking device and the other operated the computer. Net gait training time was approximately 15–20 minutes. The walking distance covered by the patient during wearable robot treatment sessions totaled approximately 2,100 m and averaged 210 m per session. Conventional physical therapy in the other

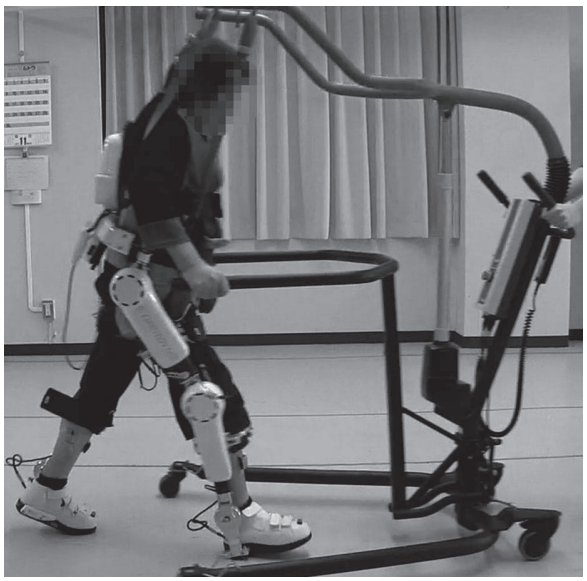

Figure 3 Intervention by the wearable robot with a walking device and a harness for safety.

facilities, such as standing exercises and gait training with a walking device, was not performed concurrently with wearable robot treatment.

Statistical analysis

The toe lift and step length from data of the VICON motion capture system were analyzed by two-factor factorial ANOVA, and then differences among means were analyzed using Bonferroni/Dunn multiple comparison tests.

Results

Improvements in gait speed, step length, and cadence for the 10-m walk test and the total walking distance covered in the 2-minute walk test were observed (Figs. 4A and 4B). The results of the 10-m walk test and 2-minute walk test are shown (Table 1). Although the patient was not able to ambulate independently without the aid of crutches before wearable robot treatment, she was able to ambulate independently without them over a distance of at least 8 m after 10 sessions of wearable robot treatment. The gait speed in the 10-m walk test was 53.4 m/minute after wearable robot treatment for 6 months. Improvements in walking ability were maintained after wearable robot treatment.

From the VICON data, the number of extracted steps were (24, 26, and 16), (38, 66, and 42) and (38, 18, and 42) for (pre-robot, robot, post-robot) for session 1, 5, and 9. While wearing the robot, toe lift and step length increased walking compared with pre-robot walking during the 1st (by 4.3 cm and 2.5 cm respectively), 5th (by 2.9 cm and 7.9 cm), and 9th (by 2.2 cm and 6.0 cm) wearable robot treatment sessions. These immediate effects persisted during walking after robot treatment, and were characterized by the increased toe lift and step length compared with the pre-robot phase in each of the 1st (by 0.2 cm and 3.5 cm), 5th (by 0.8 cm and 7.1 cm), and 9th (by 0.4 cm and 5.1 cm) sessions (Fig. 5A and B). Gait speed and cadence immediately increased from pre-robot to post-robot segments in the same wearable robot treatment session (Figs. 5C and 5D) and in subsequent sessions. Statistical analysis showed significant differences among the sessions ($P < 0.05$ for toe lift, and $P < 0.05$ for step length) and among the robot conditions ($P < 0.05$ for toe lift and $P < 0.05$ for step length). Interaction between the two factors was observed. Multiple comparison tests showed that toe lift was larger in Robot condition compared to Pre-robot ($P < 0.05$) and to Post-robot ($P < 0.05$) and step length was larger in Robot condition compared to Pre-robot ($P < 0.05$) but not compared to Post-robot ($P > 0.05$).

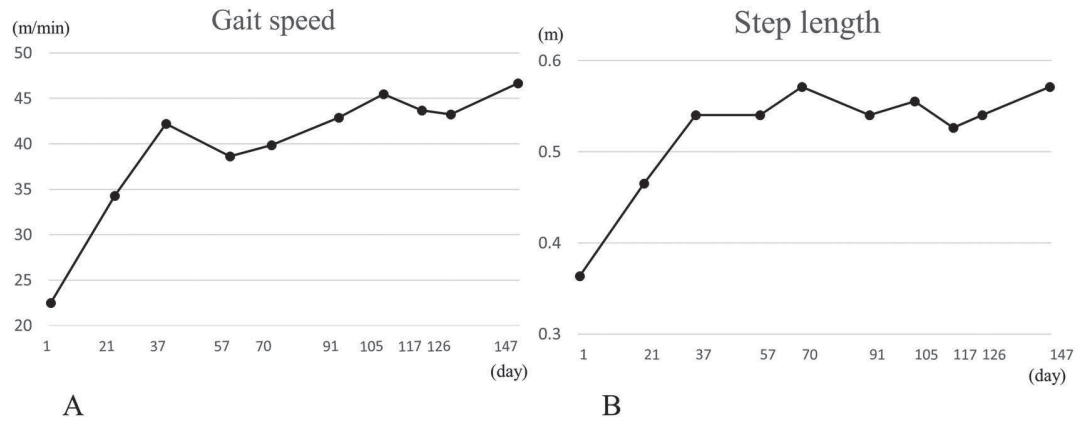

Figure 4 Change in 10-m walk test without wearable robot. (A) Gait speed and (B) Step length.

Table 1 The results of the 10-m walk test, the 2-minute walk test, and the VICON motion capture system at baseline, after the training, and 1, 5, 9 session pre and post wearable robot treatment

	10-m walk test			2-minute walk test	VICON motion capture system			
	Speed (m/min)	Step length (m)	Cadence (steps/min)	Total walking distance (m)	Toe lift (m)	Step length (m)	Speed (m/min)	Cadence (steps/min)
At baseline	22.5	0.36	61.9	63.4	NA	NA	NA	NA
After the training	46.7	0.57	81.6	103.7	NA	NA	NA	NA
1th session pre-robot	NA	NA	NA	NA	0.09	0.57	38.7	68.6
1th session post-robot	NA	NA	NA	NA	0.09	0.60	42.7	70.6
5th session pre-robot	NA	NA	NA	NA	0.11	0.61	41.0	67.2
5th session post-robot	NA	NA	NA	NA	0.11	0.68	53.1	77.3
9th session pre-robot	NA	NA	NA	NA	0.09	0.58	45.0	77.0
9th session post-robot	NA	NA	NA	NA	0.09	0.63	50.9	80.2

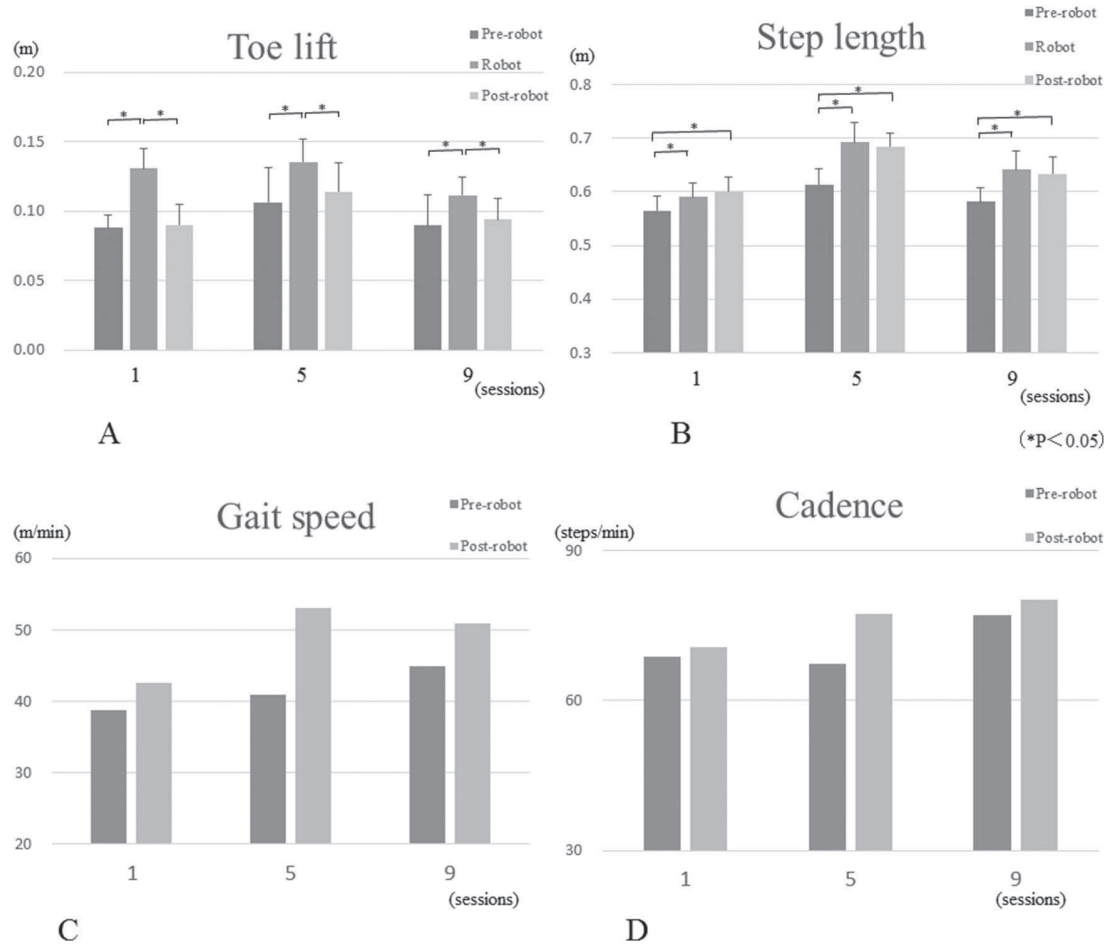

Figure 5 The results of the kinematic motion analysis using the Vicon motion capture system. (A) Toe lift, (B) Step length, (C) Gait speed, and (D) Cadence.

Table 2 The results of the ASIA motor score (lower extremity), ASIA sensory score, Frankel classification, WISCI II, and FIM motor score at baseline and after the wearable robot treatment

	ASIA motor score (lower extremity)	ASIA sensory score	Frankel classification	WISCI II	FIM motor score
At baseline	15 / 15	47 / 54	D	16	91
After the training	18 / 16	47 / 54	D	16	91

The clinical evaluation, performed after the patient's final wearable robot treatment session, revealed the following results: (i) cervical JOA score was 9/17, (ii) AIS was grade D, (iii) ASIA motor score (lower extremity) was 34 points (right: 18 points, left: 16 points), (iv) ASIA sensory score for light touch was 101 points (right: 47 points, left: 54 points), (v) the Frankel classification was grade D, (vi) WISCI II was 16, and (vii) the FIM motor score was 91 (Table 2). This study was conducted with the approval of the Ethics Committee of the Tsukuba University Faculty of Medicine. This study was registered with the University Hospital Medical Information Network (UMIN) Clinical Trials Registry (UMIN000014336).

Discussion

We have presented a case of chronic cervical myelopathy with OPLL pathology in which an improvement in walking ability was achieved following 10 wearable robot physical therapy sessions, even after her walking ability had plateaued for approximately 14 years after surgery. The gait speed post-robot was faster than it was pre-robot (Fig. 5C). We had the impression that the gait speed while wearing the robot was fairly equal to that pre-robot. Therefore, it is difficult to believe that the patient immediately learned a faster gait while wearing the robot. However, because the patient could walk repeatedly with longer step and higher toe lift with the aid of the wearable robot (Figs. 5A and 5B) without the risk of falling, we consider that gait stability might have been improved and led to the faster gait post-robot.

Some of the measurements such as toe lift regressed closer to baseline during the 9th session compared to the 5th session (Fig. 5B). This might have arisen from the assist configuration of HAL in each of the sessions. At the earlier sessions, treatment was configured so that the patient could walk safely using a reciprocal bipedal gait, therefore with larger assistance in flexing of the hip and knee to achieve a higher toe lift. In the middle sessions, treatment was configured to achieve a longer swing motion with longer step, therefore, with increased assistance in the extension motion of the hip and knee. Among the measured sessions, the largest enhancement of step length was observed in the 5th session. Toward the later sessions, assisted configuration was gradually reduced so that the patient could practice walking, gradually increasing reliance on her own ability, smoothness and efficiency while maintaining stability. By this reasoning, the amount of gait change influenced by HAL was considered to gradually decrease toward the later sessions.

Regarding improvement in gait speed and step length after 3 sessions start to plateau, we conjectured as follows. Our patient had a gait posture that was highly influenced by bilateral crutches. However, the gait of the patient changed quickly to a new gait posture during treatment by wearing the robot (longer step, higher toe lift). Therefore, improvement of gait speed and step length were observed especially in early sessions (from session 1 to 3). Later, because the patient became accustomed to her gait posture after wearing the robot after 4 sessions, we consider that the increase of gait speed and step length might have quickly plateaued.

Statistical analysis indicated that the toe lift and the step length significantly increased in the gait with Robot compared to the gait of Pre-robot (Figs. 5A and 5B). It shows that the assisted gait can be characterized by larger foot motion during swing phase. Statistical analysis also indicated that the gait changed significantly in the 5th session compared to the 1st session, and in the 9th session compared to the 5th session, in terms of the toe height and the step length (Figs. 5A and 5B). This might correspond to the above observation for the gait changes of the earlier sessions due to the removal of the crutches and of the later sessions due to the increased reliance on her own walking ability for smoother and more efficient gait. The removal of the crutches contributed to the increase of walking speed while the later changes did not, and therefore the plateau after the 3rd session (Figs. 4A and 4B). The limitation of the statistical analysis has to be noted since, first, there was only one participant in the experiments and, second, the effect of interaction between the session and the robot factors were large.

There have been several reports on robotic physical therapy for patients with chronic spinal cord injury (SCI).[4,16,17] Wirz *et al.* reported that after the robotic-assisted, bodyweight-supported treadmill training with

Lokomat three to five times a week, the 10-m walk test gait speed of 20 patients with a chronic motor incomplete SCI increased by 0.11 ± 0.10 m/s.[16] Labruyère *et al.* compared a robot-assisted gait training (RAGT) group with a strength training group of patients with chronic incomplete SCIs, and reported that mean gait speed improved from 0.62 m/second (37.2 m/minute) to 0.66 m/second (39.6 m/minute) in the RAGT group.[17] Improvement of the gait speed for our case (from 22.5 m/minute to 46.7 m/minute) was higher than the improvement (from 37.2 m/minute to 39.6 m/minute) of Labruyère *et al.* The gait speed of our patient at baseline (22.5 m/minute) was lower than the gait speed of 9 patients of Labruyère *et al.* at baseline (37.2 m/minute). For that reason, we considered that our patient might be easily influenced by gait training including conventional gait training. Therefore, the improvement of gait speed in our patient was higher than that of subjects in the study by Labruyère *et al*. Aach *et al.* showed that the HAL physical therapy, performed five times per week over 90 days, significantly improved walking ability for eight patients with chronic SCI.[4] In particular, the mean (± standard deviation) total walking distance covered during a 6-minute walk test significantly improved from 70.1 ± 130 m to 163.3 ± 160.6 m. Our case also demonstrated that significant improvements in total walking distance occurred during a 2-minute walk test, despite the comparatively reduced frequency of wearable robot physical therapy sessions (once every 2 weeks).

We speculate that the effectiveness of motor learning in relation to walking ability improvements induced by wearable robot treatment is based on the patient's voluntary control. Wu *et al*. reported that locomotor training using a cable-driven robotic locomotor support system improved the walking speed and balance in ten patients with chronic incomplete SCI.[18] Because the cable-driven robotic locomotor system constrains leg movement and allows for variability in leg kinematics during treadmill walking, assistive training is important in motor learning. On the other hand, our wearable robot treatment could induce in real-time voluntary assistive motion via the wearer's voluntary signals (i.e. bioelectrical signals). We consider that sensory feedback was enhanced during walking while wearing the wearable robot because of real-time voluntary assistive motion that promoted superior motor learning effects. We conjectured that the mechanism underpinning the recovery of functional ambulation in this case was based on changes in plasticity of the spinal cord and supraspinal centers by the wearable robot-induced motion, which can facilitate favorable feedback effects.

Further studies are needed to compare the effectiveness of wearable robot treatment and conventional rehabilitation. We consider that the development of training programs according to the indicative disease and a term of disease for wearable robot treatment is necessary. An investigation of the difference in improvement between high-frequency training and low-frequency training with our wearable robot treatment is currently underway. Future studies also should examine the influence of the severity of spinal myelopathy and incomplete spinal cord injury on the effectiveness of wearable robot treatment.

Study limitations

This case study has some limitations. First, this case study could not compare the efficacy of pure wearable robot treatment with conventional rehabilitation (gait training). Second, long-term efficacy of the wearable robot treatment could not be assessed. Third, this case study could not exclude observer bias because the same staff implemented evaluation and treatment.

Conclusion

The wearable robot treatment for chronic cervical OPLL has the potential to improve the ability of a patient to walk, even years after surgery when their walking ability appears to have plateaued. More patients will be needed to evaluate the isolated effects of wearable robot treatment.

Acknowledgment

We thank Mayuko Sakamaki and Yumiko Ito of the Center for Innovative Medicine and Engineering (CIME) at the University of Tsukuba Hospital for their excellent technical assistance.

Conflict of Interest

None

Contributor Statement

A commercial party having a direct financial interest in the results of the research supporting this article has conferred or will confer a financial benefit on 1 or more of the authors. Yoshiyuki Sankai is CEO of Cyberdyne Inc, Ibaraki, Japan. Hiroaki Kawamoto is a stockholder of the Cyberdyne. Cyberdyne is the manufacturer of the robot suit HAL. This study was proposed by the authors. Cyberdyne was not directly involved in the study design, the collection, analysis, or interpretation of data, writing the report, or the decision to submit the paper for publication. No commercial party having a direct financial interest in the

results of the research supporting this article has or will confer a benefit on the authors (Shigeki Kubota, Tetsuya Abe, Hideki Kadone, Kengo Fujii, Aiki Marushima, Tomoyuki Ueno, Yukiyo Shimizu, Yasushi Hada, Akira Matsumura, and Masashi Yamazaki) or on any organization with which the authors are associated.

Funding

This study was supported by the Industrial Disease Clinical Research Grants of the Ministry of Health Labour and Welfare, Japan (14060101-01).

ORCID

Kengo Fujii http://orcid.org/0000-0003-4450-0819
Yukiyo Shimizu http://orcid.org/0000-0001-7491-4516

References

1 Kawamoto H and Sankai Y. Power assist method based on phase sequence and muscle force condition for HAL. Adv Robot 2005;19 (7):717–34.
2 Kubota S, Nakata Y, Eguchi K, Kawamoto H, Kamibayashi K, Sakane M, *et al.* Feasibility of rehabilitation training with a newly developed wearable robot for patients with limited mobility. Arch Phys Med Rehabil 2013;94(6):1080–7.
3 Kawamoto H, Kamibayashi K, Nakata Y, Yamawaki K, Ariyasu R, Sankai Y, *et al.* Pilot study of locomotion improvement using hybrid assistive limb in chronic stroke patients. BMC Neurol 2013;13:141.
4 Aach M, Cruciger O, Sczesny-Kaiser M, Höffken O, Meindl RCh, Tegenthoff M, *et al.* Voluntary driven exoskeleton as a new tool for rehabilitation in chronic spinal cord injury: a pilot study. Spine J 2014;14(12):2847–53.
5 Maeshima S, Osawa A, Nishio D, Hirano Y, Takeda K, Kigawa H. *et al.* Efficacy of a hybrid assistive limb in post-stroke hemiplegic patients: a preliminary report. BMC Neurol 2011;11:116.
6 Nilsson A, Vreede KS, Häglund V, Kawamoto H, Sankai Y, Borg J. Gait training early after stroke with a new exoskeleton--the hybrid assistive limb: a study of safety and feasibility. J Neuroeng Rehabil 2014;2(11):92.
7 Watanabe H, Tanaka N, Inuta T, Saitou H, Yanagi H. Locomotion improvement using a hybrid assistive limb in recovery phase stroke patients: a randomized controlled pilot study. Arch Phys Med Rehabil 2014;95(11):2006–12.
8 Sakakima H, Ijiri K, Matsuda F, Tominaga H, Biwa T, Yone K, *et al.* A newly developed robot suit hybrid assistive limb facilitated walking rehabilitation after spinal surgery for thoracic ossification of the posterior longitudinal ligament: a case report. Case Rep Orthop 2013;2013:621405.
9 Fujii K, Abe T, Kubota S, Marushima A, Kawamoto H, Ueno T, *et al.* The voluntary driven exoskeleton Hybrid Assistive Limb (HAL) for postoperative training of thoracic ossification of the posterior longitudinal ligament: a case report. J Spinal Cord Med 2016;9:1–7.
10 Kubota S, Abe T, Fujii K, Marushima A, Ueno T, Haginoya A, *et al.* Improvement of walking ability using hybrid assistive limb training in a patient with severe thoracic myelopathy caused by ossification of the posterior longitudinal ligament: a case report. J Spine 2016;S7:003.
11 Sapega AA. Muscle performance evaluation in orthopaedic practice. J Bone Joint Surg Am 1990;72(10):1562–74.
12 Kirshblum SC, Burns SP, Biering-Sorensen F, Donovan W, Graves DE, Jha A, Johansen M, *et al.* International standards for neurological classification of spinal cord injury (revised 2011). J Spinal Cord Med 2011;34(6):535–46.
13 Dittuno PL and Ditunno JF Jr. Walking index for spinal cord injury (WISCI II): scale revision. Spinal Cord 2001;39(12):654–6.
14 Linacre JM, Heinemann AW, Wright BD, Granger CV, Hamilton BB. The structure and stability of the Functional Independence Measure. Arch Phys Med Rehabil 1994;75:127–32.
15 Tsuji T, Sonoda S, Domen K, Saitoh E, Liu M, Chino N. ADL structure for stroke patients in Japan based on the functional independence measure. Am J Phys Med Rehabil. 1995;74(6):432–8.
16 Wirz M, Zemon DH, Rupp R, Scheel A, Colombo G, Dietz V, *et al.* Effectiveness of automated locomotor training in patients with chronic incomplete spinal cord injury: a multicenter trial. Arch Phys Med Rehabil 2005;86(4):672–80.
17 Labruyère R and van Hedel HJ. Strength training versus robot-assisted gait training after incomplete spinal cord injury: a randomized pilot study in patients depending on walking assistance. J Neuroeng Rehabil 2014;11:4.
18 Wu M, Landry JM, Schmit BD, Hornby TG, Yen SC. Robotic resistance treadmill training improves locomotor function in human spinal cord injury: a pilot study. Arch Phys Med Rehabil 2012;93(5):782–9.

The Journal of Spinal Cord Medicine

ISSN: 1079-0268 (Print) 2045-7723 (Online) Journal homepage: http://www.tandfonline.com/loi/yscm20

Active elbow flexion is possible in C4 quadriplegia using hybrid assistive limb (HAL®) technology: A case study

Yukiyo Shimizu, Hideki Kadone, Shigeki Kubota, Akira Ikumi, Tetsuya Abe, Aiki Marushima, Tomoyuki Ueno, Ayumu Endo, Hiroaki Kawamoto, Kousaku Saotome, Akira Matsushita, Akira Matsumura, Yoshiyuki Sankai, Yasushi Hada & Masashi Yamazaki

To cite this article: Yukiyo Shimizu, Hideki Kadone, Shigeki Kubota, Akira Ikumi, Tetsuya Abe, Aiki Marushima, Tomoyuki Ueno, Ayumu Endo, Hiroaki Kawamoto, Kousaku Saotome, Akira Matsushita, Akira Matsumura, Yoshiyuki Sankai, Yasushi Hada & Masashi Yamazaki (2017): Active elbow flexion is possible in C4 quadriplegia using hybrid assistive limb (HAL®) technology: A case study, The Journal of Spinal Cord Medicine, DOI: 10.1080/10790268.2017.1305036

To link to this article: http://dx.doi.org/10.1080/10790268.2017.1305036

Published online: 29 Mar 2017.

Research article

Active elbow flexion is possible in C4 quadriplegia using hybrid assistive limb (HAL®) technology: A case study

Yukiyo Shimizu [1], Hideki Kadone[2], Shigeki Kubota[3], Akira Ikumi [4], Tetsuya Abe[4], Aiki Marushima[5], Tomoyuki Ueno[1], Ayumu Endo[1], Hiroaki Kawamoto[6], Kousaku Saotome[2], Akira Matsushita [7], Akira Matsumura[5], Yoshiyuki Sankai[6], Yasushi Hada[1], Masashi Yamazaki[4]

[1]Department of Rehabilitation Medicine, University of Tsukuba Hospital, Tsukuba, Ibaraki 305–8576, Japan, [2]Center for Innovative Medicine and Engineering, University of Tsukuba Hospital, Tsukuba, Ibaraki 305–8576, Japan, [3]Division of Regenerative Medicine for Musculoskeletal System, Faculty of Medicine, University of Tsukuba, Tsukuba, Ibaraki 305–8575, Japan, [4]Department of Orthopaedic Surgery, Faculty of Medicine, University of Tsukuba, Tsukuba, Ibaraki 305–8575, Japan, [5]Department of Neurosurgery, Faculty of Medicine, University of Tsukuba, Tsukuba, Ibaraki 305–8575, Japan, [6]Faculty of Systems and Information Engineering, University of Tsukuba, Tsukuba, Ibaraki 305–8573, Japan, [7]Department of Neurosurgery, Ibaraki Prefectural University Hospital of Health Sciences, Inashiki-gun, Ibaraki 300–0331, Japan

Context: Patients with complete quadriplegia after high cervical spinal cord injury are fully dependent with activities of daily living. Assistive technology can improve their quality of life. We examined the use of a hybrid assistive limb for single joints (HAL-SJ) in a 19-year-old man with complete C4 quadriplegia due to chronic spinal cord injury to restore function of active elbow flexion. This is the first report on the use of the HAL-SJ in a patient with spinal cord injury.

Findings: The HAL-SJ intervention for each elbow was administered in 10 sessions. Clinical assessment using surface EMG was conducted to evaluate muscle activity of the trapezius, biceps brachii, infraspinatus, and triceps brachii muscle before, and during the 2nd, 3rd, 6th, and 9th interventions. Surface electromyography (EMG) before intervention showed no contraction in the upper arms, but in the bilateral trapezius. The HAL-SJ used motion intention from the right trapezius for activation. After the 6th and 7th session, respectively, biceps EMG showed that voluntary contraction and right elbow flexion could be performed by motion intention from the right biceps. After the 10th session, voluntary bicep contraction was possible. HAL-SJ treatment on the left elbow was performed using the same protocol with a similar outcome. After completing treatment on both upper extremities, both biceps contracted voluntarily, and he could operate a standard wheelchair for a short distance independently.

Conclusion: HAL-SJ intervention is feasible and effective in restoring elbow flexor function in a patient with C4 chronic spinal cord injury and complete quadriplegia.

Keywords: Hybrid assistive limb for single joint, Spinal cord injury, Complete quadriplegia, Active elbow flexion, Surface electromyography

Introduction

Individuals with complete quadriplegia from high cervical (around the level of C4) spinal cord injury (SCI) have extensive paralysis and are dependent for all aspects of their care, including activities of daily living (ADLs).[1] Neurological recovery, especially for patients with complete SCI, is rare.[2,3] Therefore, these patients' rehabilitation plan should include environmental control systems to compensate for ADL loss.[4,5]

Regaining limb function is consistently reported as high priority by patients with SCI.[6–8] Recently, assistive technology such as functional electrical stimulation (FES)[9–11] and brain computer interface (BCI)

Correspondence to: Yukiyo Shimizu MD, Department of Rehabilitation Medicine, University of Tsukuba Hospital, 2–1-1, Amakubo, Tsukuba, Ibaraki 305–8576, Japan. E-mail: shiniyukig@md.tsukuba.ac.jp

DOI 10.1080/10790268.2017.1305036

technology[7,8,12–18] has been developed. The aim of FES is to activate individual paralyzed muscles. BCI enables patients to control assistive devices, such as robotic limbs, by using neural signals recorded directly from the brain. However, those two technologies are still in the research stage. Some types of FES require invasive medical procedures to implant electrodes necessary to activate deep muscle. Large systems are often needed.

Exoskeleton robots are available for therapeutic use, including the InMotion ARM,[19] WOTAS[20] and ReoGo.[21] The In-Motion ARM is a clinical version of MIT-MANUS.[22] However, these are large systems and therefore may be challenging for the user to physically manage. For application in a clinical setting, portable devices are preferable. The Myomo e100[23,24] is a portable upper limb therapeutic robot that has been used for patients with stroke.

The Hybrid Assistive Limb (HAL®) is a portable wearable robot that allows users to produce motion based on their voluntary drive and provides motion support to the lower limbs, of which we have previously reported experiences of its use on the lower extremity.[25–30] The HAL® Single Joint type (HAL®-SJ; Cyberdyne Inc., Ibaraki, Japan) is developed for elbow or knee joint motion support (Fig. 1). A small power unit on the lateral side of the joint consists of angular sensors and actuators, and the primary control system consists of a cybernic voluntary control (CVC), based on the motion intention using the bioelectric signals generated by the patient's muscle activities.[25]

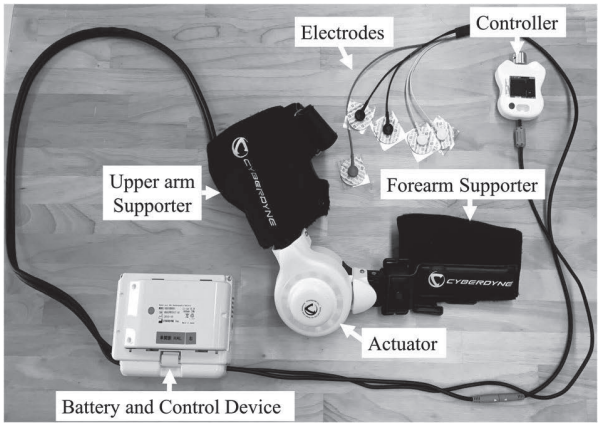

Figure 1 Hybrid assistive limb for single joint (HAL®-SJ). The HAL-SJ for the upper extremity is fitted with an upper arm supporter, forearm supporter, and small power unit placed laterally to the elbow. The power unit consists of angular sensor and an actuator. The controller is handheld and enables visual identification of bioelectric signals of the wearer. The whole system including electrodes for flexion, extension, and reference, and a control unit and battery.

To the best of our knowledge, the HAL-SJ has been utilized in 2 cases: a patient with acute stroke,[31] and postoperatively in a patient with total knee arthroplasty.[32] This is the first report on the use of HAL-SJ for a patient with chronic SCI.

Here, we used functional therapy to restore active elbow flexion using HAL-SJ in a patient with chronic SCI and C4 quadriplegia. We have also reported gait training in the same case using HAL for the lower limb.[30] This is another study on the same patient. This study was conducted with the approval of the Ethics Committee of the Tsukuba University Faculty of Medicine.

Case presentation

Patient characteristics

A 19-year-old man with chronic SCI due to cervical vertebral fracture-dislocation (C3/4) had complete quadriplegia. He presented to our hospital 3 years and 8 months after injury for HAL intervention. His neurological examination before intervention revealed muscle weakness with a manual muscle testing (MMT) score of 5/5 in the trapezius muscle and an MMT score of 0/5 in the deltoid muscle, biceps brachii, supraspinatus muscle, infraspinatus muscle (C5 level), and below. Several months prior, at a previous hospital, FES was performed; motor paralysis was unchanged following FES.

He also had severe sensory disturbances below the neck. A slight sense of pressure remained in his right upper extremity and lower extremities, but no sensation remained in other areas. Articular contracture was not present. No urinary bladder or bowel function remained. Results of the blood and urine tests were normal. He seldom experienced orthostatic hypotension in a sitting position. He had taken antispasmogenic and anticholinergic medications for 3 years after the injury. He required comprehensive care, including feeding, changing clothes, bathing, and egestion. He used a head-controlled electric wheelchair to move independently. Magnetic resonance imaging (MRI) before intervention showed a signal change (high signal at T2WI, low signal at T1WI) of the spinal cord at the level of C3/4 (Fig. 2).

Clinical evaluation before intervention showed the following: grade A (complete motor lesion) on the American Spinal Injury Association (ASIA) impairment scale (AIS), an ASIA motor score (upper and lower limb total) of 0 points, an ASIA sensory score for light touch of 62 points (right: 31 points; left: 31 points), a Barthel Index of 5/100 points, and a Total Functional Independence Measure score of 53/126

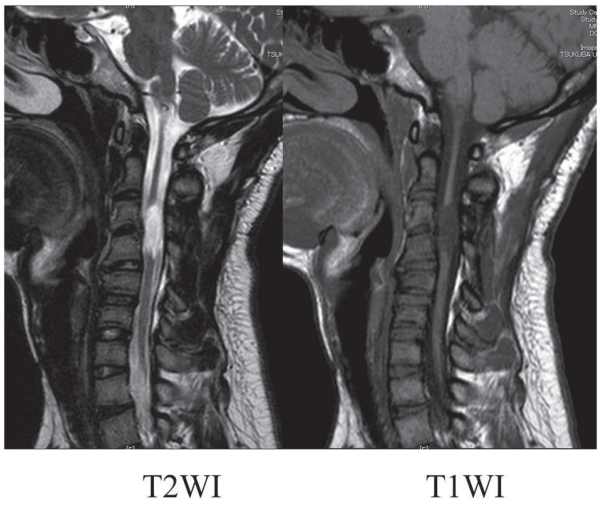

Figure 2 MRI findings before HAL-SJ intervention. Mid-sagittal section of T2-weighted and T1-weighted MR images before HAL intervention. The MR images show the signal changes in the spinal cord at the C3/4 level.

points (motor for wheelchair, 18/91 points; cognitive, 35/35 points).

HAL-SJ intervention

The patient received HAL-SJ intervention (Fig. 3) for the right upper arm 2 times per week for 5 weeks (10 sessions) in addition to standard physical and occupational therapy in the hospital. Physical therapy consisted of range of motion exercise for spasticity and standing exercises for orthostatic hypotension. Occupational therapy consisted of exercise with a portable spring balancer for maintaining a good upper arm position, and neck muscle training. He had undergone similar standard therapy for about 3 years prior to HAL intervention. Each session with the HAL lasted 50 minutes, including rest and the time required to attach and detach the device (5 minutes to attach and 5 minutes to detach). The remaining time was allocated as follows: about 20 minutes for elbow flexion and extension exercise, about 10 minutes for resting, and 10 minutes for evaluation before and after HAL intervention. A medical doctor was on staff and present in case of an emergency, a therapist and a co-operator attached and detached the HAL, and an engineer implemented motion analysis.

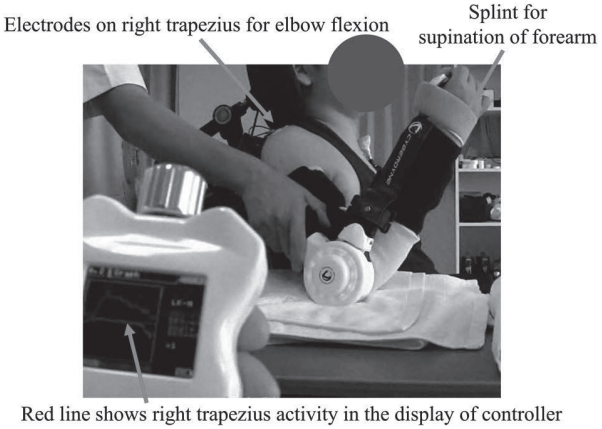

Figure 3 At the first HAL-SJ intervention. During the session, a therapist supported the patient's arm. A cock-up splint was used for maintaining the forearm in supination to align elbow flexion motion with the axis of the biceps muscle contraction. The display of the controller shows bioelectric signals from the right trapezius for elbow flexion as a red line.

A cock-up splint was used to keep the forearm supinated to fit the motion of the HAL-SJ to the axis of the biceps movement.

Twenty weeks after HAL-SJ intervention for the right upper extremity, intervention for the left upper extremity was performed for 12 weeks, once per 1 to 2 weeks (10 sessions) in the outpatient setting.

Clinical Assessment

Clinical assessments were conducted before and after intervention. A Trigno Lab wireless EMG system (Delsys, Massachusetts, USA) was used to evaluate muscle activity of the trapezius, biceps brachii, infraspinatus (ISP), and triceps brachii muscle before and during the 2nd, 3rd, 6th, and 9th intervention. Each muscle's activity was evaluated by the EMG which was collected at 2000Hz and filtered with a 30–400 Hz bandwidth passing filter; an activation envelop was computed by a 200 ms moving window average, using scripts on MATLAB 8.2 (Mathworks, Natick, MA, USA).

Results

Surface EMG before intervention showed no voluntary contraction in the bilateral upper arm, but in the bilateral trapezius (Fig. 4A). Elbow flexion could not be performed using HAL-SJ by placing the electrodes on the right biceps. Therefore, the electrodes for flexion were placed on the right trapezius and, for extension, on the left trapezius. Initially, voluntary right elbow flexion with HAL-SJ was performed by motion intention from the right trapezius in accordance with shoulder elevation. Over time, isometric contraction of the trapezius was performed; therefore, only elbow flexion was performed without shoulder elevation.

After the 6th session, an EMG of the biceps showed voluntary contraction (Fig. 4B). At the same time, the right ISP displayed voluntary contraction separately

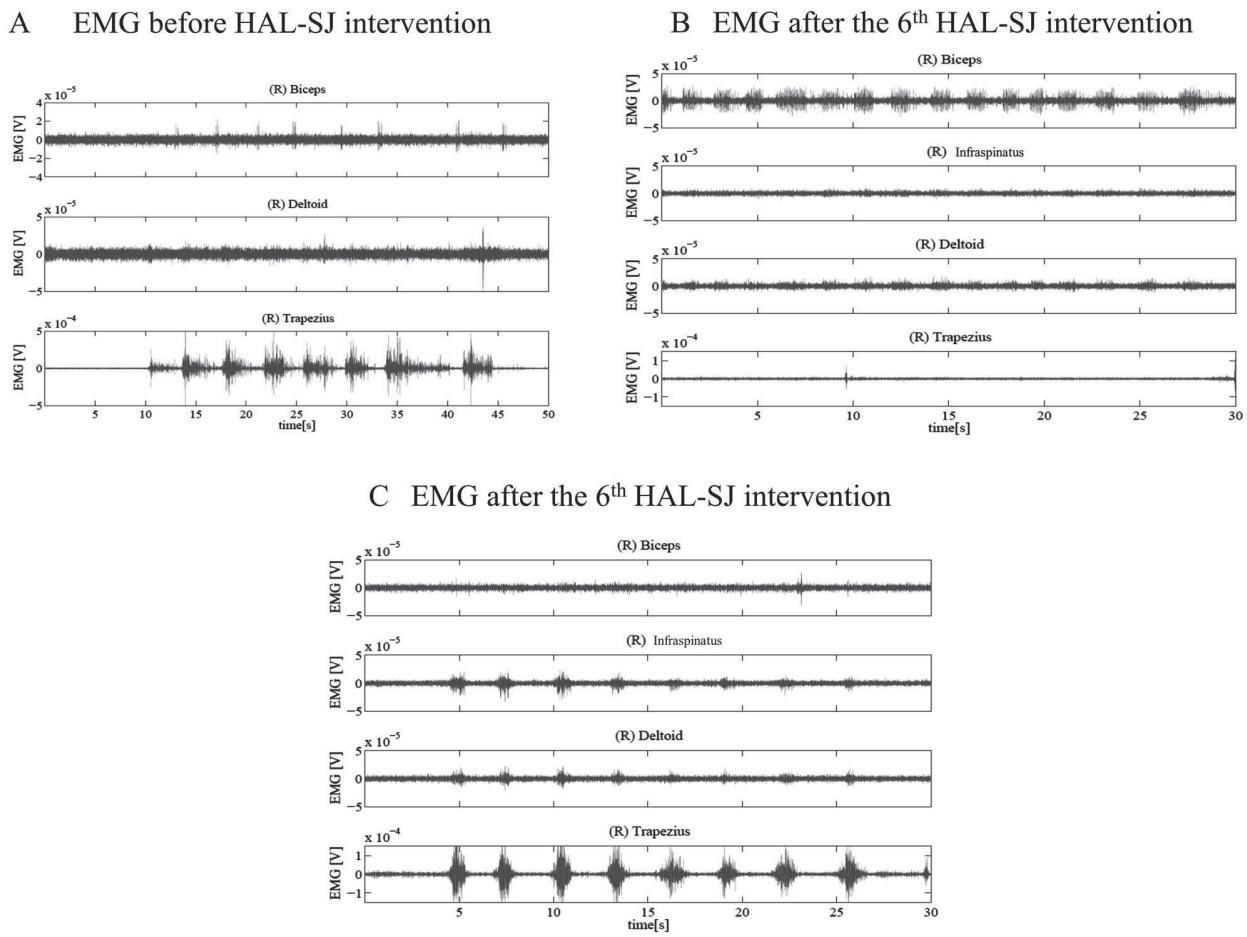

Figure 4 EMG in the right arm before and in the 6th HAL intervention. (A) EMG in the right arm before HAL-SJ intervention on the right side. There were voluntary contractions of the trapezius only. (B) EMG in the right arm after the 6th HAL-SJ intervention on the right side. There were voluntary contractions of the biceps brachii. (C) EMG in the right arm after the 6th HAL-SJ intervention on the right side. There was voluntary contraction of the infraspinatus and trapezius separate from biceps after the 6th HAL-SJ intervention on the right side.

from the right biceps (Fig. 4C). We placed the elbow flexion and extension electrodes on the right biceps and right triceps brachii, respectively, separately from the main HAL-SJ unit, to watch the movement of the HAL-SJ arm; this was done after a routine evaluation to confirm if the HAL could be triggered by the biceps muscle contraction to produce movement (see the linked video).

Right elbow flexion was observed through right biceps brachii contraction (Fig. 5). During the 7th session, voluntary right elbow flexion with HAL-SJ could be performed by placing the flexion electrodes for flexion on the right biceps. After the 10th intervention, he was able to contract the biceps voluntarily.

Following intervention on the right side, he was admitted to the hospital and continued to undergo standard physical and occupational therapy once every 1–2 weeks.

Twenty weeks after beginning intervention on the right side, intervention on the left side was started. At that time, it was difficult for him to voluntarily contract both biceps.

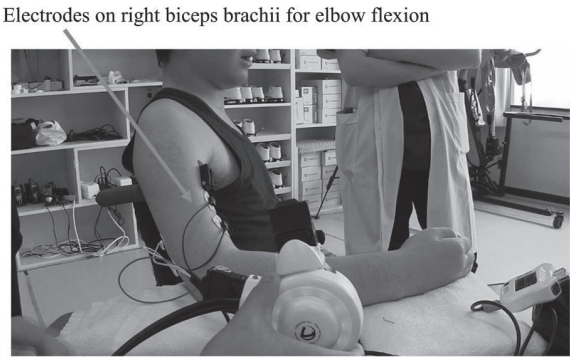

Figure 5 After the 6th HAL-SJ intervention. Electrodes for flexion were placed on the biceps. Elbow flexion was triggered by the right biceps.

Muscle activity before intervention showed bilateral trapezius and left ISP voluntary contraction. During the first session, motion intention for left elbow flexion was taken from the left trapezius. After the 1st session, the muscle activity revealed voluntary contraction of the right biceps, despite only treating the left side.

Before the 2nd session, muscle activity showed voluntary contraction of the left biceps; therefore, the electrodes for flexion were placed on the left biceps. Before the 3rd session, there was no voluntary contraction of the left biceps, and the electrodes for flexion was placed on the left trapezius; however, after the intervention, the left biceps contracted voluntarily. After that, motion intention from the left biceps was used for left elbow flexion in all interventions. While there was only a slight voluntary contraction on the left side after each intervention, voluntary contraction on the right side became stable after each intervention on the left side. The session progression is summarized in Fig. 6. No adverse events associated with HAL-SJ intervention occurred.

On clinical evaluation, Barthel Index and FIM scores remained unchanged. However, an increase in ASIA upper limb score from 0 to 2 was observed, along with an increase in MMT score of the bilateral biceps and bilateral ISP from 0 to 1.

Four months after completion of HAL intervention (1 year after HAL intervention initiation), the patient was able to voluntarily contract the bilateral biceps with right-sided dominance. After completion of HAL intervention, he underwent standard physical and occupational therapy once every 1 to 2 weeks, similar to the second (for the left side) intervention. He drove a standard wheelchair 10 meters by himself using elbow flexion during the clinical evaluation. This was done in the physical therapy room on a slightly uneven surface for about 2 minutes. We considered that this was not a practical setting; however, his progression of elbow flexion was evident.

Discussion

In this study, the HAL-SJ was used to produce active elbow flexion for a patient with complete quadriplegia from chronic SCI. The HAL is a wearable robotic device that can assist with movement according to the wearer's voluntary drive.[26] The HAL- SJ is a portable device, which is convenient for clinical setting use, even for bedridden patients.

The present case used motion intention from the trapezius to produce elbow joint motion; the trapezius is a valuable muscle that remains neurologically intact in a patient with high cervical chronic SCI. He could contract the bilateral biceps voluntarily after HAL-SJ intervention. Voluntary elbow flexion using the HAL-SJ might provide systematic feedback and is considered to have motor learning effects.

Dally and Ruff[12] describe the critical principles of motor learning for central nervous system plasticity as requiring five characteristics: near-normal movements, muscle activation driving movement practice, focused attention, repetition of desired movements, and training specificity. The motion using HAL-SJ, which is derived from volitional contraction of residual neurologically intact muscle, may allow plasticity to occur within the central nervous system.

FES is a type of assistive technology used for rehabilitation.[9–11] This mode was used in the biceps at the previous hospital in our patient; however, there was

		1	2	3	4	5	6	7	8	9	10
Right elbow flexion	Pre HAL EMG	Bil.trapezius	Bil.trapezius	Bil.trapezius			Bil.trapezius			Bil.trapezius Rt. Biceps	
	Electrode for elbow flexion	Rt.trapezius	Rt.trapezius	Rt.trapezius	Rt.trapezius	Rt.trapezius	Rt.trapezius	Rt.biceps	Rt.biceps	Rt.biceps	Rt.biceps
	Post HAL EMG	Bil.trapezius	Bil.trapezius	Bil.trapezius			Bil.trapezius Rt. ISP Rt. Biceps			Bil.trapezius Bil. ISP Rt. Biceps	
Left elbow flexion	Pre HAL EMG	Bil.trapezius Bil. ISP	Bil.trapezius Bil. ISP Bil. Biceps	Bil.trapezius Bil. ISP Rt. Biceps			Bil.trapezius Bil. ISP Bil. Biceps			Bil.trapezius Bil. ISP Bil. Biceps	
	Electrode for elbow flexion	Lt.trapezius	Lt. biceps	Lt. trapezius	Lt. biceps	Lt. biceps	Lt. biceps	Lt. biceps	Lt. biceps	Lt. biceps	Lt. biceps
	Post HAL EMG	Bil.trapezius Bil. ISP Rt. Biceps	Bil.trapezius Bil. ISP Bil. Biceps	Bil.trapezius Bil. ISP Bil. Biceps			Bil.trapezius Bil. ISP Bil. Biceps			Bil.trapezius Bil. ISP Bil. Biceps	

Figure 6 A summary of the HAL-SJ intervention. There were stained Red words for the first findings in EMG, or changes in the place of electrodes. *ISP, infraspinatus.

no effect on active elbow flexion. Elbow flexion using the HAL-SJ had both visual and performance feedback, which were reported to be effective for motor learning.[14]

Mateo *et al.*[33] reviewed studies on motor imagery training, mainly grasping, for patients with tetraplegia due to cervical SCI. They state that change in motor performance and brain plasticity reflect functional and structural changes within the central nervous system, enabling the improvement of compensated movements.

In the present case, HAL-SJ intervention resulted in active biceps contraction and might cause functional changes in the central nervous system. Interestingly, after HAL-SJ intervention for the right upper extremity, the bilateral infraspinatus (a shoulder rotator) could be voluntarily contracted and, after intervention for the left upper extremity, the right biceps could be voluntarily contracted. This volitional control of C5 level muscles, paralyzed before HAL-SJ intervention, was substantial to suggest that plasticity occurs within the central nervous system.

There are some limitations in our study. We only evaluated muscle activity through surface EMG and did not measure brain activity. In the future, we intend to evaluate changes in the central nervous system by using near-infrared spectroscopy during HAL intervention or functional MRI before and after HAL intervention.

In this case, we investigated the feasibility of rehabilitation using the HAL-SJ in an individual with C4 quadriplegia, and confirmed that HAL-SJ intervention could be implemented safely and result in positive outcomes. No HAL-SJ intervention-related adverse events occurred.

To our knowledge, there is no report regarding HAL-SJ intervention for patients with SCI. In the current case, voluntary control of the bilateral biceps emerged after HAL-SJ intervention. He had been fully dependent with the exception of locomotion through a head-controlled electric wheelchair before HAL intervention. After the intervention, he was able to actively contract bilateral elbow flexors and drive a standard wheelchair for a short distance; this was not practical ambulation, but did indicate functional improvement.

Conclusion

The HAL-SJ enabled a patient with complete quadriplegia after chronic high cervical SCI to voluntarily contract the bilateral biceps. The HAL-SJ is feasible and effective in restoring elbow flexion allowing for functional enhancement in patients with chronic SCI.

Acknowledgements

We thank Mayuko Sakamaki and Yumiko Ito, Center for Innovative Medicine and Engineering (CIME), University of Tsukuba Hospital, for their excellent technical assistance.

Disclaimer statements

Declaration of Interest None.

Funding This study was supported by the Industrial Disease Clinical Research Grants of the Ministry of Health Labour and Welfare, Japan (14060101-01).

Ethics approval This study was conducted with approval from the Ethics Committee of the Tsukuba University Faculty of Medicine.

Informed consent Written informed consent was obtained from the patient for publication of this case report and accompanying images.

Supplementary material

Supplementary Material for this article available here: 10.1080/10790268.2017.1305036

ORCID

Yukiyo Shimizu http://orcid.org/0000-0001-7491-4516
Akira Ikumi http://orcid.org/0000-0001-6034-1593
Akira Matsushita http://orcid.org/0000-0003-2335-674X

References

1 Memberg WD, Polasek KH, Hart RL, Bryden AM, Kilgore KL, Nemunaitis GA, *et al.* Implanted neuroprosthesis for restoring arm and hand function in people with high level tetraplegia. Arch Phys Med Rehabil 2014;95(6):1201–11.e1
2 Kirshblum S, Millis S, McKinley W, Tulsky D. Late neurologic recovery after traumatic spinal cord injury. Arch Phys Med Rehabil 2004;85(11):1811–7.
3 Lim PA, Tow AM. Recovery and regeneration after spinal cord injury: a review and summary of recent literature. Ann Acad Med Singapore 2007;36(1):49–57.
4 McDonald DW, Boyle MA, Schumann TL. Environmental control unit utilization by high-level spinal cord injured patients. Arch Phys Med Rehabil 1989;70(8):621–3.
5 Craig A, Tran Y, McIsaac P, Boord P. The efficacy and benefits of environmental control systems for the severely disabled. Med Sci Monit 2005;11(1):Ra32–9.
6 Anderson KD. Targeting recovery: priorities of the spinal cord-injured population. J Neurotrauma 2004;21(10):1371–83.
7 Jackson A, Zimmermann JB. Neural interfaces for the brain and spinal cord--restoring motor function. Nat Rev Neurol 2012;8(12):690–9.
8 Collinger JL, Boninger ML, Bruns TM, Curley K, Wang W, Weber DJ. Functional priorities, assistive technology, and brain-computer interfaces after spinal cord injury. J Rehabil Res Dev 2013;50(2):145.
9 Hara Y, Obayashi S, Tsujiuchi K, Muraoka Y. The effects of electromyography-controlled functional electrical stimulation on upper extremity function and cortical perfusion in stroke patients. Clin Neurophysiol 2013;124(10):2008–15.

10 Naito A, Shimizu Y, Handa Y, Ichie M, Hoshimiya N. Functional anatomical studies of the elbow movements. I. Electromyographic (EMG) analysis. Okajimas Folia Anat Jpn 1991;68(5):283–8.
11 Shimada Y, Sato K, Kagaya H, Konishi N, Miyamoto S, Matsunaga T. Clinical use of percutaneous intramuscular electrodes for functional electrical stimulation. Arch Phys Med Rehabil 1996;77(10):1014–8.
12 Daly JJ, Ruff RL. Construction of efficacious gait and upper limb functional interventions based on brain plasticity evidence and model-based measures for stroke patients. ScientificWorldJournal 2007;7:2031–45.
13 Birbaumer N, Cohen LG. Brain-computer interfaces: communication and restoration of movement in paralysis. J Physiol 2007; 579(Pt 3):621–36.
14 Buch E, Weber C, Cohen LG, Braun C, Dimyan MA, Ard T, *et al.* Think to move: a neuromagnetic brain-computer interface (BCI) system for chronic stroke. Stroke 2008;39(3):910–7.
15 Courtine G, Micera S, DiGiovanna J, del R Millán J. Brain–machine interface: closer to therapeutic reality?. Lancet 2013;381 (9866):515–7.
16 Daly JJ, Wolpaw JR. Brain-computer interfaces in neurological rehabilitation. Lancet Neurol 2008;7(11):1032–43.
17 Dobkin BH. Brain-computer interface technology as a tool to augment plasticity and outcomes for neurological rehabilitation. J Physiol 2007;579(Pt 3):637–42.
18 Cincotti F, Mattia D, Aloise F, Bufalari S, Schalk G, Oriolo G, *et al.* Non-invasive brain–computer interface system: Towards its application as assistive technology. Brain Res Bull 2008;75(6): 796–803.
19 Duret C, Courtial O, Grosmaire AG, Hutin E. Use of a robotic device for the rehabilitation of severe upper limb paresis in subacute stroke: exploration of patient/robot interactions and the motor recovery process. BioMed Res Int 2015;2015:482389.
20 Rocon E, Belda-Lois JM, Ruiz AF, Manto M, Moreno JC, Pons JL. Design and validation of a rehabilitation robotic exoskeleton for tremor assessment and suppression. IEEE Trans Neural Syst Rehabil Eng 2007;15(3):367–78.
21 Bovolenta F, Goldoni M, Clerici P, Agosti M, Franceschini M. Robot therapy for functional recovery of the upper limbs: a pilot study on patients after stroke. J Rehabil Med 2009;41(12):971–5.
22 Krebs HI, Volpe BT, Aisen ML, Hogan N. Increasing productivity and quality of care: robot-aided neuro-rehabilitation. J Rehabil Res Dev 2000;37(6):639–52.
23 Stein J. e100 NeuroRobotic system. Expert Rev Med Devices. 2009;6(1):15–9.
24 Page SJ, Hill V, White S. Portable upper extremity robotics is as efficacious as upper extremity rehabilitative therapy: a randomized controlled pilot trial. Clin Rehabil 2013;27(6):494–503.
25 Kawamoto H, Sankai Y. Power assist method based on Phase Sequence and muscle force condition for HAL. Advanced Robotics. 2005;19(7):717–34.
26 Kawamoto H, Kamibayashi K, Nakata Y, Yamawaki K, Ariyasu R, Sankai Y, *et al.* Pilot study of locomotion improvement using hybrid assistive limb in chronic stroke patients. BMC Neurol 2013;13:141.
27 Kubota S, Nakata Y, Eguchi K, Kawamoto H, Kamibayashi K, Sakane M, *et al.* Feasibility of rehabilitation training with a newly developed wearable robot for patients with limited mobility. Arch Phys Med Rehabil 2013;94(6):1080–7.
28 Fujii K, Abe T, Kubota S, Marushima A, Kawamoto H, Ueno T, *et al.* The voluntary driven exoskeleton Hybrid Assistive Limb (HAL) for postoperative training of thoracic ossification of the posterior longitudinal ligament: a case report. J Spinal Cord Med 2016:1–7. doi:10.1080/10790268.2016.1142056.
29 Fujii K, Abe T, Kubota S, Marushima A, Kawamoto H, Ueno T, Matsushita A, *et al.* The voluntary driven exoskeleton Hybrid Assistive Limb (HAL) for postoperative training of thoracic ossification of the posterior longitudinal ligament: a case report. J Spinal Cord Med 2016:1–7. doi:10.1080/10790268.2016.1142056.
30 Ikumi A, Kubota S, Shimizu Y, Kadone H, Marushima A, Ueno T, *et al.* Decrease of spasticity after hybrid assistive limb® training for a chronic spinal cord injury patient with C4 quadriplegia. J Spinal Cord Med 2016: 1–6. doi:10.1080/ 10790268.2016.1225913.
31 Fukuda H, Morishita T, Ogata T, Saita K, Hyakutake K, Watanabe J, *et al.* Tailor-made rehabilitation approach using multiple types of hybrid assistive limb robots for acute stroke patients: A pilot study. Assist Technol 2016;28(1):53–6.
32 Yoshioka T, Sugaya H, Kubota S, Onishi M, Kanamori A, Sankai Y, *et al.* Knee-Extension Training with a Single-Joint Hybrid Assistive Limb during the Early Postoperative Period after Total Knee Arthroplasty in a Patient with Osteoarthritis. Case Rep Orthop 2016;2016:9610745.
33 Mateo S, Di Rienzo F, Bergeron V, Guillot A, Collet C, Rode G. Motor imageryreinforces brain compensation of reach-to-grasp movement after cervical spinalcord injury. Front Behav Neurosci 2015;9:234.

NeuroRehabilitation 40 (2017) 87–97
DOI:10.3233/NRE-161393
IOS Press

Gait training with Hybrid Assistive Limb enhances the gait functions in subacute stroke patients: A pilot study

Kenichi Yoshikawa[a,*], Masafumi Mizukami[b], Hiroaki Kawamoto[c], Ayumu Sano[a], Kazunori Koseki[a], Kumiko Sano[a], Yasutsugu Asakawa[b], Yutaka Kohno[d], Kei Nakai[d,e], Masahiko Gosho[f] and Hideo Tsurushima[e]

[a]*Department of Physical Therapy, Ibaraki Prefectural University of Health Sciences Hospital, Ami Ibaraki, Japan*
[b]*Department of Physical Therapy, Ibaraki Prefectural University of Health Sciences, Ami Ibaraki, Japan*
[c]*Faculty of Systems and Information Engineering, University of Tsukuba, Tsukuba Ibaraki, Japan*
[d]*Department of Neurology, Ibaraki Prefectural University of Health Sciences Hospital, Ami Ibaraki, Japan*
[e]*Faculty of Medicine, University of Tsukuba, Tsukuba Ibaraki, Japan*
[f]*Department of Clinical Trial and Clinical Epidemiology, Faculty of Medicine, University of Tsukuba, Tsukuba Ibaraki, Japan*

Abstract.
BACKGROUND: The robotic Hybrid Assistive Limb (HAL) provides motion according to the wearer's voluntary activity. HAL training effects on walking speed and capacity have not been clarified in subacute stroke.
OBJECTIVES: To determine improvement in walking ability by HAL and the most effective improvement measure for use in future large-scale trials.
METHODS: Sixteen first-ever hemiplegic stroke patients completed at least 20 sessions over 5 weeks. Per session, the experimental group received no more than 20 min of gait training with HAL (HT) and 40 min of conventional physiotherapy, whereas the control group received at least 60 min of conventional physiotherapy. Primary outcome was maximum walking speed (MWS).
RESULTS: The change in MWS from baseline at week 5 was 11.6 ± 10.6 m/min (HAL group) and 2.2 ± 4.1 m/min (control group) (adjusted mean difference = 9.24 m/min, 95% confidence interval 0.48–18.01, $P = 0.040$). In HAL subjects there were significant increases in Self-selected walking speed (SWS; a secondary outcome) and in step length (a secondary outcome) at MWS and SWS compared with controls.
CONCLUSIONS: HT improved walking speed in hemiplegic sub-acute stroke patients. In future, randomized controlled trials are needed to confirm the utility of HT.

Keywords: Hybrid Assistive Limb, robot-assisted gait training, stroke

1. Introduction

Stroke is a major cause of walking disability worldwide (Feigin, Lawes, Bennett, Barker-Collo, & Parag, 2009). More than 60% of stroke patients have walking disability and approximately 50% find it impossible to walk at disease onset (Jorgensen, Nakayama, Raaschou, & Olsen, 1995). Walking function in stroke patients, including walking speed and gait symmetry, are poorer than in the healthy population (Kollen, Kwakkel, & Lindeman, 2006; Patterson, Gage, Brooks, Black, & McIlroy, 2010a,

*Address for correspondence: Kenichi Yoshikawa, 4733 Ami, Ami-Machi, Inashiki-County, Ibaraki 300-0394, Japan. Tel.: +81 29 888 9216; Fax: +81 29 888 9279; E-mail: yoshikawak@ami.ipu.ac.jp.

2010b; Perry, Garrett, Gronley, & Mulroy, 1995; Suzuki, Imada, Iwaya, Handa, & Kurogo, 1999). Improving the walking ability of stroke patients is therefore an important goal, and various interventions have been tested in the past. In recent years, task-specific training, such as bodyweight-supported treadmill training and a combination of treadmill training and functional electric stimulation, has been recommended from the perspective of recovery of neuroplasticity (Langhorne, Bernhardt, & Kwakkel, 2011; Langhorne, Coupar, & Pollock, 2009; Peurala, Karttunen, Sjogren, Paltamaa, & Heinonen, 2014). However, further training methods need to be developed to promote neuroplasticity and motor learning (Bowden, Woodbury, & Duncan, 2013; Krakauer, Carmichael, Corbett, & Wittenberg, 2012).

Robot-assisted training—a type of task-oriented training—has been developed since the early 2000 s. In a systematic review, Mehrholz, Elsner, Werner, Kugler, and Pohl (2013a, 2013b) reported that patients who receive robot-assisted gait training (RAGT) in combination with physiotherapy after stroke are more likely to achieve independent walking than people who receive gait training without these devices. However, they concluded that this apparent benefit for patients was not supported by the secondary outcomes associated with improvements in walking velocity or walking capacity.

For motor learning of a new task, training that incorporates active participation, whereby the subject voluntarily produces a movement, is thought to be essential for inducing changes in motor performance, cortical activity, and neuroexcitability (Lotze, Braun, Birbaumer, Anders, & Cohen, 2003; Pennycott, Wyss, Vallery, Klamroth-Marganska, & Riener, 2012). However, patient voluntary contribution during most robot-assisted walking has been limited so far, and devices that incorporate active participation are required (Dobkin, 2009; Pennycott et al., 2012).

The Hybrid Assistive Limb (HAL), a robot-assisted training device, was developed by Cyberdyne Corporation (Tsukuba, Japan). HAL is a wearable robot that interactively provides motion according to the wearer's voluntary drive (Kawamoto et al., 2013). Details of the HAL system have been reported in preliminary research (Kawamoto & Sankai, 2002; Kawamoto et al., 2010; Suzuki, Mito, Kawamoto, Hasegawa, & Sankai, 2007). HAL detects the bioelectrical signals generated by the patient's muscle activity or the floor-reaction-force signals caused by the patient's intended weight shifts, or both. HAL enables locomotor training with voluntary drive, and it has the advantages of both voluntary drive and ambulatory performance. Most other exoskeletons use autonomously generated predefined motion. In contrast, HAL generates motion in response to the wearer's voluntary drive. The wearer operates HAL by adjusting his or her muscle activity. Thus HAL is able to conduct locomotor training by providing motion support in response to the user's volition. In addition, other exoskeletons are designed for walking on a treadmill; therefore, they provide a simulated gait that differs from that of walking on a flat floor. In contrast, as a wearable system, HAL delivers locomotor training in an actual ambulatory environment. Clinical trials of gait training using HAL (HAL training; HT) for stroke patients have been already conducted in the chronic stage (Kawamoto et al., 2013; Kubota et al., 2013) and during convalescence (Nilsson et al., 2014; Watanabe, Tanaka, Inuta, Saitou, & Yanagi, 2014) and clinical safety has been confirmed in these studies. However, a systematic review of preliminary research on HT alone reported that reliable clinical trials deserving of meta-analysis had not yet been conducted (Wall, Borg, & Palmcrantz, 2015). The trial by Watanabe et al (2014) has been the only randomized controlled trial comparing HT and conventional gait training for 20 min a day, three times a week in a group of 22 stroke patients in the subacute stage. Their evaluation of walking independence, walking speed, balance function, lower limb motor function, and lower limb muscle strength revealed that only walking independence (functional ambulation category; FAC) showed significant improvement. This result was similar to the conclusions of the above-mentioned systematic reviews of RAGT by Mehrholz et al. (2013b).

As Watanabe et al. indicated, the most effective number and frequency of HT training sessions have not yet been established. According to a review of clinical trials of RAGT, however, at least 20 training sessions over 4 weeks have been used in most clinical trials; in two-thirds of the studies in which only 10 to 12 sessions were used, the efficacy of training in the experimental group could not be confirmed (Schwartz & Meiner, 2015). Therefore, it may be possible that the small number of training sessions used in the clinical trials of Watanabe et al. influenced their finding that HT was efficacious only for improving walking independence.

In the subacute stroke phase recovery varies widely among individuals (Hillis & Tippett, 2014) degree of recovery is associated with severity of paralysis (Ward & Cohen, 2004); level of activities of daily

living (ADL) (Jørgensen et al., 1995; Jorgensen et al., 1995; Stineman & Granger, 1998; Suzuki, Majima, Tsurukawa, & Imasuzuki, 2004; Ween, Alexander, D'Esposito, & Roberts, 1996) in the early days after onset; and age (Kugler, Altenhoner, Lochner, Ferbert, & Hessian Stroke Data Bank Study Group, 2003; Prabhakaran et al., 2007; Tokunaga et al., 2014) (although opinion is divided as to whether age is in fact associated with recovery after stroke). Also, in the stroke recovery process, the area activated vicariously by the brain differs depending on the area and volume of cerebral damage (Ward & Cohen, 2004). Stinear, Byblow, and Ward (2014) reported that there is currently no predictive algorithm for the recovery of lower limb function, although recent evidence indicates that assessment of motor-evoked potential and measurement of fractional anisotropy by diffusion tensor imaging could be of some use.

As above, various factors are connected with functional recovery of stroke patients in the subacute phase. Intervention studies during the early period of recovery in stroke patients admitted to convalescent hospitals or wards may need to be multicenter and large-scale. Wall et al. (2015), the authors of the above-mentioned systematic review, pointed out that post-acute studies are challenging and expensive, because they have to consider not only the impact of spontaneous recovery early after the event but also post-acute health problems.

Therefore, to make it easy to find an effect, we intervened with HAL after the recovery rate of walking ability had reached a plateau in standard rehabilitation. The purpose of our study was to determine the improvement effect of HT on walking ability and to work out the most effective measure for use in a later large-scale trial.

2. Method

2.1. Subjects

Subjects were recruited from an inpatient rehabilitation unit at Ibaraki Prefectural University of Health Sciences Hospital, Japan. All subjects were admitted to our hospital between October 2013 and August 2015 through acute care hospitals to receive acute medical care and acute rehabilitation.

Inclusion criteria were diagnosis of first infarction or hemorrhage with hemiparesis and, for suitability for HAL, height from 150 to 185 cm and weight from 40 to 80 kg. Exclusion criteria were subarachnoid hemorrhage; high-risk heart disease; uncontrollable or severe high blood pressure; severe chronic respiratory disease; severe diabetes mellitus; severe consciousness disorder; severe receptive aphasia; severe cognitive deficit; neuromuscular disorder; marked ataxia; severe orthopedic disease of the lower limbs; significant limitation of range of motion of a lower limb joint; other need for severe risk control in physical therapy; judgment by a medical doctor that intervention would be difficult; or class 4 (independent walking inside the hospital) or class 5 (independent outdoor walking) on the Functional Ambulation Categories Classification (FAC). After having obtained the permission of the chief medical doctor treating each subject, we explained the purpose of the study to the patients by document and word of mouth and obtained written consent from all patients or their legal representatives. After having met the criteria for intervention start, subjects who withdrew their consent; had problems with pain during continuous gait training; manifested a risk of heart disease; developed new epileptic seizures; were extremely easily fatigued; were discharged from hospital before the start of intervention; or were able to walk independently outdoors without a cane or orthosis were excluded. This study was not a randomized clinical trial. Subjects admitted between October 2013 and June 2014 were assigned to the intervention group, and those admitted between July 2014 and July 2015 were assigned to the control group. The second period started straight after the first, without pause. The study design is presented in Fig. 1. The ethics committee of Ibaraki Prefectural University of Health Sciences approved the study, which was part of a research project, the protocol of which was registered with the University Hospital Medical Information Network Clinical Trials Registry (UMIN 000012760).

2.2. Decision on intervention initiation time

To determine when to start the intervention, we measured the subjects' 10-m maximum walking speed (MWS) once a week from the time of admission to our hospital onward. To smooth out individual variabilities, the simple moving average (SMA) of walking speed in the preceding 3 weeks was then calculated. To assess the improvement rate, we calculated the change in the rate by dividing the difference between the present SMA and the previous week's SMA by the previous SMA. We intervened at a time when the rate of improvement of MWS was stable.

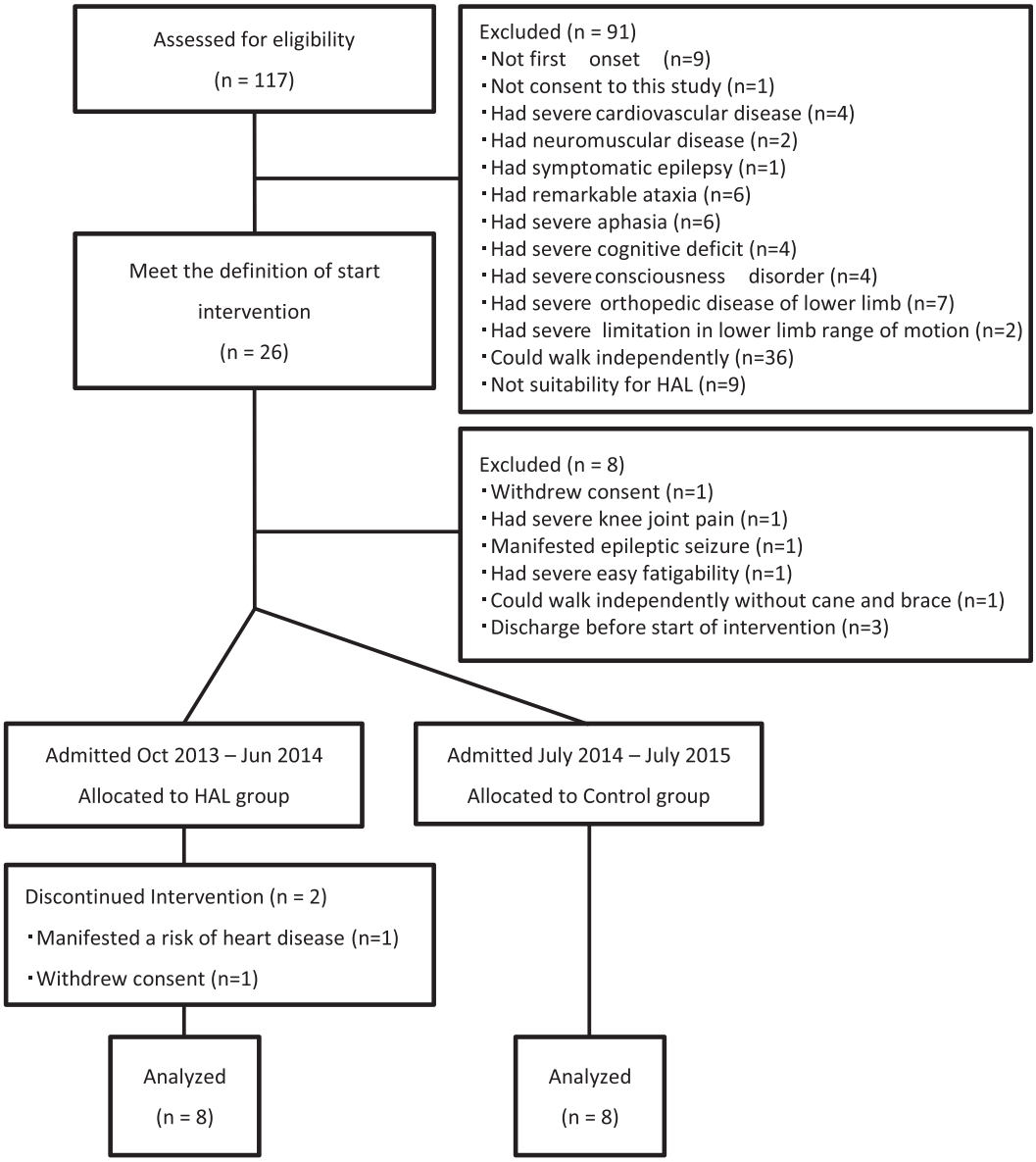

Fig. 1. Flow chart of subject participation.

We defined this as occurring when the change in the rate was less than 10% in the first week and 5% in the second and third weeks consecutively. We then monitored whether or not the change in rate was stable for 3 consecutive weeks. After confirming that this definition had been met, we started the intervention.

2.3. Intervention

The single-leg version of HAL was placed on the subject's paretic side. To prevent falls, the HAL attached to the patient was connected to a mobile suspension system (All-In-One Walking Trainer, Ropox A/S, Næstved, Denmark) without the patient bearing weight (to prevent falls) (Fig. 2). During the intervention, gait training was implemented at a speed judged by the therapists to be as fast as possible while still maintaining good gait posture on level ground. HT was done 4 or 5 times a week for 5 weeks. One gait training session with HAL took no more than 20 min a day, excluding the device-fitting time and rest time. In consideration of variations in the physical condition of the subjects and the occurrence of public holidays, the total number of interventions ranged from 20 to 25. When we had reached this number range, the intervention was considered complete.

During each training session, walking was continuously assisted by HAL. The design and control system for HAL have been described in detail elsewhere (Kawamoto & Sankai, 2002; Kawamoto et al.,

Fig. 2. Walking training with HAL and a mobile suspension system.

2010; Suzuki et al., 2007). The exoskeletal frame was fixed to the pelvis and the lower limbs by thigh and lower leg cuffs. Active actuators were installed at the hip and knee joints and generated assistive extension or flexion torque of these joints. HAL has two control systems, namely Cybernic Voluntary Control (CVC) mode and Cybernic Autonomous Control mode (CAC) (Suzuki et al., 2007). CVC mode drives the amount and timing of the assistive torque provided to each joint for walking on the basis of bioelectrical signals from the flexor and extensor muscles at the hip and knee (Kawamoto & Sankai, 2002). The CAC mode can autonomously generate torque according to the walking pattern by referring to information from the floor reaction force. We used the CVC mode. The gain in assistive torque at each joint in response to these bioelectrical signals was controlled by a therapist so that the walk pattern was as normal and symmetrical as possible. The physical therapists who conducted the HT had attended a class in safe use of the HAL robot suit and had at least 2 years' experience in using HAL. The physical therapist directed the subject to walk with as great an effort as possible at the start of HT. After confirmation that the subject's walking pattern was stable after the start of training, we induced the maximum speed possible at which the patient could maintain a smooth walk with HAL assistance.

During the HT intervention period in the intervention group (HAL group), subjects received no more than 40 min per day of conventional physical therapy and received a total HT walk time of no more than 20 min. In an equivalent period during an intervention period, control group subjects were provided with conventional physical therapy for 60 min or more a day and 5 sessions or more a week for 5 weeks.

2.4. Outcome measures

The primary outcome was Maximum Walking Speed (MWS). The primary outcome was evaluated at the start of intervention, once a week in the intervention period, and at the end of intervention. Time taken to cover the intermediate 10 m of a total distance of 16 m was measured; subjects were allowed 3 m for acceleration and 3 m for deceleration. Time was measured with an electronic stopwatch. Measurement was performed three times and the fastest time used.

Secondary outcomes were the 2-min walk test (2MT), self-selected walking speed over 10 m (SWS), FAC, Fugl-Meyer Assessment of the lower extremity (FMA), Berg Balance Scale (BBS), Functional Independence Measure (FIM), gait asymmetry ratio (AR), cadence at MWS and SWS, and mean step length (SL) at MWS and SWS. Secondary outcomes were evaluated at the start and end of intervention. We set a walk course of 40 m in the physical therapy room to measure 2MT. We started the walk with a signal and measured the distance walked in 2 min by using a digital measuring wheel (DWM-190P, STS Corporation, Nagoya, Japan). Walking speed was self-selected. In the 2MT, subject started from the same starting line as used in the MWS. During the 2MT, we also measured the time taken to cover the intermediate 10 m with a stopwatch, as we had done in the MWS, and calculated the SWS. The evaluator judged FAC by examining the degree of independence in walking during the walk tests. The assessment of the FIM was taken from the latest medical record, which was evaluated regularly by the attending nurse, the charge physical therapist, and an occupational therapist. By using the following formula, AR was calculated from the paretic side single-support time and the non-paretic-side single-support time, which were obtained from the gait analysis during SWS measurement: (Hsu, Tang, & Jan, 2003; Michael D Lewek, Bradley, Wutzke, & Zinder, 2014; Lewek & Randall, 2011; Patterson et al., 2010b).

$$AR = \frac{\text{non-paretic side single support time}}{\text{paretic side single support time}}$$

We videoed subjects with a camera (Sony HDR-CX 390, Tokyo, Japan; sampling rate 30 Hz) for gait analysis from the sagittal plane and the frontal plane. We took the sagittal plane video from a position on the paretic side that was 5 m away from, and at angle to, the course center, such that 5 m of the center of the walk course fitted into the angle of view. The frontal plane video was captured from the right front of the subjects. The videos were analyzed by using two-dimensional movement analysis software (Frame DIAS-V, DKH, Tokyo). The frame numbers of the paretic and non-paretic limb swing phase (as the opposite of the single support time on the other side) from the point of sole off to the point of sole contact were judged and the AR calculated from the two times. This analysis was conducted over 1 min for three gait cycles, and the mean was taken as the representative value. To calculate walking rate and SL, the number of steps in the 10-m measurement section of the MWS or SWS test was counted.

2.5. Statistical analysis

Descriptive statistics are presented as means ± standard deviation (SD) or medians (range: 25% to 75%) or number (%). Differences between the HAL and control groups in terms of subject characteristics at baseline were analyzed by using an unpaired *t*-test or the Wilcoxon's rank sum test, as appropriate, for continuous variables and Fisher's exact test for categorical variables. The change scores at week 5 from baseline in the primary and secondary outcomes were analyzed by using analysis of covariance (ANCOVA), including group as a factor and baseline value as a covariate. All analyses were performed with SPSS version 22.0 (IBM SPSS Statistics version 22.0, USA). Statistical significance was set at $P < 0.05$.

3. Results

One-hundred-seventeen patients were admitted to our rehabilitation hospital post hemiplegic stroke and assessed for eligibility during the test periods. Ninety-one subjects met the exclusion criteria on admission, and eight subjects were excluded after having met the criteria for the start of intervention. Among the 10 subjects allocated to the HAL group, 1 withdrew consent and 1 could not continue rehabilitation because of manifestation of a risk of heart disease. Sixteen subjects were ultimately analyzed (Fig. 2).

All baseline characteristics did not differ significantly between the two groups, although the quantity of standard rehabilitation during intervention in the control group was somewhat larger than that including HT in the HAL group (Table 1).

The change in MWS from baseline at week 5, which was the primary endpoint, was 11.6 ± 10.6 m/min for the HAL group and 2.2 ± 4.1 m/min for the control group; there was a significant difference between the two groups (adjusted mean difference = 9.24; 95% confidence interval (CI) 0.48–18.01; $P = 0.040$) (Table 2). In the group comparison of changes in secondary outcomes, the HAL group had a large and significant increase in SWS (difference = 7.34 m/min, 95% CI 1.75–12.93, $P = 0.014$), SL at MWS (difference = 0.06 m, 95% CI 0.02–0.11, $P = 0.008$), and SL at SWS (difference = 0.05 m, 95% CI 0.00–0.10, $P = 0.037$) (Table 2). In the HAL group, SWS, MWS, and 2MT increased in similar ways during the 5-week intervention period (Fig. 3).

Table 1
Characteristics of subjects at baseline

Characteristics		HAL group ($n = 8$)	Control group ($n = 8$)	*P*
Age		58.6 ± 16.9	62.6 ± 11.5	0.59*
Sex	Male	5	6	1.00†
	Female	3	2	
Time since stroke at the start of intervention (day)		132.6 ± 18.5	129.6 ± 23.3	0.78*
Type of stroke	Hemorrhagic	5	6	1.00†
	Ischemic	3	2	
Side of paresis	Right	5	4	1.00†
	Left	3	4	
Quantity of Physical Therapy during intervention period including HT (h)‡		27.7 ± 1.83‡	32.9 ± 7.42	0.09*

Values are n or mean ± SD. *Unpaired *t* test. †Fisher's exact test. ‡Including HAL training only in HAL group.

Table 2
Differences between groups for all outcomes

Response	Visit	HAL group ($n = 8$)	Control group ($n = 8$)	Diff 95% CI	P
MWS (m/min)	Pre	49.8 ± 20.1	47.9 ± 24.9		
	Post	61.4 ± 26.6	50.1 ± 25.0		
	Diff	11.6 ± 10.6	2.2 ± 4.1	9.24 (0.48, 18.01)	0.040*
SWS (m/min)	Pre	38.6 ± 17.2	36.6 ± 20.3		
	Post	50.0 ± 20.3	40.6 ± 20.6		
	Diff	11.5 ± 5.4	4.0 ± 4.7	7.34 (1.75, 12.93)	0.014*
2MT (m)	Pre	78.9 ± 33.3	69.7 ± 33.9		
	Post	100.1 ± 40.6	80.1 ± 38.3		
	Diff	21.1 ± 12.4	10.4 ± 8.9	9.46 (–1.59, 20.5)	0.087
FAC	Pre	3.1 ± 0.8	3.1 ± 0.6		
	Post	3.5 ± 0.9	3.4 ± 0.5		
	Diff	0.4 ± 0.5	0.3 ± 0.5	0.13 (–0.40, 0.65)	0.614
FMA	Pre	23.8 ± 3.7	22.9 ± 7.4		
	Post	24.5 ± 4.3	23.6 ± 6.9		
	Diff	0.8 ± 1.5	0.8 ± 1.2	0.03 (–1.45, 1.52)	0.965
BBS	Pre	46.4 ± 6.6	43.8 ± 9.8		
	Post	48.8 ± 7.8	43.8 ± 8.4		
	Diff	2.4 ± 3.4	0.0 ± 2.9	2.65 (–0.84, 6.13)	0.125
FIM	Pre	76.6 ± 9.0	69.1 ± 11.9		
	Post	79.5 ± 8.1	71.5 ± 11.6		
	Diff	2.9 ± 2.7	2.4 ± 2.6	1.13 (–1.90, 4.17)	0.434
AR at SWS	Pre	1.60 ± 0.30	1.50 ± 0.45		
	Post	1.48 ± 0.21	1.67 ± 0.55		
	Diff	–0.12 ± 0.26	0.18 ± 0.27	–0.28 (–0.58, 0.01)	0.057
Cadence at MWS (steps/min)	Pre	98.5 ± 20.7	100.5 ± 37.1		
	Post	105.6 ± 21.6	105.1 ± 36.9		
	Diff	7.1 ± 10.7	4.6 ± 5.0	2.43 (–6.85, 11.71)	0.581
Cadence at SWS (steps/min)	Pre	84.4 ± 17.9	84.7 ± 26.5		
	Post	96.2 ± 19.2	93.7 ± 29.0		
	Diff	11.8 ± 3.1	9.0 ± 7.9	2.78 (–3.83, 9.38)	0.380
SL at MWS (m)	Pre	0.49 ± 0.12	0.46 ± 0.15		
	Post	0.56 ± 0.17	0.47 ± 0.17		
	Diff	0.07 ± 0.06	0.00 ± 0.02	0.06 (0.02, 0.11)	0.008**
SL at SWS (m)	Pre	0.44 ± 0.13	0.42 ± 0.15		
	Post	0.51 ± 0.15	0.44 ± 0.16		
	Diff	0.07 ± 0.05	0.02 ± 0.04	0.05 (0.00, 0.10)	0.037*

Abbreviations: MWS, Maximum walking speed; SWS, Self selected walking speed; FAC, functional ambulation categories classification; FMA, Fugl-Meyer Assessment of Motor Recovery after Stroke; BBS, Berg Balance Scale; FIM, Functional independence measure; AR, Asymmetry ratio; SL, Step length. Analyzed by using ANCOVA including group as a factor and baseline as a covariate. *$P < 0.05$, **$P < 0.01$.

4. Discussion

The HAL group had a significantly greater increase in MWS than the control group during the intervention period. Conventional physical therapy plus HT improved MWS more than did conventional physical therapy. SWS also significantly increased. Improvement in walking speed of hemiplegic stroke patients is connected directly to ADL and social participation (Perry et al., 1995; Schmid et al., 2007). The increases in MWS and SWS by HT were socially significant. Therefore, walking speed was found to be effective outcome measure in the design of this study.

Furthermore, we found increases in SL at MWS and SWS with improvement in walking ability. Goldie, Matyas, and Evans (2001) reported that subjects with stroke spent more time in the two double-limb support (DLS) phases and in unaffected single limb support (SLS) than did control healthy subjects. This extended duration contributed to low gait speed; if the goal of treatment is to increase gait velocity and to improve gait pattern, then treatment strategies should be directed toward reducing the two DLS phases and the unaffected SLS. In addition, weight shift to the paretic side is essential in walking, as it allows the non-paretic limb to be moved and, consequently, a step to be taken (Perry & Davids, 1992). The ability to maintain single-limb support is an important determinant of gait stability (Gunes, 2007; Perry & Davids, 1992). Thus,

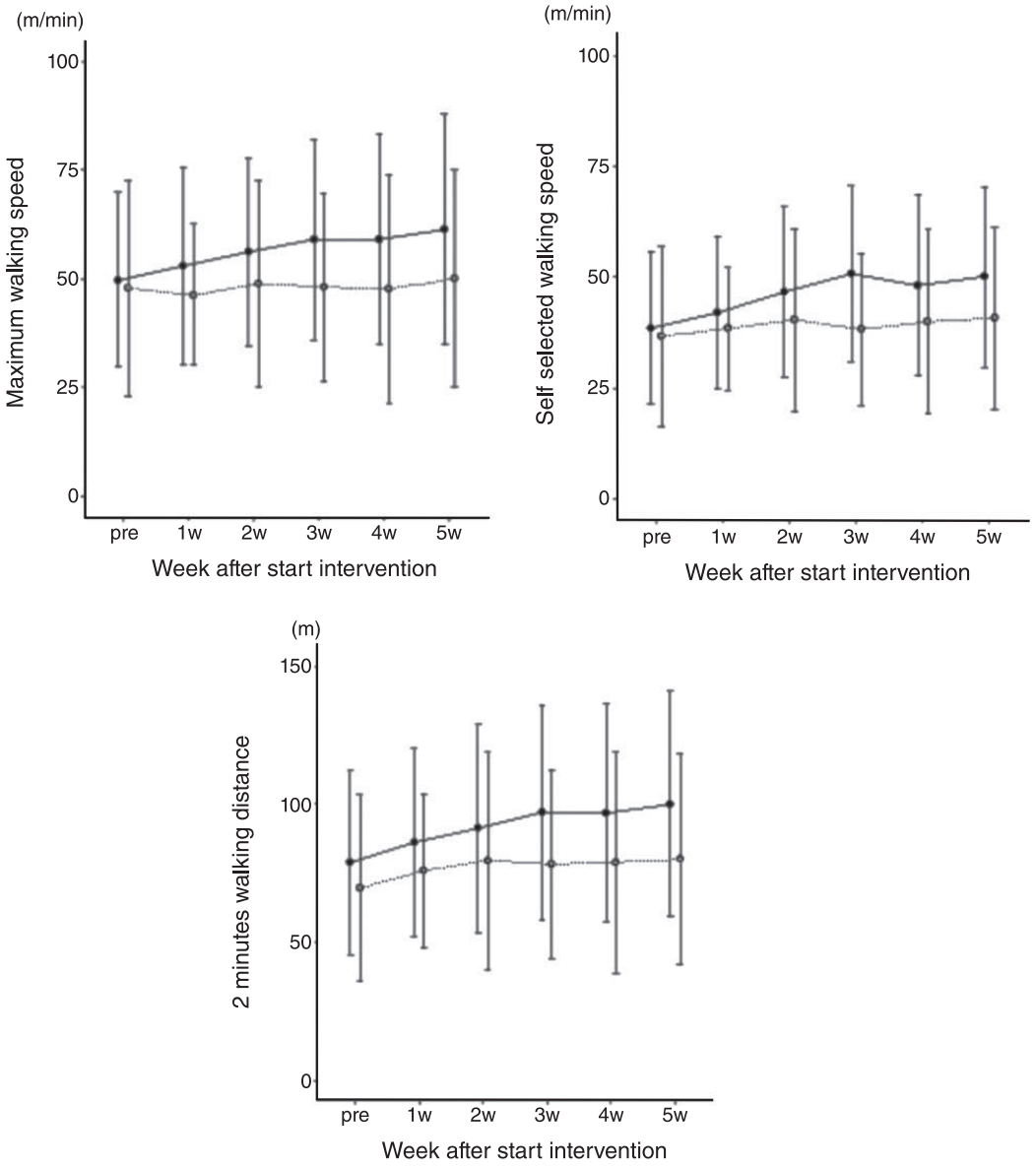

Fig. 3. Transition of primary outcome mean values. Black circles and solid lines, HAL group. White circles and dashed lines, control group. Some values are missing in the control group at 2 weeks ($n = 6$) and 4 weeks ($n = 7$).

single-support stability training helps to achieve more symmetric gait in stroke patients with hemiparesis (Gunes, 2007; Olney & Richards, 1996). Through walking with HAL, wearers are provided assistance to reach near-normal timing in the stance phase and the swing phase. We therefore speculated that SL changed because, through HT, subjects learned a gait pattern that was near normal. In addition, although there was no statistically significant difference in AR between the groups, there was a trend toward improvement of gait asymmetry in the HAL group ($P = 0.057$). The AR result was likely influenced by the small sample size, but in practice the change in AR probably supported the change in gait pattern in the HAL group. Gait asymmetry ratios like the AR have a negative relationship with walking speed (Patterson et al., 2010b; 2008), and the change in walking pattern with HT may have contributed to the increase in walking speed. From the perspective of motor learning, repetitive movement and voluntary exercise are important elements (Dobkin, 2009; Lotze et al., 2003; Pennycott et al., 2012). In HT, the physical therapist can adjust the joint torque, which HAL assists, in real time according to size of the muscle action potential from the subject's muscles. Thus therapists can regulate the degree of effort made by the subjects while they maintain a near-normal walking pattern. Therefore, the change in walking

pattern as a result of changes in SL and AR was considered to result from motor learning effects due to the HT.

Here, we obtained improvements in walking speed by using four or five HT sessions a week for 5 weeks. However, the optimum number and frequency of training sessions for effective HT have not yet been established (Watanabe et al., 2014). Interestingly, the gait function parameters we tested during intervention increased in similar ways during the 5-week intervention period (Fig. 3)—especially in the first 3 weeks (12 to 15 sessions). Therefore, the results of the clinical trials of Watanabe et al. (2014), who found that only walking independence was influenced by HT, may have reflected an insufficient frequency and number of training enforcement sessions. However from our results and those of Watanabe et al., we were not able to extract information on the effects of duration or number of training sessions on walking speed. In a further trial we will need to examine the duration and number of training sessions to determine the maximum cost effectiveness of HT.

We confirmed here that both groups started intervention approximately 19 weeks on average from stroke onset. In preliminary research that measured the maximum walking speed of subjects with hemiplegic stroke every week from onset (Kollen et al., 2006), maximum walking speed was found to reach a plateau from approximately 18 weeks onward. Furthermore, Kwakkel et al. Kwakkel, Wagenaar, Twisk, Lankhorst, and Koetsier (1999), in a randomized clinical trial of intensity training of the upper or lower limbs in stroke patients, reported that, in an intense arm-training group and an intense leg-training group, improvement of maximum walking speed was not found after 20 weeks from stroke onset in either group. We found here that walking speed reached a plateau in our study groups at approximately the same time as in these earlier studies. We therefore consider than the definition of intervention start that we used here was valid as a decision-making tool in individual subjects.

Because we had only a small sample size and our study was not a strictly randomized trial, in future we will need to run a large-scale randomized clinical trial. Despite the small sample size, our results indicated that the improvements we obtained in walking speed and gait pattern by HT were meaningful. We also presented a means of adjusting the time of intervention under particular conditions so as to test each patient effectively.

5. Conclusion

We found here that HT improved walking speed in hemiplegic sub-acute stroke patients. We considered that improvement in walking pattern contributed to the improvement in walking speed. Also, we obtained consistent validation of the selection criteria, the intervention method, and the time of intervention start. In future, randomized controlled trials are needed to confirm the utility of HT.

Contributions

KY participated in the design of the study, performed the data collection, analysis, and interpretation, and drafted and revised the manuscript. MM participated in the design of the study, collected patient's informed consent and drafted the manuscript. AS and KK performed the HT.

KS performed the assessments. MG conducted the statistical analysis and interpretation and edited the manuscript. HK participated in the design of the study and provided the HAL suits and technical support. YA, YK, HN, KN, and HT participated in the coordination and design of the study and in finalizing the manuscript.

Conflict of interest

Kenichi Yoshikawa, Masafumi Mizukami, Ayumu Sano, Kazunori Koseki, Kumiko Sano, Masahiko Gosho, Hiroaki Kawamoto, Yasutsugu Asakawa, Yutaka Kohno, Hiroshi Nagata, Kei Nakai, and Hideo Tsurushima have no competing interests to declare. Hiroaki Kawamoto is a founder, shareholder, and external director of CYBERDYNE Inc., which produces HAL.

Funding

This work was supported by a Grant-in-Aid for Project Research (1247) from Ibaraki Prefectural University of Health Sciences, Japan.

References

Bowden, M. G., Woodbury, M. L., & Duncan, P. W. (2013). Promoting neuroplasticity and recovery after stroke: Future directions for rehabilitation clinical trials. *Current Opinion in Neurology*, *26*(1), 37-42. doi:10.1097/WCO.0b013e32835c5ba0

Dobkin, B. H. (2009). Motor rehabilitation after stroke, traumatic brain, and spinal cord injury: Common denominators within recent clinical trials. *Current Opinion in Neurology*, *22*(6), 563.

Feigin, V. L., Lawes, C. M., Bennett, D. A., Barker-Collo, S. L., & Parag, V. (2009). Worldwide stroke incidence and early case fatality reported in 56 population-based studies: A systematic review. *Lancet Neurology*, *8*(4), 355-369. doi:10.1016/s1474-4422(09)70025-0

Goldie, P. A., Matyas, T. A., & Evans, O. M. (2001). Gait after stroke: Initial deficit and changes in temporal patterns for each gait phase. *Archives of Physical Medicine and Rehabilitation*, *82*(8), 1057-1065.

Gunes, Y. (2007). Walking after stroke. *Journal of Physical Medicine and Rehabilitation Sciences*, *1*, 1-8.

Hillis, A. E., & Tippett, D. C. (2014). Stroke recovery: Surprising influences and residual consequences. *Adv Med*, *2014*, 1-10. doi:10.1155/2014/378263

Hsu, A. L., Tang, P. F., & Jan, M. H. (2003). Analysis of impairments influencing gait velocity and asymmetry of hemiplegic patients after mild to moderate stroke. *Archives of Physical Medicine and Rehabilitation*, *84*(8), 1185-1193. doi:10.1016/s0003-9993(03)00030-3

Jørgensen, H. S., Nakayama, H., Raaschou, H. O., Vive-Larsen, J., Støier, M., & Olsen, T. S. (1995). Outcome and time course of recovery in stroke. Part II: Time course of recovery. The copenhagen stroke study. *Archives of Physical Medicine and Rehabilitation*, *76*(5), 406-412.

Jorgensen, H. S., Nakayama, H., Raaschou, H. O., & Olsen, T. S. (1995). Recovery of walking function in stroke patients: The Copenhagen Stroke Study. *Archives of Physical Medicine and Rehabilitation*, *76*(1), 27-32.

Kawamoto, H., Kamibayashi, K., Nakata, Y., Yamawaki, K., Ariyasu, R., Sankai, Y., . . . & Ochiai, N. (2013). Pilot study of locomotion improvement using hybrid assistive limb in chronic stroke patients. *BMC Neurology*, *13*, 141. doi:10.1186/1471-2377-13-141

Kawamoto, H., & Sankai, Y. (2002). Power assist system HAL-3 for gait disorder person *Computers helping people with special needs* (pp. 196-203): Springer.

Kawamoto, H., & Sankai, Y. (2002). Power assist system HAL-3 for gait disorder person. *Computers helping people with special needs*, 19-29.

Kawamoto, H., Taal, S., Niniss, H., Hayashi, T., Kamibayashi, K., Eguchi, K., & Sankai, Y. (2010). Voluntary motion support control of Robot Suit HAL triggered by bioelectrical signal for hemiplegia. Paper presented at the Engineering in Medicine and Biology Society (EMBC), 2010 Annual International Conference of the IEEE.

Kollen, B., Kwakkel, G., & Lindeman, E. (2006). Hemiplegic gait after stroke: Is measurement of maximum speed required? *Archives of Physical Medicine and Rehabilitation*, *87*(3), 358-363.

Krakauer, J. W., Carmichael, S. T., Corbett, D., & Wittenberg, G. F. (2012). Getting Neurorehabilitation Right What Can Be Learned From Animal Models? *Neurorehabilitation and Neural Repair*, *26*(8), 923-931.

Kubota, S., Nakata, Y., Eguchi, K., Kawamoto, H., Kamibayashi, K., Sakane, M., . . . & Ochiai, N. (2013). Feasibility of rehabilitation training with a newly developed wearable robot for patients with limited mobility. *Archives of Physical Medicine and Rehabilitation*, *94*(6), 1080-1087. doi:10.1016/j.apmr.2012.12.020

Kugler, C., Altenhoner, T., Lochner, P., Ferbert, A., & Hessian Stroke Data Bank Study Group, A. S. H. (2003). Does age influence early recovery from ischemic stroke? A study from the Hessian Stroke Data Bank. *Journal of Neurology*, *250*(6), 676-681. doi:10.1007/s00415-003-1054-8

Kwakkel, G., Wagenaar, R. C., Twisk, J. W., Lankhorst, G. J., & Koetsier, J. C. (1999). Intensity of leg and arm training after primary middle-cerebral-artery stroke: A randomised trial. *The Lancet*, *354*(9174), 191-196.

Langhorne, P., Bernhardt, J., & Kwakkel, G. (2011). Stroke rehabilitation. *Lancet*, *377*(9778), 1693-1702. doi:10.1016/S0140-6736(11)60325-5

Langhorne, P., Coupar, F., & Pollock, A. (2009). Motor recovery after stroke: A systematic review. *Lancet Neurology*, *8*(8), 741-754. doi:10.1016/S1474-4422(09)70150-4

Lewek, M. D., Bradley, C. E., Wutzke, C. J., & Zinder, S. M. (2014). The relationship between spatiotemporal gait asymmetry and balance in individuals with chronic stroke. *Journal of Applied Biomechanics*, *30*(1), 31-36.

Lewek, M. D., & Randall, E. P. (2011). Reliability of spatiotemporal asymmetry during overground walking for individuals following chronic stroke. *Journal of Neurologic Physical Therapy*, *35*(3), 116-121. doi:10.1097/NPT.0b013e318227fe70

Lotze, M., Braun, C., Birbaumer, N., Anders, S., & Cohen, L. G. (2003). Motor learning elicited by voluntary drive. *Brain*, *126*(Pt 4), 866-872.

Mehrholz, J., Elsner, B., Werner, C., Kugler, J., & Pohl, M. (2013a). Electromechanical-assisted training for walking after stroke. *Cochrane Database Syst Rev*, *7*, Cd006185. doi:10.1002/14651858.CD006185.pub3

Mehrholz, J., Elsner, B., Werner, C., Kugler, J., & Pohl, M. (2013b). Electromechanical-assisted training for walking after stroke updated evidence. *Stroke*, *44*(10), e127-e128.

Nilsson, A., Vreede, K. S., Haglund, V., Kawamoto, H., Sankai, Y., & Borg, J. (2014). Gait training early after stroke with a new exoskeleton–the hybrid assistive limb: A study of safety and feasibility. *Journal of Neuroengineering and Rehabilitation*, *11*, 92. doi:10.1186/1743-0003-11-92

Olney, S. J., & Richards, C. (1996). Hemiparetic gait following stroke. Part I: Characteristics. *Gait and Posture*, *4*(2), 136-148.

Patterson, K. K., Gage, W. H., Brooks, D., Black, S. E., & McIlroy, W. E. (2010a). Changes in gait symmetry and velocity after stroke: A cross-sectional study from weeks to years after stroke. *Neurorehabilitation and Neural Repair*, *24*(9), 783-790. doi:10.1177/1545968310372091

Patterson, K. K., Gage, W. H., Brooks, D., Black, S. E., & McIlroy, W. E. (2010b). Evaluation of gait symmetry after stroke: A comparison of current methods and recommendations for standardization. *Gait and Posture*, *31*(2), 241-246. doi:10.1016/j.gaitpost.2009.10.014

Patterson, K. K., Parafianowicz, I., Danells, C. J., Closson, V., Verrier, M. C., Staines, W. R., . . . & McIlroy, W. E. (2008). Gait asymmetry in community-ambulating stroke survivors. *Archives of Physical Medicine and Rehabilitation*, *89*(2), 304-310. doi:10.1016/j.apmr.2007.08.142

Pennycott, A., Wyss, D., Vallery, H., Klamroth-Marganska, V., & Riener, R. (2012). Towards more effective robotic gait training for stroke rehabilitation: A review. *Journal of Neuroengineering and Rehabilitation*, *9*, 65. doi:10.1186/1743-0003-9-65

Perry, J., & Davids, J. R. (1992). Gait analysis: Normal and pathological function (Vol. 12). NJ: Slack.

Perry, J., Garrett, M., Gronley, J. K., & Mulroy, S. J. (1995). Classification of Walking Handicap in the Stroke Population. *Stroke*, *26*(6), 982-989. doi:10.1161/01.str.26.6.982

Peurala, S. H., Karttunen, A. H., Sjogren, T., Paltamaa, J., & Heinonen, A. (2014). Evidence for the effectiveness of walking training on walking and self-care after stroke: A systematic review and meta-analysis of randomized controlled trials. *Journal of Rehabilitation Medicine*, *46*(5), 387-399. doi:10.2340/16501977-1805

Prabhakaran, S., Zarahn, E., Riley, C., Speizer, A., Chong, J. Y., Lazar, R. M., … & Krakauer, J. W. (2007). Inter-individual variability in the capacity for motor recovery after ischemic stroke. *Neurorehabilitation and Neural Repair*, *22*(1), 64-71.

Schmid, A., Duncan, P. W., Studenski, S., Lai, S. M., Richards, L., Perera, S., & Wu, S. S. (2007). Improvements in speed-based gait classifications are meaningful. *Stroke*, *38*(7), 2096-2100. doi:10.1161/STROKEAHA.106.475921

Schwartz, I., & Meiner, Z. (2015). Robotic-assisted gait training in neurological patients: Who may benefit? *Annals of Biomedical Engineering*, *43*(5), 1260-1269.

Stinear, C. M., Byblow, W. D., & Ward, S. H. (2014). An update on predicting motor recovery after stroke. *Annals of Physical and Rehabilitation Medicine*, *57*(8), 489-498. doi:http://dx.doi.org/10.1016/j.rehab.2014.08.006

Stineman, M. G., & Granger, C. V. (1998). Outcome, Efficiency, and Time-Trend Pattern Analyses for Stroke Rehabilitation1. *American Journal of Physical Medicine and Rehabilitation*, *77*(3), 193-201.

Suzuki, E., Majima, M., Tsurukawa, T., & Imasuzuki, T. (2004). A case-mix study of stroke patients in the post acute stage. *Jpn J Rehabil Med*, *41*(8), 540-547.

Suzuki, K., Imada, G., Iwaya, T., Handa, T., & Kurogo, H. (1999). Determinants and predictors of the maximum walking speed during computer-assisted gait training in hemiparetic stroke patients. *Archives of Physical Medicine and Rehabilitation*, *80*(2), 179-182.

Suzuki, K., Mito, G., Kawamoto, H., Hasegawa, Y., & Sankai, Y. (2007). Intention-based walking support for paraplegia patients with Robot Suit HAL. *Advanced Robotics*, *21*(12), 1441-1469.

Tokunaga, M., Watanabe, S., Nakanishi, R., Yamanaga, H., Yonemitsu, H., Mita, S., … & Yamaga, M. (2014). The influence of stroke type, gender, and age on FIM improvement. *Japanese Journal of Comprehensive Rehabilitation Science*, *5*, 136-140.

Wall, A., Borg, J., & Palmcrantz, S. (2015). Clinical application of the Hybrid Assistive Limb (HAL) for gait training—a systematic review. *Frontiers in Systems Neuroscience*, *9*, 48. doi:10.3389/fnsys.2015.00048

Ward, N. S., & Cohen, L. G. (2004). Mechanisms underlying recovery of motor function after stroke. *Archives of Neurology*, *61*(12), 1844-1848. doi:10.1001/archneur.61.12.1844

Watanabe, H., Tanaka, N., Inuta, T., Saitou, H., & Yanagi, H. (2014). Locomotion improvement using a hybrid assistive limb in recovery phase stroke patients: A randomized controlled pilot study. *Archives of Physical Medicine and Rehabilitation*, *95*(11), 2006-2012. doi:10.1016/j.apmr.2014.07.002

Ween, J. E., Alexander, M. P., D'Esposito, M., & Roberts, M. (1996). Factors predictive of stroke outcome in a rehabilitation setting. *Neurology*, *47*(2), 388-392.

Abnormal Distribution of $GABA_A$ Receptors in Brain of Duchenne Muscular Dystrophy Patients

Yuji Suzuki, MD, PhD[1,2], Shinya Higuchi, MD[2], Izumi Aida, MD[2], Takashi Nakajima, MD, PhD[2], Tsutomu Nakada, MD, PhD[1]

[1] Center for Integrated Human Brain Science, Brain Research Institute, University of Niigata, Niigata, Japan

[2] National Hospital Organization, Niigata National Hospital, Niigata, Japan

Acknowledgment

The study was supported by grants from the Ministry of Education, Culture, Sports, Science, and Technology (Japan) and University of Niigata. The authors thank Shuichi Tomizawa, Yousuke Yonemochi, Motoi Fujita and Satoru Kinoshita for the clinical assistance, Naoyuki Shibayama for his help in the neuropsychological assessments.

Correspondence to:

Yuji Suzuki, MD, PhD

Center for integrated Human Brain Science

Brain Research Institute, University of Niigata

1-757 Asahimachi, Niigata 951-8585, Japan;

Tel: 81-25-227-0683/Fax: 81-25-227-0822

E-mail: yuji-s@bri.niigata-u.ac.jp

Running title: $GABA_A$-Rs in DMD

Abstract

Introduction: We sought to: (1) determine the distribution of $GABA_A$ receptors ($GABA_A$-Rs) in the brain of Duchenne muscular dystrophy (DMD) patients; and (2) ascertain if the distribution pattern correlates with cognitive dysfunction.

Methods: Fourteen DMD patients [young adults (n=7, 18-25 year-old and older adults (n=7, 30-37 year-old) groups] and 16 age-matched normal volunteers participated. $GABA_A$-R distribution was assessed using ^{123}I-IMZ-SPECT. Neuropsychological assessments were performed using 3 different test batteries, WAIS-III, WMS-R, and Wisconsin Card Sorting Test (WCST).

Results: All DMD patients showed significant decline in ^{123}I-IMZ uptake in the prefrontal cortex ($P<0.05$). While no differences were detected in the WAIS-III and WMS-R, the WCST scores of DMD patients (2.8 ± 1.9) were significantly lower ($P<0.01$) than those of normal volunteers (5.4 ± 0.7). Both abnormalities were more pronounced in older adult patients.

Conclusion: These findings demonstrate that DMD is accompanied by a reduction in the prefrontal cortex distribution of $GABA_A$-Rs.

Abbreviations: DMD, Duchenne muscular dystrophy; DGC, dystrophin-glycoprotein complex; $GABA_A$-R, gamma-aminobutyric $acid_A$ receptor; IMZ, Iomazenil; ^{123}I-IMZ-SPECT, ^{123}I-IMZ single photon emission computed tomography; WAIS-III, Wechsler Adult Intelligence Scale-Third Edition; WMS-R, Wechsler Memory Scale-Revised; WCST, Wisconsin Card Sorting Test; VIQ, verbal intelligence quotient;

VMS, verbal memory score; CA, categories achieved

Key Words:

Duchenne muscular dystrophy; ^{123}I-iomazenil-SPECT; brain; $GABA_A$ receptor; cognitive dysfunction

INTRODUCTION

Dystrophin, a cytoplasmic protein encoded by a 2.5 megabase gene at locus Xp21, is expressed abundantly in the cerebral cortex, cerebellum, and hippocampus [1,2]. Its precise function in the brain unknown. In skeletal muscle, dystrophin forms part of the dystrophin-glycoprotein complex (DGC), which acts as a physical bridge between the extracellular matrix and muscle fiber cytoskeleton. Dystrophin may have a similar connecting function in the brain. However, studies attempting to determine its specific role have been complicated by the presence of isoforms (Dp260, Dp140, Dp116, Dp71, and Dp40), splice variants, and DGC components, such as dystroglicans, syntrophins, sarcoglycans, and dystrobrevins [3,4].

Duchenne muscular dystrophy (DMD) is caused by an absence of dystrophin expression. Although brain structure is thought to be unaffected by DMD and appears grossly normal, many studies have indicated CNS involvement. Meta-analysis of DMD patients has shown that intelligence quotients (IQ) are normally distributed around a mean of 80.2, which is approximately 1 standard deviation lower than that of normal individuals [2,5]. Furthermore, some imaging studies suggested that the lack of dystrophin may be associated with alterations in cortical function and brain metabolism [6,7].

Dystrophin, its various isoforms, and DGC components in the CNS may bridge receptors and channels for clustering and anchoring at specific regions of the cell membrane. Recent studies have found that dystrophin colocalizes with gamma-aminobutyric $acid_A$ receptor ($GABA_A$-R) clusters at the postsynaptic membrane [8-11]. Dystrophin-deficient *mdx* mice show a reduction in the number and size of

$GABA_A$-R clusters [8], as well as fewer functional receptors [10]. The results suggest a previously undocumented functional linkage between dystrophin and $GABA_A$-R. The GABAergic system plays a key role in a variety of distinct neuronal processes, including regulation of neuronal excitability, synchronicity of local networks, and neuronal plasticity. Recently, the impact of the $GABA_A$ receptor on cognitive function has been emphasized in many diseases, such as schizophrenia, trauma and autism [12-15]. It is plausible, therefore, that the brains of DMD patients may have significant functional alteration in GABAergic systems.

Iomazenil (IMZ) is a $GABA_A$-R antagonist that specifically and reversibly binds to the $GABA_A$-R alpha subunit. ^{123}I-IMZ single photon emission computed tomography (^{123}I-IMZ-SPECT) has been used widely for quantitative analysis of $GABA_A$-Rs in the human brain [16].

Accordingly, in this study, we investigated $GABA_A$-R distribution in DMD patients using ^{123}I-IMZ-SPECT to identify alterations of $GABA_A$-R distribution that may be linked to dystrophin deficiency. Furthermore, we considered the relationship between the risk of cognitive dysfunction and the alterations of $GABA_A$-R.

METHODS

Participants

The study was performed between Jun 2014 and February 2015 in accordance with the human research guidelines of the Internal Review Board of Niigata National Hospital and the University of Niigata. Written informed consent was obtained from

each subject or legal guardian prior to initiating any study-specific procedure. Fourteen patients with DMD (age range 18-37 years) and 16 normal, age-matched volunteers (age range 19-38 years) participated in this study. The DMD diagnosis was confirmed by a genetic study (detection of exon deletions) or by muscle biopsy (absence of dystrophin). None of the patients or volunteers take any medicine that would affect the uptake of Iomazenil. The average ages of independent ambulation loss and initiation of respiratory support were 10.3 ± 1.4 and 19.7 ± 2.2 years, respectively. The clinical status of each patient is summarized in table 1. The project was registered at the UMIN Clinical Trials Registry as UMIN000014250 (http://www.umin.ac.jp/ctr/index.htm).

Neuropsychological Testing

All patients underwent a neuropsychological assessment that included the Wechsler Adult Intelligence Scale-Third Edition (WAIS-III), Wechsler Memory Scale-Revised (WMS-R), and the Wisconsin Card Sorting Test Keio version (WCST). Specifically, verbal intelligence quotient (VIQ), verbal memory score (VMS), and categories achieved (CA) score were assessed by the WAIS-III, WMS-R, and WCST, respectively. These tests were feasible for adult DMD patients to perform, and from which we are able to estimate general cognitive functions, including IQ, global memory, and executive function. Statistical analyses were performed using Mann-Whitney U-test (2-tailed) on the statistical package for the social sciences (IBM SPSS Statistics 19, IBM Corp, Chicago, IL, USA).

^{123}I-IMZ-SPECT

SPECT imaging was performed using a combined SPECT/CT scanner (Symbia T2, SIEMENS Healthcare, Erlangen, Germany). Images were acquired in a 64 × 64 matrix at 5 degree angular steps at 50s/step. No attenuation correction was applied. The final reconstructed pixel size was 5.38 × 5.38 × 5.38 mm. Image acquisition was initiated at 3 hours post administration of a uniform radioligand dose (222 MBq ^{123}I-IMZ) for all subjects. Subsequently, images were analyzed by iNEUROSTAT++ (Nihon Medi+Physics). After stereotactic anatomical standardization, ^{123}I-IMZ accumulation in each image was determined based on a predefined set of surface pixels (3-dimensional stereotactic surface projection, 3D-SSP).

Institutional control values for adults were determined based on the database obtained in this study's 10 normal volunteers (age range 21-35 years) by defining a Z-score on a pixel-by-pixel basis as follows: Z-score = (average pixel level in the control group – pixel level in a patient) / (standard deviation of control group). A cluster of pixels with a significant difference (P<0.05) relative to the standard value (Z-score>2.0) is identified on the Z-score images. Subsequently, group comparison was performed between the young adult group (n=7, age range 18-25 years) and the older adult group (n=7, age range 30-37 years) using a 2-sample Student t-test on a pixel-by-pixel basis. Calculated t values were converted to Z values using a probability integral transformation.

RESULTS

Z-score images of all DMD patients are shown in Figure 1. A Z>2.0 indicates a

significant reduction in ^{123}I-IMZ ($p<0.05$). A higher Z score reflects a greater reduction in ^{123}I-IMZ uptake. All DMD patients showed a significant decline in ^{123}I-IMZ uptake in the prefrontal cortex. Group comparison between young adult and older adult patients was performed, and its Z-score images are shown in Figure 2. There was a significant reduction ($P<0.05$) in the older adult group compared to the young adult group ($Z>2.0$), shown similar to Figure 1.

The results of neuropsychological assessments are summarized in table 2. The VIQ (91.2 ± 10.9) and VMS (99.4 ± 12.1) scores of DMD patients were all within the accepted normal range. No significant differences in VIQ (91.0 ± 6.5 vs. 91.4 ± 15.4) and VMS (98.2±11.2 vs. 101.3±13.7) were found between the young adult and older adult groups. In contrast, CA in the WCST was significantly lower ($P<0.01$) for the DMD patients (2.8 ± 1.9) compared to normal volunteers (5.3 ± 0.6). There was a significant difference in CA ($P<0.05$) between the young adult and older adult groups (4.0 ± 1.5 vs. 1.5 ± 1.5).

DISCUSSION

In this study, we identified a significant decline in $GABA_A$-R within the prefrontal cortices in DMD patients. The observed decline is more pronounced in older adult DMD patients, indicating that the observed decline in $GABA_A$-R is likely to be part of the disease process. Furthermore, we detected cognitive dysfunction in the WCST, although IQ and global memory were virtually unaffected. The WCST is used widely to assess executive functions, such as strategic planning, organized searching, utilization

of environmental feedback to shift cognitive sets, behavioral direction toward achieving a goal, and modulation of impulsive responses. Moreover, age-related differences in WCST scores in the DMD group suggested that cognitive dysfunction would be progressive, which appears consistent with similar changes identified in ^{123}I-IMZ SPECT.

Neuroimaging studies correlating WCST performance and regional brain activity using PET, SPECT, and MRI have revealed significant activation in the prefrontal cortex[17,18], the same area most affected by DMD according to our ^{123}I-IMZ SPECT study. Studies on *mdx* mice also revealed a marked decrease in the number and size of $GABA_A$ receptor clusters at the postsynaptic membrane and a dysfunction of the GABAergic system [8,11] . Therefore, the behavioral abnormalities in DMD patients may suggest that a defect in GABAergic neurotransmission contributes to cognitive dysfunction. Our findings unequivocally demonstrate that there is progressive $GABA_A$-R functional abnormality in DMD patients, and that the observed $GABA_A$-R abnormality is likely to be a result of dystrophin deficiency.

At present, the mechanisms responsible for CNS dysfunctions in DMD patients remain unclear. Hence, systematic investigation of cortical dysfunction in DMD patients related to the GABAergic and other dependent systems are warranted.

Identification of dystrophin isoforms may also provide some insight into the clinical spectrum of DMD. Among various isoforms, the loss of Dp71 appears to most correlate with cognitive impairment [19,20]. We believe this correlation suggests involvement of aquaporin 4 (AQP-4), the membrane integral water channel most abundant in the brain,

in the DMD clinical spectrum. Recent studies have shown Dp71 forms part of the protein complex associated with AQP-4 clustering in astrocytic endfeet membranes [21-25]. A defect in AQP-4 concentration in those membranes was identified in Dp71-deficient mice,[25] which have subsequently been found to have impaired spatial learning and memory[26]. It is now generally accepted that AQP-4 is essential for various fundamental physiological factors that maintain cortical functionality, from beta-amyloid clearance to neural-flow coupling [27,28]. Indeed, serious BBB alterations and dysfunction, involving both endothelial and glial cells associated with the reduction of dystrophin-associated proteins and AQP-4, have been revealed in the *mdx* mouse [22,23]. It is likely, therefore, that a decline in higher function in DMD patients may be multifactorial, including a decline in $GABA_A$-R and dysfunction of AQP-4. Accordingly, we anticipate that further studies would lead to elucidation of precise dystrophin functions in CNS.

In conclusion, we report a decrease in $GABA_A$-Rs in the prefrontal cortex of DMD patients using ^{123}I-IMZ-SPECT. Neuropsychological assessments were fully compatible with the findings indicating prefrontal cortex oriented dysfunction. Both abnormalities were more pronounced in older adult DMD patients. A progressive $GABA_A$-R decline and prefrontal lobe function appear to be a serious component of the clinical spectrum of DMD patients.

REFERENCES

1. Lidov HG, Byers TJ, Watkins SC, Kunkel LM. Localization of dystrophin to postsynaptic regions of central nervous system cortical neurons. Nature. 1990;348:725-728.
2. Anderson JL, Head SI, Rae C, Morley JW. Brain function in Duchenne muscle dystrophy. Brain. 2002;125:4-13.
3. Piluso G, Mirabella M, Ricci E, Belsito A, Abbondanza C, Servidei S, et al. Gamma1- and gamma2-syntrophins, two novel dystrophin-binding proteins localized in neuronal cells.J Biol Chem. 2000;275:15851-15860.
4. Blake DJ, Nawrotzki R, Loh NY, Górecki DC, Davies KE. β-dystrobrevin, a member of the dystrophin-related protein family.Proc Natl Acad Sci U S A. 1998;95:241-246.
5. Cotton S, Voudouris NJ, Greenwood KM. Intelligence and Duchenne muscular dystrophy: full-scale, verbal, and performance intelligence quotients. Dev Med Child Neurol. 2001;43:497-501.
6. Lee JS, Pfund Z, Juhász C, Behen ME, Muzik O, Chugani DC, et al. Altered regional brain glucose metabolism in Duchenne muscular dystrophy: a pet study. Muscle Nerve. 2002;26:506-512.
7. Lv SY, Zou QH, Cui JL, Zhao N, Hu J, Long XY, et al. Decreased gray matter concentration and local synchronization of spontaneous activity in the motor cortex in Duchenne muscular dystrophy. Am J Neuroradiol. 2011;32:2196-2200.
8. Knusel I, Zuellig RA, Schaub MC, Mastrocola M, Bornhauser B. Altered synaptic

clustering of GABAa receptors in mice lacking dystrophin (mdx mice). Eur.J.Neurosci. 1999;11:4457-4462

9. Brünig I, Suter A, Knuesel I, Lüscher B, Fritschy JM. GABAergic terminals are required for postsynaptic clustering of dystrophin but not of GABA(A) receptors and gephyrin. J Neurosci. 2002;22:4805-4813.
10. Levi S, Grady RM, Henry MD, Campbell KP, Sanes JR, Craig AM. Dystroglycan is selectively associated with inhibitory GABAergic synapses but is dispensable for their differentiation. J.Neurosci. 2002;22:4274-4285
11. Kueh SL, Dempster J, Head SI, Morley JW. Reduced postsynaptic GABAa receptor number and enhanced gaboxadol induced change in holding currents in Purkinje cells of the dystrophin-deficient mdx mouse. Neurobiol Dis. 2011;43:558-564.
12. Rudolph U, Möhler H. GABAA receptor subtypes: Therapeutic potential in Down syndrome, affective disorders, schizophrenia, and autism. Annu Rev Pharmacol Toxicol. 2014;54:483-507.
13. Hines RM, Hines DJ, Houston CM, Mukherjee J, Haydon PG, Tretter V, et al. Disrupting the clustering of GABAA receptor α2 subunits in the frontal cortex leads to reduced γ-power andcognitive deficits. Proc Natl Acad Sci U S A. 2013;110:16628-16633.
14. Tse MT, Piantadosi PT, Floresco SB. Prefrontal cortical gamma-aminobutyric acid transmission and cognitive function: drawing links to schizophrenia from preclinical research. Biol Psychiatry. 2015;77:929-939.
15. Nariai T, Inaji M, Tanaka Y, Hiura M, Hosoda C, Ishii K, et al. PET molecular

imaging to investigate higher brain dysfunction in patients with neurotrauma. Acta Neurochir Suppl. 2013;118:251-254.

16. Beer HF, Blauenstein PA, Hasler PH, Delaloye, B, Riccabona, G, Bangerl I, et al. In vivo and in vitro evaluation of iodine-123-Ro 16-0154: a new imaging agent for SPECT investigations of benzodiazepine receptors. J Nucl Med. 1990;31:1007-1014.
17. Berman KF, Ostrem JL, Randolph C, Gold J, Goldberg TE, Coppola R, et al. Physiological activation of a cortical network during performance of the Wisconsin Card Sorting Test: a positron emission tomography study. Neuropsychologia. 1995;33:1027-1046.
18. Lie CH, Specht K, Marshall JC, Fink GR. Using fMRI to decompose the neural processes underlying the Wisconsin Card Sorting Test. Neuroimage. 2006;30:1038-1049.
19. Taylor PJ, Betts GA, Maroulis S, Gilissen C, Pedersen RL, Mowat DR, et al. Dystrophin gene mutation location and the risk of cognitive impairment in Duchenne muscular dystrophy. PLoS One. 2010;5:e8803
20. Wingeier K, Giger E, Strozzi S, Kreis R, Joncourt F, Conrad B, et al. Neuropsychological impairments and the impact of dystrophin mutations on general cognitive functioning of patients with Duchenne muscular dystrophy. J Clin Neurosci. 2011;18:90-95.
21. Frigeri A, Nicchia GP, Repetto S, Bado M, Minetti C, Svelto M. Altered aquaporin-4 expression in human muscular dystrophies: a common feature?

FASEB J. 2002;16:1120-1122.

22. Nico B, Tamma R, Annese T, Mangieri D, De Luca A, Corsi P, et al. Glial dystrophin-associated proteins, laminin and agrin, are downregulated in the brain of mdx mouse. Lab Invest. 2010;90:1645-1660.
23. Nico B, Paola Nicchia G, Frigeri A, Corsi P, Mangieri D, Ribatti D, et al. Altered blood-brain barrier development in dystrophic MDX mice. Neuroscience. 2004;125:921-935.
24. Waite A, Brown SC, Blake DJ. The dystrophin-glycoprotein complex in brain development and disease. Trends Neurosci. 2012;35:487-496.
25. Nicchia GP, Rossi A, Nudel U, Svelto M, Frigeri A. Dystrophin-dependent and -independent AQP4 pools are expressed in the mouse brain. Glia. 2008;56:869-876.
26. Daoud F, Candelario-Martínez A, Billard JM, Avital A, Khelfaoui M, Rozenvald Y, et al. Role of mental retardation-associated dystrophin-gene product Dp71 in excitatory synapse organization, synaptic plasticity and behavioral functions. PLoS One. 2008;4:e6574.
27. Igarashi H, Suzuki Y, Kwee IL, Nakada T. Water iInflux into cerebrospinal fluid is significantly reduced in senile plaque bearing transgenic mice, supporting beta-Amyloid clearance hypothesis of Alzheimer disease. Neurol Res. 2014;36:1094-1098.
28. Nakada T. Review: Virchow-Robin space and aquaporin-4: New insights on an old friend. Croatian Med J .2014;55:328-336.

Figure legends

Figure 1: Individual results of ^{123}I-IMZ SPECT. A significant reduction in ^{123}I-IMZ uptake compared to the normalized counts of the global brain (GLB) is mapped on standardized brain surface MRI in 2 directions (superior and anterior views). For easier comparison, images were segregated into 2 groups, namely, young adult (A) and older adult (B) patients. Color bar indicates corresponding Z-score. SUP, superior; ANT, anterior.

Figure 2: Group comparison between young adult and older adult patients groups. Reduction in ^{123}I-IMZ uptake in the older adult group was compared to that of the young adult group shown in 8 directions, exhibiting further significant reduction in ^{123}I-IMZ uptake in older adult patients. A Z-score image was generated similar to individual analysis where reduction in ^{123}I-IMZ uptake was compared to the GLB.

RT. LAT; right lateral, LT.LAT; left lateral, SUP; superior, INF; inferior, ANT; anterior, POST; posterior, RT.MED; right medial, LT.MED; left medial.

Table 1, Summary of clinical characteristics for patients involved in this study

Pt	Age	Diagnosis (Exon deletions / Muscle biopsy)	Ventilation	Age of Ambulation Loss	Respiratory Support (age of start)
1	18	absence of dystrophin	INIV	8Y1M	18Y0M
2	18	absence of dystrophin	INIV	10Y10M	18Y1M
3	19	absence of dystrophin	INIV	9Y4M	18Y9M
4	20	45,47,48,49,50,51,52	INIV	13Y2M	17Y2M
5	21	absence of dystrophin	INIV	11Y0M	19Y6M
6	23	48,49,50	INIV	8Y1M	17Y1M
7	25	44	CIV	9Y10M	20Y3M
8	30	47,48	CIV	11Y3M	20Y1M
9	31	8	CNIV	10Y1M	21Y1M
10	32	49,50	CNIV	12Y0M	24Y7M
11	35	51,52	CIV	8Y10M	17Y9M
12	36	44	CIV	10Y5M	19Y3M
13	37	50,51,52	CIV	10Y2M	22Y1M
14	37	absence of dystrophin	CIV	12Y0M	25Y4M

INIV, Intermittent noninvasive ventilation; CNIV, continuous noninvasive ventilation; CIV, continuous invasive ventilation.

Table 2, Results of neuropsychological assessments

		average age	WAIS-III	WMS-R	WCST
DMD patients	(n=14)	27.3±7.5	91.2±10.9	99.4±12.1	2.8±1.9*
young adult	(n=7)	20.6±2.6	91.0±6.5	98.2±11.2	4.0±1.5
older adult	(n=7)	34.0±2.9	91.4±15.4	101.3±13.7	1.5±1.5†
Volunteers	(n=16)	28.2±5.7	105.6 ±8.3	105.0±12.1	5.3±0.6
young adult	(n=8)	23.5±2.8	106.4 ±9.9	105.1±13.9	5.4±0.5
older adult	(n=8)	33.0±2.9	104.9 ±6.8	104.8±10.9	5.3±0.7

Data expressed as mean ± standard deviation.

* Significantly lower than normal volunteers (P<0.01).

† Significantly lower in comparisons between the young adult and older adult patient groups. (P<0.05). Mann-Whitney U-test (2-tailed)

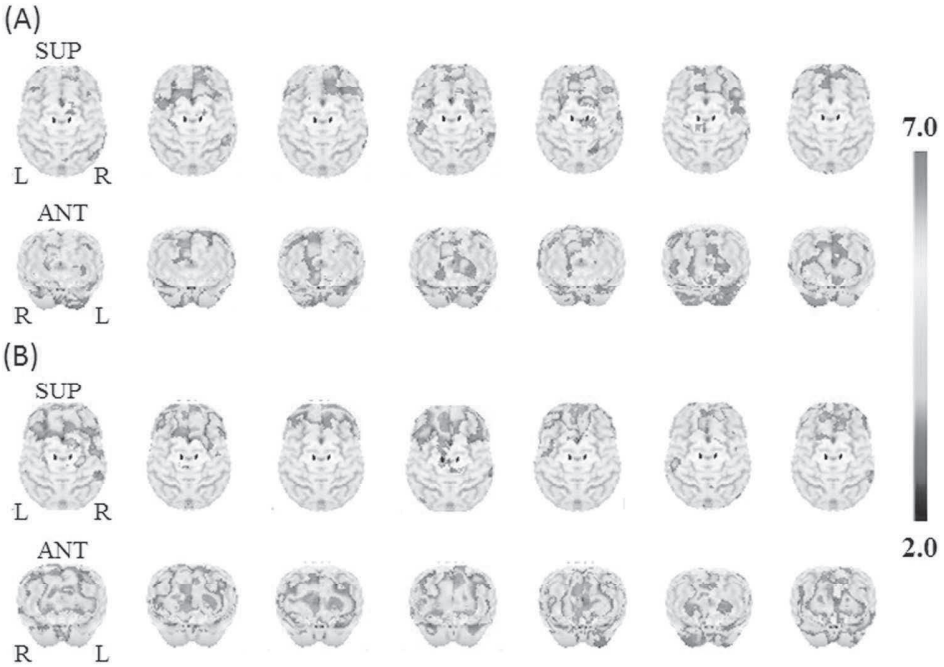

Figure 1: Individual results of 123I-IMZ SPECT
Significant reduction in 123I-IMZ uptake compared to the normalized counts of the global brain (GLB) is mapped on standardized brain surface MRI in two directions (superior and anterior views). For easier comparison, images were segregated into two groups, namely, young adult (A) and older adult (B) patients. Color bar indicates corresponding Z-score. SUP, superior; ANT, anterior.

170x121mm (300 x 300 DPI)

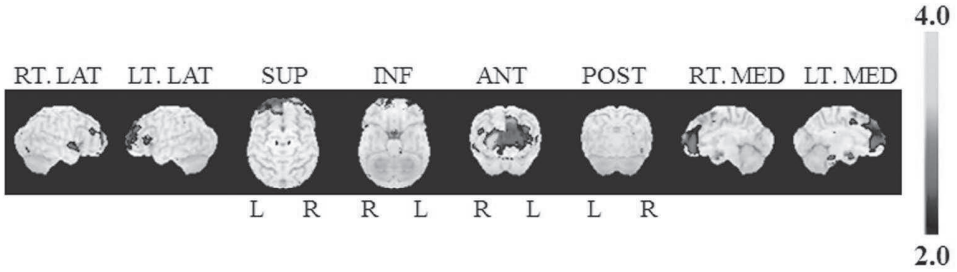

Figure 2: Group comparison between young adult and older adult patients groups\r\nReduction in 123I-IMZ uptake in the older adult group was compared to that of young adult group shown in eight directions, exhibiting further significant reduction in 123I-IMZ uptake in older adult patients. Z-score image was generated similar to individual analysis where reduction in 123I-IMZ uptake was compared to the GLB. \r\nRT. LAT; right lateral, LT.LAT; left lateral, SUP; superior, INF; inferior, ANT; anterior, POST; posterior, RT.MED; right medial, LT.MED; left medial.\r\n

170x52mm (300 x 300 DPI)

SCIENTIFIC REPORTS

OPEN

Microglia preconditioned by oxygen-glucose deprivation promote functional recovery in ischemic rats

Received: 31 August 2016
Accepted: 12 January 2017
Published: 14 February 2017

Masato Kanazawa[1], Minami Miura[1], Masafumi Toriyabe[1], Misaki Koyama[1], Masahiro Hatakeyama[1], Masanori Ishikawa[1], Takashi Nakajima[2], Osamu Onodera[1], Tetsuya Takahashi[1], Masatoyo Nishizawa[1] & Takayoshi Shimohata[1]

Cell-therapies that invoke pleiotropic mechanisms may facilitate functional recovery in stroke patients. We hypothesized that a cell therapy using microglia preconditioned by optimal oxygen-glucose deprivation (OGD) is a therapeutic strategy for ischemic stroke because optimal ischemia induces anti-inflammatory M2 microglia. We first delineated changes in angiogenesis and axonal outgrowth in the ischemic cortex using rats. We found that slight angiogenesis without axonal outgrowth were activated at the border area within the ischemic core from 7 to 14 days after ischemia. Next, we demonstrated that administration of primary microglia preconditioned by 18 hours of OGD at 7 days prompted functional recovery at 28 days after focal cerebral ischemia compared to control therapies by marked secretion of remodelling factors such as vascular endothelial growth factor, matrix metalloproteinase-9, and transforming growth factor-β polarized to M2 microglia *in vitro/vivo*. In conclusion, intravascular administration of M2 microglia preconditioned by optimal OGD may be a novel therapeutic strategy against ischemic stroke.

More than half of patients who survive ischemic stroke suffer from motor disabilities[1]. To date, physical rehabilitation has remained the only effective therapeutic option to prompt functional recovery in these patients[2]. It is necessary, therefore, to establish other therapeutic strategies to facilitate functional recovery in stroke patients in the subacute and chronic phases.

It has been demonstrated that angiogenesis is a necessary process for functional recovery after ischemia in the heart[3], which raises the possibility that enhancement of angiogenesis is one strategy for facilitating functional recovery after ischemic stroke[4]. In fact, a previous study using a rodent model demonstrated that enhanced angiogenesis via the intravenous administration of vascular endothelial growth factor (VEGF) at 2 days after cerebral ischemia promoted functional recovery[5]. However, systemic injection of VEGF causes adverse effects, including hypotensive and tachycardic responses in various animals[6–8]. Furthermore, early administration of VEGF might prompt blood-brain barrier (BBB) disruption that causes cerebral oedema and haemorrhagic transformation[5]. Therefore, a therapeutic strategy that enhances angiogenesis without these adverse effects is desirable.

"Single-target" therapies may be insufficient because ischemic cerebral injury involves several mechanisms. It has been proposed that therapeutic approaches should target multiple cell types to enhance protection and recovery[9]. Cell therapies using bone marrow mononuclear cells or bone marrow-derived mesenchymal stem/stromal cells may be an effective "multi-target" therapeutic strategy to facilitate functional recovery in stroke patients in the subacute and chronic phases via pleiotropic mechanisms[9,10]. One such mechanism observed in cell-based therapies using neural progenitor cells, bone marrow stromal cells, and mesenchymal stem cells was the induction of angiogenesis via secretion of VEGF or brain-derived neurotrophic factor (BDNF)[11–13]. Enhancement of axonal outgrowth after such cell-based therapy also was reported[13,14]. However, a recent multi-centre randomized controlled trial demonstrated that there was no beneficial effect of intravenous administration of bone marrow

[1]Department of Neurology, Brain Research Institute, Niigata University, 1-757 Asahimachi-dori, Chuoku, Niigata, Japan. [2]Department of Neurology, Niigata National Hospital, National Hospital Organization, 3-52 Akasaka-cho, Kashiwazaki, Niigata, Japan. Correspondence and requests for materials should be addressed to M.Kanazawa (email: masa2@bri.niigata-u.ac.jp) or T.S. (email: t-shimo@bri.niigata-u.ac.jp)

mononuclear stem cells among patients with ischemic stroke[15]. In addition, there remain several clinical concerns, including the efficiency with which bone marrow-derived cells cross the BBB[16] and the technical safety of bone marrow-derived cell collection in patients who are undergoing anticoagulant or antiplatelet therapy for secondary prevention of stroke.

Cell-based therapies using microglia might be a promising novel therapeutic strategy because glial cells are the main source of the above-mentioned growth factors in the CNS[9,17]. Although several studies have demonstrated that microglia might expand cerebral infarct volume in the acute phase[18,19], microglia after cerebral ischemia in the subacute and chronic phases are known to play protective roles via tissue and vascular remodelling[19,20]. These ischemia-induced protective microglia are called M2 microglia, and their protective effect is considered to be due to the secretion of remodelling factors, such as VEGF and BDNF, matrix metalloproteinase-9 (MMP-9), and transforming growth factor-beta (TGF-β) after ischemia[17,20–25], that may facilitate anti-inflammation, angiogenesis, and axonal outgrowth after cerebral ischemia. In addition, transplanted microglia can cross the BBB, particularly in the ischemic condition[26–28]. Therefore, we speculated that a cell-based therapy using microglia preconditioned by optimal ischemic condition might be an ideal and convenient therapeutic strategy for ischemic stroke.

In the present study, we hypothesized that microglia preconditioned by oxygen-glucose deprivation (OGD) and administered intra-arterially may cross the BBB, secrete remodelling factors in the brain parenchyma, and exert pleiotropic therapeutic effects via the promotion of angiogenesis and axonal outgrowth against focal cerebral ischemia even in the subacute phase. To test this hypothesis, we first delineated temporal changes in angiogenesis and axonal outgrowth in the ischemic core and penumbra in a rat model of transient focal cerebral ischemia. Then, we investigated whether primary microglia preconditioned by optimal OGD promoted functional recovery via enhancement of angiogenesis and axonal outgrowth after focal cerebral ischemia.

Results

Angiogenesis on the border of the ischemic core in the subacute phase of focal cerebral ischemia. To determine the detailed localization and temporal changes of angiogenesis after transient focal cerebral ischemia, we performed immunofluorescence staining against the ischemic cortex of Sprague-Dawley rats using an antibody against the endothelial and angiogenesis marker, cluster of differentiation (CD)31 (Fig. 1A and B). Confocal microscopic studies revealed that the immunoreactivity for CD31 volume per unit volume on the border area within the ischemic core defined as microtubule-associated protein 2 (MAP2)-negative area decreased at 1 day after cerebral ischemia and reached a minimum level at 3 days after cerebral ischemia compared to sham-operated rats (all $P < 0.001$) (Fig. 1B). However, immunoreactivity for CD31 volume per unit volume in the same area was increased at 7 and 14 days after cerebral ischemia compared to that of 3 days after cerebral ischemia ($P = 0.013$ and $P < 0.001$, respectively). In contrast, no significant changes in the immunoreactivity for CD31 volume per unit volume were observed compared to sham-operated rats in the ischemic penumbra defined as MAP2-positive region ($P = 0.083$) (Fig. 1B).

We next investigated which cells were involved in angiogenesis after cerebral ischemia. We found that Ki67 was expressed in the border area within the ischemic core, but not in the ischemic penumbra or in sham-operated rats (Fig. 1C). Additionally, Ki67-positive cells on the border area within the ischemic core were slightly increased at 3 days and markedly increased at 7 days after cerebral ischemia (Fig. 1D and E). Ki67 expression was observed in the nuclei of endothelial cells, pericytes, and microglia but not in the nuclei of astrocytes (Fig. 1D, Supplementary Fig. 1). Ki67-positive endothelial cells on the border area within the ischemic core also were markedly increased at 7 days after cerebral ischemia in a rat autologous thromboembolic model with tissue plasminogen activator (Supplementary Fig. 2).

No axonal outgrowth in the ischemic core and penumbra until 14 days after focal cerebral ischemia. To investigate neuronal regeneration after focal cerebral ischemia in the ischemic cortex of Sprague-Dawley rats, we performed immunofluorescence staining using antibodies against an axonal marker, SMI31 and a dendrite marker, MAP2, respectively[29]. Confocal microscopic studies revealed that there was no immunostaining of SMI31 and MAP2 in the ischemic core (Figs 1A and 2A). Furthermore, the immunoreactivity for SMI31 per unit volume on the border area within the ischemic penumbra decreased gradually after cerebral ischemia, and was not recovered even at 14 days after cerebral ischemia (day 3, $P = 0.018$; day 7, $P < 0.001$; day 14, $P < 0.001$) (Fig. 2A and B). In contrast, a transient decrease in the immunoreactivity for MAP2 per unit volume was observed only at 1 day after cerebral ischemia ($P = 0.06$) (Figs 1A and 2C).

Therapeutic effects of microglia preconditioned by OGD against focal cerebral ischemia. To investigate the effects of transplantation of primary microglia preconditioned by OGD against focal cerebral ischemia, we compared neurological outcomes among the no cell control group, OGD-preconditioned primary astrocytic transplantation group, and OGD-preconditioned microglial transplantation group by a sensorimotor scale after focal cerebral ischemia. Neurological deficit as measured by the corner test was significantly improved in the OGD-preconditioned microglial transplantation group compared to both the no cell control group and OGD-preconditioned astrocytic transplantation group at 28 days after cerebral ischemia ($P = 0.006$ and 0.024, respectively) (Fig. 3A). There were no significant differences in body weight at 1, 3, 7, 14, 21, and 28 days after cerebral ischemia among the three groups ($P = 0.281$) (Supplementary Fig. 3A).

Next, to investigate the effects of OGD preconditioning on functional recovery by microglial transplantation, we analysed neurological outcomes between the OGD-preconditioned microglial transplantation group and normoxia-microglial transplantation group by a sensorimotor scale after focal cerebral ischemia. Neurological deficit as measured by the corner test was significantly improved in the OGD-preconditioned microglial transplantation group compared with the normoxia-microglial transplantation group at 28 days after cerebral ischemia

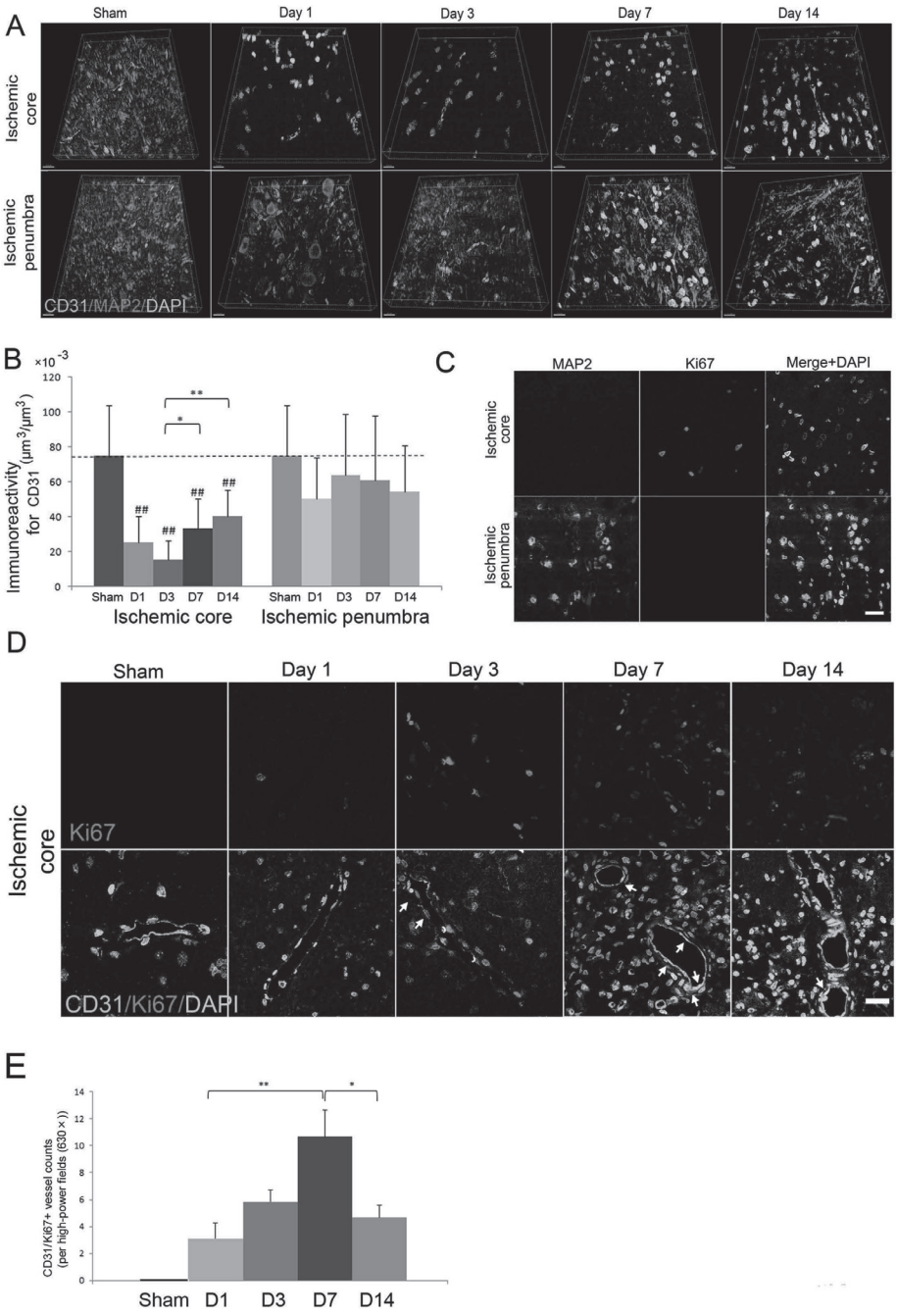

Figure 1. Temporal changes in angiogenesis in the rat cerebral cortex after focal cerebral ischemia. (**A**) Cluster of differentiation 31 (CD31; green)/microtubule-associated protein 2 (MAP2; red)/4′,6′-diamidino-2-phenylindole (DAPI; blue) triple labelling of cerebral cortices in the non-ischemic (sham-operated) and ischemic core and penumbra at 1, 3, 7, and 14 days after cerebral ischemia examined by confocal microscopy. CD31 and MAP2 are markers for angiogenesis and neuronal dendrites, respectively. Three-dimensional reconstruction images show temporal changes in angiogenesis and neuronal dendrites in the ischemic core and penumbra. A secondary-only antibody control confirms its specificity. Scale bars, 15 μm. (**B**) The immunoreactivity of CD31-positive volume (μm^3) per unit volume (μm^3) at 1 (D1), 3 (D3), 7 (D7), and 14 (D14) days after cerebral ischemia (N = 21). *P < 0.05, **P < 0.01, $^{\#\#}$P < 0.01 versus sham-operated rats. (**C**) MAP2 (green)/Ki67 (red)/DAPI (blue) triple labelling of cerebral cortices in the ischemic core and penumbra examined by confocal microscopy. Ki67 is a marker for cellular proliferation at 7 days after cerebral ischemia. Scale bars, 20 μm. (**D**) CD31 (green)/Ki67 (red)/DAPI (blue) triple labelling of cerebral cortices in the non-ischemic (sham-operated) and ischemic core at 1, 3, 7, and 14 days after cerebral ischemia examined by confocal microscopy. Arrows indicate Ki67-positive angiogenic endothelial nuclei. Scale bars, 20 μm. (**E**) The numbers of CD31/Ki67 double-positive vessels from the ischemic core at 1 (D1), 3 (D3), 7 (D7), and 14 (D14) days after cerebral ischemia (N = 21). *P < 0.05, **P < 0.01.

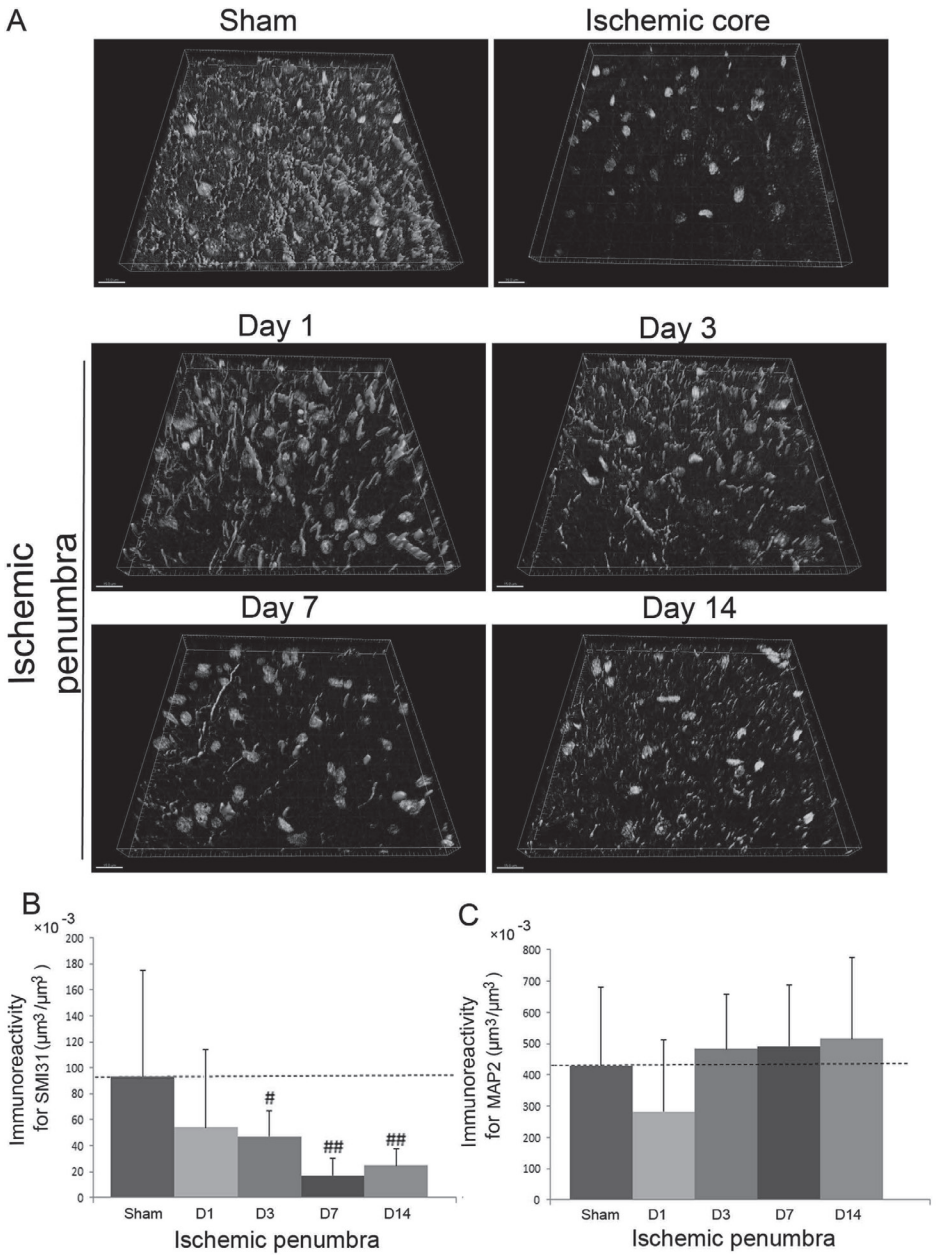

Figure 2. Temporal changes in neuronal axons and dendrites in the rat cerebral cortex after focal cerebral ischemia. (**A**) SMI31 (green)/4′,6′-diamidino-2-phenylindole (DAPI; blue) double labelling in the non-ischemic (sham-operated), ischemic core, and ischemic penumbra cortices at 1, 3, 7, and 14 days after cerebral ischemia examined by confocal microscopy. SMI31 is a marker for neuronal axons. A secondary-only antibody control confirms its specificity. Scale bars, 15 μm. **(B)** The immunoreactivity for SMI31 volume (μm^3) per unit volume (μm^3) in the ischemic penumbra at 1 (D1), 3 (D3), 7 (D7), and 14 (D14) days after cerebral ischemia (N = 21). $^{\#}P < 0.05$ and $^{\#\#}P < 0.01$ versus sham-operated rats. **(C)** The immunoreactivity for MAP2 volume in the ischemic penumbra (μm^3) per unit volume (μm^3) at 1 (D1), 3 (D3), 7 (D7), and 14 (D14) days after cerebral ischemia (N = 21).

(P = 0.023) (Fig. 3B). There were no significant differences in body weight at 1, 7, 14, 21, and 28 days after cerebral ischemia between the groups (P = 0.71) (Supplementary Fig. 3B). We did not observe any allergic reactions or symptoms of graft versus host diseases after transplantation.

To confirm whether microglia and astrocytes preconditioned by OGD migrated into the brain parenchyma across the BBB, we administered both OGD-preconditioned primary microglia and astrocytes derived from green fluorescent protein (GFP) transgenic mice[28,30]. After intra-arterial administration of these cells, OGD-preconditioned GFP microglia were observed in the border area between the ischemic core and penumbra at 3 days after transplantation (Fig. 3C) but not at 21 days after transplantation. In contrast, no

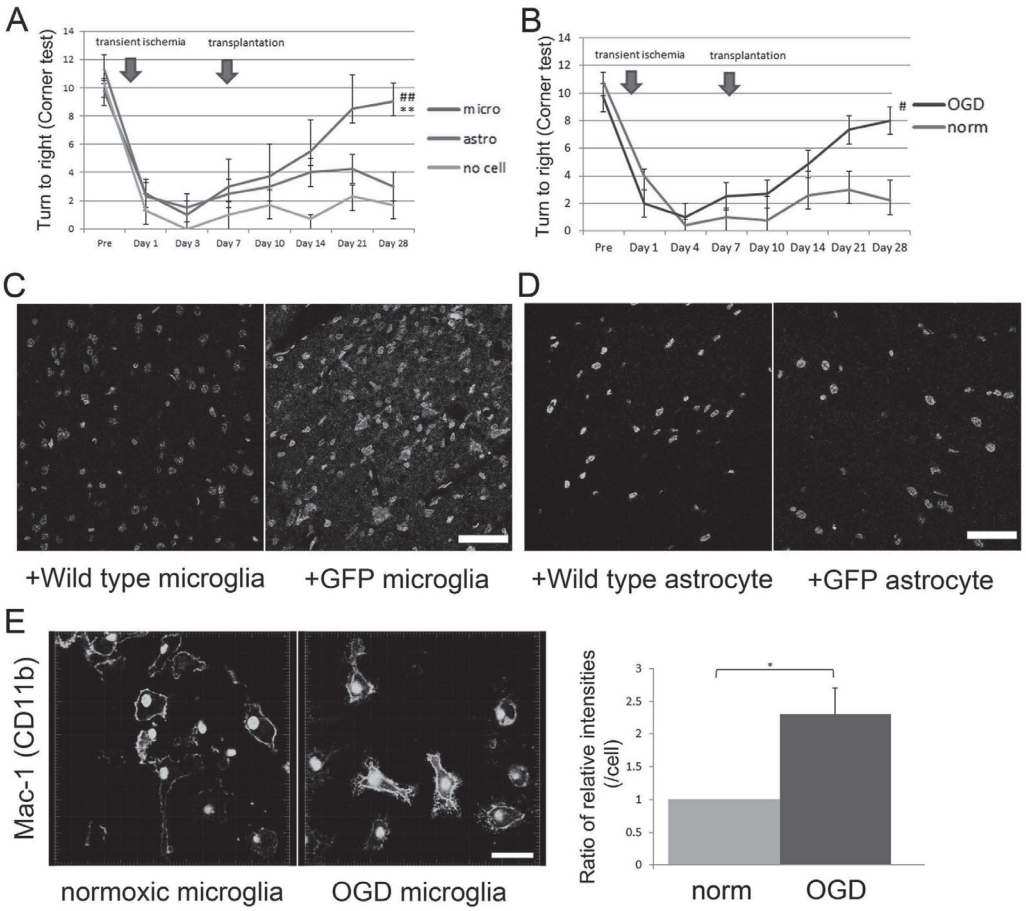

Figure 3. Improvements in neurological outcomes after oxygen-glucose deprivation (OGD)-preconditioned microglial transplantation. (**A**) Significantly better functional recovery on the corner test (performed 20 times) is observed in the OGD-preconditioned microglial transplantation group (micro group) compared with the vehicle-injected control group (no cell control group) and OGD-preconditioned astrocytic transplantation group (astro group); $^{\#\#}P < 0.01$ vs astro group, $^{**}P < 0.01$ vs no cell control group (N = 4 per group). (**B**) Significantly better functional recovery on the corner test (performed 20 times) is observed in the OGD-preconditioned microglial transplantation group compared with the normoxic microglial transplantation group (norm); $^{\#}P < 0.05$ (N = 6). OGD-preconditioned microglia (**C**), but not OGD-preconditioned astrocytes (**D**), from GFP mice (green) migrate into the border area between the ischemic core and penumbra compared with those from wild-type mice at 3 days after transplantation. Scale bar, 50 μm. (**E**) Representative figures and bar graphs showing the relative signal intensities of adhesion receptor macrophage-1 antigen (Mac-1) (CD11b/CD18; green) from primary microglia under normoxic and OGD conditions. Confocal microscopic images of Mac-1 (green)/DAPI (blue) double labelling of microglia. White scale bars, 15 μm. The bar graph depicts the relative ratio of the signal intensities per cell of the normoxic samples to that of OGD-preconditioned samples (N = 5). A secondary-only antibody control was used to confirm specificity. $^{*}P < 0.05$.

OGD-preconditioned GFP astrocytes were observed at either 3 or 21 days after transplantation (Fig. 3D). The leukocyte adhesion receptor macrophage-1 antigen (Mac-1) (CD11b/CD18) is a β2 integrin that is constitutively expressed on the surface of leukocytes and microglia, as well as quantitatively upregulated by inflammatory mediators and ischemia. Mac-1 mediates the firm adhesion of leukocytes to the blood vessel by binding to its endothelial ligand, intercellular adhesion molecule-1 (ICAM-1)/CD31. Deficiency in Mac-1 might decrease susceptibility to infiltration and migration after cerebral ischemia[31,32]. To investigate the effect of preconditioning by OGD on microglia, we compared the levels of Mac-1 expression on microglia under normoxic and OGD conditions. We found that the levels of Mac-1 after OGD preconditioning were twice those under normoxic conditions (P = 0.038) (Fig. 3E).

Marked changes in levels of growth factors and MMP-9 secreted by OGD-preconditioned glial cells. To investigate the effect of preconditioning by OGD on microglia, we compared levels of VEGF and BDNF in microglial and astrocytic-conditioned media under normoxic and OGD conditions. As described in the Methods section, we previously determined that the optimal incubation time under the OGD condition was 18 h, because this condition induced sufficient oxidative and hypoglycaemic stress without causing cell death[33,34].

Additionally, M2 microglia after cerebral ischemia were detectable starting from 12 h, maximally increased at 24 h, and markedly decreased at later time points[20]. Therefore, we incubated microglia under OGD conditions for 18 h before transplantation.

We found that the levels of VEGF from microglial and astrocytic-conditioned media after OGD preconditioning were markedly higher than those under the normoxic condition ($P = 0.006$ and <0.001, respectively) (Fig. 4A, Supplementary Fig. 4A). In addition, the levels of BDNF from astrocytic-conditioned media but not microglial-conditioned media after OGD preconditioning were higher than those under the normoxic condition ($P = 0.004$ and $P = 0.198$, respectively) (Fig. 4A, Supplementary Fig. 4B).

We also measured the levels of MMP-9 in microglial and astrocytic-conditioned media after OGD preconditioning, because sources of MMP-9 after cerebral ischemia include microglia[35] and potentially astrocytes[36]. We found that the levels of MMP-9 from microglial and astrocytic-conditioned media after OGD preconditioning were higher than those under the normoxic condition ($P = 0.001$ and 0.005, respectively) (Fig. 4B, Supplementary Fig. 4C).

Finally, to determine changes in the cytokine profiles of microglia preconditioned by OGD, we compared levels of several cytokines from microglia under normoxic and OGD conditions. Generally, M2 microglia secretes interleukin (IL)-10 and TGF-β, whereas M1 microglia secretes tumour necrosis factor alpha (TNF-α), IL-1β, and IL-6[19,20]. We found that the levels of anti-inflammatory cytokine TGF-β after OGD preconditioning were 25 times as high as those under the normoxic condition ($P = 0.002$), and that the levels of pro-inflammatory cytokine IL-6 after OGD preconditioning were half as much as those under the normoxic condition ($P < 0.001$). In contrast, pro-inflammatory cytokines TNF-α and IL-1β after OGD preconditioning were three and four times as high as those under the normoxic condition ($P < 0.001$ and $P < 0.001$, respectively), whereas there was no difference in the level of anti-inflammatory cytokine IL-10 from microglia between the OGD-preconditioning and normoxic conditions ($P = 0.35$) (Fig. 4C). The ratio of TGF-β per TNF-α, which reflects the polarization of M1 and M2 microglia[3], from microglia preconditioned by OGD, was six times as high as that from microglia under the normoxic condition ($P = 0.009$) (Fig. 4D). Taken together, these results demonstrate that preconditioning by the optimal OGD condition can prime microglia into the anti-inflammatory M2 dominant subtype.

Microglial M2 switch after intra-arterial administration of 18 h-OGD-preconditioned microglia. To investigate the effect of OGD-preconditioned microglial transplantation on the injured brain parenchyma, we performed immunohistochemical analyses of the brains of transplanted rats at 3 days after transplantation using antibodies against inducible nitric oxide synthase (iNOS, M1 marker) (Fig. 5A) and CD206 (M2 marker) (Fig. 5B). Confocal microscopic examination revealed that the number of iNOS-positive cells in the border area between the ischemic core and the penumbra at 3 days after transplantation in the OGD-preconditioned microglial transplantation group was less than that in the normoxic microglia transplantation group ($P < 0.001$) (Fig. 5A and C). In contrast, the number of CD206-positive cells in the border area between the ischemic core and the penumbra at 3 days after transplantation in the OGD-preconditioned microglial transplantation group was more than that in the normoxic microglia transplantation group ($P = 0.13$) (Fig. 5B and C). The ratio of CD206-positive cells to iNOS-positive cells, which reflects the polarization of M1 and M2 microglia[19], in the OGD condition was twenty times that in the normoxic condition ($P = 0.001$) (Fig. 5D). Taken together, these results demonstrate that OGD-preconditioned microglial transplantation can prime microglial M2 switch.

VEGF, MMP-9, and TGF-β expression by OGD-preconditioned microglial transplantation. To confirm whether functional recovery after transplantation of microglia preconditioned by OGD was associated with upregulation of VEGF, MMP-9, and TGF-β in the injured brain parenchyma, we performed immunohistochemical analyses of the brains of transplanted rats using antibodies against VEGF, MMP-9, and TGF-β at 28 days after cerebral ischemia. Whereas expressions of VEGF, MMP-9, and TGF-β were undetectable in the brains of sham-operated rats, significant expressions of VEGF, MMP-9, and TGF-β were observed in the border area within the ischemic core and penumbra at 28 days after cerebral ischemia (21 days after transplantation). Analyses of immunoreactivity intensities demonstrated that the expressions of these remodelling factors were more prominent in the OGD-preconditioned microglial transplantation group than in the no cell control group and the OGD-preconditioned astrocytic transplantation group (both $P < 0.001$) (Fig. 6A–C). VEGF and MMP-9 expressions were observed not only in the microglia but also in pericytes, endothelial cells, and neurons within the ischemic cortex (Supplementary Figs 5 and 6). In addition, TGF-β expression was observed in microglia as well as pericytes and neurons within the ischemic cortex (Supplementary Fig. 7).

Promotion of angiogenesis by OGD-preconditioned microglial transplantation. We speculated that expressions of VEGF, MMP-9, and TGF-β by OGD-preconditioned microglial transplantation might promote angiogenesis. Thus, we investigated the effects of OGD-preconditioned microglial transplantation on angiogenesis by immunofluorescence staining of the ischemic cortex at 28 days after cerebral ischemia using an antibody against the angiogenesis marker, CD31 (Fig. 7A). Confocal microscopic studies revealed that immunoreactivity for CD31 per unit volume in the border area within the ischemic core in the OGD-microglial transplantation group was more prominent than that in the no cell control group and OGD-preconditioned astrocytic transplantation group at 28 days after cerebral ischemia (at 21 days after transplantation) ($P < 0.001$ and $P < 0.001$). However, there was no significant difference in the immunoreactivity for CD31 per unit volume within the ischemic penumbra among the three groups.

Promotion of axonal outgrowth by OGD-preconditioned microglial transplantation. We investigated the effects of OGD-preconditioned microglial transplantation on axonal outgrowth by immunofluorescence staining of the ischemic cortex at 28 days after cerebral ischemia using an antibody against the neurofilament

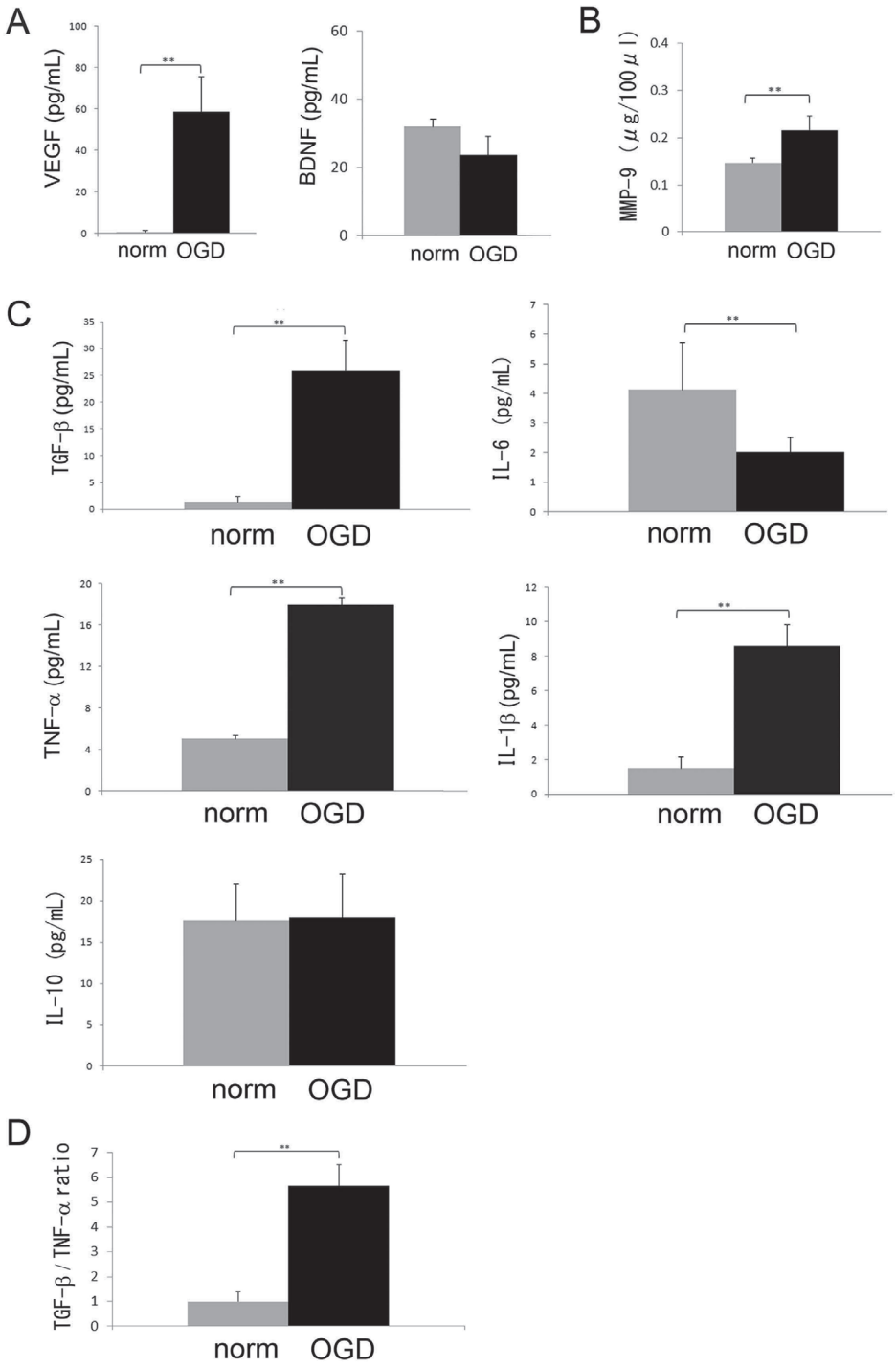

Figure 4. Characteristics of murine primary-cultured microglia preconditioned by oxygen-glucose deprivation (OGD). (**A**,**B**) The levels of secretory vascular endothelial growth factor (VEGF), brain derived neurotrophic factor (BDNF) (**A**) and matrix metalloproteinase-9 (MMP-9) (**B**) from conditioned media of murine primary-cultured microglia subjected to normoxia (norm) or OGD (N = 6–8 each). **P < 0.01. (**C**) The levels of secretory anti-inflammatory cytokines such as transforming growth factor-β (TGF-β) and interleukin-10 (IL-10), and pro-inflammatory cytokines such as IL-6, tumour necrosis factor-α (TNF-α), and IL-1β from conditioned media of murine primary-cultured microglia subjected to normoxia (norm) or OGD (N = 6 each). **P < 0.01. (**D**) The ratio of TGF-β per TNF-α, which reflects microglial polarization after normoxia and OGD preconditioning (N = 6 each). The increase in the ratio of TGF-β per TNF-α reveals the polarization of M2 microglia after OGD preconditioning. **P < 0.01.

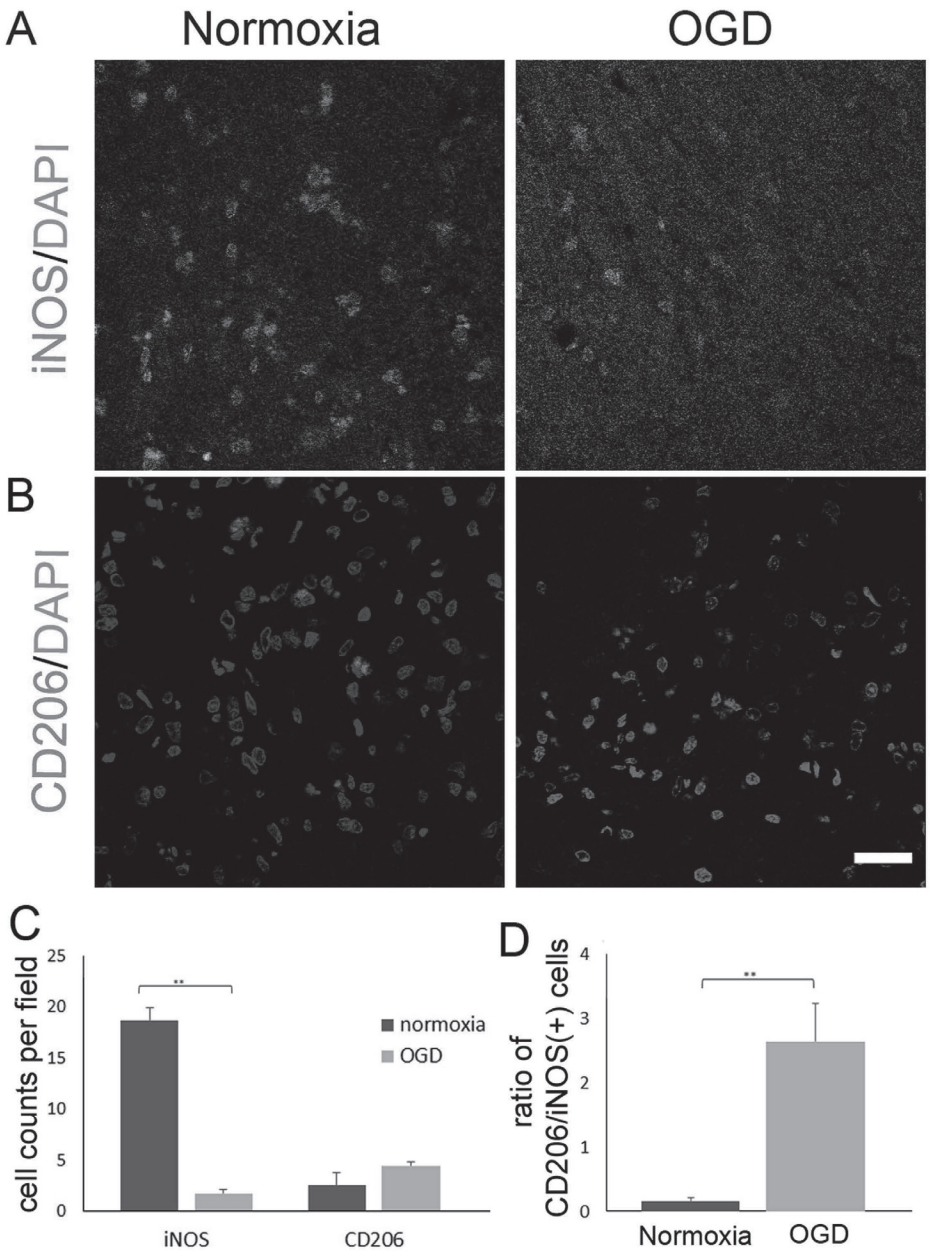

Figure 5. Transplantation of microglia preconditioned with oxygen-glucose deprivation (OGD) primes M2 microglial switch in the border area between the ischemic core and the penumbra at 3 days after transplantation. Representative figures indicate the number of cells positive for M1-specific marker (inducible nitric oxide synthase, iNOS) (**A**) and M2-specific marker (cluster of differentiation 206, CD206) (**B**) in the border area between ischemic core and penumbra from cerebral cortices of the normoxic microglial transplantation group or the OGD-preconditioned microglial transplantation group at 3 days after transplantation (10 days after cerebral ischemia). Confocal microscopic images showing iNOS or CD206 (red)/4′,6′-diamidino-2-phenylindole (DAPI; blue) double labelling in the ischemic cortices. Scale bars, 15 μm. (**C**) Bar graphs depicting the number of iNOS- and CD206-positive cells in the border between ischemic core and penumbra from cerebral cortices of the normoxic microglial transplantation group or OGD-preconditioned microglial transplantation group at 3 days after transplantation. (**D**) Bar graphs depicting the ratio CD206-positive cells to iNOS-positive cells, which reflects microglial polarization after normoxia and OGD preconditioning ($N > 21$). $^{**}P < 0.01$.

protein marker, SMI31. The expression of SMI31 in the ischemic penumbra in the OGD-preconditioned microglial transplantation group was more prominent than that in the no cell control group and OGD-preconditioned astrocytic transplantation group ($P < 0.001$ and $P < 0.001$, respectively) (Fig. 7B). Additionally, the expression

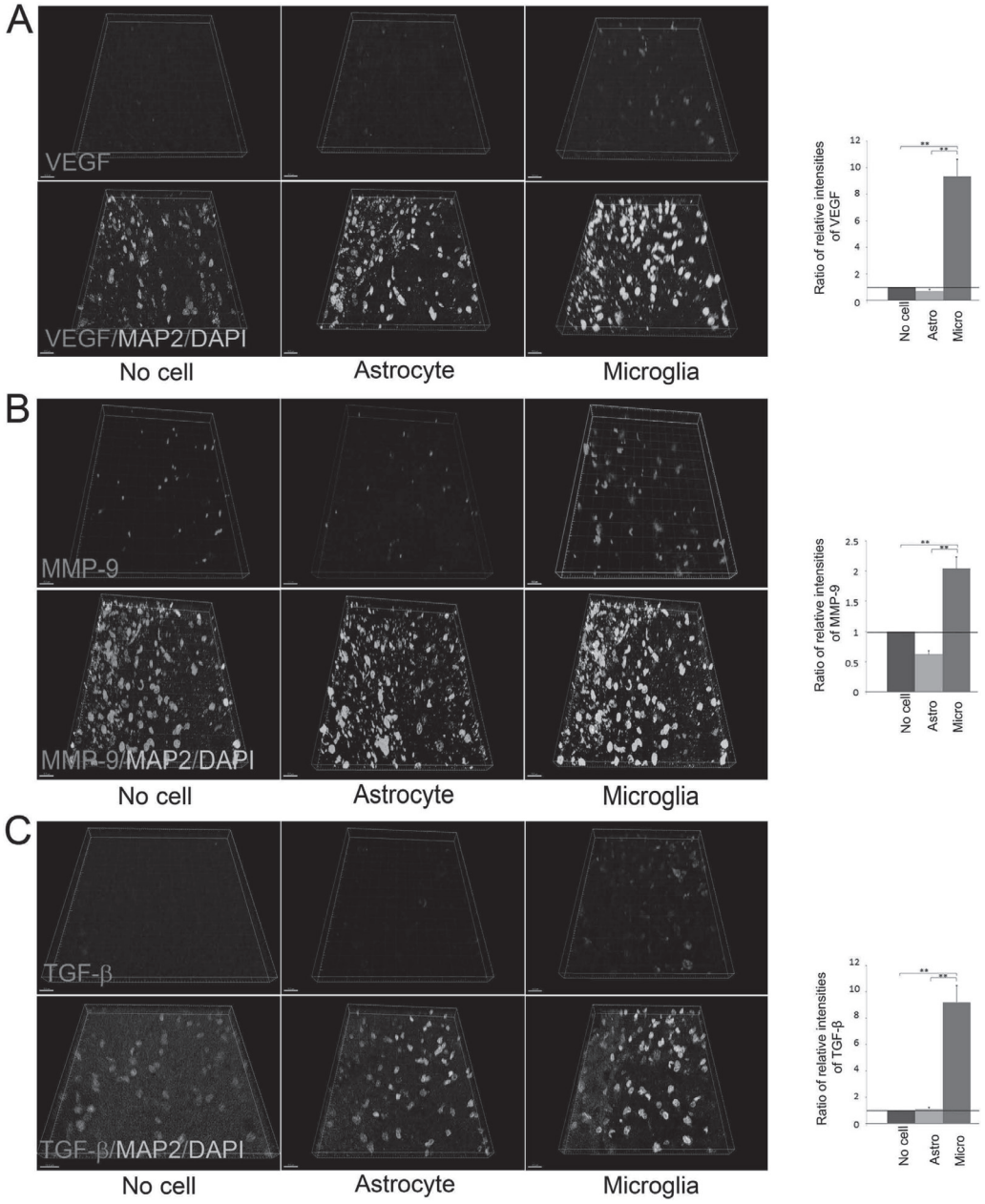

Figure 6. Transplantation of OGD-preconditioned microglia promotes expression of remodelling factors at 28 days after cerebral ischemia. (**A–C**) Representative figures and the relative signal intensities of vascular endothelial growth factor (VEGF) (**A**), matrix metalloproteinase-9 (MMP-9) (**B**), and transforming growth factor-β (TGF-β) (**C**) from cerebral cortices of the no cell control group and the microglia or astrocyte transplanted groups at 28 days after cerebral ischemia. VEGF (**A**), MMP-9 (**B**), and TGF-β (**C**) (red)/MAP2 (green)/DAPI (blue) triple labelling of cerebral cortices in the border between the ischemic core and penumbra at 28 days after reperfusion as examined by confocal microscopy. A secondary-only antibody control confirms its specificity. Scale bars, 15 μm. Bar graphs represent relative signal intensities of ischemic brain samples compared with those of no cell control samples (N = 21–28). $^{**}P < 0.01$.

of another axonal outgrowth marker, growth associated protein 43 (GAP43)[14], in the ischemic penumbra in the OGD-preconditioned microglial transplantation group also was more prominent than that in the no cell control group and OGD-preconditioned astrocytic transplantation group ($P < 0.001$ and $P < 0.001$, respectively) (Supplementary Fig. 8). In contrast, there was no significant difference in the expressions of MAP2 in the ischemic penumbra among the three groups (Fig. 7B).

To determine the mechanism by which OGD-preconditioned microglial transplantation promotes axonal outgrowth, we evaluated the expression of chondroitin sulphate proteoglycan (CSPG), because it inhibits axonal outgrowth[37] and is cleaved and degraded by MMP-9[38]. To confirm our hypothesis that an increase in MMP-9

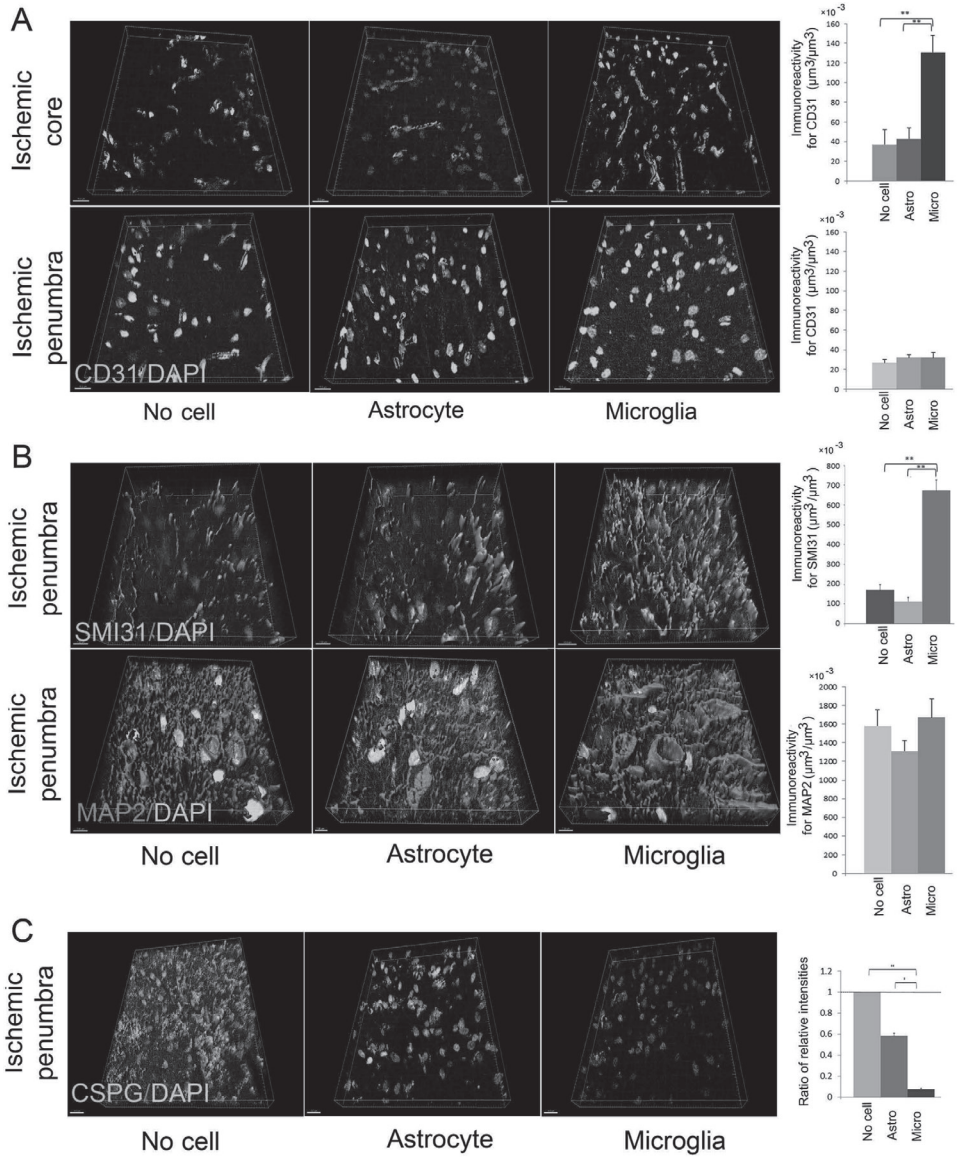

Figure 7. Transplantation of oxygen-glucose deprivation (OGD)-preconditioned microglia promotes angiogenesis in the border area within the ischemic core and axonal outgrowth in the ischemic penumbra at 28 days after cerebral ischemia. (**A**) Representative figures and bar graphs representing immunoreactivity for CD31 volume per unit volume, expressed as μm^3 per μm^3, in the ischemic core and penumbra from cerebral cortices of the no cell control group, OGD-astrocyte, or OGD-microglia transplanted groups at 28 days after cerebral ischemia. The cluster of differentiation (CD31; green)/4′,6′-diamidino-2-phenylindole (DAPI; blue) double labelling in the ischemic cortices at 28 days after cerebral ischemia as examined by confocal microscopy. Scale bars, 15 μm. (**B**) Representative figures and bar graphs representing immunoreactivity for SMI31 and MAP2-positive volumes per unit volume, expressed as μm^3 per μm^3, in the ischemic penumbra from the cerebral cortices of the no cell control group and OGD-preconditioned astrocyte or OGD-preconditioned microglia transplanted groups at 28 days after cerebral ischemia. SMI31 (green) or microtubule-associated protein 2 (MAP2; red)/DAPI (blue) double labelling in the ischemic cortices at 28 days after cerebral ischemia as examined by confocal microscopy. Scale bars, 7 μm. (**C**) Representative figures and bar graphs representing the relative signal intensities of chondroitin sulphate proteoglycan/neuron-glial antigen 2 (CSPG/NG2; green) from the cerebral cortices of the no cell control group and the OGD-preconditioned astrocyte or OGD-preconditioned microglia transplanted groups at 28 days after cerebral ischemia. CSPG/NG2 (green)/DAPI (blue) double labelling of the cerebral cortices in the ischemic penumbra at 28 days after cerebral ischemia as examined by confocal microscopy. Scale bars, 15 μm. The graph represents the relative signal intensities of the microglia or astrocytes transplanted into ischemic brain samples compared with samples from the no cell control group (N = 21–28). The bar graph represents the relative ratio of the signal intensities of the ischemic brain samples compared with that of sham-operated rat samples (N = 21–28). Moreover, a secondary-only antibody control confirms its specificity. *$P < 0.05$, **$P < 0.01$.

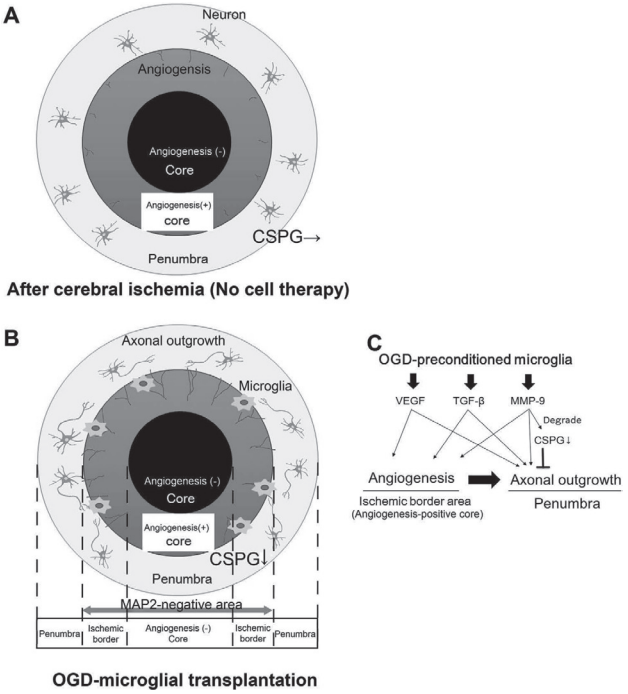

Figure 8. Mechanism of oxygen-glucose deprivation (OGD)-preconditioned microglial transplantation after cerebral ischemia. (**A**) The schema of angiogenesis after cerebral ischemia. The ischemic core is defined as the MAP2-immunonegative ischemic cortex. Angiogenesis (red lines) is slightly activated at the border area within the ischemic core, which we define as the "angiogenesis-positive core" (dark grey), by cell therapy. Thus, the MAP2-negative ischemic core consists of the angiogenesis-positive core and angiogenesis-negative core (black), which develops irreversible change. (**B**) The schema of angiogenesis and axonal outgrowth (regeneration, green cells; neurons) by OGD-preconditioned microglial transplantation (blue cells) after cerebral ischemia. OGD-preconditioned microglial transplantation markedly activated angiogenesis (red lines) at the angiogenesis-positive core (ischemic border area). In addition, the decrease in the expression of chondroitin sulphate proteoglycan (CSPG, grey and diagonal area), which is known to be an axonal outgrowth inhibitor, was observed in the ischemic penumbra after cerebral ischemia. An axonal outgrowth of neuronal cells (green) by OGD-preconditioned microglial transplantation was observed in the ischemic penumbra. (**C**) A diagram of therapeutic effects of OGD-preconditioned microglial transplantation after cerebral ischemia. Transplanted OGD-preconditioned microglia directly secreted vascular endothelial growth factor (VEGF), transforming growth factor-β (TGF-β), and matrix metalloproteinase-9 (MMP-9). These factors may also be associated with changes in resident native endothelial cells, astrocytes, pericytes, neurons, and microglia caused by the paracrine action of OGD-preconditioned M2 microglia. These factors directly prompt angiogenesis in the angiogenesis-positive core (ischemic border area). MMP-9 from microglia might degrade the axonal outgrowth inhibitor CSPG. Angiogenesis might facilitate the induction of axonal outgrowth. In addition, VEGF, TGF-β, and MMP-9 also might directly induce axonal outgrowth.

expression by OGD-preconditioned microglial transplantation may cause degradation of CSPG, resulting in axonal outgrowth, we performed immunofluorescence staining using an anti-CSPG/neuron-glial antigen 2 (NG2) antibody (NG2 is a major component of CSPG) (Fig. 7C). We compared intensities of CSPG/NG2 expression in sham-operated rats and transplanted rats at 28 days after cerebral ischemia. Confocal microscopic studies revealed that expression of CSPG/NG2 in the ischemic penumbra of the OGD-preconditioned microglial transplantation group was much lower than that in the no cell control group ($P < 0.001$) and OGD-preconditioned astrocytic transplantation group ($P = 0.038$) at 21 days after transplantation (at 28 days after cerebral ischemia).

Discussion

First, we investigated both temporal changes and the detailed location of angiogenesis and axonal outgrowth (neuronal regeneration) after cerebral ischemia, because angiogenesis and axonal outgrowth in the peri-infarct area were considered to promote functional recovery[13,39]. We demonstrated that endothelial proliferation and subsequent angiogenesis were activated at the border area within the MAP2-negative ischemic core but not in the ischemic penumbra from 7 days after cerebral ischemia. We confirmed these findings using a different ischemic model. Although there are several definitions of the ischemic core, the ischemic core in animal models is generally defined as the MAP2-negative lesion[40,41]. However, the present study demonstrated for the first time that the MAP2-negative ischemic core is not homogenous; angiogenesis was observed only in the border area within the MAP2-negative area (Fig. 8A). We speculated that the border area within the MAP2-negative ischemic core

might be a novel therapeutic target area against cerebral ischemia. In contrast, axonal outgrowth was not observed in either the ischemic core or penumbra until 14 days after cerebral ischemia. This result was consistent with a previous report that axonal outgrowth was not observed until 28 days after cerebral ischemia[42]. These findings indicate that it could be difficult to promote axonal outgrowth, which is a prerequisite for functional recovery, without any sort of interventions after cerebral ischemia.

We demonstrated evident functional recovery by OGD-preconditioned microglial transplantation but not by OGD-preconditioned astrocytic transplantation. We also found that OGD-preconditioned microglia but not OGD-preconditioned astrocytes could cross the BBB to reach the injured brain parenchyma. This finding was consistent with several reports showing that primary microglia could cross the BBB[27] and reach the injured brain parenchyma[22,26,28]. As Mac-1 mediates leukocyte and microglial adhesion to the endothelial surface, it might be important for the infiltration of these cells into the affected brain parenchyma[31,32]. Increasing the levels of Mac-1 after OGD preconditioning may enable the microglia to cross BBB and reach the injured brain parenchyma. Several studies have demonstrated that the chemokine stromal-derived factor-1 (SDF-1, also known as CXCL12) plays an important role in the homing of bone marrow-derived cells, especially microglia, monocytes, and stem cells, to areas of ischemic injury[43–45]. SDF-1 may play a role in the homing of microglia to areas of ischemic brain parenchyma. Interestingly, the homing of bone marrow-derived cells has been observed in the ischemic border between ischemic core and penumbra, similar to our results, and the expression of SDF-1 has been observed in the ischemic penumbra[44]. This ability of OGD-preconditioned microglia is crucial to the success of this cell-based therapy, although the mechanism by which OGD-preconditioned microglia reach the injured brain parenchyma remains to be elucidated.

Next, we demonstrated that optimal OGD preconditioning can induce anti-inflammatory M2 microglia, which are considered to have protective effects via the secretion of remodelling factors such as VEGF and TGF-β after cerebral ischemia[19,25,46]. Temporal analyses of microglial phenotypes in ischemic animals demonstrated that M2 microglia were detectable from 12 h, temporally increased at 1 to 3 days, and decreased after several days after cerebral ischemia[19,20]. In the present study, we chose 18 h incubation as the optimal OGD condition, because 18 h incubation induced predominantly M2 microglia whereas 24 h incubation caused cell death[33,34]. In fact, this OGD condition induced increased secretion of VEGF, MMP-9, and TGF-β *in vitro*, indicating the polarization of M2 microglia (Fig. 4). The administration of OGD-preconditioned microglia resulted in overexpression of remodelling factors such as VEGF, TGF-β, and MMP-9. These results showed the possible effects of OGD treatment on microglial M2 switch. The upregulation of these remodelling factors also was observed *in vivo,* more specifically in the injured brain parenchyma after OGD-preconditioned microglial transplantation.

We consider that the secretion of remodelling factors from OGD-preconditioned microglia were limited in duration because no GFP-positive OGD-preconditioned microglia were observed in the ischemic lesion at 21 days after transplantation. However, we observed the expression of these remodelling factors not only in the microglia but also in other cells at 28 days after transplantation, suggesting that changes in resident native endothelial cells, astrocytes, pericytes, neurons, and microglia might be caused by the paracrine action of OGD-preconditioned M2 microglia.

We speculate that pleiotropic effects of OGD-preconditioned M2 microglia, including the paracrine actions of the remodelling factors, and degradation of CSPG by MMP-9, might promote angiogenesis and axonal outgrowth (i.e., neuronal regeneration). We demonstrated that angiogenesis was activated at the border area within the MAP2-negative ischemic core, which we defined as the "angiogenesis-positive core" (Fig. 8B). In this region, we observed diminished expression of CSPG, one axonal outgrowth inhibitor[37], which might be degraded by MMP-9[38] (Fig. 8C). We also demonstrated that axonal outgrowth was observed only in the ischemic penumbra, especially around the region exhibiting angiogenesis. We consider that VEGF, MMP-9, and TGF-β might promote not only angiogenesis but also axonal outgrowth *in vivo* (Fig. 8B and C), because several studies have reported that these angiogenic factors are also involved in axonal outgrowth[23,47,48]. Interestingly, Lyden and others had proposed a 'clean-up hypothesis' whereby newborn vessels serve to facilitate macrophage/microglia infiltration and clear cellular debris from pan-necrotic tissue to facilitate angiogenesis and remodelling[49,50]. OGD-preconditioned microglia might induce this phenomenon in the "angiogenesis-positive core" and its surrounding tissue (i.e., penumbra) after cerebral ischemia. Based on these findings, we consider that cell-based therapies that cause a switch from M1- to M2-dominant microglia/macrophages might be promising.

In conclusion, we demonstrated that transplantation of microglia preconditioned by OGD may be a novel therapeutic strategy for ischemic stroke. We consider that the following therapeutic mechanisms might be involved: (i) migration of OGD-preconditioned microglia into the "angiogenesis-positive core", (ii) secretion of remodelling factors from the M2 microglia stimulated by optimal OGD preconditioning, (iii) changes in resident native endothelial cells, astrocytes, pericytes, neurons, and microglia by paracrine actions of the M2 microglia, and (iv) angiogenesis and axonal outgrowth.

Methods

This study was carried out in strict accordance with the recommendations from the Guide for the Care and Use of Laboratory Animals of the National Institutes of Health (Bethesda, MD, USA). The protocol was approved by the Niigata University Administrative Panel on Laboratory Animal Care. All surgeries were performed under inhalation of halothane and according to ARRIVE (Animal Research: Reporting of *In Vivo* Experiments) guidelines[51]. Rats and mice were maintained under controlled light (lights on, 5:00–19:00), temperature (23 ± 1 °C), and humidity (55 ± 10%) conditions and given free access to food and water.

Focal cerebral ischemia. Transient focal cerebral ischemia was induced in male Sprague-Dawley rats weighing 290–320 g using an intraluminal filament suture technique[52,53]. After 90 min of ischemia, the suture was withdrawn to restore blood flow. This model provides an area of the ischemic core and penumbra determined by

the presence of MAP2 with a high degree of reproducibility, and demonstrates that the time window for salvage of penumbral tissues by reperfusion was 90 min. Focal cerebral ischemia also was induced using a different model of focal embolic ischemia using an autologous thrombi technique[54–56]. Tissue plasminogen activator was administered intravenously in the form of Alteplase (Mitsubishi Tanabe Pharma Co., Osaka, Japan) at a dose of 10 mg/kg per animal at 4 h after cerebral ischemia for recanalization and reperfusion. Core body temperature, which was monitored via rectal probe, was maintained at 37.0 ± 0.5 °C using a heating pad.

Experimental design. Sample size calculations were performed prior to the experiments to determine the number of animals needed to detect differences between cell-based therapy and control conditions. Based on a pilot study of N = 4 animals in the treatment group, we determined the sample size needed to detect differences in motor outcomes between the OGD-preconditioned microglial transplantation group and the control and normoxia groups (α, 0.05; one-sided analysis). Rats were randomly assigned to various experimental groups, and analyses were performed by an investigator blinded to the treatment.

Immunofluorescence staining and confocal microscopy. The rats that survived for 1, 3, 7, 14, and 28 days after cerebral ischemia were euthanized with an overdose of halothane, followed by transcardial perfusion with cold normal saline followed by perfusion with cold 4% paraformaldehyde in 0.1 M phosphate-buffered saline (PBS; pH 7.4). Brains were removed and embedded in paraffin wax. Serial sections (4-μm thick) were cut from the paraffin blocks and stained using antibodies as described previously[53]. We also stained free-floating sections (50-μm thick)[53]. Sections were mounted with Vectashield 4′, 6′-diamidino-2-phenylindole (DAPI) (Vector Laboratories, Burlingame, CA, USA). Information about the primary antibodies is described in Supplementary Table 1. The sections were examined under a confocal laser-scanning microscope (LSM510 META; Carl Zeiss, Oberkochen, Germany). Cortical tissues corresponding to the ischemic core or penumbra were defined by MAP2 staining as described previously[52,53].

Immunocytochemistry. Microglial cells on coverslips were washed with PBS and fixed with 100% methanol for 10 seconds. After fixation, the cells were incubated with the primary fluorescein isothiocyanate (FITC)-conjugated anti-Mac-1 monoclonal antibody (Supplementary Table 1). Sections were mounted with DAPI (Vector Laboratories, Burlingame, CA, USA).

Quantitative analysis of brain tissue structures and Mac-1 expression by immunostaining. To perform quantitative analyses of brain tissue structures, tissue sections were immunostained with antibodies against CD31 (a marker of endothelial cells and angiogenesis), MAP2 (a marker of neuronal dendrites), SMI31 and GAP43 (markers of neuronal axons), VEGF, TGF-β, and MMP-9 (Supplementary Table 1), and counted as described previously[55]. Briefly, seven randomly chosen non-overlapping high-power fields (630× or 1260×) at the level of the anterior commissure of the sham-operated or ischemic cortex in the MCA territory were examined. Data were acquired from stereotaxically identical 0.03-mm^3 regions of interest (ROIs). Three-dimensional reconstructions and z-sections collected at 0.15-μm z-intervals were created and automatically quantified in blinded fashion as the intensity of total immunoreactive structure volumes (immunoreactive volume/examined ROI volume) using IMARIS imaging software (BitplaneAG, Zurich, Switzerland)[55–57]. The results were confirmed in three or four independent samples (N > 21–28).

For comparing the expression levels of Mac-1 in microglia under normoxic and OGD conditions, high-power fields (630×) were examined. Two-dimensional reconstructions were created and the intensity of total immunoreactivity per cell was quantified in a blinded manner using the IMARIS imaging software[34] (N = 5).

Cell counting protocol. To determine the frequency of cells positive for Ki67, a proliferative marker[39], after cerebral ischemia, seven randomly chosen non-overlapping high-power fields (630×) at the level of the anterior commissure of the sham-operated or ischemic cortex (i.e., the border area of the ischemic core and penumbra) were examined at 1, 3, 7, and 14 days after cerebral ischemia (N = 21)[53,58].

To determine the numbers of cells positive for M1 microglia-specific marker (iNOS) and M2-specific marker (CD206)[19,20], seven randomly chosen non-overlapping high-power fields (630×) at the level of the anterior commissure of the ischemic cortex (i.e., the border area between the ischemic core and penumbra) were examined at 3 days after transplantation (10 days after cerebral ischemia (N > 21)[53,58].

Primary cell cultures. Primary murine microglia and astrocytes were obtained as previously described[33]. Primary mixed glial cultures were established from the forebrains of postnatal C57Bl/6 mice by dissociating isolated cerebral cortices in papain and then growing the resulting cell suspension for 10 days in Dulbecco's modified Eagle's medium (DMEM) supplemented with 10% foetal bovine serum (FBS). After 10 days, flasks were shaken for 15 min to remove loosely attached microglia. The purity of these microglial cultures was 99% as determined by Mac-1 (CD11b/CD18) immunoreactivity in flow cytometry[33]. For astrocytes, flasks were then shaken overnight to remove microglia and oligodendrocyte precursors. The remaining monolayer was determined as >95% astrocytes by glial fibrillary acidic protein (GFAP) immunoreactivity[33].

Oxygen–glucose deprivation. The standardized conditions for OGD have been described in detail elsewhere[33,35]. The cultures containing low-glucose medium were placed in a hypoxia chamber (Billups-Rothenburg, Del Mar, CA, USA), which was flushed with a mixture of 95% N_2 and 5% CO_2 for 1 h, and then closed for 18 h. Twenty-four h incubation under OGD conditions promoted cell death, whereas 18 h incubation under OGD conditions did not cause cell death as evaluated by propidium iodide[33] and lactate dehydrogenase assays[34]. Additionally, M2 microglia were detectable starting from 12 h, maximally increasing at 24 h,

and markedly decreased at later time points[20]. Given these findings, we chose 18 h for the OGD condition in this study.

Enzyme-linked immunosorbent assay (ELISA). After overnight incubation under OGD conditions, we measured the levels of VEGF, BDNF, TNF-α, TGF-β, IL-1β, IL-6, and IL-10 in the conditioned media using the VEGF Quantikine ELISA Kit (RRV00), BDNF Quantikine ELISA Kit (DBD00), TNF-α Quantikine ELISA Kit (MTA00B00), TGF-β Quantikine ELISA Kit (MB100B), IL-1β Quantikine ELISA Kit (MLB00C), IL-6 Quantikine ELISA Kit (M6000B), and IL-10 Quantikine ELISA Kit (M1000B) (all R&D Systems, Minneapolis, MN, USA), respectively, according to the manufacturer's instructions (N = 5–6).

Active MMP-9 assay. The Fluorimetric SensoLyte™ 520 (AnaSpec Corp. San Jose, CA, USA) was used to quantify the specific enzymatic activity of active MMP-9 using a fluorescence resonance energy transfer (FRET) peptide containing a fluorescent donor and quenching acceptor[55,59]. We measured MMP-9 activities of the samples according to the manufacturer's instructions. The protein concentrations of the samples were determined using a bicinchoninic acid protein assay kit (Pierce, Rockford, IL, USA). Samples (170 μg) were placed in a 96-well plate containing 50 μl of assay buffer. The proteolytic activities of MMP-9 were quantified using the FRET peptide.

Cell transplantation. We excluded rats that weighed 2 SD below the mean at 7 days after cerebral ischemia to include only rats in the same physiological condition. Cells (1×10^6, microglia or astrocytes) were diluted with 300 μL of PBS[13]. Rats subjected to transient MCA occlusion at 7 days after cerebral ischemia were randomly assigned to one of the cell-treated groups, in which transplantations of microglia or astrocytes were slowly infused through the stump of the external carotid artery over the course of 3 min (microglia group and astrocyte group, respectively), or the no cell control group. The same volume of PBS was injected in all groups.

Sensorimotor assessment. Sensorimotor assessments were performed at 0, 1, 4, 7, 10 (3 days after transplantation), 14 (7 days after transplantation), 21 (14 days after transplantation), and 28 days (21 days after transplantation) after cerebral ischemia using the corner test[60]. Analyses of therapeutic effects were performed by an investigator blinded to treatment.

Green fluorescent protein (GFP) mice. To determine whether transplanted microglia and astrocytes can translocate from the blood into the brain parenchyma to exert their beneficial effects after intra-arterial administration, we used primary microglia and astrocytes from GFP mice[30]. GFP transgenic mice were produced by breeding heterozygous pairs in the Genome Information Research Centre, Osaka University, Japan and maintained in the Department of Comparative and Experimental Medicine, Brain Research Institute, Niigata University. After preconditioning primary microglia and astrocytes from GFP mice by the OGD condition, we administered these cells intra-arterially at 7 days after cerebral ischemia. We performed confocal microscopic examination at 3 and 21 days after transplantation.

Statistical analyses. All data are presented as the mean ± standard error of the mean (SEM). Differences in the parameters were analysed using one-way or two-way ANOVA followed by Bonferroni's *post hoc* test or unpaired *t*-test. Statistical analyses were performed using IBM SPSS Statistics for Windows, Version 21.0 (Armonk, NY, USA). Differences in frequencies were assessed with Fisher's exact test. All tests were considered statistically significant at a P value < 0.05.

References

1. Mozaffarian, D. *et al.* Heart disease and stroke statistics–2015 update: a report from the American Heart Association. *Circulation* **131,** e29–322 (2015).
2. Winstein, C. J. *et al.* Guidelines for Adult Stroke Rehabilitation and Recovery: A Guideline for Healthcare Professionals From the American Heart Association/American Stroke Association. *Stroke* **47,** e98–169 (2016).
3. Freytes, D. O. *et al.* Macrophages modulate the viability and growth of human mesenchymal stem cells. *J. Cell. Biochem.* **114,** 220–229 (2013).
4. Arai, K. *et al.* Brain angiogenesis in developmental and pathological processes: neurovascular injury and angiogenic recovery after stroke. *FEBS J* **276,** 4644–4652 (2009).
5. Zhang, Z. G. *et al.* VEGF enhances angiogenesis and promotes blood-brain barrier leakage in the ischemic brain. *J. Clin. Invest.* **106,** 829–838 (2000).
6. Hariawala, M. D. *et al.* VEGF improves myocardial blood flow but produces EDRF-mediated hypotension in porcine hearts. *J. Surg. Res.* **63,** 77–82 (1996).
7. Yang, R. *et al.* Effects of the vascular endothelial growth factor on hemodynamics and cardiac performance. *J. Cardiovasc. Pharmacol.* **27,** 838–844 (1996).
8. Yang, R. *et al.* Substantially attenuated hemodynamic responses to Escherichia coli-derived vascular endothelial growth factor given by intravenous infusion compared with bolus injection. *J. Pharmacol. Exp. Ther.* **284,** 103–110 (1998).
9. Moskowitz, M. A. *et al.* The science of stroke: mechanisms in search of treatments. *Neuron* **67,** 181–198 (2010).
10. Liu, X. *et al.* Cell based therapies for ischemic stroke: from basic science to bedside. *Prog. Neurobiol.* **115,** 92–115 (2014).
11. Li, Q. *et al.* Modeling the neurovascular niche: VEGF- and BDNF-mediated cross-talk between neural stem cells and endothelial cells: an *in vitro* study. *J. Neurosci. Res.* **84,** 1656–1668 (2006).
12. Moriyama, Y. *et al.* Intravenous injection of neural progenitor cells facilitates angiogenesis after cerebral ischemia. *Brain Behav.* **3,** 43–53 (2013).
13. Ishizaka, S. *et al.* Intra-arterial cell transplantation provides timing-dependent cell distribution and functional recovery after stroke. *Stroke* **44,** 720–726 (2013).
14. Andres, R. H. *et al.* Human neural stem cells enhance structural plasticity and axonal transport in the ischaemic brain. *Brain* **134,** 1777–1789 (2011).
15. Prasad, K. *et al.* Intravenous autologous bone marrow mononuclear stem cell therapy for ischemic stroke: a multicentric, randomized trial. *Stroke* **45,** 3618–3624 (2014).

16. Seto, T. *et al.* Brain magnetic resonance imaging in 23 patients with mucopolysaccharidoses and the effect of bone marrow transplantation. *Ann. Neurol.* **50,** 79–92 (2001).
17. Iadecola, C. & Anrather, J. The immunology of stroke: from mechanisms to translation. *Nat. Med*. **17,** 796–808 (2011).
18. Mabuchi, T. *et al.* Contribution of microglia/macrophages to expansion of infarction and response of oligodendrocytes after focal cerebral ischemia in rats. *Stroke* **31,** 1735–1743 (2000).
19. Hu, X. *et al.* Microglia/macrophage polarization dynamics reveal novel mechanism of injury expansion after focal cerebral ischemia. *Stroke* **43,** 3063–3070 (2012).
20. Perego, C. *et al.* Temporal pattern of expression and colocalization of microglia/macrophage phenotype markers following brain ischemic injury in mice. *J. Neuroinflammation* **8,** 174 (2011).
21. Crain, J. M. *et al.* Microglia express distinct M1 and M2 phenotypic markers in the postnatal and adult central nervous system in male and female mice. *J. Neurosci. Res.* **91,** 1143–1151 (2013).
22. Imai, F. *et al.* Neuroprotective effect of exogenous microglia in global brain ischemia. *J. Cereb. Blood Flow Metab.* **27,** 488–500 (2007).
23. Rosenberg, G. A. Matrix metalloproteinases and their multiple roles in neurodegenerative diseases. *Lancet Neurol.* **8,** 205–216 (2009).
24. Vivien, D. & Ali, C. Transforming growth factor-beta signalling in brain disorders. *Cytokine Growth Factor Rev.* **17,** 121–128 (2006).
25. Stanković, N. D. *et al.* Microglia-blood vessel interactions: a double-edged sword in brain pathologies. *Acta. Neuropathol.* **131,** 347–363 (2016).
26. Hughes, P. M. *et al.* Monocyte chemoattractant protein-1 deficiency is protective in a murine stroke model. *J. Cereb. Blood Flow Metab.* **22,** 308–317 (2002).
27. Neumann, H. Microglia: a cellular vehicle for CNS gene therapy. *J. Clin. Invest.* **116,** 2857–2860 (2006).
28. Wattananit, S. *et al.* Monocyte-derived macrophages contribute to spontaneous long-term functional recovery after stroke in mice. *J. Neurosci.* **36,** 4182–4195 (2016).
29. Ueno, Y. *et al.* Axonal outgrowth and dendritic plasticity in the cortical peri-infarct area after experimental stroke. *Stroke* **43,** 2221–2228 (2012).
30. Okabe, M. *et al.* Green mice' as a source of ubiquitous green cells. *FEBS Lett.* **407,** 313–319 (1997).
31. Soriano, S. *et al.* Mice deficient in Mac-1 (CD11b/CD18) are less susceptible to cerebral ischemia/reperfusion injury. *Stroke* **30,** 134–139 (1999).
32. Ahn, G. O. *et al.* Inhibition of Mac-1 (CD11b/CD18) enhances tumor response to radiation by reducing myeloid cell recruitment. *Proc. Natl. Acad. Sci. USA* **107,** 8363–8368 (2010).
33. Milner, R. *et al.* Responses of endothelial cell and astrocyte matrix-integrin receptors to ischemia mimic those observed in the neurovascular unit. *Stroke* **39,** 191–197 (2008).
34. Kanazawa, M. *et al.* Multiple therapeutic effects of progranulin on experimental acute ischaemic stroke. *Brain* **138,** 1932–1948 (2015).
35. del Zoppo, G. J. *et al.* Microglial cell activation is a source of metalloproteinase generation during hemorrhagic transformation. *J. Cereb. Blood Flow Metab.* **32,** 919–932 (2012).
36. Arai, K. *et al.* Essential role for ERK mitogen-activated protein kinase in matrix metalloproteinase-9 regulation in rat cortical astrocytes. *Glia* **43,** 254–264 (2003).
37. Galtrey, C. M. & Fawcett, J. W. The role of chondroitin sulfate proteoglycans in regeneration and plasticity in the central nervous system. *Brain Res. Rev.* **54,** 1–18 (2007).
38. Larsen, P. H. *et al.* Matrix metalloproteinase-9 facilitates remyelination in part by processing the inhibitory NG2 proteoglycan. *J. Neurosci.* **23,** 11127–11135 (2003).
39. Wang, Z. *et al.* Chronic valproate treatment enhances postischemic angiogenesis and promotes functional recovery in a rat model of ischemic stroke. *Stroke* **43,** 2430–2436 (2012).
40. Dawson, D. A. *et al.* Acute focal ischemia-induced alterations in MAP2 immunostaining: description of temporal changes and utilization as a marker for volumetric assessment of acute brain injury. *J. Cereb. Blood Flow Metab.* **16,** 170–174 (1996).
41. Zhao, H. *et al.* Akt contributes to neuroprotection by hypothermia against cerebral ischemia in rats. *J. Neurosci.* **25,** 9794–9806 (2005).
42. Li, Y. *et al.* Neuronal damage and plasticity identified by microtubule-associated protein 2, growth-associated protein 43, and cyclin D1 immunoreactivity after focal cerebral ischemia in rats. *Stroke* **29,** 1972–1980 (1998).
43. Lu, D. Y. *et al.* SDF-1alpha up-regulates interleukin-6 through CXCR4, PI3K/Akt, ERK, and NF-kappaB-dependent pathway in microglia. *Eur. J. Pharmacol.* **613,** 146–154 (2009).
44. Hill, W. *et al.* SDF-1 (CXCL12) is upregulated in the ischemic penumbra following stroke: association with bone marrow cell homing to injury. *J. Neuropathol. Exp. Neurol.* **63,** 84–96 (2004).
45. Robin, A. *et al.* Stromal cell-derived factor 1a mediates neural progenitor cell motility after focal cerebral ischemia. *J. Cereb. Blood Flow Metab.* **26,** 125–134 (2006)
46. Cherry, J. D. *et al.* Neuroinflammation and M2 microglia: the good, the bad, and the inflamed. *J. Neuroinflammation* **11,** 98 (2014).
47. Sondell, M. *et al.* Vascular endothelial growth factor has neurotrophic activity and stimulates axonal outgrowth, enhancing cell survival and Schwann cell proliferation in the peripheral nervous system. *J. Neurosci.* **19,** 5731–5740 (1999).
48. Ho, T. W. *et al.* TGFβ trophic factors differentially modulate motor axon outgrowth and protection from excitotoxicity. *Exp. Neurol.* **161,** 664–675 (2000).
49. Manoonkitiwongsa, P. S. *et al.* Angiogenesis after stroke is correlated with increased numbers of macrophages: the clean-up hypothesis. *J. Cereb. Blood Flow Metab.* **21,** 1223–1231 (2001).
50. Yu, S. W. *et al.* Stroke-evoked angiogenesis results in a transient population of microvessels. *J. Cereb. Blood Flow Metab.* **27,** 755–763 (2007).
51. Kilkenny, C. *et al.* National Centre for the Replacement, Refinement and Reduction of Amimals in Research. Animal research: reporting *in vivo* experiments—the ARRIVE guidelines. *J. Cereb. Blood Flow Metab.* **31,** 991–993 (2010).
52. Memezawa, H. *et al.* Penumbral tissues salvaged by reperfusion following middle cerebral artery occlusion in rats. *Stroke* **23,** 552–559 (1992).
53. Kanazawa, M. *et al.* Biochemical and histopathological alterations in TAR DNA binding protein-43 after acute ischemic stroke in rats. *J. Neurochem.* **116,** 957–965 (2011).
54. Okubo, S. *et al.* FK-506 extended the therapeutic time window for thrombolysis without increasing the risk of hemorrhagic transformation in an embolic rat stroke model. *Brain Res.* **1143,** 221–227 (2007).
55. Kanazawa, M. *et al.* Inhibition of VEGF signaling pathway attenuates hemorrhage after tPA treatment. *J. Cereb. Blood Flow Metab.* **31,** 1461–1474 (2011).
56. Kawamura, K. *et al.* Effects of angiopoietin-1 on hemorrhagic transformation and cerebral edema after tissue plasminogen activator treatment for ischemic stroke in rats. *PLoS One* **9,** e98639 (2014).
57. Zhang, L. *et al.* Atorvastatin extends the therapeutic window for tPA to 6 h after the onset of embolic stroke in rats. *J. Cereb. Blood Flow Metab.* **29,** 1816–1824 (2009).
58. Katchanov, J. *et al.* Mild cerebral ischemia induces loss of cyclin-dependent kinase inhibitors and activation of cell cycle machinery before delayed neuronal cell death. *J. Neurosci.* **21,** 5045–5053 (2001).

59. Lin, C. W. *et al.* Quercetin inhibition of tumor invasion via suppressing PKCδ/ERK/AP-1-dependent matrix metalloproteinase-9 activation in breast carcinoma cells. *Carcinogenesis* **29,** 1807–1815 (2008).
60. Balkaya, M. *et al.* Characterization of long-term functional outcome in a murine model of mild brain ischemia. *J. Neurosci. Methods* **213,** 179–187 (2013).

Acknowledgements

We thank Prof. Masanori Fukushima (Translational Research Informatics Center, Japan) for helpful suggestions. We thank Prof. Masahito Ikawa and Prof. Masaru Okabe (Genome Information Research Centre, Osaka University, Japan) for providing GFP transgenic mice (C57BL/6-Tg(CAG-EGFP)C14-Y01-FM131Osb). We also thank Moe Ono, B.S. for her technical assistance. This work was supported by a Grant-in-Aid for Scientific Research (Research Project Number: 15K19478 and 25860702), a grant from SENSHIN Medical Research Foundation, Uehara Memorial Foundation, and Takeda Science Fundation, Young Investigator Okamoto Award, and Research Promoted Award from Yujin Memorial Foundation (MK).

Author Contributions

M.Kanazawa performed the experiments and analyzed the data, developed the concept designed the experiments, drafted the manuscript. M.M participated in ELISA experiments, and helped the culture and immunohisotochemistry. M.T helped the culture and immunohisotochemistry. M.Koyama contributed to the focal ischemic experiments. M.H. helped immunohisotochemistry. M.I., T.N., O.O. T.T. and M.N. advised experiments. M.K. and T.S. were responsible for analyzed the data. T.S. supervised all aspects of this project. All authors read and approved the final manuscript.

Additional Information

Supplementary information accompanies this paper at http://www.nature.com/srep

Competing financial interests: The authors declare no competing financial interests.

How to cite this article: Kanazawa, M. *et al.* Microglia preconditioned by oxygen-glucose deprivation promote functional recovery in ischemic rats. *Sci. Rep.* **7**, 42582; doi: 10.1038/srep42582 (2017).

Publisher's note: Springer Nature remains neutral with regard to jurisdictional claims in published maps and institutional affiliations.